

13172

NATIONAL LIBRARY
OTTAWA



BIBLIOTHÈQUE NATIONALE
OTTAWA

NAME OF AUTHOR.....Hendrik Jan Ritsema van Eck.....

TITLE OF THESIS.....Digital Computer Simulation of Cardiac
.....Excitation and Repolarization in Man
.....

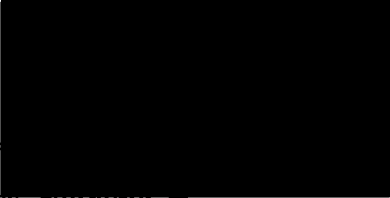
UNIVERSITY.....Dalhousie University, Halifax, N.S.....

DEGREE FOR WHICH THESIS WAS PRESENTED.....Ph.D.....

YEAR THIS DEGREE GRANTED.....1972.....

Permission is hereby granted to THE NATIONAL LIBRARY
OF CANADA to microfilm this thesis and to lend or sell copies
of the film.

The author reserves other publication rights, and
neither the thesis nor extensive extracts from it may be
printed or otherwise reproduced without the author's
written permission.

(Signed) 

PERMANENT ADDRESS:

... 32. Bongweg.....

... Poortugaal.....

... The Netherlands.....

DATED. September 5, 19 72

NL-91 (10-68)

- 1 -

DIGITAL COMPUTER SIMULATION
OF CARDIAC EXCITATION AND REPOLARIZATION
IN MAN

by

Hendrik Jan Ritsema van Eck

Submitted in partial fulfillment of the requirements
for the Degree of Doctor of Philosophy at Dalhousie
University, Halifax, N.S., Canada, September 5, 1972.

Approved by the Members of the Official Examining
Committee, appointed by the Faculty of Graduate Studies.


Dr. G. van Herpen
External Examiner


Dr. A.G. Hunter


Dr. W.T. Josenhans


Dr. D.L. Roy


Dr. P.M. Rautaharju
Thesis Supervisor

Ex Officio: Dr. G. Langstroth
Faculty of Graduate Studies
Chairman of the Committee

DALHOUSIE UNIVERSITY

Date Sept. 5, 1972

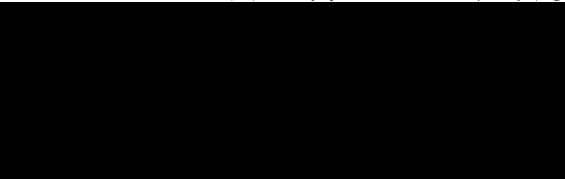
Author Hendrik Jan Ritsema van Eck

Title Digital Computer Simulation of Cardiac Excitation and
Repolarization in Man

Department or School Department of Physiology and Biophysics

Degree Ph.D. Convocation Fall Year 1972

Permission is herewith granted to Dalhousie University to circulate and to have copied, at its discretion, the above title upon the request of individuals or institution.



Signature of Author

EXTENSIVE QUOTATION OR FURTHER REPRODUCTION OF THIS MATERIAL FOR COMMERCIAL PURPOSES BY PERSONS OR AGENCIES OTHER THAN DALHOUSIE UNIVERSITY MAY NOT BE MADE WITHOUT THE EXPRESS PERMISSION OF THE AUTHOR.

DIGITAL COMPUTER SIMULATION OF
CARDIAC EXCITATION AND REPOLARIZATION IN MAN

Dedicated to Renske

A TABLE OF CONTENTS

1.	INTRODUCTION	1
1.1	Electrical and mechanical activity	1
1.2	The cardiac cell	3
1.3	The cardiac syncytium	11
1.4	Electrical sources due to cellular excitation and recovery	14
1.5	Relation between heart vectors and leads	21
1.6	Impulse conduction in excitable elements	24
1.7	Models in electro- and vectorcardiography	26
1.8	Models in general	28
1.9	Purpose of the present investigation	29
2.	REVIEW	32
3.	EXPERIMENTAL PROCEDURE	42
3.1	Introduction	42
3.2	Assumptions	43
	3.2.1 Anatomical structure	43
	3.2.2 Functions	45
	3.2.3 Physical representation	48
3.3	Modelling unit	49
	3.3.1 Introduction	49
	3.3.2 The rhombododecahedron (RDH)	51
	3.3.3 The representing grid points; hexagonal coordinates	54
3.4	Programs HEXCITE and VECTORS	56
	3.4.1 Introduction	56
	3.4.2 Program HEXCITE	57
	3.4.3 Program VECTORS	65

3.5	Error analysis	66
3.5.1	Introduction	66
3.5.2	Experimental errors	67
3.5.3	Procedural errors	70
3.6	Summary	72
4.	NORMAL EXCITATION AND REPOLARIZATION	74
4.1	Introduction	74
4.1.1	Normal excitation and recovery	75
4.2	Methods	90
4.2.1	Normal excitation	90
4.2.2	Heart vectorcardiogram - depolarization	92
4.2.3	Heart vectorcardiogram - repolarization	93
4.2.4	The lead systems	102
4.3	Results	104
4.3.1	Normal excitation	104
4.3.2	Heart vectorcardiogram - depolarization	104
4.3.3	Heart vectorcardiogram - repolarization	108
4.3.4	The lead systems	124
4.4	Discussion	130
4.4.1	Normal excitation	130
4.4.2	The heart VCG depolarization	132
4.4.3	The heart VCG repolarization	133
4.4.4	The lead systems	143
4.5	Conclusions and Summary	148
5.	IMPULSE CONDUCTION UNDER REPETITIVE STIMULATION	151
5.1	Introduction	151
5.2	Formulation of the interaction	151
5.2.1	Refractory periods	152
5.2.2	Conduction velocity	155
5.2.3	Impulse conduction with repetitive stimulation	155
5.2.4	Selfsustaining activity	156
5.2.5	Ventricular myocardium model	157

5.3	Methods	
5.3.1	Action-potential duration	158
5.3.2	Conduction velocity	163
5.3.3	A simple structure of 2500 elements	164
5.3.4	Ventricular myocardium model	165
5.4	Results	168
5.4.1	Impulse conduction with repetitive stimulation	168
5.4.2	Selfsustaining activity	174
5.4.3	Ventricular myocardium model	179
5.5	Discussion	179
5.5.1	The relationship functions	179
5.5.2	Selfsustaining activity	187
5.5.3	Ventricular myocardium model	191
5.6	Conclusions and Summary	192
6.	SUMMARY AND CONCLUSIONS	193
7.	BIBLIOGRAPHY	196
8.	APPENDICES AND TABLES	211

ABSTRACT

A digital computer model was developed of ventricular excitation and repolarization. The geometry of the model was based on accurately collected anatomical data, and the properties of the activation process were constrained according to the electrophysiological behaviour of excitable cells.

In general, a good agreement with data reported in the literature is obtained. Some discrepancies are observed, however, in comparative evaluation of the terminal depolarization sequences.

The electromotive forces associated with the excitation wavefronts were computed on the basis of cellular action potential waveforms.

Body surface potential distributions were computed with the aid of a numerical substitute of a realistic three-dimensional model of the human torso.

The simulated 12 lead electrocardiograms were compared with the actually recorded 12 lead electrocardiograms of the subject whose heart excitation pattern, as studied post mortem with multielectrode needles, served as guideline in the simulation of the normal excitation. A good agreement was observed.

A comparison was made between the computed vectorcardiograms of four commonly used VCG lead systems and the VCG constructed from the dipolar activity of the heart. The overall performance of the McFee & Parungao lead system is most

satisfactory, followed by the Frank system and SVEC III-system; the Burger system is less satisfactory.

The electromotive forces associated with the repolarization were simulated with the aid of profile vectors defined according to the classical ventricular gradient concept.

Four models of the ventricular repolarization sequence were tested. One of the hypotheses, based on currently accepted histological-electrophysiological evidence, was more satisfactory than models based on the reported or speculated effects of temperature or stress distribution on action potential waveforms.

The influence of the inhomogeneous, realistically shaped human torso was found to cause particularly an anterior and slightly inferior displacement of the repolarization vectors.

Dynamic behaviour of a conglomerate of excitable elements was studied. A second stimulus, following within a quite narrow "vulnerable" period after the first stimulus, resulted in a chaotic, self-sustaining, relatively random activity.

A LIST OF DEFINITIONS OF ABBREVIATIONS AND SYMBOLS USED

A	area (scalar); (meter ²)
A	also action potential duration
a	cartesian x component of the lead vector (ohm/meter)
a	also real-constant
APD	action potential duration
AV-node	atrioventricular node, node of His - Tawara
aVL, aVR, aVF	'augmented' ECG leads
b	cartesian y component of the lead vector (ohm/meter)
C	cycle length (sec)
c	cartesian z component of the lead vector (ohm/meter)
c _m	membrane capacitance (farad)

cos	cosine
CV	conduction velocity
d	distance (meter)
d l	scalar differential of distance (meter)
$d\vec{S}$	vector differential element of the surface with direction of the normal to the surface element and length equal to the area of the surface element (meter ²)
dV	scalar differential of potential
dV	also decivolt
dV	scalar differential element of volume (meter ³)
d Ω	scalar differential of the solid angle Ω ($d\Omega = \frac{\vec{r} \cdot d\vec{S}}{r^3}$)
\vec{E}	intensity of the electric field (vector); (volt/meter)
\vec{E}_i	intensity of impressed electric field (vector); (volt/meter)

e	voltage of membrane
E_A	equilibrium potential for ion A
E_m	actual transmembrane potential
e_s	voltage of stimulus
F	Faraday constant $\equiv 96,487$ coulomb/mole
F	function
f	function
FRP	functional recovery period
\vec{G}	gradient vector, integral of heart vector (\vec{H}) over a part or the whole period of one cycle
g_A	chord conductance for ion A
\vec{H}	'heart vector', $\vec{H} = \int_V \vec{J}_i dv$, where integration is over the whole heart 'region' (ampere meter)
h	variable

HVCG	heart vectorcardiogram
I	electric current (ampere)
i	running index, as in a_i , $i=1, \dots, n$
\vec{J}	current density vector; current per unit area (ampere/meter ²)
\vec{J}_i	impressed current density vector, \vec{J}_i has the dimensions of a dipole moment per unit volume (ampere/meter ³)
j	running index, see i
K	constant
\vec{K}_i	current dipole moment per unit surface area (ampere/meter ²)
K_i	reciprocal of absolute refractory period of point P_i
\vec{L}_i	lead vector (ohm/meter)
LV	left ventricle

\vec{m}	dipole moment (vector), is current times separation, directed from negative to positive
N	difference number
N,n	general symbol of integer
N,n	also epoch number
n	normal to membrane, directed outwards
n	also running index, see i
\vec{P}_i	profile vector at point i, $\vec{P}_i = -\sigma \int_{\text{cycle}} \nabla \Phi_i dt$
q	electric charge (coulomb)
R	the gas constant
R	also resistance (ohm)
R	also refractory period
r	positive distance between source and field point (scalar) $r = \vec{r} $ (meter)

RDH	rhombododecahedron
r_i	axoplasmic resistance (ohm)
r_m	membrane resistance (ohm/cm ²)
RV	right ventricle
SA-node	sinu-auricular node, node of Keith-Flack
sin	sinus
T	absolute temperature (degrees Kelvin)
t	time (seconds)
tg	tangens
U	unknown in equation
V	potential difference (scalar); (volt)
v	volume (meter ³)
v	conduction velocity (meter/second)
V_m	transmembrane potential

X	cartesian x component of the 'heart vector' (ampere meter)
x	cartesian coordinate
X_o	orthogonal cartesian coordinate
X_h	hexagonal cartesian coordinate
X_1	hypothetical factor governing ionic current I_{x1}
Y	cartesian y component of the 'heart vector' (ampere meter)
y	cartesian coordinate
Y_o	orthogonal cartesian coordinate
Y_h	hexagonal cartesian coordinate
Z	cartesian z component of the 'heart vector' (ampere meter)
z	cartesian coordinate

z_o	orthogonal cartesian coordinate
z_h	hexagonal cartesian coordinate
\AA	Ångström (10^{-8})
α	time constant of x_1 activation function
β	time constant of x_1 deactivation function
ΔV	scalar differential of potential
Δl	scalar differential of distance
ϵ_0 (epsilon)	constant; dielectric permittivity of the free space $\epsilon_0 = 8.8549 \cdot 10^{-12}$ (farad/meter)
λ (lambda)	wavelength
λ_m	space constant of membrane
μm	micrometer
π (pi)	constant; the ratio of the length of circumference of a circle to the diameter, $\pi \approx 3.14159$

Φ (phi)	scalar potential of electromagnetic field
Φ_i	scalar impressed potential of source electromagnetic field
ρ (rho)	density of charge, i.e. charge per unit volume (coulomb/meter ³)
ρ (rho)	also resistivity of medium (ohm/meter)
σ (sigma)	volume electric conductivity of the material; function of position (mho/meter)
τ (tau)	time interval
τ_m (tau)	time constant of membrane
Ω (omega)	solid angle;
ω (omega)	angular velocity (radians/second)
∇ (nabla)	linear vector operator, operating on the field coordinates $\nabla \approx \frac{\partial}{\partial x} + \frac{\partial}{\partial y} + \frac{\partial}{\partial z}$
∇^2 (nabla square)	Laplacian operator, operating on the field coordinates (scalar) $\nabla^2 \approx \frac{\partial^2}{\partial x^2} + \frac{\partial^2}{\partial y^2} + \frac{\partial^2}{\partial z^2}$

∂, ∂^2 (curly d)

indicates partial differentiation as in

$$\frac{\partial f(x, y, z)}{\partial x} \quad \text{or in}$$
$$\frac{\partial^2 f(x, y, z)}{\partial x^2}$$

· (dot)

indicates scalar or dot (inner) product of two vectors

\approx

symbolic replacement of

\approx

approximately equal

$=$

equal

\equiv

identical

* (asterisk)

Fortran symbol indicating multiplication of two scalars

\int_V, \int_S

volume and surface integral sign

\rightarrow

indicates vector quantity

\geq

(is) greater than or equal to

$>$

(is) greater than

\leq

(is) less than or equal to

< (is) less than

% per cent; per hundred

| | (vertical bars) indicate absolute value

$\sqrt{\quad}$ square root

° degree (angular)

ACKNOWLEDGEMENTS

I would like to express appreciation and gratitude to my supervisor, Professor Pentti M. Rautaharju, Director of the Medical Biophysics and Bioengineering Research Laboratory, Faculty of Medicine, Dalhousie University. His originality, energetic enthusiasm and, moreover, his warm attention and active interest made this study possible.

I am indebted to Dr. B.M. Horacek for many lengthy discussions and close cooperation, practical and theoretical, during almost all parts of this study. He also kindly made available his torso model for the computation of the body surface potential distributions.

My thanks go to Dr. M. Okajima from Nagoya University, Japan, who initiated in this laboratory the search for the solution of the forward problem.

Mr. Paul MacInnis was of crucial importance in the development of programs Hexcite and Vectors. His skill enabled me to realize a much more extensive and ambitious investigation than would have been otherwise possible.

Mr. Emilio Macchi helped me with endless patience on the collection and preparation of the anatomical data. I wish to thank all other members of the biophysics group for their criticism and valuable advice in minor and major problems encountered.

The recorded 12-lead electrocardiogram was generously made available for reproduction by Prof. Dr. D. Durrer, Dept. of Cardiology, Wilhelmina Gasthuis, Amsterdam, The Netherlands.

Last but not least, I would like to express my gratitude towards Mrs. Virginia McDougall, Mrs. Barbara McDonald, Miss Kathryn MacLeod, and Miss Pamela Lutz, who suffered many hours under the load of my scribblings.

Throughout this study, I have been generously supported by a fellowship of the Canadian Heart Foundation. This project has been partially supported by research grants from MRC and the Nova Scotia Heart Foundation, awarded to Dr. P.M. Rautaharju.

Chapter 1

INTRODUCTION

- 1.1 Electrical and mechanical activity
- 1.2 The cardiac cell
 - 1.2.1 Histological aspects
 - 1.2.2 Membrane potential
 - 1.2.3 Subthreshold stimuli
 - 1.2.4 The action potential
- 1.3 The cardiac syncytium
- 1.4 Electrical sources due to cellular excitation and recovery
- 1.5 Relation between heart vectors and leads
- 1.6 Impulse conduction in excitable elements
- 1.7 Models in electro- and vectorcardiography
- 1.8 Models in general
- 1.9 Purpose of the present investigation

' *The closest model to a human heart is another one, or preferably the same heart.* '

After Arturo Rosenblueth and Norbert Wiener, 1945.

1.1 *Electrical and mechanical action*

The ancient Greeks believed that the human mind was situated in the heart. Before the discovery of the circulation by Harvey, mysterious functions were generally attributed to this organ. After his discovery it has been established over and over again how important a role is played by the heart in the total circulation. At the time of discovery of the electrogram and the electrocardiogram it was believed that these electrical phenomena only accompanied the contraction of the heart. Later the importance of the electrical activity of the heart in initiation of the contractions, and thus in timing and coordination of the mechanical activity, was realized.

Due to this link between electrical and mechanical heart activity, it seemed to be and proved very fruitful to study the electrocardiogram in order to assess the condition and function of the heart. Waller, (148) in 1887, was the first to describe the excitation wave passing over the ventricle, giving rise to an electromotive force in the direction in which it travelled. With the introduction of the string galvanometer to electrocardiography by Einthoven (45) in 1903, a sufficiently sensitive and accurate measuring instrument was available to record reliable electrocardiograms. Sir Thomas Lewis (76) in the mid 1920's was among the first to establish a link between the excitation process, its distribution in space and time, and the shape of the electrocardiogram. He carefully mapped on the inner and outer surfaces of the ventricles the arrival time of excitation, evaluating the relative contribution of the left and right ventricle to the electrocardiogram.

He also showed the prime importance of the Purkyne fiber network in the sequence of ventricular activation. His detailed description of the pathway of excitation in a case with auricular flutter is still among the best documented to date (77). After his monumental work, relatively little has been done to increase the theoretical understanding of the electrocardiogram.

With the introduction of the glass microelectrodes by Ling and Gerard (79) in 1949, a new era of intensive study of cellular behaviour started, triggering a renewed interest in the excitation process as a whole.

In 1953, Scher (122) using needles with multielectrode terminals inside the ventricular wall, carefully mapped the spread of excitation in canine hearts. From these 'classic' maps he derived a qualitative relationship between the sequence of cardiac excitation and recorded electrocardiograms in humans, under the assumption that the human heart is activated in a way similar to the dog heart (123, 120). Durrer and co-workers (44^a, 44^b) also started experimenting with dog hearts. Later, however, they published the first extensive data on the excitation of the human heart (41, 42, 43). Boineau, et al. (12, 13) demonstrated the relationship of the activation sequence and body surface potential distribution. This last relationship is particularly important since in clinical electrocardiography the invasive multipolar needle technique is too crude and damaging a means of acquiring knowledge about the state of the heart, and is certainly unsuitable for routine investigations. The desired knowledge about the state of the heart has to be derived from the surface potential distribution.

Ultimately, the state of each cardiac cell is our concern, since this state determines the action and interaction of the individual cell and its neighbours, and is thus responsible for the total heart action. For this reason, the following paragraphs describe the cardiac cell and its function in general.

1.2 *The cardiac cell*

The cellular properties of interest to this report are mainly excitability and impulse conduction. The molecular structure of the membrane is of basic interest to anyone who studies excitation and conduction. However, the molecular structure is beyond the scope of this introduction. The histological aspects of the cells are dealt with insofar as the structural details discussed are of particular importance in relation to the electrical properties of cardiac muscle.

1.2.1 *Histological aspects of the cardiac cell*

The cell membrane of cardiac fibers, the sarcolemma, is approximately 200 to 300 Å in thickness, and consists of two dense layers, separated by a less dense structure or space. The basement membrane, which is the outer layer of the sarcolemma, is uninterrupted. In contrast, the plasma membrane, the inner layer, seems to be continuous with certain intracellular structures, such as the intercalated disks and endoplasmic reticulum. The intercalated disc is a complex structure, where two sarcolemmas of two adjacent cells come into close contact.

A gap of 100 Å is found along the disc except for the nexal region. In the nexus the outer layers actually fuse, leaving no extracellular space between the cells.

All other histological aspects are similar to those of skeletal muscle. Regularly spaced filaments compose the myofibrils. The myofibrils show, in contrast to smooth muscle myofibrils, cross striating, which consists of M and Z bands. The myofibrils are separated by dense chains of mitochondria. The cell nuclei, which in skeletal muscle are located close to the sarcolemma, are located, in myocardial cells, amidst the myofibrils in the center of cells. The cells differ considerably in dimensions, ranging in the adult heart, from approximately 50 μm to 100 μm in length, and having on the average a diameter of 15 μm . Cells contact each other abundantly. As viewed through the light microscope, one gets the impression that the cells divide and join as in a sponge-like structure. Here the intercalated disks appear as plasma bridges between cells. This observation, and the fact that in terms of its electrical and mechanical function the myocardium appears to act as a syncytial structure, led many investigators to forward the idea that the heart, in fact, was a syncytium. However, since the structure of these 'bridges' was revealed (131, 91, 7), it is clear that the cardiac cells, though in close contact with each other at the side of the intercalated disks, are otherwise perfectly separated cells. The myofibrils, as well as other intracellular elements, do not cross the disks.

In the subsequent paragraphs, the term 'membrane' will refer to the sarcolemma, without distinction into basement membrane and plasma membrane.

1.2.2 Membrane potential

The 'potassium-sodium-pump' affects potassium and sodium in the sense that K^+ is actively transported into the cell and sodium actively extruded from the cell, creating concentration gradients for these ions across the membrane, which give rise to the existence of a Gibbs-Donnan equilibrium.

The potential which arises when a solution with a certain concentration of ions $[A_i^+]$ is separated by a membrane, selective permeable to A^+ , from its surrounding with a concentration $[A_o^+]$ is described by the Nernst equation:

$$E_A = \frac{RT}{F} \lg \frac{[A_i^+]}{[A_o^+]} \quad (1)$$

R, T and F are the gas constant, the absolute temperature and the Faraday constant, respectively.

For example, the value of concentrations inside and outside the cardiac cell for K^+ and Na^+ , in cat heart muscle are reported (111) to be

$$[K_i^+] = 151 \text{ mEq/l} \quad (2^a)$$

$$[K_o^+] = 4.8 \text{ mEq/l} \quad (2^b)$$

$$[Na_i^+] = 6.5 \text{ mEq/l} \quad (3^a)$$

$$[Na_o^+] = 159 \text{ mEq/l} \quad (3^b)$$

which results in

$$E_K = -61.5 \log \frac{(151)}{(4.8)} = -92.6 \text{ mV} \quad (4^a)$$

and

$$E_{Na} = -61.5 \log \frac{(6.5)}{(159)} = +84 \text{ mV} \quad (4^b)$$

In which E_K and E_{Na} are the equilibrium potentials for potassium and sodium respectively.

If I_A denotes a current density in which charge is carried by means of the movement of A^+ ions and R_A the resistance $/\text{cm}^2$ to flow by the membrane to ions A^+ , then

$$E_M - E_A = I_A R_A \quad (5)$$

or if g_A denotes the conductance of the membrane to ion A^+ (which is the reciprocal of the resistance):

$$E_M - E_A = \frac{I_A}{g_A} \quad (6)$$

The voltage difference across the membrane caused by each ion A thus depends on the ionic current I_A , the conductance of the membrane and, if we consider a voltage-time relationship, on the capacitance of the membrane.

In the resting cardiac cells the transmembrane potential differs for the various types of cells encountered. In general, the resting transmembrane potential is between 80-100 mV, the inside of the cell being negative in respect to the outside (66,pp. 44,45).

Slightly smaller values of the resting potential are encountered in the cells of the atria, the S.A. node and AV node, whereas Purkyne fibers have slightly larger values. The resting potential is close to the equilibrium potential for potassium, and indeed, the potassium conductance in the resting cell is considerably larger than the sodium conductance.

Let us now consider changes in the resting potential due to either external stimuli (i.e. current) or to different transmembrane potentials of neighbouring cells.

1.2.3 *Subthreshold stimuli*

If only small amounts of current are applied, the first changes in transmembrane potential can be explained in terms of the 'core conductor' properties of the cells, i.e. membrane conductance and capacitance and longitudinal resistance of extracellular fluid and cytoplasm. The two properties of main interest are the time constant and the space constant. The time constant $\tau_m = r_m c_m$ depends only on the properties of the membrane and is a measure of the rate of voltage change in time. The space constant is $\lambda = \sqrt{r_m / r_i}$, if we consider the resistance of the extracellular fluid negligibly small as compared with the axoplasmic resistance. It is a measure of the rate at which an applied voltage falls off with distance. The space constant is independent of the capacity, and because of its relation to membrane resistance and axoplasmic resistance, dependent on fiber diameter. The voltage course in time due to an applied step voltage ϵ_s (156) is:

$$\epsilon(t) = \epsilon_s (1 - e^{-t/\tau}) \quad (7)$$

where τ is the time constant, and the voltage course in space due to an applied step voltage ϵ_s (156) is:

$$\epsilon(x) = \epsilon_s e^{-x/\lambda} \quad (8)$$

where x is the distance between the measured location and the site of application of ϵ_s , and λ the space constant. Both changes in time and in space are exponential.

Both constants are of great importance for the conduction velocity of impulses. A large time constant will lower the conduction velocity, a large space constant will enhance the conduction velocity. The space constant is also an important factor in the electrotonic spread of impulses. Later changes due to the application of small amounts of currents include not only the voltage changes described above, but also changes in the Gibbs-Donnan equilibrium, and even more important changes in the state of the different factors which influence the membrane conductances of the ions involved in the Gibbs-Donnan equilibrium.

1.2.4 *The action potential*

If a larger amount of depolarizing current is applied, a chain of reactions is set off which results in the action potential for each cell typical voltage time course. The different phases of the action potential are normally labelled according to the terminology introduced by Coraboeuf and Weidmann (31). The resting transmembrane potential changes rapidly on excitation from about -90 mV to a positive value of about $+30$ mV (phase 0). This depolarization is immediately followed by an initially rapid repolarization (phase 1), a slow phase 2 (commonly

referred to as plateau), and a final faster phase 3. The transmembrane potential reached at the end of phase 3 is normally the maximal potential reached in the whole cycle. During the following phase 4, most cells remain at their resting transmembrane potential, whereas the so-called pacemaker cells exhibit during phase 4 the typical diastolic depolarization which leads sooner or later to a new action potential.

Most of the knowledge of the ionic events associated with the action potential is based on data obtained by the voltage clamp technique. Lesser data are obtained with microperfusion or radioactive tracing techniques. On the basis of these data, several models for ionic events in the membrane have been proposed. Most of these models approach the membrane from the electrophysical point of view, and are in essence electrical analogues with capacitors, resistors, rectifiers, etc. A few models have been proposed on the basis of the knowledge of the membrane structure. However, the electrophysical models describe in an accessible way the time course of events under normal conditions. Little doubt exists about the origin of the transmembrane potential, and the explanation given in paragraph 1.2.2 is generally accepted. General agreement also exists on the initiation of the depolarization which is thought to be mainly dependent on Na^+ inward current. The role of Ca^{++} and other ions (as Cl^-) is not well established. The first fast repolarization is thought to be due to an increased K^+ outward current. So far, the first model as proposed by Hodgkin and Huxley (63) for the giant squid action, is also accepted for striated muscle, heart muscle, and smooth muscle. However, for the remaining parts of the action potential, several different views

exist for heart muscle tissue and Purkyne fiber tissue.

The two main opposing views held on plateau phase and repolarization are those by the group of Trautwein and the group of Noble. Most preparations used are from Purkyne fibers, which confines results to this category.

Peper and Trautwein (105) hold a 'dynamic current' responsible for plateau duration. This current is carried by Cl^- ions at potentials positive to -30 mV and by positive ions (Na^+ and Ca^{++}) at potentials negative to -30 mV. It holds the membrane at the plateau level until it has been deactivated. Deactivation is only time-dependent.

According to Noble and co-workers (99, 100, 101) the 'dynamic current' is only responsible for the first fast repolarization, whereas the much slower activation of I_{x1} terminates the plateau phase, and starts the repolarization.

Though voltage clamp data are very informative about the membrane properties, they do not inform us about the dynamic group behaviour of cells as part of an excitable tissue. The membrane potential in the voltage clamp technique is assumed to be uniformly distributed throughout the cell. The 'cable' properties are avoided in these models, which reconstruct action potentials (64, 98, 81, 62), by assuming the net membrane current to be zero. This is, however, not the case if impulse conduction in interconnected cells is considered, which is self-evident if one realizes that membrane currents generated by the 'neighbours' of a cell constitute a current load on the cell itself.

Another aspect is the apparent relation between contraction and action potential duration. It is well known that the mechanical relaxation

is closely related to the repolarization. Whether the repolarization is dependent on the relaxation, or the relaxation on the repolarization, is not clear. As long as these and similar problems are not solved or sufficiently explained by the proposed models, they should serve more as a comprehensive description of events than as an interpretation of events.

1.3 *The cardiac syncytium*

In the previous paragraphs cellular properties were emphasized. However, the properties of the heart as a whole are certainly as important. The microscopic details of the intercalated disks were revealed by Sjöstrand et al. (131), who showed that at the nexus the membranes fuse to a double layer about 100 Å thick. Contrary to the view of Sperelakis (134,135), it is generally accepted that the intercalated disks are low resistance connections between adjacent cells unifying them as far as impulse conduction is concerned to one large functional syncytium. Though connected to each other functionally, different cells of the myocardium possess clearly distinct features. The following is a brief description of events during a cardiac cycle, in the heart as a whole, with special emphasis on parts which are of particular interest to this report.

Under normal conditions excitation starts in the sinoauricular node. The cells of the S.A. node possess so-called 'pacemaker' properties; that is, spontaneous diastolic depolarization and 'firing' when a certain threshold value is reached. By virtue of the intercellular connections,

this impulse spreads over the atria. Not all parts of the atria are reported to conduct with similar conduction velocity, especially in the S.A. node the conduction velocity is very low (147). The conduction in the atria is such that the AV-node is more or less simultaneously reached from several directions (86,117,72). Conduction in the AV-node is very slow. The AV-node is functionally divided according to the type of action potential encountered in an upper, middle and lower portion (66). In the lower portion of the AV-node, Hisbundle and Purkyne fibers, the recorded action potential becomes gradually longer until just in front of the 'transitional fibers' (94). In these transitional fibers, an apparent decrease in action potential duration and change of shape occurs from the typical Purkyne fiber action potential via the transitional fiber 'spike and dome' configuration, into the typical myocardial action potentials. Concomitant with the increase in action potential duration in the Purkyne fibers is an increase in conduction velocity, which in the ventricular myocardium decreases again to values below 50 cm/sec.

Meyerberg et al. (99) pointed out that the increasing action potential duration in the Purkyne fibers distally from the AV-node is associated very closely with an increasing refractory period, the fibers close to the transitional zone having the longest action potential duration. This long refractory period in this region is functionally important since early premature beats, either from supraventricular origin, or from ventricular origin, are most likely to be blocked in this 'gate'. However, as soon as a localized disease affects the particular part of the endocardium, or Purkyne network, the refractory periods of these gates might become much shorter, and their protective mechanism

against early premature beats lost. The transitional fibers between 'true' Purkyne fibers and 'true' ventricular muscle fibers exhibits the so-called spike and dome configuration (80). Explanation for the 'dome' is the current load imposed on the fibers by the underlying muscle fibers. The reported data are almost all confined to Purkyne fiber/papillary muscle preparations, so no knowledge has yet been accumulated on the extent of the Purkyne fibers inside the ventricular cavities. Only a few intracellular recordings are made from human hearts (17,141), so speculation on distribution of action potentials is wide open. The refractory periods reported (37,73,90) serve as a guideline, however, not all measurements are in agreement with each other. This spread of excitation in ventricular tissue is accepted as generally uniform in all directions (107,132,6).

Observations of non uniform velocities reported in an earlier report (119) can be questioned on the basis of techniques used in these investigations. However, a more recent study (116) also indicates non-uniform velocities in ventricular myocardium. Excitation is shown in atria to be faster along the fiber direction, than perpendicular to it (58). In the ventricular myocards this could still result in a net outward spreading excitation wave. The idea that the net resultant excitation wave generally propagates with uniform velocity is supported by the reports of Durrer et al. (44a,44b,43,42), Casella and Taccardi (28), and Scher and Young (123).

Relatively few reports deal with the repolarization process (38,37). Though generally accepted that the sequence of repolarization is not identical to the sequence of depolarization, no satisfactory explanation for this difference has been given as yet.

The heart as a whole is richly supplied by nerve endings of the autonomous nervous system, the influence of which is undoubtedly a major mechanism in adaptation and regulation of the heart function (30). Histologically, nerve fiber endings are found in practically every part of the heart (114). The influence of both sympathetic and parasympathic stimulation of the heart action are subjects of many research reports. The influence of these stimulations on the total activation process in the ventricles has not been reported. Vagal influence on repolarization was studied in relation to possible factors influencing the onset of fibrillation (59,5); the repolarization process as a whole, however, was not considered.

1.4 *Electrical sources due to cellular excitation and recovery*

The formulation followed is mainly after Plonsey (106). The electro-magnetic field within the torso arises from charge distribution which accumulates on membrane capacitances. It is estimated (107) that the relative importance of the magnetic effects on the electric field is negligible as compared with potentials due to charge separation. The charge separation, which takes place across the cell membrane, causes an electric field \vec{E} in the surrounding medium. At any point we assume the current density, \vec{J} , to be linearly related to this electric field (Ohms Law), so

$$\vec{J} = \sigma \vec{E} \quad (9)$$

Within the heart region the total electric field at any point is the sum of the electric field set up by other points and the impressed electric field, caused by the point itself, thus

$$\vec{J} = \sigma \vec{E} + \sigma \vec{E}_i \quad (10)$$

or, replacing \vec{E}_i by \vec{J}_i , the impressed current density, Eq (10) becomes

$$\vec{J} = \sigma \vec{E} + \vec{J}_i \quad (11)$$

Outside the region of the sources, propagation effects of electromagnetic waves can be ignored [Geselowitz (56), Plonsey (107)]. Consequently, the electric field at each instant can be obtained from the scalar potential, Φ ,

$$\vec{E} = -\nabla \Phi \quad (12)$$

Neglecting of tissue capacitance implies that as the sources vary, charges on boundaries and interfaces redistribute themselves in a negligibly short time, or equivalently

$$\nabla \cdot \vec{J} = 0 \quad (13)$$

In the membrane, however, the capacitive displacement current cannot be ignored. Formally we will include this current in the impressed current density, \vec{J}_i .

From Eq (11), (12) and (13) it follows that outside the region of the sources

$$\begin{aligned}\nabla \cdot \vec{J} = 0 &= \nabla \cdot \sigma \vec{E} + \nabla \cdot \vec{J}_i \\ &= -\sigma \nabla^2 \Phi + \nabla \cdot \vec{J}_i \\ \nabla^2 \Phi &= \frac{\nabla \cdot \vec{J}_i}{\sigma}\end{aligned}\tag{14}$$

Equation (14) is a Poisson's equation. The quantity $\nabla \cdot \vec{J}_i$ constitutes a current source density.

The integral solution for (14) is

$$\Phi = -\frac{1}{4\pi\sigma} \int_V \frac{\nabla \cdot \vec{J}_i}{r} dV\tag{15}$$

since

$$\frac{\nabla \cdot \vec{J}_i}{r} = \nabla \cdot (\vec{J}_i / r) - \nabla (1/r) \cdot \vec{J}_i\tag{16}$$

and also for a volume containing all sources

$$\int_V \nabla \cdot (\vec{J}_i / r) dV = \int_S 1/r \vec{J}_i \cdot d\vec{S} = 0\tag{17}$$

Substitution of Eq (16) into (15) yields

$$\Phi = \frac{1}{4\pi\sigma} \int_V \vec{J}_i \cdot \nabla(1/r) dV \quad (18)$$

Noting that a dipole potential field set up by a current source and sink with a dipole moment \vec{m} (current times separation, directed from negative to positive), has the form

$$\Phi = \frac{1}{4\pi\sigma} \vec{m} \cdot \nabla(1/r) \quad (19)$$

we see that \vec{J}_i in Eq (18) has the form of a current dipole moment per unit volume.

This impressed current density, \vec{J}_i , is localized in the cell membrane. For all practical purposes, the cell membrane can be considered to have no thickness, in which case \vec{J}_i in Eq(18) gets the form of current dipole moment per unit surface area \vec{K}_i , and Eq (18) transforms into

$$\Phi = \frac{1}{4\pi\sigma} \int_S \vec{K}_i \cdot \nabla(1/r) dS \quad (20)$$

Consider a cell with potential Φ_1 and Φ_2 , respectively, inside and outside and σ_1 and σ_2 as conductivity inside and outside. On the cell membrane S

$$\sigma_1 \frac{\partial \Phi_1}{\partial n} = \sigma_2 \frac{\partial \Phi_2}{\partial n} \quad (21)$$

where n is the normal to the membrane directed outwards. This is necessarily so, since the current density normal to the membrane must be continuous. The scalar function $\sigma\Phi$ is discontinuous across S and has a continuous normal derivative. Only a dipole layer source provides the appropriate singularity at S . The strength of a dipole layer equals its potential function discontinuity. Using Eq (19), the potential at point P is:

$$\Phi_P = \frac{1}{4\pi\sigma_p} \int_S (\sigma_1 \Phi_1 - \sigma_2 \Phi_2) d\vec{S} \cdot \nabla(1/r) \quad (22)$$

in which σ_p may be either σ_1 or σ_2 .

Noting that $d\vec{S} \cdot \nabla(1/r)$ is an element of solid angle, $d\Omega$, Eq (22) can be rewritten as

$$\Phi_P = \frac{1}{4\pi\sigma_p} \int_S (\sigma_1 \Phi_1 - \sigma_2 \Phi_2) d\Omega \quad (23)$$

In case the external region is extensive and taken as reference, then $\Phi_2 = 0$ and thus

$$\Phi_P = \frac{1}{4\pi} \frac{\sigma_1}{\sigma_p} \int_S \Phi_1 d\Omega \quad (24)$$

in which Φ_1 , is equal to the transmembrane potential, V_m . The coefficient σ_1/σ_p is unity for points inside the cell and since the solid angle inside is 4π , $\Phi_P = V_m$, as expected.

Outside the cell the coefficient equals σ_1/σ_2 . If all parts of the membrane are at identical potential, the surface integral for any outside point evaluates as zero, thus only spatial variation of V_m contributes to current flow. Consider now several or all cardiac cells active at a particular moment. If in one type of fiber in a certain region activation spreads with constant speed, temporal and spacial events are interchangeable and linked by the conduction velocity. In general, the length of cardiac cells is much greater than their width. Consider then a propagating wave front, travelling not necessarily along the fiber axis. If we assume that all points of the membrane in a plane perpendicular to the direction of propagation of the wavefront are at the same membrane potential, then we can think of a small differential volume, bounded by the cell membrane and two equipotential surfaces, both perpendicular to the propagation direction. The potential field due to such differential volume can be found using Eq (24), or by replacing the current source of the membrane by an equivalent source in the bounding equipotential surfaces, with identical dipole double layer density as the membrane. Under the assumption that the potential at the boundaries is equal and uniform, the external potential field of such differential volume is zero (uniform potential over a closed surface). Thus the equivalent source on the bounding equipotential surfaces is equal (if reversed in direction) to the one of the bounding membrane. For an adjacent volume element the V_m is increased by ΔV and at the interface between the two elements a net double layer has the strength ΔV . All interfaces between all the differential elements with membrane

potential V_m and $V_m + \Delta V$ together form an electromotive surface with strength ΔV and an area equal to the extent of the part of the propagating wavefront with transmembrane potential V_m . The total spatial action potential can be divided (stratified) into equipotential surfaces (laminae), separated a differential distance Δl . The strength of the net double layer ΔV can be found from

$$\Delta V = \frac{\partial V_m}{\partial l} \Delta l \quad (25)$$

and thus the double layer density is equal to $\Delta V/\Delta l$. If this double layer density is evaluated against the spatial distributed action potential, it is expected to be, roughly, an error function (107). This expectation is confirmed by experimental data of Solomon et al. (133). A similar line of reasoning applies also to the repolarization process. For all practical purposes, the spatial rise time (depolarization) is short enough (about 0.8 mm) to collapse all stratified lamina into one net double layer. (This does not hold for the repolarization.) The strength of such net double layer is

$$\vec{K}_e = - \int \frac{\partial V_m}{\partial l} dl \frac{dA}{dS} \quad (26)$$

where the correction factor dA/dS is the ratio of the area occupied by each fiber to the total area. For the repolarization a similar correction function should be introduced in the calculation of dipole double layer strength for each lamina.

The above discussion assumes the isochronous surfaces to be normal to the direction of spread, in which case spatial and temporal events could be exchanged in this direction. If, however, the direction of the spread is along the fiber axis, then, due to the structure of the heart, still a net outward moving activation results, but the electromotive surface amplitude and velocity are reduced by the ratio of radial pathlength to transverse pathlength.

1.5 *Relation between heart vectors and leads*

The first formulation of the relationship between electromotive force in the heart and the body surface potentials is from Einthoven (46). The potential difference measured in the limb-leads equals the projection of the 'manifest potential' onto the appropriate side of the 'Einthoven triangle'. Based on the observations of Craib (34), who showed that the electromotive force is located in the surface formed by the wave of excitation, Wilson (152) derived a formulation for the electrocardiogram, assuming the body to be a homogeneous infinite medium. He pointed out that the electromotive surface actually acts as a simple dipole. He also extended the Einthoven triangle into a three dimensional lead system by adding one more electrode on the back (151). This system is now known as the Wilson-tetrahedron lead system, in which the relation between dipole (equivalent to Einthoven's 'manifest potential' and Lewis 'electrical axis') and measured potential differences are simply the projection of the dipole (as a vector) onto the appropriate side of the tetrahedron. It was pointed out by Burger and van Milaan (23) that the simple relationship given in the equilateral triangle between 'manifest

potential difference' and the limb leads is only a crude approximation. Under the simplifying assumption that the total excitation activity can be represented by a single dipole (the heart vector), they set out to give a firm physical foundation to the relationship of such a dipole and potential differences recorded at the body surface.

Under the assumption of quasi static conditions the relation of the heart vector (\vec{H}_i) and the surface potential (V_i) is given by

$$V_i = (\overrightarrow{X, Y, Z}) \cdot (\overrightarrow{a, b, c}) = a_i X + b_i Y + c_i Z \quad (27)$$

where X, Y and Z are the orthogonal components of the heart vector under consideration. The coefficients a, b, c are dependent on surface location of point i, body geometry and origin of the heart vector. As seen in equation (27), this coefficient can be interpreted as a vector ($\overrightarrow{a, b, c}$). It is termed the lead vector, \vec{L}_i (24). For any heart vector, i.e. any source location, a large set of lead vectors describes the relation of this source to the surface points. The tips of all the lead vectors of one source location together form an 'image' surface. An image surface is merely a geometrical representation of the lead vectors, i.e. of the relation between source (c.q. heart vector) and leads. Though the concept of the lead vectors was introduced by Burger and van Milaan (25), the first to publish extensive experimental results was Frank (51). His data are based on torso tank measurements. McFee and Johnston (82) extended the concept of lead vectors to that of the lead field. The relation between lead-field and lead-vector is that at any point the

current density of the lead-field multiplied by the resistivity is exactly equal to the lead-vector at that point (16).

Using the information about source-surface relation, as condensed in the image surfaces, Frank devised a lead system (52) which specifically tried to reconstruct the dipolar activity from the measured surface potentials. Since he used a homogeneous torso to perform his measurements, the basic assumptions underlying his lead-system are: (a) the electrical activity of the heart can be represented by a single dipole, fixed in location; (b) the human torso behaves as a homogeneous medium.

Other vectorcardiographic lead-systems have also been proposed, all based on dipolar approximation of the cardiac activity. Geselowitz (57) correctly pointed out that the electrical activity on the body surface can be accurately accounted for by an equivalent multipole source in a homogeneous medium, and only approximately by an equivalent dipole. This view is supported by the observed distribution of surface potentials (96,139,70,140). It is impossible to create similar distributions by a single dipole. However attractive and physically correct the equivalent multipole source approach, one disadvantage is that the direct relation between the excitatory process and source is no longer present. Furthermore, no inhomogeneities are considered in this approach. The effects of inhomogeneities are lumped in the equivalent source. Whereas the dipole approximation cannot account for the potential distribution on the body surface, the equivalent multipole source misses the link with the excitation distribution in the heart. An intermediate solution is

to represent the excitation wavefronts by multiple distributed dipoles, each with their own set of lead-vectors. The more dipoles used, the closer the calculated surface potential approaches to the real one. Each dipole itself only represents the heart tissue in its immediate vicinity, and is directly related to the excitation process, as far as the tissue which is represented is concerned. Recently a large set of lead-vectors for a large set of dipole source locations were computed in this laboratory (68), for homogeneous and non-homogeneous torso. An identical result can be obtained by direct computation of the body surface potential from a large number of distributed dipoles (69), representing the cardiac electrical activity.

1.6 *Impulse conduction in excitable elements*

Relatively independent of the problem of potential distribution and equivalent heart source is another aspect of electrocardiography, which deals with the impulse conduction throughout the heart. The cell to cell conduction is dependent on the cell properties, as is the automaticity of certain regions. Under special conditions a chaotic excitation pattern will occur, namely fibrillation. Auricular fibrillation was first described as such by Engelman (47), who also offered the theory that multiple foci, caused by an increased excitability, are responsible for this condition. Rothberger and Winterberg (115) thought that one single ectopic focus with a high frequency of firing could cause this condition.

Mines (87) and Garrey (54), on the other hand, confirmed a theory proposed by Porter (108) that impediment to the propagation of a stimulus causes the excitation to deviate from its normal pathway and finally to return to the point of origin, and so to perform a closed loop or 'circus' movement, which can be maintained indefinitely. Lewis (78) extended this to flutter, for which condition he also pinpointed that the pathway of the circus movement included the superior and inferior venae cavae.

Evidence in favour of either theory has been brought forward and still no *communis opinio* exists on the nature of fibrillation.

It has been shown that several factors or agencies can produce ectopic foci with high firing frequency (138). On the other hand, well documented cases in favour of the circus movement theory have been forwarded (113,32). Independent of the aforementioned theories is the multiple wavelet hypothesis (88), which states that once a chaotic pattern is created, multiple wavelets independent of each other will maintain this disorganized state. This last hypothesis does not necessarily include either an ectopic focus or a point of reentry. The nature of this pattern will still be dependent on cellular properties and intercellular relations.

It is generally accepted that a spatial distributed dispersion in refractory periods is essential to set the stage for fibrillation. Recently, more detailed information on the cellular behaviour in repetitive stimulation became available (146,60,50). However, whether the facts revealed are important in fibrillation has not been assessed as yet.

1.7 Models in electro- and vectorcardiography

The solution of Eq (27) for X,Y and Z from measured surface potentials V_i is the aim of practical electro- or vectorcardiography. However, this is an impossibility since for each measured V_i three unknown coefficients a_i, b_i, c_i are introduced. In the simplest case, where a solution is sought for one dipole the number of unknowns (U) is related to the number (n) of surface locations measured as

$$U_n = 3n + 3 \quad (28)$$

The only possible way to arrive at a solution is to determine the coefficients a_i, b_i, c_i . For technical and ethical reasons this has so far proven to be difficult in living subjects. Cadavers have been used (11), for which however the results are questionable due to post-mortem changes in organ position, membrane structure, blood distribution, etc. For this reason, extensive use has been made of torso models, either mathematical and physical. The mathematical models are usually confined to simple geometrical structures such as spheres, cylinders, discs; whereas, the physical models usually were shaped after human (male or female) torsos and filled with electrolytic solution with or without additional structures. These models are used to specify the behaviour of the human body, the torso. In terms of Eq (27), they help solve the coefficients a_i, b_i, c_i . Once solved the heart vector can be found from the surface potentials. Whether the heart as source is determined as a single dipole, multipole, multipole dipoles, or even restricted multiple dipoles is immaterial.

Another approach was already indicated by Scher (121), who proposed that X,Y and Z are determined and then the coefficients calculated from the measured surface potentials. The determination of X,Y and Z in vivo, however, is difficult if not impossible. It is, of course, possible to reconstruct from measured isochronous maps the isochronous surfaces. The next step will then be to calculate from these isochronous surfaces the surface potential distribution, using a set of coefficients, or using a surface potential distribution to calculate a set of coefficients. Casts of the isochronous surfaces have also been made (103) and energized in electrolytic tank torso models, which yielded surface potential distributions on the torso. Here again a logical approach is to make a model which dynamically simulates the activation process and will yield isochronous surfaces which can be used in further computation. Indeed, this approach is now used by several investigators, and is also the subject of the present investigation.

This last type of model can also be useful in two more respects: (a) to study the excitation process itself, and (b) to study the mechanisms involved in the electrical behaviour of the heart during repolarization.

Two models have been published dealing with the excitation process itself. Wiener and Rosenblueth (150) published their study in 1946 on impulse conduction in excitable elements, especially focussing attention on atrial flutter and fibrillation, whereas Moe et al. (89) simulated atrial fibrillation using a digital computer.

For the mechanisms involved in the potential distribution during repolarization, only one real model has been published so far. This one by the group of Abildskov (61, 4), approaches the problem in a rather indirect way, constructing an equivalent T-loop ('primary T-loop'), which represent those parts of the repolarization which cannot be predicted by the depolarization.

1.8 *Models in general*

The first model ever built was man (143). "God created man according to his image". Ever since, models have been built and used for various purposes. In science, models have been and are extensively used. The reason for this was expressed by Rosenblueth and Wiener (112) as follows: "No substantial part of the universe is so simple that it can be grasped and controlled without abstraction. Abstraction consists in replacing the parts of the universe under consideration by a model of similar but simpler structure."

Scientific inquiry aims at understanding parts of the universe. It follows that modelling is an essential part of any scientific procedure. Probably not all research workers are aware of their modelling effort, but speak in terms of 'concepts' and 'hypothesis'.

Models can be intellectual or formal, on the one hand, or material on the other. Formal models are a symbolic assertion in logical terms of an idealized relatively simple situation. A material model is the representation of a complex system, by a system which is assumed simpler, but also is assumed to have some properties similar to those selected for study in the original complex system. More complex classifications of models have been proposed (95), which, however, are not relevant in this

context. The structure of any model can be partitioned in smaller structures which, in themselves, form models. Consequently, a largely material model might contain several formal models. Digital computer models are an excellent example of this 'mixed' type of model, since each computer model finally breaks down into abstract numbers.

The model to be described in this report is mainly a material model. It is deterministic in setup, which means that none of the operating characteristics is given by a probability function. The power of such a setup is the direct logical connection, however complex, between input and output.

1.9 Purpose of the present investigation

The two aspects of electrocardiography described above, i.e. the relationship of sequence of depolarization and repolarization to the body surface electrocardiogram and the behaviour of impulses conducted in conglomerates of interconnected excitable elements are subjects of this report. Both problems have their common root in the membrane of the myocardial cells. It applies equally to both problems that studying the membrane properties and the cell itself will not solve the problem. This is partly caused by the fact that the cells influence each other in their behaviour, which makes the functional and anatomical relationship of the cells to each other important, and partly by the fact that the heart, as electrical source, is embedded in a nonhomogeneous conducting medium, the torso.

The complex interrelationship of cellular microscopic and macroscopic events during excitation and repolarization, as well as the complex electrophysical behaviour of the human torso leads to a complicated relationship of cellular membrane phenomena (i.e. propagated depolarization and subsequent repolarization) and body surface potential distribution (i.e. the electrocardiogram). However with the availability of experimental data on the cellular level, and more realistic data on electrophysical behaviour of the human torso the possibility emerges to perform a synthesis of these data to one unifying model, which links anatomical and electrophysical data on one hand with the electro- and vectorcardiogram on the other.

* The primary purpose of the present investigation is to develop, based on realistic anatomical and physiological data, a model of the human ventricles, which can serve as a practical tool in investigations of the electrical activity of the ventricles in depolarization as well as in repolarization.

* Simulation of a normal excitation is attempted, and compared with the data obtained from a normal subject.

* A comprehensive comparison is made of dipolar content of the cardiac electrical activity and the body surface potential distribution, as reflected in the various commonly used lead-systems.

* Hypothetical explanations of the electrical activity associated with the repolarization are tested.

* A preliminary analysis is made of the conduction properties of impulses under repetitive stimulation.

Realization of the above aims is tried for by the construction of a digital model of interconnected excitable elements, shaped according to the geometry of a human heart. With some limiting restrictions, both anatomy and function of heart cells are preserved in the model. In order to calculate the body surface potential distributions use is made of a numerical substitute of the human torso, previously developed in this laboratory. This last model and the present heart model complement each other.

Although the heart model is anatomically based on the data obtained from one human heart, generality of the results is provided by sufficient amount of unpredetermined factors, such as identification of the endings of the His-bundle, extent of the Purkyne fiber network, smoothing of the data, choice of conduction velocity, etc. Furthermore, no quantitative study is made of the surface potentials involved.

Chapter 2

REVIEW

This review of pertinent literature will be limited to models of the excitation and repolarization of the human heart used in electro and vectorcardiography. Equivalent dipoles and multipoles will not be considered to constitute such a heart model. Though the ingredients necessary for construction of a model of the excitation process are not too complex, surprisingly few attempts have been made as yet to do so, Even fewer reports deal with the repolarization.

In 1946 Wiener and Rosenblueth (150) published in one paper two models, one of cardiac flutter, the other of cardiac fibrillation.

The definition of flutter adopted by these authors is: "Flutter consists of a wave or waves of activity in a conducting system with a regular cyclic recurrence of paths, and therefore with a well defined regular wavefront and period. Flutter differs from the ordinary heart beat in that flutter activity is continuous, while beats are separated by periods of total rest (diastole of cardiac muscle)". For the properties of impulse conduction in interconnected excitable elements three postulates are made:

- (a) The cardiac impulses spread with a constant velocity equal in all directions.
- (b) Amplitude of the stimulating process remains constant and exceeds the threshold of regions which are in the "resting condition", (see below).
- (c) Any given region of a fiber exists only in one of three conditions:
 1. The active state
 2. The refractory state
 3. The resting state

These postulates make the following simplifications:

- Homogeneity and isotropy of the heart muscle in respect of action potential properties; duration, depolarization phase, and tissue properties; time and space constants.
- Neither summation nor inhibition is considered.
- No transition between states is considered; the states are discretized.

An 'epoch number' is assigned to each state. The epoch number zero is assigned to the active state, an epoch number one to the resting state, an epoch number between zero and one to the refractory state. The laws of propagation are symbolically expressed as follows:

Let n be the epoch number as a function of point P_i of space X , Y and Z (or fewer dimensions, as the case may be) and time t . Then

$$(1) \quad dn = K_i dt \quad \text{when } 0 \leq N \leq 1, \quad (29)$$

where K_i is the reciprocal of the absolute refractory period of point P_i , and

$$(2) \quad dn = 0 \quad \text{when } N = 1 \quad (30)$$

Except that when at a certain point (x_0, y_0, z_0) $N=0$, and at a neighbouring point (x_1, y_1, z_1) placed within a sphere with center at x_0, y_0, z_0 and with radius $v dt$ (where v is the conduction velocity) at the same time $N=1$, then over the whole segment between these points

$$(3) \quad dn = -1 \quad (31)$$

A wavelength is defined at P_i as

$$\lambda = \frac{v}{K_i} \quad (32)$$

With these postulates and propagation laws, the possibility of self-perpetuating steady state waves in one and two dimensional systems are investigated.

For one dimensional 'open circuit' systems it is concluded that no self sustained activity is possible under the assumptions adopted. For one dimensional 'closed circuit' systems self-sustained activity is possible if a wave can be originated, which spreads in one direction only. Conditions to set up such a wave are discussed. At least one second stimulus has to be applied to a region properly chosen and distinct from site of application of the first stimulus.

In a two dimensional system, self-sustained waves can exist only if the waveforms are involutes of an obstacle. This implies that there is no self-sustaining propagation in a simply connected sheet of elements. An obstacle must have a minimum perimeter exceeding a wavelength. If at any time there is only one wavefront, then the perimeter of the obstacle must be the pacemaker. However, it is possible, under certain conditions, to start a single wave moving around an obstacle of appropriate length. One of the conditions is to apply stimuli to an area in such a way that not in all directions an excitation wave spreads. Normally when a stimulus is applied, excitation waves are concentric circles growing in diameter. By an appropriate set of stimuli one of them gives rise to an excitation wave which is not a closed circle, but a circle segment. They named these waves 'single fifth wave'. If such a wave hits an obstacle 'and-on' self-sustaining activity will ensue. In other words, flutter occurs. Obstacles of varying dimensions and shapes are considered, also combinations of obstacles. It is concluded that the 'effective'

perimeter of an obstacle or a set of obstacles should exceed one wavelength.

Three dimensional systems are readily seen to be too complicated for simple mathematical analysis. A single example is given in which flutter can occur. The above described model gives a continuous description of the space. The influence of obstacles on impulse conduction as related to selfsustaining activity is exhaustively studied. The model is, however, not able to handle more complicated situations, either three dimensional or with inhomogeneities in respect to either conduction velocities or refractory periods. The most important conclusions from this study are:

1. It is possible to set up one-way waves with an appropriate stimulus pattern.
2. Selfsustaining activity is possible under homogeneous conditions if obstacles are present.
3. The resulting activity is regular and related to conduction velocity and obstacle size.

They conclude that the definition of flutter as given by them is in agreement with their own experimental results and clinical findings of others.

The definition of fibrillation adopted is: "Fibrillation consists of a continuous activity over randomly varying paths in a network of connected conducting elements".

The main difference between flutter and fibrillation, according to these definitions, is the random nature of fibrillation as opposed to the regularity of flutter activity. The authors state about their model

based on this definition of fibrillation: "That such fibrillation exists and is what we usually mean by the term is an assumption".

At the onset of the development of a model of fibrillation, Wiener and Rosenblueth state: "The approach to the problem of fibrillation from the standpoint of regularly or semi-regularly repeated short paths is contradicted by the lack of periodicity indicated by the electrograms recorded under the conditions". Then they proceed accordingly to give a first statistical mathematical description of fibrillation, considering the node points of a network randomly distributed in space, the activity of the node points randomly distributed in time, and finally to combine these distributions with the previously given conduction rules, to arrive at activity distribution in time.

In the final discussion, however, they abandon their view of fibrillation in order to adopt the suggestion from Lewis that fibrillation is merely a quantitatively different form of flutter, and suggest to use the terms 'slow flutter' and 'fast flutter', the latter replacing the term fibrillation.

As already indicated by Wiener and Rosenblueth, more complex geometrical structures are difficult to handle on a mathematical basis. Further attempts to model the activation process were not made until sufficiently large and powerful computers were available. By discretizing both space and time, and by considering at each point only the influence of the neighbouring points, it is possible to replace the more complex mathematical formulation by simple ones. This, however, requires a tremendous increase in the number of computations to be performed, which

is only feasible with the use of high speed computers.

Rheinboldt and associates (110) described in 1963 such an attempt, using a digital computer. A heart (diagrammed after 48 progressive cross-sections of the ventricles of a dog heart) is divided into cubic cells, of which a number are labelled P (Purkyne) cells and the other O (ordinary) cells. The P-cells are programmed to 'fire' at predetermined times. A sequence of 'firing' (depolarizing) cells is established by 'firing' each O-cell which borders a cell which fired during the previous time step. As neighbour cells are considered cells which are bordering at least by one corner, thus a cell may be surrounded by as many as 26 neighbouring cells. Unit vectors are established between cells firing at time $t-1$ and each neighbour firing at time t , to give after vectorial summation an electrocardiographic vector for this time-step. No results are presented in this paper.

In 1965, Moe, Rheinboldt and Abildskov (89) published their report on a computer simulation of atrial fibrillation. Whereas the previous model concentrated all efforts on the anatomical aspects of the model, this model of atrial fibrillation focused attention mainly on interactive behaviour of the elements. A simple sheet of interconnected elements was used. Elements were recognized to be in one of five states. State 5 was considered the resting state, state 1 the state of absolute refractoriness, states 2, 3, and 4 were considered to represent various degrees of relative refractoriness. If cells are excited in one of the states of relative refractoriness, they will transmit excitation, however with considerable delay. The length of the refractory period was determined by

the previous cycle length, according to the formula

$$R = \sqrt{KC} \quad (33)$$

where C is the preceding cycle length, R the length of the following refractory period and K a constant assigned to the heart cells. Assignment of values between 10 and 20, at random, to the parameter K, introduces a spatial inhomogeneity in respect of response to stimuli. On repetitive stimulation a selfsustaining activity ensued, which stopped only on termination of the computer run. To show the nature of the selfsustaining activity the authors used several parameters, such as average refractory period, average cycle duration, average number of units firing per time step, average number of units in excited state but not yet fired, average excitation time and average "wavelength". They attempted to assess the influence of the inhomogeneity as well as the boundaries on the fibrillatory action. They concluded that with the parameters used an activity resembling that of atrial fibrillation could be produced and they proposed the use of a "fibrillation number", which is a measure of susceptibility for fibrillatory activity.

An attempt to take into account both geometry and physiological parameters, was made by Okajima (102) et al. They proceeded along the same lines as Rheinboldt. 27,000 cubes of 3 mm x 3 mm x 3 mm arranged in 30 layers, comprising 30 rows and 30 columns were identified either as muscle cells, Purkyne cells or nonexcitable elements. For each layer, the data for identification was obtained from photographs of 3mm sections of a human heart. The cubes adjacent to the ventricular cavities were assigned to be Purkyne elements.

Excitation was started at predetermined intervals in the Purkyne elements, and were spread 10 times faster in these elements than in the ordinary muscle cells. Much attention was paid to correction of the directional error in conduction velocity. The excitation wavefront was assumed to exist on the transition of 'fired' and 'not yet fired' elements, and unit vectors were assigned normal to the interfaces of these elements.

In later work, this model was extended to include the transfer impedance vectors of each element to specified body surface locations. They successfully simulated the normal Frank-VCG, as well as the VCG encountered in infarction.

In the same year, Arntzenius (6) published a model of excitation of the human heart, also based on the anatomy of a human heart as obtained from photographs of 2 mm sections of a normal heart. In the drawings made of these photographs, excitation waves were constructed, as concentric spheres around the termination points of the left and the right bundle. He drew special attention to the cancellation effects which take place during excitation, and to the changes in resulting vectors at the time of breakthrough of the wavefronts at the epicardial surface. The timing of this breakthrough, seen as 'deflection' points in the planar projections of the VCG loops, was shown to be a good parameter for differential diagnosis between left ventricular hypertrophy, right ventricular hypertrophy and normal.

A simulation of myocardial activation using a digital computer-model was published by Solomon and Selvester (132) in 1970. Selvester and co-workers have been working in previous years on several equivalent source models (125,127,126,128), which they used to study a variety of clinical

conditions, in both homogeneous sphere, homogeneous torso and non-homogeneous torso. Their model of myocardial activation used representing points on a 1 mm orthogonal grid. The algorithm used to calculate the spreading of excitation is based on finding the neighbouring points around a point of origin, which are within a sphere with radius vdt , in which v is the assumed conduction velocity. After three time increments all points reached so far serve as new origin points and the procedure is started again. This procedure is very similar to the way Huygens constructed wavefronts. Restart of the procedure after three time steps is necessary to avoid a large directional error in conduction velocity. The surface area of the spheres, rather than that of the envelop, is used to find the appropriate equivalent electromotive surface. Activation is calculated separately for the Purkyne fiber system. The results of the Purkyne fiber excitation serve as start for the computation of the excitation in the myocard itself.

The models described above are mainly concerned with the depolarization process. Only one theoretical model of the T-wave has been described so far. In this model by Harumi (61) et al. the sequence of depolarization is taken to determine the sequence of repolarization.

Action potentials of appropriate duration were assigned to each area of the ventricle represented by an activation front. The offset of action potentials was made to correspond to the normal sequence of repolarization. Action potentials were divided into time units, and the difference in the height of the action potential at the beginning and end of each time unit

was taken as the potential difference during that time unit of repolarization. The direction of repolarization vectors during each time unit was determined by relating the time phase of action potential up-strokes to that of down-strokes. With this model it is possible to account for the polarity and form of T-waves as recorded in animals. A computer iteration procedure was used to determine the differences in action potential duration, for optimal T-wave simulation.

Chapter 3

EXPERIMENTAL PROCEDURE

3.1 Introduction

3.2 Assumptions

- 3.2.1 Anatomical structure
- 3.2.2 Functions
- 3.2.3 Physical representation

3.3 Modelling unit

- 3.3.1 Introduction
- 3.3.2 The rhombododecahedron (RDH)
- 3.3.3 The representing grid points; hexagonal coordinates
- 3.3.4 Vector operations in hexagonal coordinates

3.4 Programs HEXCITE and VECTORS

- 3.4.1 Introduction
- 3.4.2 Program HEXCITE
- 3.4.3 Program VECTORS

3.5 Error analysis

- 3.5.1 Introduction
- 3.5.2 Experimental errors
- 3.5.3 Procedural errors

3.6 Summary

3.1 *Introduction*

A digital model of the ventricles of the heart was developed. This development divides into two parts.

Part I consists of the collection of anatomical data of a normal human heart into suitable digital form. For the collection of anatomical data, a technique was used known in our laboratory thanks to Dr. Okajima of the Nagoya University, Nagoya, Japan. This technique is described in full detail in Appendix I. The anatomical data collected were further processed and converted into suitable digital form. The procedures followed are described in Appendix II.

Part II consisted of the development of a computer program. This development took place in three stages. In stage I a preliminary study was done on the feasibility of using the rhombododecahedron as elemental units. Several basic operations (for example, approximation of configurations in orthogonal coordinates by structures composed of elemental units and described in hexagonal coordinates) were tested in this stage, as well as algorithms developed to be used in later stages. For this purpose a simple rectangular structure and a mathematical approximation of the ventricles was used. The latter consisted of three half ellipsoids, one for the outer boundary of the ventricular myocardium and two others for the left and right cavity.

In Stage II the program was used in simple form on the anatomical data collected. Conduction velocity was limited to only two different values, only one excitation cycle was considered at a time. Results presented at the Satellite Symposium of the 12th International Congress

of Physiological Sciences "The Electrical Field of the Heart", (89) were obtained during this stage. In the third stage, a more sophisticated program was devised which contains a large number of features. Attention was especially paid to flexibility and generality of the program. In section 3.4 the structure and features of this last program will be discussed. Section 3.2 deals with the assumptions made, whereas section 3.3 describes the modelling unit and its properties.

3.2 *Assumptions*

The assumptions are arbitrarily divided into three categories. Most of the assumptions were made because of limitations in the procedure used. Not included in this list are assumptions made in the context of specific experiments, which will be dealt with in the discussion following each experiment.

3.2.1 *Assumptions made in connection with the anatomical structure.*

(A1) *The anatomical structure of the heart is adequately represented by regular elements of 1.28 mm^3 in volume.*

The resolution achieved in representation of the anatomical structure depends primarily on the resolution of the photoprints of the specimen used. In these photographs the limiting factor is the uncertainty in identification of the borderline of the muscle masses. If the information about the anatomical structure is sufficiently detailed, the total number of elements could be greatly increased. However, the number of elements which could be handled conveniently is directly dependent on the computer

memory size. The size of the real heart cells is not important, since the myocardium is assumed to be piecewise homogeneous. (Assumption A2) The finest structure modelled in this report is still at least represented by a layer of two elements, which preserves two degrees of freedom for the direction of spread.

Representation of a structure by a single layer is bound to be in error since only one degree of freedom is available for this direction.

(A2) *Myocardium is piecewise homogeneous.*

Each element represents only one type of myocardial cells.

(A3) *No fine structure exists within each representing element.*

Although the physical volume of an element would be occupied by several myocardial cells, no such subdivisions into smaller cardiac cells are considered. As a result, fiber orientation is lost.

(A4) *Purkyne fibers extend as a continuous network on the surface of the ventricular cavities, without penetrating into the myocardium.*

The Purkyne fibers are added to the anatomical structure on a functional basis. Little is known about the distribution of the fibers across the surface. It is unlikely that the Purkyne fibers should not penetrate the myocardium at all. In canine hearts, the fibers are known to penetrate the myocardium (43). Effectively, the distribution over the surface is equivalent to an endocardial penetration of half unit diameter.

(A5) *The geometry is fixed during the whole cardiac cycle.*

No change during depolarization or repolarization of the elements in relative position are considered. The muscle is not 'contracting'.

3.2.2 *Functions*

Since each element represents several cardiac cells, it is tempting to allow for different properties in the different regions of an element. However, in so doing, we get into conflict with the anatomical resolution. It is unrealistic to make functional distinctions in a volume element in which no anatomical distinctions are made. The opposite approach is to consider each element as one large cardiac cell. This view is also dangerous. Most considered phenomena are membrane phenomena, but the axoplasm and its properties will undoubtedly influence these phenomena. For instance, the total surface area of the plasma membrane and its extension, the endoplasmic reticulum, are related to the membrane capacity, which in turn influences the impulse conduction velocity. Calculating these qualities for a 'giant' cell will result in values quite different from the actual ones. In order to be able to use data collected from single cell studies, we still consider the element to represent several cardiac cells. The above considerations lead, in conjunction with assumption no. (A2) from the previous paragraph to the following assumption.

B1) *All functional properties of an element are assigned to its centerpoint.*

Real heart muscle is an organized structure and most likely the conduction speed is greater along the fiber axis than perpendicular to the fiber axis. On the macroscopic level however, this has never been proven conclusively. In human hearts, excitation seems to spread rather uniformly in all directions. A simplifying view often adopted is that each excited cell serves as a starting point from which excitation spreads

in all directions with equal speed. This is referred to as Huygens principle, in analogy with light wave transmission.

Christian Huygens (1629-1695)

The Huygens principle divides into two hypothesis:

1. Every point on an advancing wavefront can be considered as a source of secondary waves, which in an isotropic medium move forward as spherical wavelets. The wave amplitude at any point ahead can be obtained by superposition of these wavelets.
2. From a given position of an uninterrupted wavefront, a later position of the wavefront can be determined as the envelope of the secondary wavelets.

In the model, no information is preserved about fiber direction, which together with the previous assumption leads to the next assumption:

(B2) *Impulses spread in the 12 directions normal to the faces of the rhombododecahedra with equal speed.*

The impulse strength in the cell to cell conduction is proportional to the action potential height. This height varies in different parts of the heart muscle, however, also varying from cell to cell are the space constants and the time constants. These three factors together determine the reaction of a resting cell to a propagated impulse. Ventricular myocardium under normal conditions is quite uniform in respect to these properties. In order to economize coding of information, the parameters representing cellular interaction are specified solely within the state code of the cell which is receiving an impulse. This leads to the following assumption:

(B3) *Impulses are of unit strength*

The sequence of cellular reactions upon stimulation serves as a physiological basis for the properties assigned to each cell. In analogy to this sequence the condition of a cell is described as either at rest,

activated, refractory or recovering. These different conditions are labelled as four different states. Though rather arbitrarily defined, this division into states is convenient in the light of the fact that anatomical and physiological conditions are lumped in the center of the cell.

(B4) *Each cell is in one of four distinct states, and no transitions between states are considered. The state of each element is evaluated at discrete time intervals.*

The state of an element is only changed upon stimulation, either by one of its neighbours or by external intervention. In real heart muscle tissue there exists a continuous influence of neighbouring cells on each other, however the most distinct influence occurs during the fast depolarization period. Since the mechanisms of the other influences are not well described on the cellular level they are left out of consideration.

(B5) *Only elements which are activated (state 2) influence the state of their adjacent neighbours.*

(B6) *Duration of state 3 (absolute refractory period) is only dependent on the properties of the element itself.*

Closely related to the various states of a cardiac cell is its membrane potential. For the purpose of calculating the electric field caused by the cell membranes in the various states, the voltage time course of the action potential is used. Assumption number 8 then follows from assumption number 7:

(B7) *Voltage time course of an element is independent of the voltage time course of its neighbours.*

(B8) *No electronic impulse conduction is considered.*

Though it is known that Purkyne fibers show spontaneous depolarization and that, under abnormal conditions also myocardial cells show spontaneous impulse formation, this is not considered:

(B9) *No spontaneous impulse formation occurs.*

3.2.3 *Physical representation*

Assumptions made in connection with the electromagnetic properties of heart muscle and torso.

In order to evaluate the impressed electric fields \vec{E}_i the contribution of each element is separately evaluated. The gradient of the impressed potential field is calculated at the center point of each element. A current dipole, proportional to this gradient, is then assigned to each cell. The first four assumptions are after Horacek (68):

(C1) *The medium of heart muscle and torso is isotropic, that is, the physical properties in the neighbourhood of some arbitrary interior point are the same in all directions.*

(C2) *The medium is homogeneous, that is, the physical properties in the interior of a medium do not vary from point to point.*

(C3) *The medium is linear, that is, the relations between electric displacement vector (\vec{D}), current density vector (\vec{J}), and electric field intensity vector (\vec{E}) and also between magnetic induction vector (\vec{B}) and magnetic field intensity vector (\vec{H}) are linear under considered conditions.*

(C4) *Quasistatic conditions prevail, that is, the tissues are essentially resistive, and coupling between electric and magnetic fields can be neglected.*

- (C5) *The potential gradient inside an element is constant in direction and magnitude.*
- (C6) *The potential of an element is only evaluated in its center.*
- (C7) *The impressed electric field is continuous.*

3.3 *Modelling unit*

3.3.1 *Introduction*

The choice of the modelling unit is rather important. Associated with this choice is the whole philosophy on which the development of the program HEXCITE is based, and a number of necessary assumptions follow from this.

Two approaches, opposing in principle, to the choice of the modelling unit can be distinguished.

One starts with the choice of a convenient unit and works out in which way this unit can represent the structure to be modelled. An important consideration is how the units can be packed. A regular packing of units allows the choice of a coordinate system in such a way as to assign each unit integer coordinates, which simplifies storage and calculation problems. A second important consideration is the distance between adjacent units. If the Huygens principle for wave transmission is adopted, this distance plays an important role, especially if this distance varies in different directions.

The other approach starts with the consideration of how to represent optimally a three dimensional structure. Since the representation will be point wise, it seems logical to use spheres, these being the units with

the smallest surface area per volume unit. All points of the three dimensional structures falling within one sphere are then represented by this sphere's centerpoint. Using spheres with equal diameter there exists a large variety of ways of packing these spheres. No matter how packed, there will always be an open space between the spheres, so each of the points of the three dimensional structure in this open space has to be represented by the nearest sphere. Effectively the influence sphere of a centerpoint is increased by this addition. The amount of volume added to each sphere is good measure for the closeness of the packing of the spheres. Another way of looking at it is to imagine the spheres to grow, without growing into each other, until the total volume is occupied. The additional growth is the volume difference between the final "grown" sphere and the real one, or, in other words, between the final structure and its inscribed sphere.

If we pack spheres in such a fashion that their centerpoints are located along straight lines parallel to the X-axis, Y-axis, and Z-axis of an orthogonal cartesian coordinate system, then they are equidistant and each sphere is surrounded by 6 neighbours. By "growing" the spheres to fill all spaces they obtain the shape of a hexahedron. The difference volume of a hexahedron and its inscribed sphere is 47.64% of the total volume.

If we, however, pack the spheres so that their centerpoints are located along straight lines parallel to the X-axis, Y-axis, and Z-axis of an hexagonal cartesian coordinate system, then they are still equidistant, but now each sphere is surrounded by twelve neighbours.

By "growing" the spheres to fill all spaces they obtain the shape of rhombododecahedron, for which the difference volume is 25.95% of the total volume. Since the hexagonal packing of spheres is the closest regular packing (49), any other packing of equal size with less neighbours will less sufficiently represent a three dimensional structure.

It can be shown that 12 spheres comprise the maximum number which can be packed around a center sphere (49).

In view of the above facts, we made a choice for a point representation where each point is the node of a grid. The grid lines are parallel to the X_h, Y_h , or Z_h -axis, and are located on integer coordinates. Consequently, the grid points have all integer coordinates, and the distance between each point and its closest neighbours is unity. Each point is surrounded by twelve neighbours at this distance. The solid represented by one single point has consequently the shape of a rhombododecahedron. (Fig. 3.1) It is convenient to think of the model presented here as built from solid rhombododecahedra; this is actually not the case; it is merely a pointwise representation of an anatomical structure.

A perspective drawing of X_h, Y_h , and Z_h -axis is seen in Fig. (3.2), which also shows the location of the centers of the twelve adjacent neighbours.

3.3.2 *The rhombododecahedron (R.D.H.)*

Rhombododecahedra belong to the family of polyhedra. It is a semi-regular solid with 12 faces, which are all rhombi. If properly packed it

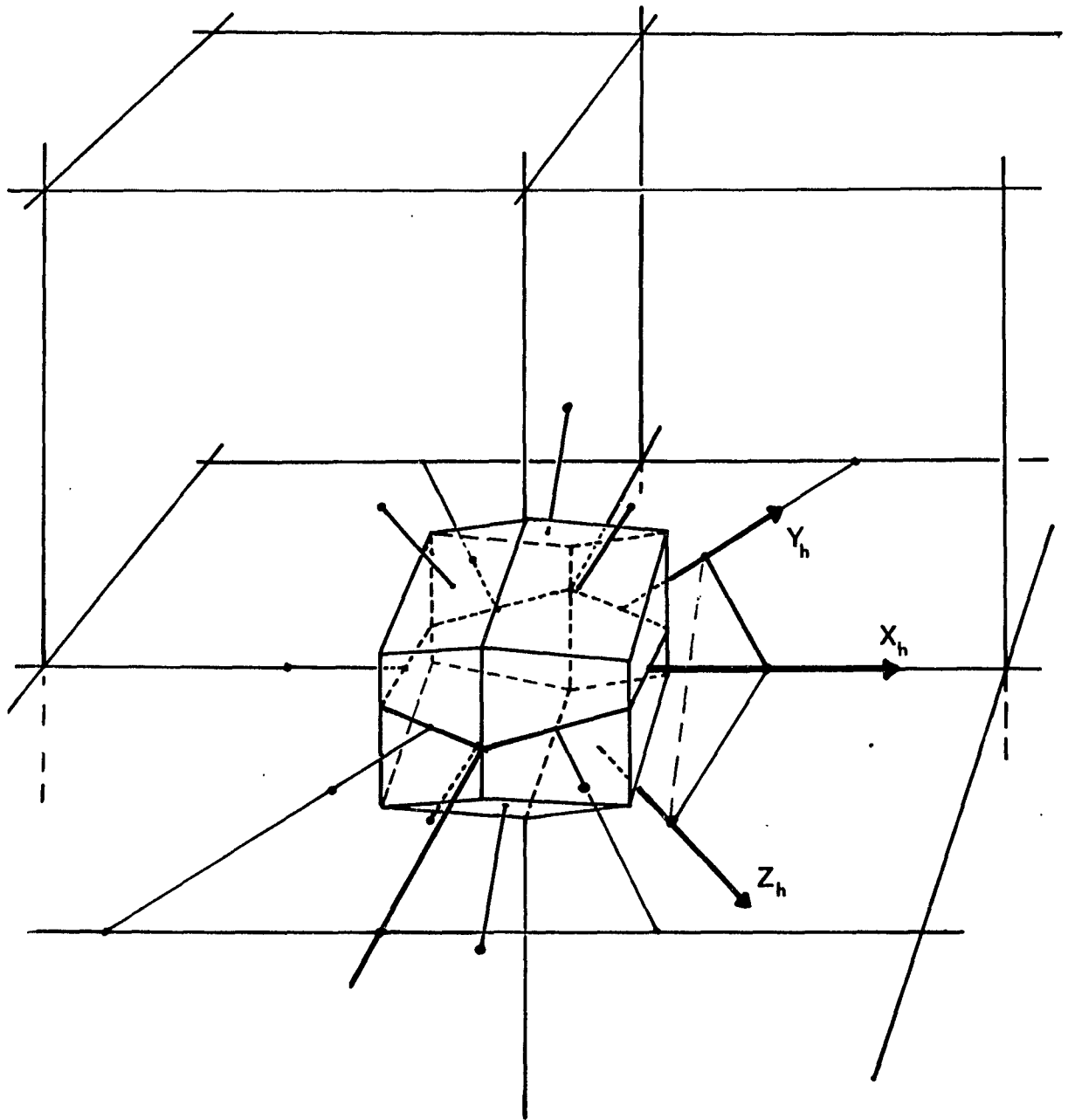


Fig. 3.1 A rhombododecahedron. A perspective drawing of a rhombododecahedron. The hexagonal coordinate axes are labelled X_h, Y_h, Z_h . The intersection with X_h, Y_h plane forms a hexagon. The normals to each rhombic face are also seen.

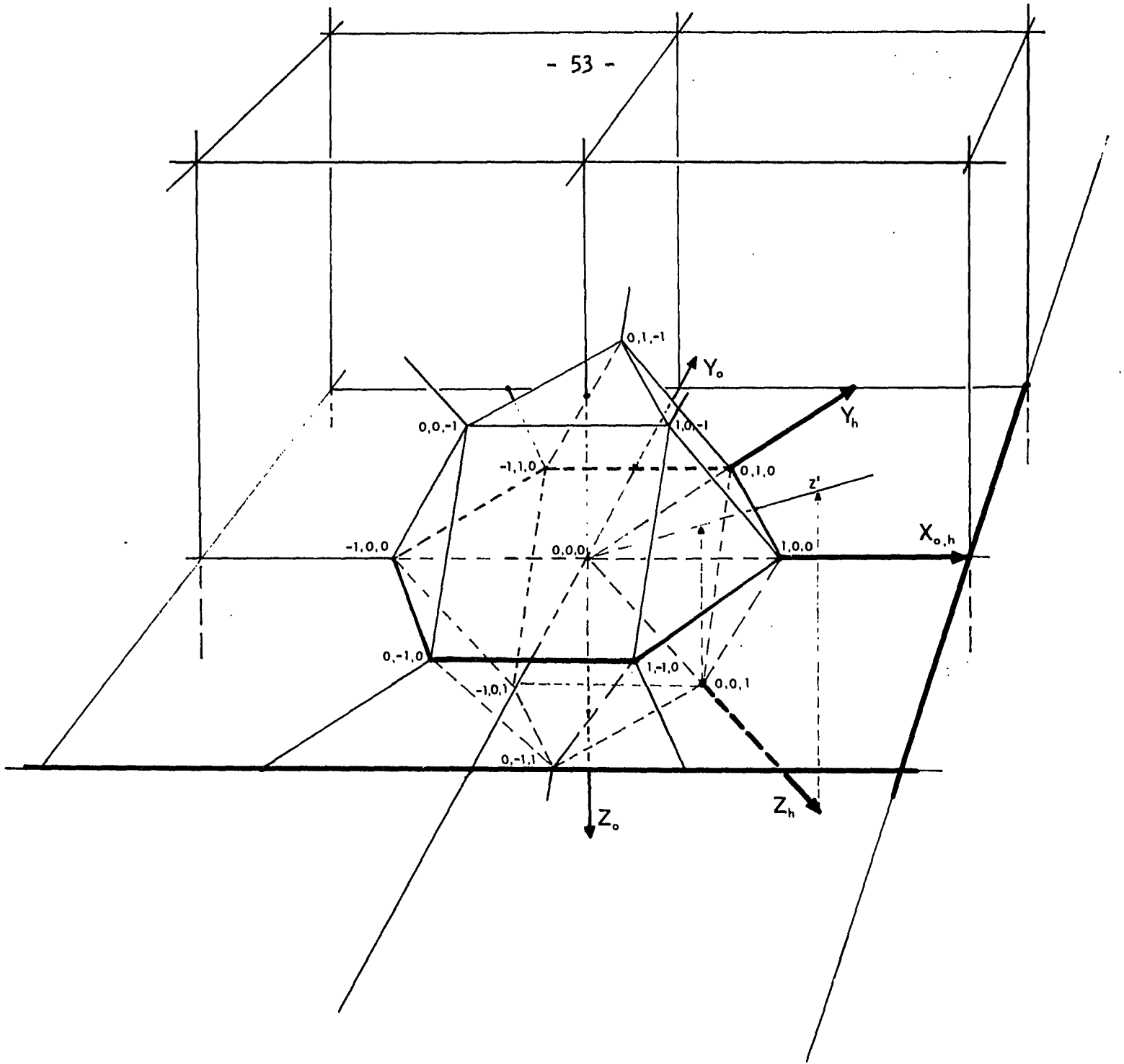


Fig. 3.2 Hexagonal grid points. In this perspective drawing both hexagonal X_h, Y_h, Z_h (and orthogonal X_o, Y_o, Z_o) coordinate axes are labelled. The twelve grid points surrounding grid point $(0,0,0)$ are labelled with their hexagonal coordinates. Taking the surrounding grid points as vertices of a solid, a cuboctahedron is formed. The angle Z_h , origin, Z' is $54^\circ, 44'$.

fills all space just once. A more detailed description of the rhombododecahedron is found in Appendix III.

3.3.3 *The Representing Grid Points: Hexagonal Coordinates*

As discussed above and as implied from the assumptions made, the author prefers to think of a point-wise representation of the space. The representing points are the grid knots of gridlines parallel to either the X, Y, or Z axis in hexagonal space and unit distance apart.

The volume which is represented by one gridpoint is comprised in the above described rhombododecahedron. This does not necessarily mean that the total volume of the RDH was occupied by ventricular muscle tissue mass. If the coordinates of a grid point (in hexagonal cartesian coordinates) are X,Y,Z, then the twelve surrounding grid points can be obtained by incrementing or decrementing the coordinates by (1,0,0), (0,1,0), (0,0,1), (1,-1,0), (1,0,-1), (0,1,-1).

As can be seen in figure (3.2) for point (0,0,0), these points are unit distance apart from the center point. A more precise proof of the previous statement is given in Appendix IV. The twelve points around the center also form a semi-regular polyhedron, the cuboctahedron. The distance, in orthogonal coordinates, between two successive layers of points was chosen to be 1 mm. Reasons for this were: (a) an estimation of the total amount of representing points matched the available computer memory capacity, (b) the slicing technique used does not allow for the making of much thinner slices, (c) the volume of the elements comprises 12-20 real heart cells in which case the assumptions made in respect to homogeneity and radial spread are reasonable.

(d) all areas of the ventricles are at least represented by a double layer.

The choice of a hexagonal cartesian coordinate system was made in order to assure integer coordinates for each grid knot point. Integer coordinates are easier to handle and occupy less space in the computer memory. Also, simple coding of coordinates triplets into one number (occupying one word) is possible, without loss of precision.

Properties of an hexagonal cartesian coordinate system are described in detail in Appendix IV. Vector operations, as far as they differ from ordinary vector operations are also discussed in this Appendix.

3.4 *The Program - HEXCITE and VECTORS*

3.4.1 *Introduction*

HEXCITE was developed with two major objectives:

- (a) The first is to preserve the anatomical structure presented to it and to organize this structure into suitable form.
- (b) The second is to allow the largest possible freedom to the user to specify the rules for interaction of the elements.

The first objective was easily met by generalizing the form of acceptable data. Assumed in the program is a description of data in hexagonal coordinates, though minor changes will allow acceptance of orthogonal data. The different histological structures are stored by type-numbers. The total amount of different types possible depends on the number of bits allocated for this purpose (see paragraph #3.4.2.3, variable bit allocation). A theoretical maximum of 8,192 different types is possible, though such a large set reduces the freedom for other specifications.

The second objective is accomplished by users interaction at the intermediate level (I.M. level, see below). Each element is upon excitation presented to a users supplied subroutine together with the relevant information, such as type, time, direction of spread, length of excitation or recovery period. The decision how the element reacts is then up to the user, as well as the determination of the duration of the following periods. The program as used allowed only one way operation, i.e. the state of an element can only be changed into the "active" state, state 2.

3.4.2 *Program HEXCITE*

The computer program HEXCITE divides into two parts.

The first part organizes the anatomical data given to the computer in coordinate strings into the model proper, whereas the second part actually computes the sequence of activation within these anatomical data, starting from users specified origins.

3.4.2.1 *Organization of the Model*

The design of the program is such that any anatomical structure, if represented in suitable form, can be used, and the only limitation is the maximum number of representing points in one horizontal plane. This maximum is (2780) on the computer used (XDS-Sigma 5). The anatomical data are read in from magnetic tape in coordinate strings. One string consists of the consecutive coordinate triplets parallel to the X_h axis. Such a string is coded into one word, which contains the Z_h , Y_h coordinates of all triplets and the first and last X_h coordinate of the string. All elements in one string must be of the same type. Series of strings of the same type are followed by the type code. Each element occupies 16 bits in core (one half word) in which the type code is stored, as well as information necessary for the computation of the sequence of activation. The location in memory (the half word address) is specific for one element, and from this address the X_h , Y_h , and Z_h coordinates can be derived by means of an index table, and vice versa, i.e. knowing the X_h , Y_h , and Z_h coordinates the representing half word can be found. One layer of elements immediately outside the anatomical structure is assigned to be "shell" and forms a functional barrier to the spread of activation.

A temporary storage of data on a rad file is used, organized in sections, from which at execution time the necessary sections are brought into memory.

3.4.2.2 *Computation of Sequence of Activation*

The computation of sequence of activation is controlled by several factors. The users can influence these factors at three levels:

- (a) Factors built in excitation program, lowest level of control
- (b) Factors specified for one run, intermediate level of control
- (c) Factors controlled at execution time, highest level of control

(a) *Factors built-in in excitation program; lowest level of control*

At the lowest level of organization occurs the basic computation of spreading of the activation in all directions, provided that no activation spreads outside the heart muscle or into the shell structure surrounding the heart muscle. This computation is done in time steps, that is all activity in the structure is computed and completed before the next time moment is considered. The element status is the only parameter which can be changed at this influence level. The status is numbered. An element is either in Status 1, 2, 3, or 4. Status 1 is comparable with "at rest", Status 2 with "depolarizing". Status 3 "absolute refractory" and Status 4 "relative refractory". Under "normal" conditions each element passes through these four states in the above stated sequence. Status 1 is of undefined length and only terminated upon excitation of the element under consideration by an adjacent neighbour or by external stimulation.

In the former case control is passed on to the I.M. level, in the latter the interruption of the state is forced from the highest level of control and is passed on to I.M. level. Once an element entered stage 2, the duration of this state and of the following state 3 must be specified. Without further interruption by either another excitation from one of the neighbours or external stimulation the elements automatically passes through these stages into state 4, which has a predetermined duration and finally terminates with the element re-entering state 1.

Schematically the parts of one cycle are seen in figure 3.3 which depicts a discontinuous function $Y=F(t)$

The function $Y=f(t)$ is defined as follows:

$$\begin{aligned} dY &= 0, \text{ for } t < t_0 \\ dY &= -adt, \text{ for } t_0 < t < t_e, \text{ and } dY = Y_1, \text{ for } t = t_0 \\ dY &= 0, \text{ for } t > t_e \end{aligned}$$

, where t_0 is time of excitation and t_e the time the element is not under control anymore; a is set equal to $Y_3 /$ maximum number in counterfield.

The element is in state 1 if $Y=0$,

$$\text{in state 2 if } Y_1 \geq Y > Y_2$$

$$\text{in state 3 if } Y_2 \geq Y > Y_3$$

$$\text{in state 4 if } Y_3 \geq Y > 0$$

Since state 1 is of undefined duration, a more attractive way of schematizing the possible events for one element is by imagining the

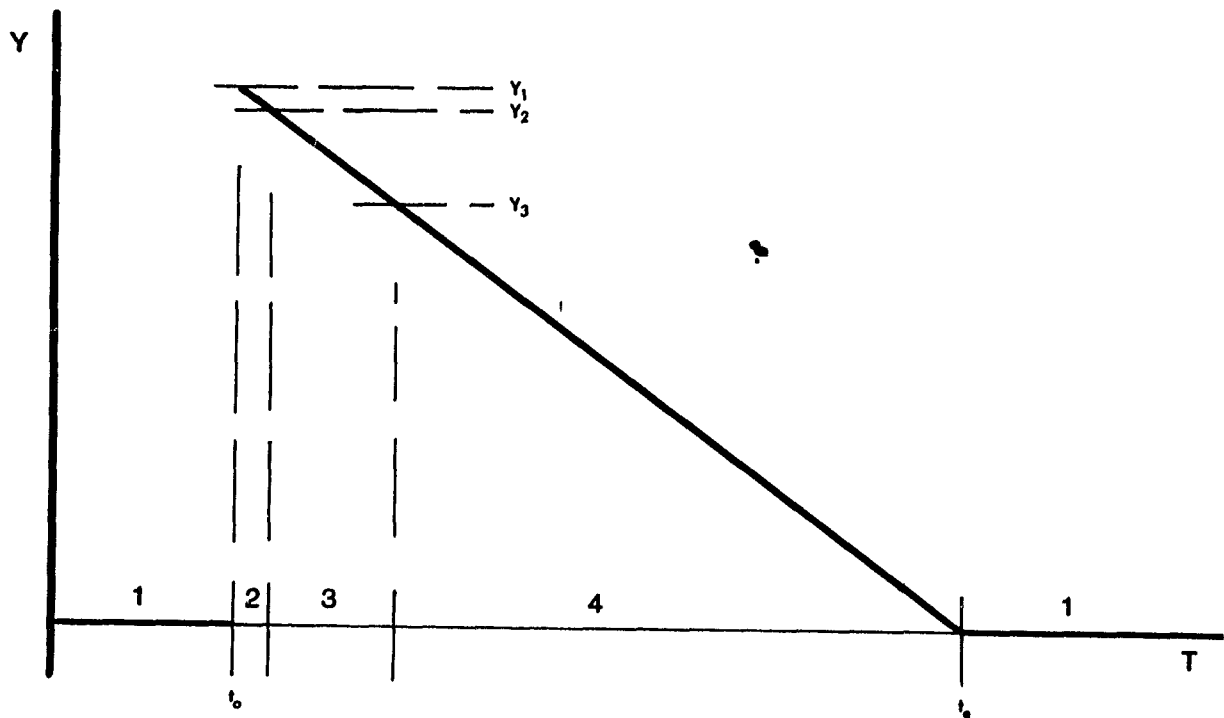


Fig. 3.3 Function $Y = f(t)$ determining the state of an element excited at time $t_0 \cdot dy = -adt$, when $t_0 < t < t_e \cdot dy = 0$ when $t_e < t < t_0, dy = Y_1$ for $t = t_0, a = Y_3/\text{maximum number allowed in counter field of half word}$. The state number of the element is indicated just above the time axis.

elements to be represented by a point in a plane within a circle with radius r_2 (Fig. 3.4). Upon excitation the point is placed on the circle with radius r_2 and enters state 2.

From there on it starts circling around the center with a constant angular velocity and (at constant rate) decreasing distance (d) from the center. If the point intersects the circle with radius r_3 the state of the point changes from state 2 into state 3, on intersection with circle with radius r_4 , it enters state 4. On intersection with circle with radius r_1 , d stops decreasing and the point enters state 1. From here on, it can continue to circle around indefinitely till the next excitation which places the point back on circle r_2 . If a point gets excited at any time in any state it can only stay either untouched or it is placed on circle r_2 . The basic cycle length (duration of state 4) is determined by the biggest number which can be stored in the bits allocated at loading time to serve as timestep counter. The radius of circle r_2 and r_3 is determined at the I.M. influence level at the moment an element is excited. At the intersection of circle r_3 , the element tries to excite its neighbouring 12 elements, which, if its state allows it, are placed on their respective r_2 circles.

A correction algorithm is used to correct for the directional error in conduction velocity. This correction is used if the excitation is calculated in the steps of .5 msec. The normal conduction (conduction velocity of 49 cm/sec.) from one element to the other takes then 5 timesteps. If, however, an element is excited twice within one timestep, only four timesteps are used for the conduction time from one element to the other.

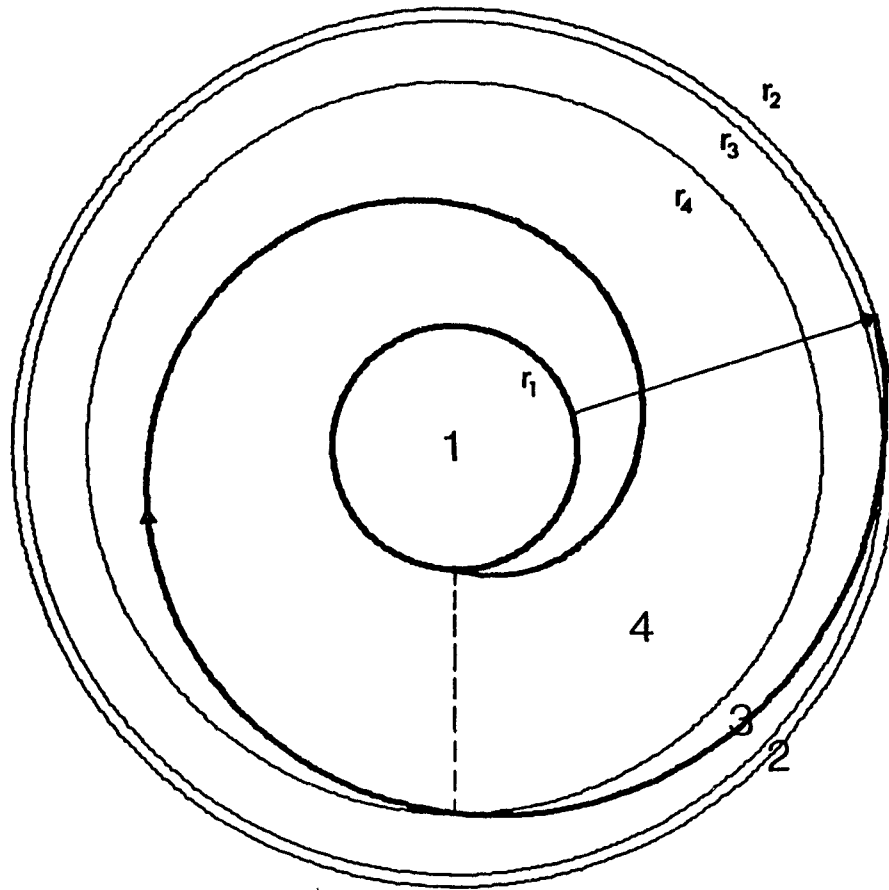


Fig. 3.4 Excitation cycle. Upon excitation the element is placed on circle r_2 , starts circling around the center with constant angular velocity (ω) and at a constant rate (a) decreasing distance (d) to the center, under the condition that:

$$2\pi/\omega a = r_4 - r_1$$

in which $r_4 - r_1$ = maximum number allowed in counter field of an element half-word, and that $a = 0$ if $d = r_1$. The state in which the element is, is indicated in the circles.

(b) *Factor specified for one run; control at intermediate level.*

At the time an element is excited, control is passed on to a user supplied subroutine. In this subroutine the user knows the current status of the element, the timestep, its type, the type of the element which excites this element, the direction from which excitation reaches the cell, how long the cell will be in the present state if unchanged (for elements in state 2 or 3) or how long ago the last change took place (for elements in state 4).

All parameters can be changed under the following conditions:

1. If the state is changed, it has to be changed into state 2
2. The time step cannot be changed
3. If specifications are made for duration of state 2 and 3, these durations have to be within the allowable limits. These limits are dependent on the number of bits allocated for these parameters within the half word.

(c) *Factors specified at execution time; highest level of control*

Influencing the activation procedure during execution time can only be done by means of external "excite" cards, which specify at which time step, which element is to be excited. At this level is also controlled the total number of time steps to be computed, as well as are specifications made for which mode the program has to execute, i.e. writing the wavefronts on to tape, or saving at certain time steps the total situation of the model by means of a dump of the sections on tape, etc.

3.4.2.3 *Variable Bit Allocations*

In order to keep the program as flexible as possible the allocations of the bits of the half word is done for each run separately. Each half

word stores the following parameters:

- (a) The status of the element i.e. 1,2,3, or 4. The first two bits are allocated for these parameters.
- (b) The duration of the refractory period.
- (c) The delay time after the start of the excitation.
- (d) The time at which the last refractory period ended.

Since parameters b and c on one hand and the parameter d on the other hand are never used at the same time, the same bit allocations are used for these parameters. It is up to the user to make use of these control possibilities. For instance, if five bits are allocated for storage of the types of the elements, a maximum of 31 types are possible, and nine bits left over to serve as post refractory periods counter, or to contain delay time and absolute refractory period duration. These nine bits allow a maximum number of 511. In case less bits for typing of the elements are used more space is available for the other parameters. A flow chart of the program as outlined above is found in Appendix V. In this flow chart, page V.1 depicts the highest level of control, the black box on page V.2 the intermediate level of control and the other content of page V.2 the lowest level of control.

3.4.2.4 *Output of HEXCITES.*

As controlled by control cards either "wavefront" tapes are generated or "model" tapes. "Wavefront" tapes contain the coordinate triplets of the model in sequence in which they entered state 2.

As additional information can be added type of element or the length of the time the element will stay in state 2. At the end of each step a small record is added which labels this time step. "Model" tapes contain a copy of the model at a certain time step, with all necessary additional information to restart from this copy the program HEXCITE. It should be noted that the output of HEXCITE is in the form of spacially distributed points. No other functional relationships are given. In order to compute an equivalent source the program VECTORS is used.

3.4.3 *Program VECTORS*

The program VECTORS is used to calculate for each element an equivalent current dipole moment for the time steps considered. The voltage time course of each element can be specified according to type or any other relevant parameter, such as, location, previous excitation interval, duration of refractory period. At each time instant for each element, the surrounding potential field is evaluated on the basis of the potential of the 12 surrounding elements. Each element is assigned a current dipole which is proportional to the negative gradient of its surrounding potential field. These current dipoles are used in the direct computation of the body surface potential distribution as described by Horacek et al (69) or vectorially summed in which they form the 'single dipole' equivalent source.

This equivalent dipole then combined with the lead vectors associated with its source location, also yield surface potentials.

A third possibility is to compute several distributed equivalent dipoles over the heart region. Each of the dipoles is the vectorial sum

of all current dipoles of the elements of a region. In this way the heart is chopped into regions, an equivalent dipole is computed for each region and this dipole is located close to the center of gravity of the region (dipole-source location; DSL). The contribution of a region to the surface potential at any defined location is equal to the dot product of the equivalent dipole moment vector of the region and its lead vector to the surface point. To find the surface potential at a certain body surface point the potential contributions of all dipole sources to the surface point are summed.

VECTORS is designed in such a way that it is possible to use any set of measured data, for instance real action potentials, as voltage time course of each element.

3.5 *Error analysis*

3.5.1 *Introduction*

In the following paragraphs, the error discussion is divided into two parts.

The first part deals with errors in the data collection, approximation procedure, smoothing and alignment of the sections. These errors are referred to as experimental errors.

The second part evaluates the errors involved in the procedure used to calculate the spreading of the activation and to compute the equivalent source (or sources). These last errors are not errors in a statistical sense, since no variation occurs with repeated measurements.

3.5.2 *Experimental Errors*

Orientation of the heart in respect to the torso was preserved by means of the two orientation needles. These were inserted in the heart in a direction perpendicular to the autopsy table. Two possible sources of error are encountered here, first of all 'perpendicular' insertion of the needles is done to the best knowledge of the pathologist. Secondly the position of various internal organs will change after death. Due to loss of the muscle tonus of abdominal muscles and diaphragm an unpredictable change in position of the diaphragm will occur, which will affect the heart position. It is known that heart position and movement are partially affected by blood pressure in aorta and pulmonary arteries, resulting in a change of heart position after death.

Orientation in the fixation box as far as the orientation needles are concerned is quite accurate, which fact was witnessed during the slicing procedure, where in section 14 and 50 the holes caused by the needles were cut in half and evenly found in the sections above and below these levels.

Finally a check was done on the proper orientation by projecting the heart outlines and cavity outlines onto a frontal plane. The heart was rotated around the Y-axis stepwise from -60° to $+60^{\circ}$ in steps of 15° and around the X-axis from -15° to $+15^{\circ}$. A total of 27 frontal plane projections were obtained for various combinations of these stepwise rotations.

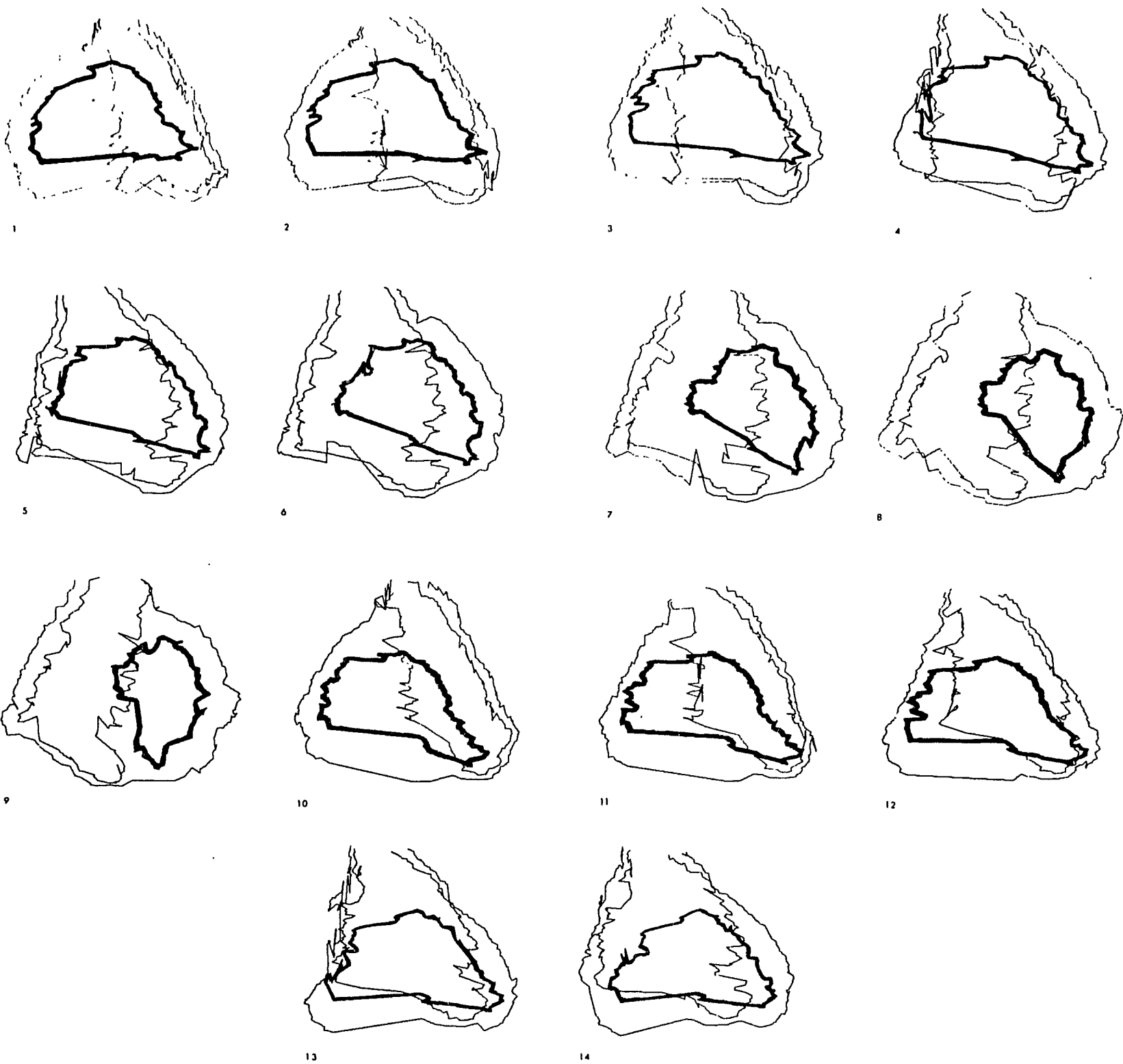
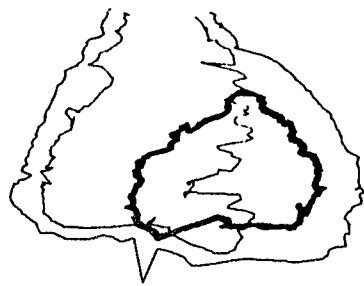


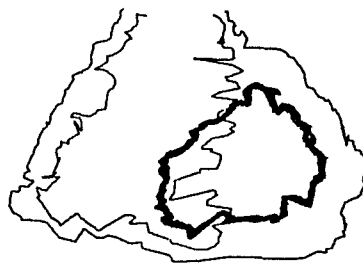
Fig. 3.5 Frontal plane projections of the heart model. Outer line is outside contour of muscle mass, inside thin line is inside contour of right ventricle, inside thick line is inside contour of left ventricle. Picture 1-9, 10-18, and 19-27 give the projections onto the frontal plane after rotation of the heart around the X_0 -axis for -15° , $+15^\circ$ and 0° in a clockwise direction (viewed from left sagittal).



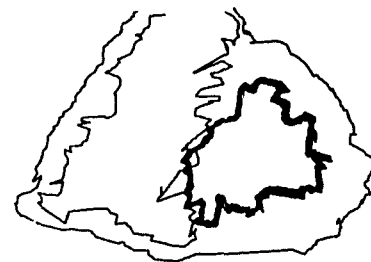
15



16



17



18



19



20



21



22



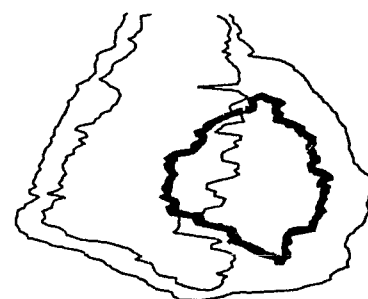
23



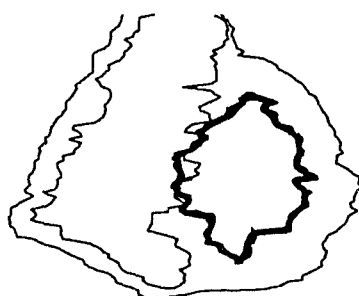
24



25



26



27

Within each series of nine the location around the Y_0 -axis (head-foot axis) ranges from -60° to $+60^\circ$ in increments of 15° . Thus projection 2, 10 and 30 are comparable with the right anterior oblique projection, 5, 14 and 23 with the postero anterior projection, and 8, 17 and 26 with the left anterior oblique projection.

(Figure 3.5) These projections were first of all compared with standard "normal" projections (#163) and secondly handed out to 7 clinicians, (5 cardiologists, and 2 radiologists) who had to choose independently of each other the correct antero-posterior projection, LA oblique and RA oblique projection. These projections are generally used in cardiac radiology when cineangiograms are made, and thus they are familiar to the cardiologists. In figure 3.5, number 23 and 24 are compatible with a normal A P projection, whereas 26, and 27 are compatible with the LAO projection and 20, 21 with the RAO projection. The choice of the majority of the 7 clinicians was compatible with these projections. From these results it was decided that the orientation of the heart is reasonably correct; and no rotational correction was made. Another encouraging fact was encountered while positioning the heart in the torso. It appears that the area previously allocated for the ventricles, on the basis of cross section anatomical data (48) and roentgenograms of the subject which served as standard for the torso model (68) fitted neatly, without rotation, around the ventricular masses of the heart model. It was concluded that the orientation of the heart was close to normal and did not need any further corrections.

The next possible error source is the digitizing of the coordinates. The D-mac digitizer pencil follower itself has a high resolution (0.001mm.) which makes the involved error negligibly small compared with the error made in identifying the boundaries on the photographs. Important factors in this identifying procedure are the quality of the photographs and the orientation of the boundary at the area of intersection. If the boundary surface makes an oblique angle with the plane of cut, a double edge appears

on the photograph. Consistently the upper edge was taken. It was also sometimes difficult to identify the nature of the tissue looked at. Errors resulting from this will result in a distorted geometry and there is no way to avoid them. However, the visual check following the alignment of the sections gives a reasonable estimate of the magnitude of this error. The first alignment was done when the sections were actually made. At that time they were manually aligned to the background paper with grid. The second alignment was done after digitizing, by calculating for each section the center of gravity (see Appendix II). The visual inspection of constructed vertical sections was relied on more heavily than computed results whenever errors were suspected. The third alignment involved the calculation of the difference area, again followed by visual inspection. This last method yielded such satisfactory results that no further adjustments appeared necessary. This also gave support to the thought that the digitizing procedure must have been quite accurate. As a yardstick during visual inspection served a smooth transition between sections, in their frontal projections. In the approximation procedures, a definite error is involved which can be at most .61 mm displacement for each point. However, since a large set of points is approximated the overall error is small, as compared with the size of the heart.

3.5.3 *Procedural Errors*

All parameters in which the time is implicitly involved are subject to error. This is caused by the discrete time step with which time is incremented. For simulation under normal conditions a time step comparable to .5 msec was chosen, which makes the time truncation errors to be maximally .25 milliseconds. The only phenomenon which is in sizable

proportions affected by this is the upstroke of the action potential. For this reason it is not attempted to distinguish elements as being partly in the action potential upstroke. More seriously affected by this discretization of time are the proportions of different conduction velocities. For example, if the unit time step is .5 msec, then the maximum conduction velocity cannot be higher than unit distance/unit time (i.e. $1.22 \text{ mm}/.5 \text{ msec} = 245 \text{ cm/sec}$). Lower conduction velocities are all multiples of the integer reciprocals. For the same unit time step normal conduction velocity in the ventricle muscle is approximated by unit distance/5 unit time steps, which is 49 cm/sec, but the nearest distinguishable velocities are 61.25 cm/sec and 41 cm/sec. These values are respectively +25% and -16 2/3% of the 'normal' velocity. The lower the conduction velocity, the higher the resolution.

It is assumed within an element that conduction velocity is constant in all directions. This holds for the 12 main directions, however, outside these 12 main directions a cumulative error occurs. This error is largest in the direction of the vertices of the RDH where four sides meet. In the nearest gridpoint in this direction arrival time of the excitation is estimated 41.4% too late. By applying a simple correction algorithm (see page 61) this error is reduced to 27.28%. In the direction of the sides of the rhombododecahedron (for example $+30^\circ$ in the horizontal plane) the error is 15.5% and using the correction algorithm 3.92%. It is difficult to assess how much this directional error influences the computed results. In the heart model we deal with an irregular surface (the endocardium) from which at different

times and at different locations the activation spreads outwards through the myocardium. For the thickest wall, the left ventricle, this error could amount to approximately 6 msec difference in real and computed arrival time of the excitation provided the excitation started from one single endocardial point.

In the calculation of the equivalent source only the time resolution for the voltage function of each element is subject to error. As mentioned above, the upstroke of the action potential will be liable to error if any distinctions are made in this part of the voltage time function. Other parts of the action potential are changing sufficiently slowly to allow this error to be neglected. To avoid ambiguities the elements are either in phase 0 or in phase 2 of the action potential as far as voltage calculations are concerned (assumption B4). Since we assume uniform conduction speed in all directions, time and space variations of the action potential are interrelated by the conduction velocity. With a conduction velocity of 49 cm/sec and an action potential rise time of 1 msec, the region occupied by phase 1 of the action potential is 490μ , which is well within the distance of two grid points (1.22 mm). It follows that the above-mentioned error source is efficiently avoided by assumption (B4), which itself does not lead to any serious error.

3.6 *Summary*

The structure of the human ventricles was described with sufficient accuracy by the knot points of a grid. Orientation of these grid knot points in hexagonal space provided optimal representation of the three

dimensional structure. The anatomical resolution obtained was mainly dependent on the resolution of the used photographs. Physiological properties of heart muscle cells served as a basis for a computer program HEXCITE which computes in time and space, once excitation is started, the propagation and distribution of this excitation. The electric field associated with this process could be computed with the program VECTORS on the basis of the cellular voltage time course, for which either artificial functions or measured action potentials can be used. The experimental errors were evaluated and judged negligible. From the procedural errors the discretization in time and the directional accumulation of conduction velocity error are more serious. It was seen that the conduction velocity is seriously affected by both. However, in an irregular structure such as that of the ventricles the results will be qualitatively barely affected as long as the resolution sought is not too high.

Chapter 4

NORMAL EXCITATION AND REPOLARIZATION

4.1 Introduction

4.1.1 Normal excitation and recovery

4.2 Methods

4.2.1 Normal excitation

4.2.2 Heart vectorcardiogram - depolarization

4.2.3 Heart vectorcardiogram - repolarization

4.2.4 The lead systems

4.3 Results

4.3.1 Normal excitation

4.3.2 Heart vectorcardiogram - depolarization

4.3.3 Heart vectorcardiogram - repolarization

4.3.4 The lead systems

4.4 Discussion

4.4.1 Normal excitation

4.4.2 The heart VCG depolarization

4.4.3 The heart VCG repolarization

4.4.4 The lead systems

4.5 Conclusions and summary

4.1 *Introduction*

In this chapter normal excitation and recovery will be discussed. Unfortunately, normal excitation and normal repolarization defy strict definition; at best we can consider the excitation and repolarization of a normal heart. It is already obvious from the large variation in electrocardiograms of healthy adults, that the complex cycle of events which leads to the electrocardiogram as recorded is different from subject to subject. These differences are caused by differences in body structure and composition (torso conductor properties) and, of course, differences in the individual hearts (source generator properties). However, from beat to beat in one individual these differences are remarkably small, which suggests that all factors involved are rather constant individually. The primary purpose of this chapter is to use the available measured data (most of them measured in a few hearts of cardiologically normal humans) in order to simulate the normal excitation patterns. As in any simulation experiment, a reasonable agreement between simulated and measured excitation patterns will provide support for the validity of the model and will justify the use of this approach for further studies to determine equivalent sources and surface potentials. Simulation of repolarization is also undertaken in this chapter. In contrast to the excitation experiments these repolarization studies are based on much less specific and more general speculative models, due to lack of specific physiological measurements. Certain hypotheses commonly offered as explanations of the repolarization patterns in electrocardiograms will be tested. 'Profile' vectors are

introduced to facilitate analysis of excitation and repolarization relationships in the context of the classical ventricular gradient concept. These 'profile' vectors are a more generalized form of the ventricular gradient vector, as introduced by Burger (19). The influence of the non-homogeneous torso on derived X,Y and Z components of the heart vector is studied by combining the author's model with a torso model previously developed in this laboratory (68).

4.1.1 *Normal excitation and recovery*

4.1.1.1 *Depolarization*

From the very few reports on excitation of human hearts, the one by Durrer et al. (42^a) was taken as a guideline to determine the locations and relative timing of the onset of excitation. These points are believed to be the first terminations of left and right bundle branch (6). For the right ventricle this point is reported (145) to be located with some variation at the base of the anterior papillary muscle close to the interventricular septum. Onset of excitation is accordingly either in the interventricular septum or the base of the papillary muscle. In the excitation pattern shown by Durrer et al. (42^a) (p.902) the onset is more towards the base of the papillary muscle. The left bundle divides high on the septum into a posterior and anterior portion. Normally, the anterior left bundle is the smaller one (142). Its terminations are at the base of the anterior papillary muscle (145). The large area around the anterior papillary muscle is excited almost

at once because of the widespread ramifications of the terminal branches of the bundle. The posterior branch of the left bundle terminates just below the posterior sleeve of the mitral valve at the junction of the posterior wall and septum, and on the ventricular septum (145). The septal endings of the posterior branch of the left bundle are normally the first to activate, followed within 5 msec by the other parts of the left bundle. The activation due to the right bundle is normally 10-15 msec later than on the left side. In order to be able to directly compare our resulting excitation wavefront patterns with those by Durrer et al., sections were constructed in comparable planes. These planes are perpendicular to an axis through the left ventricular apex and the mitral valve opening at 1 cm intervals starting from the base. The corresponding sections are labelled A,B,C H (Fig. 4.1).

4.1.1.2 *Equivalent source during depolarization*

The current dipole source representation is chosen for each element. This current dipole is proportional in strength to the impressed electric field. The impressed electric field in the center point of each element is evaluated as the gradient of the potential field, whereas the potential field in each point is assumed to be proportional to a hypothetical transmembrane potential. A simulated action potential defined in section 4.2.3.1, was used as voltage time function of the transmembrane potential. The equivalent source (for the whole heart muscle) will only be given in the form of an equivalent dipole in an

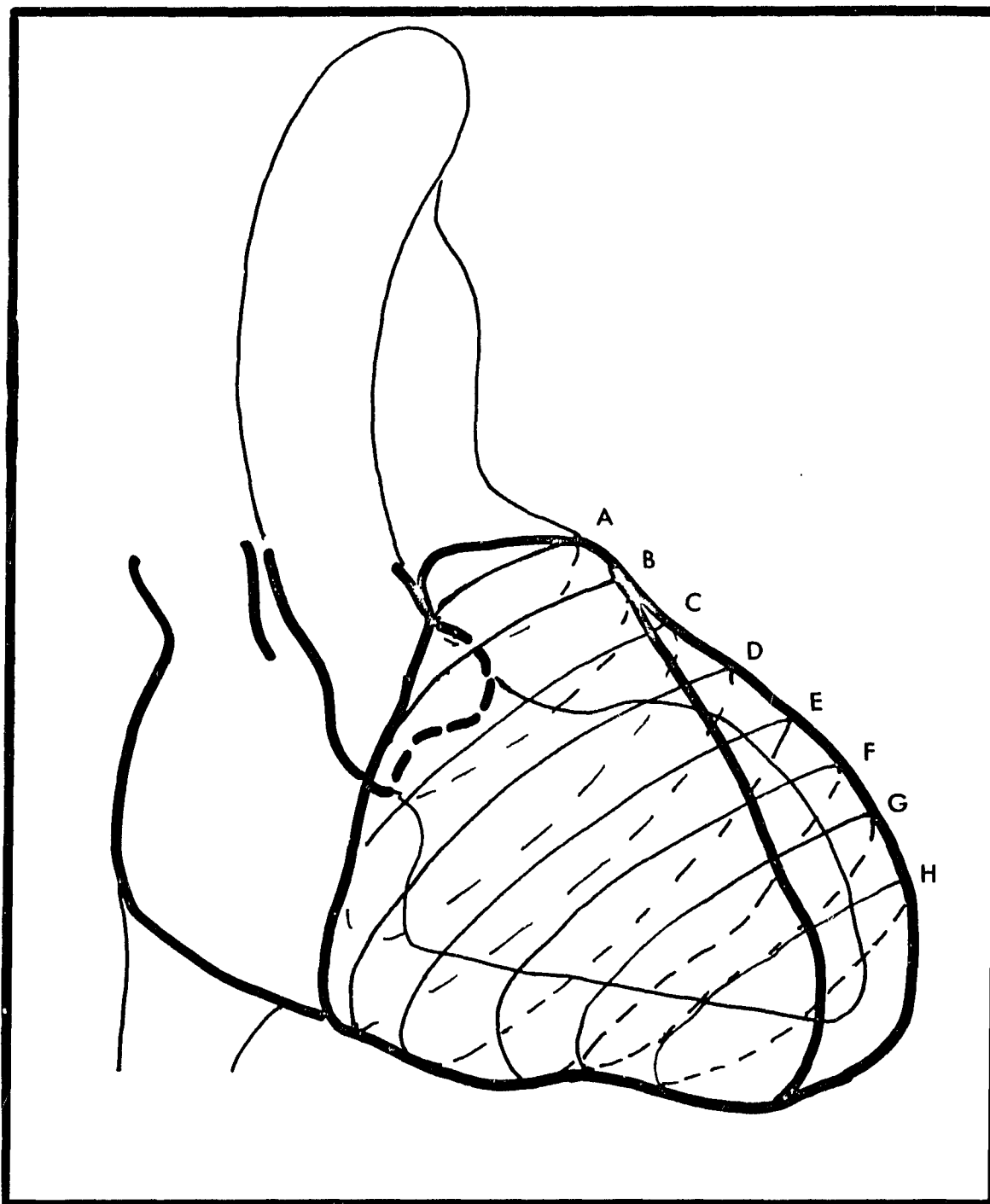


Fig. 4.1 Frontal view of the heart. Redrawn from computer plots of the outline of the cavities and ventricles. The thick lines were actually drawn by the computer, whereas the thin lines (aorta and venae cavae) are added by hand. The left ventricle cavity is also a direct copy from the computer plot. The 8 intersections of the planes for which sections were reconstructed, are labelled from base to apex, A to H. The 8 planes had normals parallel to an axis through the opening of the mitral valve and the left ventricle apex. Scale is 1:1.

infinite homogeneous medium. This equivalent dipole is derived by vectorial summations of the current dipole sources for each element; when treated as a function of time, this vector function of time is called 'heart vector cardiogram' (HVCG). Vectorcardiograms computed from the body surface potential distribution are labelled with the name of the corresponding lead system (i.e. Frank-vectorcardiogram). The heart vector is, generally speaking, an equivalent dipole in an infinite, homogeneous medium measured sufficiently far from the source to make the quadrupole and higher order terms negligible. For the computation of the body surface potential distribution the multiple dipole approach was chosen. This approach consists of the computation of multiple equivalent dipoles, each representing a volume compartment within the heart. For this purpose, the heart was partitioned into 1239 compartments. The center of each compartment lies on regular grid points in hexagonal space, 5 units apart. An equivalent dipole is computed separately for each compartment. The 1239 dipoles acquired by this procedure are used as an equivalent source in the torso model. The torso model and its properties have been described elsewhere (68).

4.1.1.3 *Equivalent source during repolarization*

The heart vector for repolarization is calculated in a similar fashion as for the depolarization. Depolarization is assumed to be a non-conducted phenomenon. This implies that the duration of the absolute refractory periods and the time course of repolarization in each muscle

element is assumed to be predictable at the time of excitation of this element. In contrast to depolarization, repolarization of a muscle element is assumed not to influence its neighbours. These assumptions may turn out to be erroneous. Lack of experimental data on normal sequence of repolarization, however, does not justify inclusion of any features of possible propagated response during repolarization in this model. Few reports deal with the duration of the refractory periods as measured by excitability (37,73), where the first moment of response to an artificial stimulus signifies the end of the refractory period. However, no data are available on normal repolarization. Reasons for this are partly of a technical nature; the needle electrodes used to measure depolarization yield tracings which are very difficult to interpret as far as repolarization is concerned. It is also believed that, whereas the depolarization is hardly affected by the electrodes, the repolarizing process is. No measurement has been done with micro-electrodes which systematically maps the whole heart. Furthermore, the repolarization is a gradual process extending over several hundred msec. Even in good tracings are available, the error in interpretation will be large. However, the lack of experimental data is easily made up for by the number of speculations about the repolarization process.

There are numerous reports which have attempted to analyze either quantitatively or qualitatively the excitation and repolarization relationships from body surface electrocardiograms and vectorcardiograms. Measurements reported in the context of the ventricular gradient concept can be used to evaluate the results of the present models of repolarization.

4.1.1.4 *Ventricular gradient concept*

Wilson et al. (153) found experimentally that integrals of electrocardiographic potentials over the time of one heart cycle in any lead are far from zero. He associated with this residual voltage-time integral the name 'ventricular gradient' and concluded that 'the sum of the areas of the initial and final deflections of any curve, which represents the excitation of the ventricular muscle is a measure of the effects produced by local variations in the excitatory process, and particularly by local variations in duration of the excited state.'

Later Burger (19) defined ventricular gradient as the time integral of the heart vector over the period of one heart cycle:

$$\vec{G}_{QRS,T} = \int_{\text{cycle}} \vec{H} dt \quad (34)$$

which is therefore intrinsically a spatial vector quantity. Following Burger's line of thought [Burger (20) (pp 98-102)] we will next derive some important properties of the ventricular gradient; first, we assume the transmembrane potential to be a square wave and then we will extend this concept to any arbitrary function which returns to an initial value within the period of integration. Let us assume the myocardium to be a volume of arbitrary shape. At a given instance, we assume a part of the muscle to be excited, whereas the remainder is still not excited. The surface between non-excited and excited areas can be expressed as a function of coordinates and time:

$$F(x, y, z, t) = 0 \quad (35)$$

in which x, y and z are orthogonal coordinates and t is time. From the above equation t can be formulated as a function of coordinates:

$$t = f(x, y, z) \quad (36)$$

Since the transition between excited and non-excited zone is infinitesimally small due to the square wave 'action potential' at each cell, we can describe the electrical behaviour of such isochronous surface as a dipole layer; quantitatively, this dipole layer will be characterized by a quantity \vec{K}_i , with physical dimension of current dipole moment per unit area.

Since the gradient of the function $f(x, y, z)$ has the direction of the normal, $d\vec{n}$, to the surface, we can state that

$$dt = |\nabla f| dn \quad (37)$$

The 'heart vector' is defined as a vector sum of all elemental current dipole sources in the heart region; when the source is confined to the dipolar layer, the definition has the form

$$\vec{H} = \int \vec{K}_i ds \quad (38)$$

and the 'ventricular gradient' is then, for the depolarization process alone:

$$\vec{G}_{QRS} = \iint \vec{K}_i ds dt = \iint \vec{K}_i ds |\nabla f| dn \quad (39)$$

Since vectors ∇f and \vec{K}_i have the same direction and $ds dn = dv$, equation (39) can be rewritten in another form:

$$\vec{G}_{QRS} = \vec{K}_i \int \nabla f dv \quad (40)$$

We assume that the repolarization occurs at time \mathcal{T} after depolarization. Because this time interval is not the same for all parts of the myocardium, \mathcal{T} should also be a function of the coordinates; $\mathcal{T} = \mathcal{T}(x, y, z)$

Equation (40) solved for the repolarization will give a result analogous to that for the depolarization:

$$\vec{G}_T = -\vec{K}_i \int (\nabla f + \nabla \mathcal{T}) dv$$

In the above formula, the minus sign at \vec{K}_i appears due to the reverse polarization of the dipole layer.

For the whole depolarization - repolarization cycle, therefore, the ventricular gradient is:

$$\vec{G}_{QRS,T} = -\vec{K}_i \int \nabla \mathcal{T} dv \quad (41)$$

From equation (41) it follows that the ventricular gradient is independent of the way in which excitation passes through the heart. So far, Burger's line of thought was followed.

To evaluate the relationship of the ventricular gradient with a general time varying source distribution, we should first make several assumptions.

(a) Each cardiac cell has its own time-potential function which can be initiated by the neighbouring cell, but otherwise proceeds on its own and is not influenced by the fields of other cells (Assumption B7).

(b) The source region is homogeneous and isotropic (constant conductivity σ) for intercellular source currents (Assumptions C1 and C2).

Excitation and repolarization of the heart can be expressed as a time varying distribution of potentials in the source region. Let us use for this 'impressed' potential the notation Φ_i to distinguish it from the actual potential Φ . (Note that the actual potential satisfies Poisson's equation, whereas the 'impressed' potential is an effective field which would exist before all boundary conditions of the surrounding volume conductor are met.)

We use the 'impressed' current density \vec{J}_i for description of the sources; this quantity has the dimensions of a current dipole moment per unit volume and evolves, where above assumptions are met, from the 'impressed' potential (Ohm's Law):

$$\vec{J}_i = -\sigma \nabla \Phi_i \quad (42)$$

Since the heart vector is defined by:

$$\vec{H} = \int \vec{J}_i dv \quad (43)$$

and by combining equations (34) and (43) we have for the ventricular gradient:

$$\vec{G}_{QRS,T} = \int_{\text{cycle}} \int_V \vec{J}_i dv dt = \int_V \left(\int_{\text{cycle}} \vec{J}_i dt \right) dv \quad (44)$$

The term in brackets, expressed as 'impressed potential' becomes:

$$\int_{\text{cycle}} \vec{J}_i dt = -\sigma \int_{\text{cycle}} \nabla \Phi_i dt \quad (45)$$

Since this term has physical dimensions of surface charge density (electric displacement vector), we can give an interesting physical interpretation of the ventricular gradient as a contribution of apparent charges, which appear on boundary surfaces between subvolumes of source regions. In each subvolume cells are of identical time course of impressed potential and differences exist in the time course of the impressed potential from subvolume to subvolume. The profile vector \vec{P}_i is defined as:

$$\vec{P}_i = -\sigma \int_{\text{cycle}} \nabla \Phi_i dt \quad (46)$$

With substitution of \vec{P}_i in equation (44), the ventricular gradient becomes:

$$\vec{G}_{QRS,T} = \int \vec{P}_i dv \quad (47)$$

which is only a finite value for non zero values of \vec{P}_i .

If the shape and duration of the action potential are assumed to be dependent only on their location, then \vec{P}_i is constant for each region, independent of the course of depolarization. Non-zero values of \vec{P}_i only happen if adjacent subvolumes have different action potentials, either by different durations, or different slopes, or different resting potentials. In the last case, a constant potential difference exists continuously. The term \vec{G} can, of course, also be evaluated for parts of the cycle. From its definition, equation (34) follows that \vec{G} is a measure of the average direction and size of the vectors. If equation (47) has zero value, \vec{G} for the depolarization (\vec{G}_{QRS}) must be equal to \vec{G} for the repolarization (\vec{G}_T) and opposite in direction.

This is illustrated in Figs. 4.2 and 4.3. In Fig. 4.2 a square wave was taken as transmembrane potential function of each element of our model; the resulting ventricular gradient over one cycle of excitation and repolarization was zero. Fig. 4.3 shows the results if a simulated action potential is assigned which is identical for all elements. The ventricular gradient which resulted was also zero. The \vec{P}_i 's are dependent on location only, their size and direction is

Fig. 4.2 Heart V.C.G. computed with square wave as elemental potential function. In the left column are seen from top to bottom the X-component, -Y component, Z component of the pure dipole. The amplitude scale for X, Y, and Z components is arbitrary, the time scale is indicated just below the Z-component. Note that the Y component is displayed with reversed polarity. In the right hand column are seen from top to bottom the projection of the V.C.G. loop on transverse, frontal and left sagittal principle plane, respectively. The inscription direction is indicated with an arrow, for the depolarization.

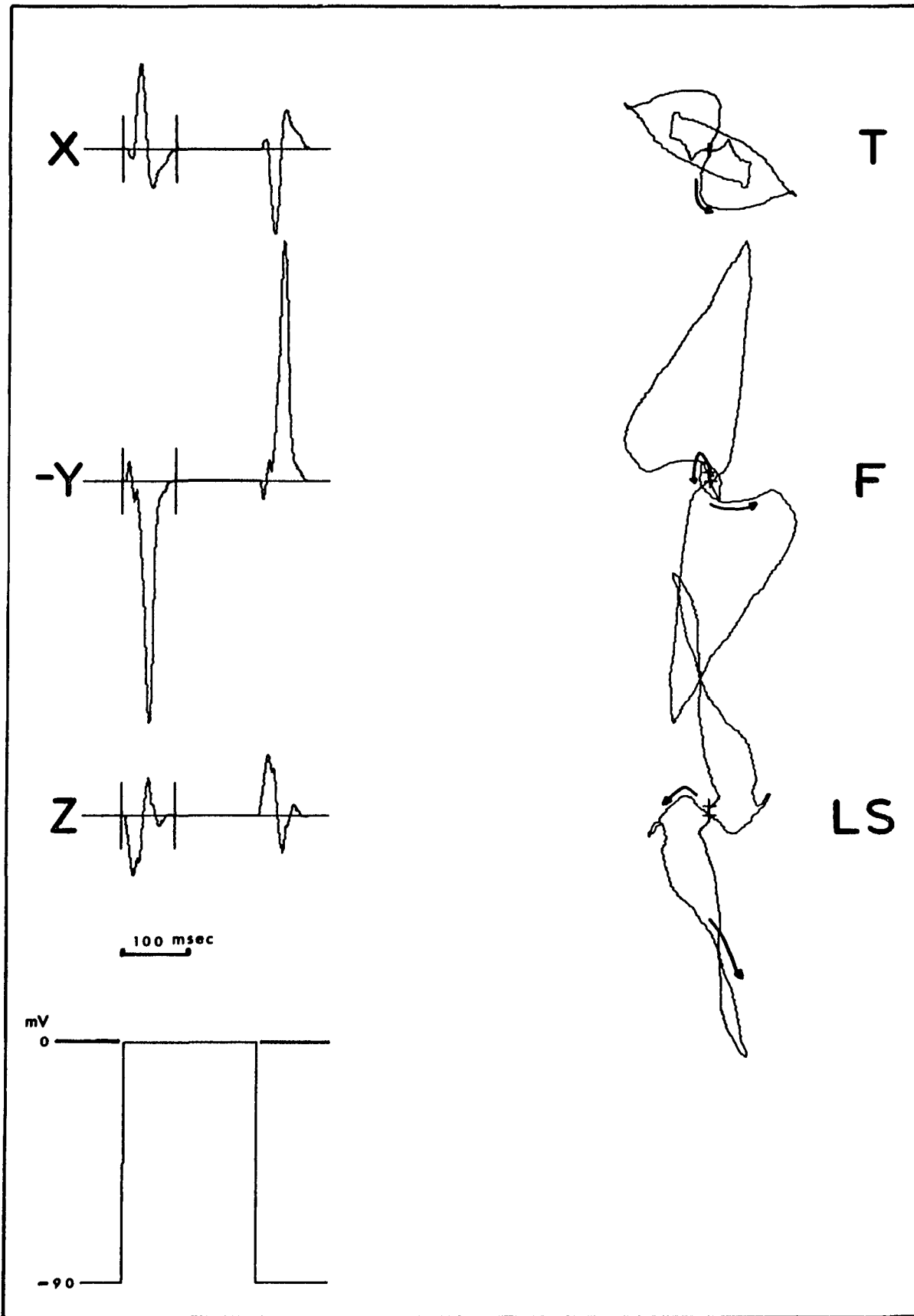


Fig. 4.2

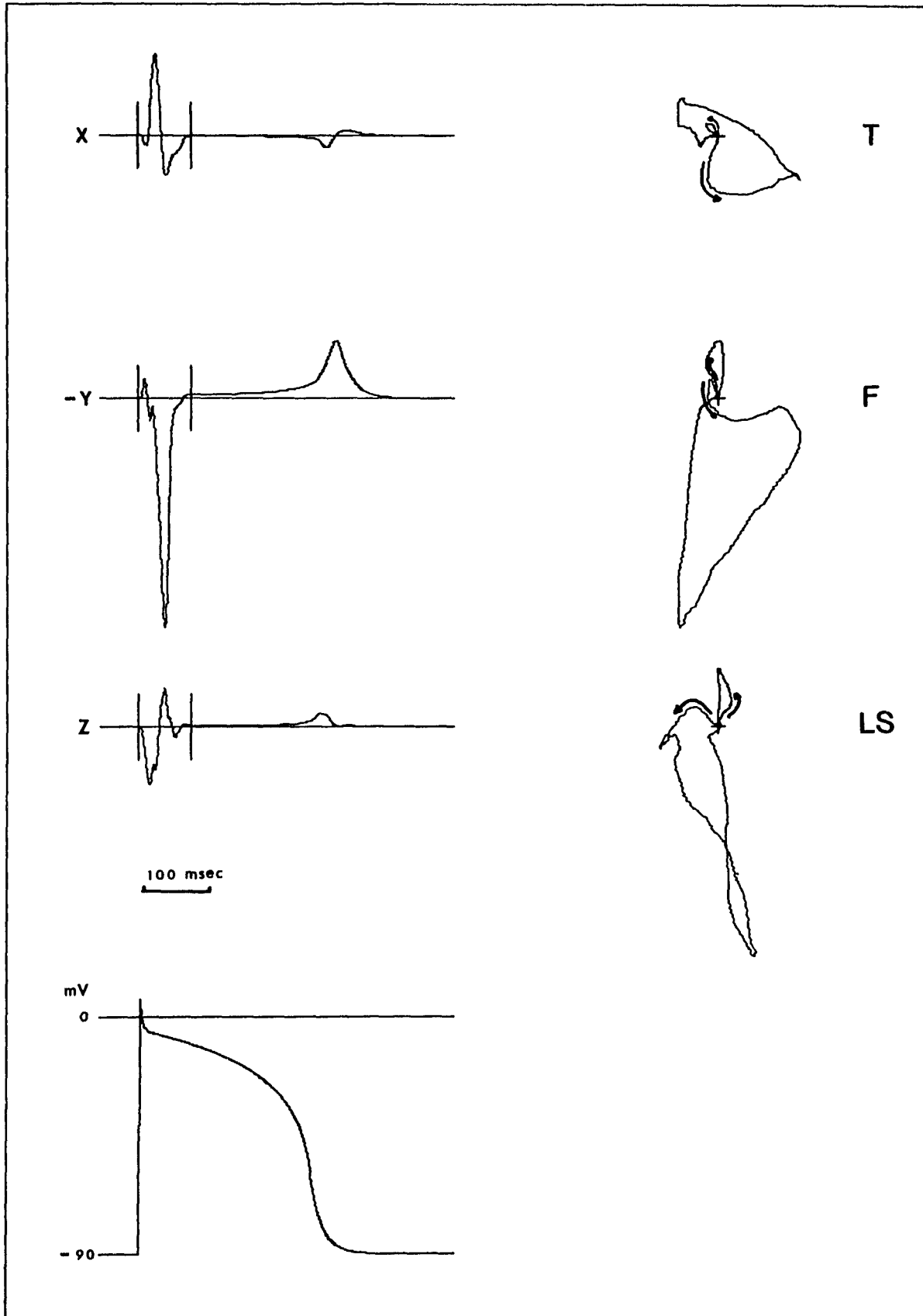


Fig. 4.3 Heart V.C.G. computed with action potential uniform throughout the heart. Layout is identical to the one in Fig. 4.2

dependent on the action potential in the subvolumes of the surrounding heart region. Use of the term 'profile' vectors is proposed, since these vectors establish for a given heart the contribution of each separate region to the total gradient vector. These vectors are not necessarily identical in all subregions and thus establish a profile of contributions for all different subregions. The slope of a profile is proportional to the size of the profile vectors. The slope of the profile is said to be constant if all profile vectors are identical in magnitude.

An ability to account for the existence of these profile vectors is one basic requirement for any model of the ventricular repolarization.

4.1.1.5 *Hypothesis about $G_{QRS,T}$*

The hypothesis put forward, can be divided into two categories.

I. Explanation of differences in action potentials purely on the basis of differences in location, i.e. relative position of the various elements in anatomical sense.

Explanations for differences in action potential duration on the basis of differences in location are evidently considering factors in the conditions of the heart cells which influence the action potential duration and which are not evenly distributed throughout the heart.

Put forward as such factors were:

A. temperature differences (75,65,97)

B. fiber-stress distribution. (118)

II. Explanation of differences in action potential duration on the basis of differences in time of excitation, i.e. relative position of the elements in physiological sense.

From measurements on leads in the frontal plane (standard leads I, II, III) it was concluded that the only possible way of explaining the T-wave polarity was to assume the sequence of repolarization to be the reverse of the sequence of depolarization, though no obvious reason is present for this 'reversed' sequence (55).

4.1.1.6 *Hypothesis*

The following hypothesis is put forward:

The ventricular gradient of normal human hearts can be explained if it is assumed that:

A. The action potential duration of the cells of the Purkyne fiber network is longer than the action potential duration of ventricular muscle cells, and

B. That the elements of the transitional cells have action potentials which are intermediate in duration to Purkyne fiber network cells and ventricular muscle cells, and

C. That the action potential duration of muscle fibers of the right ventricle is shorter than that of the left ventricular muscle fibers.

It has been reported that the action potential durations of the Purkyne fiber network are the longest close to the last termination, just before penetration into the muscle fibers (92).

The transitional fibers reveal action potentials intermediate to the typical Purkyne fibers and the typical ventricular muscle fibers (80).

A close relationship is observed between mechanical and electrical systole. As well known mechanical systole of the right ventricle is shorter than that of the left ventricle. It is thus conceivable that the action potential duration in general will be shorter in the right ventricular wall than in the left ventricular wall. It has also been reported that the action potential duration is dependent on the mass of tissue, being longer if the mass is larger (29).

4.2 *Methods*

4.2.1 *Normal excitation*

The point labelled R1 in section 31 (Fig. 4.4B) was used as a starting point of excitation in the right ventricle. This point is located in the Purkyne fiber network at the base of the anterior papillary muscle. In the left cavity four starting locations were selected; L1 in the Purkyne network at the septum (Fig. 4.4D), L2 in the Purkyne network paraseptally at the posterior wall (Fig. 4.4E), L3A and L3B, paraseptally at the anterior wall (Fig. 4.4A,C). Points L1 and L3A fired at time 0, L2, L3B after 2 msec and R1 after 10 msec.

Conduction velocities were chosen to be close to those reported by Durrer et al., i.e. 49 cm/sec for ventricular myocardium and 245 cm/sec for Purkyne fibers. The correction algorithm mentioned in page 61 was used. The previous interval was assumed to be of infinite length, which results in maximum refractory periods for each element. In both right and left ventricular Purkyne network activation was allowed for a limited number of timesteps, in preliminary runs.

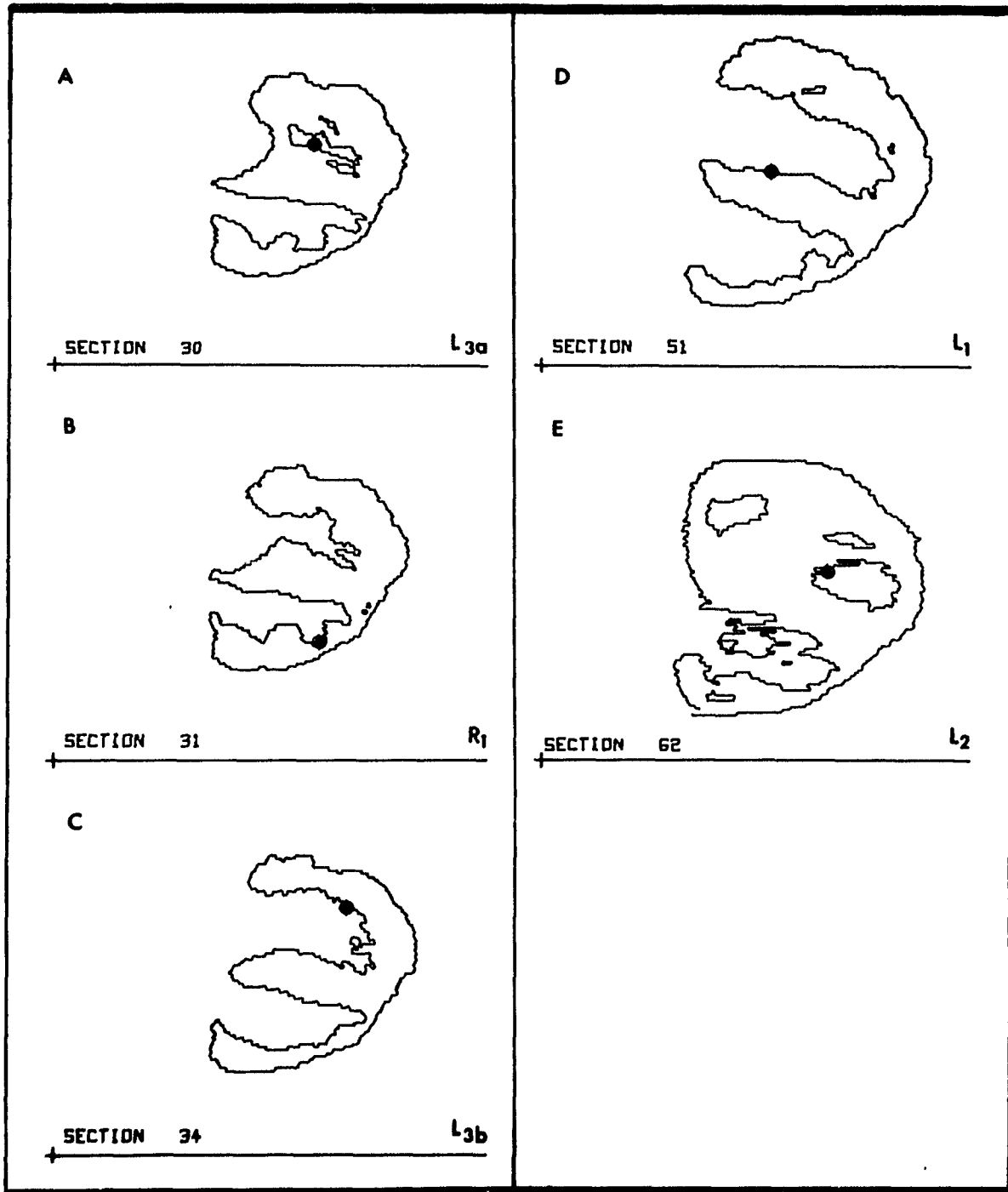


Fig. 4.4 Starting locations for a normal excitation. For the 5 starting locations used the sections are seen. The black dots indicate in the sections the starting locations itself. At the 5 starting locations the indicated elements are 'excited' at predetermined times, reflecting arrival of the excitation from the left and the right bundles. Time of excitation: L₁ and L_{3a} at time 0. L₂, L_{3b} at 2 msec, R₁ at 10 msec.

In the final runs Purkyne network activation was allowed up till 50 timesteps (25 msec) after onset of excitation at any starting point. This model is referred to as 'restricted' model on page 225.

4.2.2 Heart vectorcardiogram - depolarization

Either a step function or the initial part of an artificial action potential was used as voltage time function for each element (Fig.4.5). The differences between the two functions are mainly in the size of the signal (90 mV for the step function and 100 mV for the action potential), and the first fast repolarization (phase 1) of the action potential.

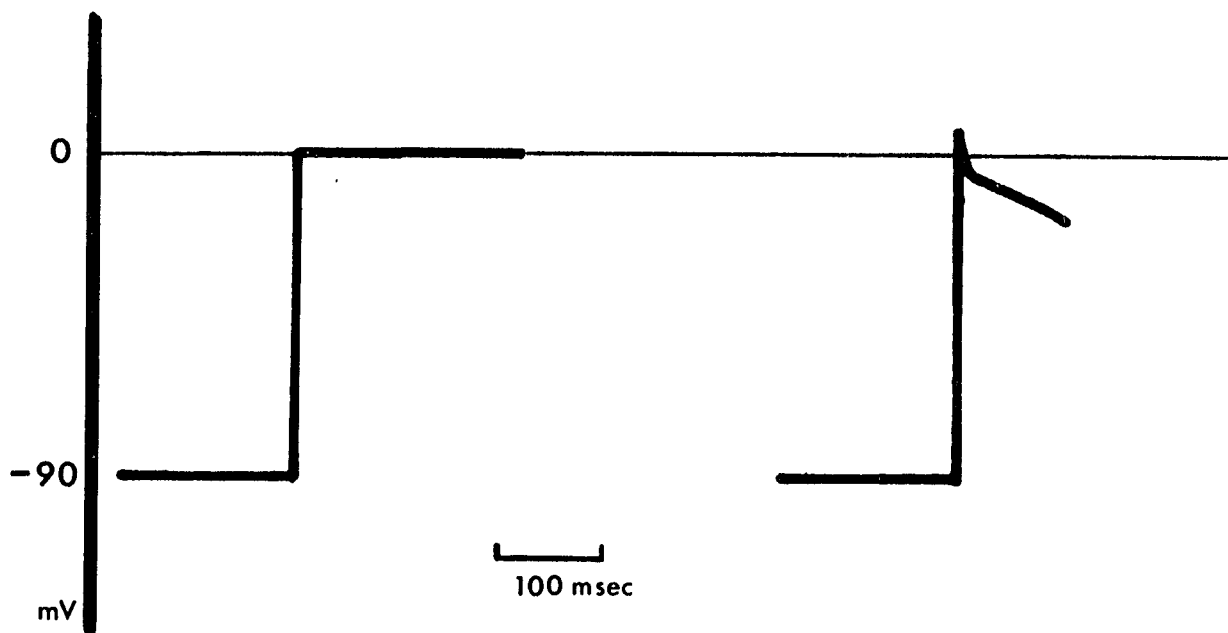


Fig. 4.5 *Elemental potential functions.*

The potential functions seen in this figure were used for the calculation of the heart VCG during depolarization. At left side a step function, at right the initial part of a simulated action potential.

4.2.3 *Heart vectorcardiogram - repolarization*

Different shapes of action potentials of varying duration are assigned to the various elements, by means of the element type number. Systematically the type numbers from 5 to 15 were used. Type numbers from 1 to 4 were reserved for Purkyne fiber elements and special type elements. The algorithm which connects type number and action potential duration or slope, is such that the lower type numbers are associated with action potentials of which the voltage time integral is large and high type numbers with small voltage time integrals. The profile vectors thus point from elements with the lower number towards elements with the higher numbers. Two variables were used to regulate from experiment to experiment the size of the profile vectors. The first variable controlled the differences in duration of the action potential, the second variable controlled the slope of the plateau phase of the action potential. Other variables specifying the shape of the action potential (see below) were held constant. A linear transition of action potential duration and slope variables is assumed between the consecutive type numbers, unless otherwise specified.

4.2.3.1 Waveforms used as action potential

Artificial action potentials are used. Though it is possible in the model to use actual measured action potentials, artificial ones are preferred, since they are easier to manipulate. As basic action potential duration was chosen 260 msec. For an element type 5 a 'normal' action potential is seen in Fig. 4.6. This normal action potential is specified by:

$$V_m(t) = V_p + I_g \left(1 - \frac{t(1 - e^{-\alpha(V_p + 0.6)})}{APD} \right) + (V_o - V_p) e^{-\gamma t} \quad (48)$$

if $t_o < t < t_o + APD$, where $\alpha = .0333/FS$ and $\gamma = .0666/OT$, and

$$V_m(t) = V_R - (V_R + 0.6) e^{-g\alpha(t - APD)} \quad (49)$$

if $t_o + APD < t$

- a) Resting potential of -90mV ($V_R = -.9$ dV)
- b) Overshoot peak of +10mV ($V_o = .1$ dV)
- c) A fast repolarization within 10 msec (OT = .010 sec)
- d) A plateau at -5mV ($V_p = -.05$ dV)
- e) A duration of 260 msec, measured at a
transmembrane potential of -60 mV (APD = .260 sec)
- f) The slope of phase 3 is specified by the membrane voltage
('slope voltage') at which the second exponential function
is within .03% of its asymptote. (dashed extension).
(FS = -1.10 dV)

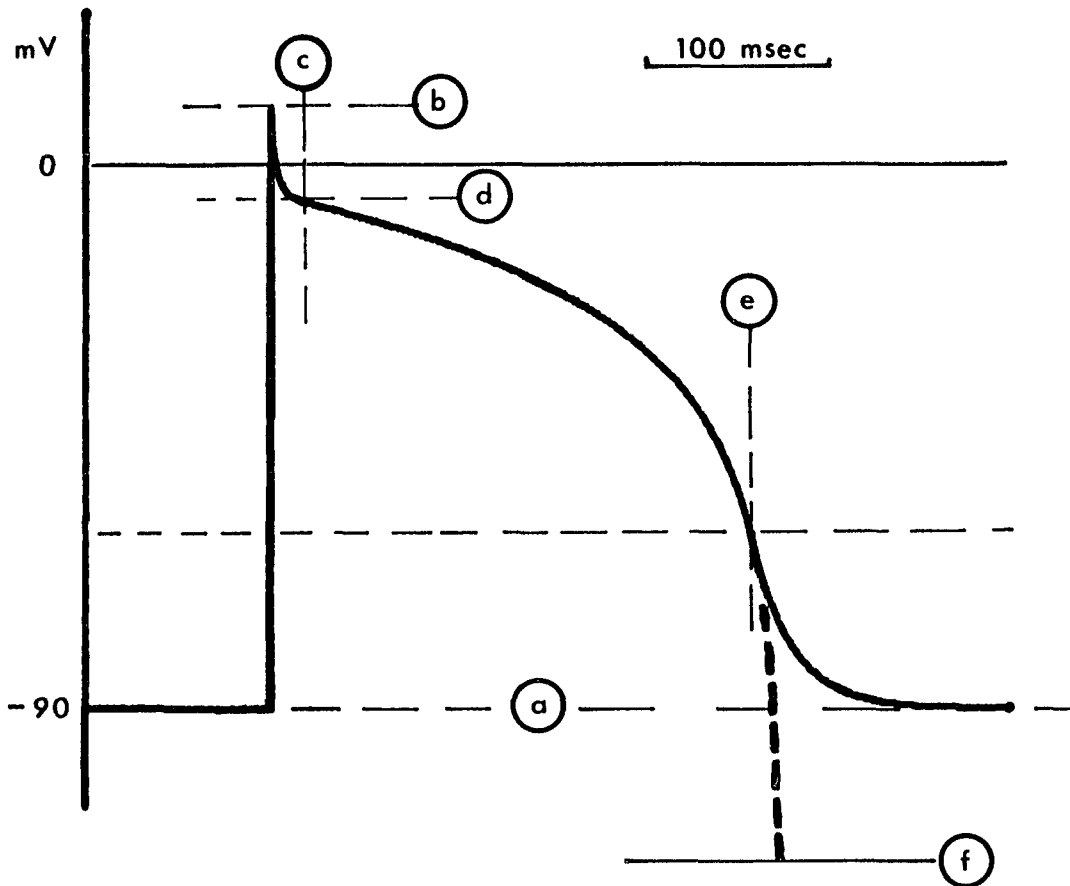


Fig. 4.6 The artificial action potential. A standard action potential for normal fibers. The parameters specifying the shape of the potential function are indicated.

a = the resting potential, b = overshoot peak

c = the duration of the first fast repolarization

d = plateau voltage

e = duration of the action potential

f = parameter regulating the slope

The artificial action potential is made up of 3 exponential functions. The first for the fast repolarization, the second for the slower repolarization following the plateau phase, the third (which is independent of the previous two) for the repolarization during the relative refractory periods.

For similar specifications, except for a duration of 130 msec and a 'slope voltage' (sub f above) of -270 mV the resulting action potential is seen in Fig. 4.7. This action potential was used for the transitional infarction fibers of the experiment in paragraph 5.2.5 (see below). The profile vectors arising between two elements of different types can be found by the difference area of the two superimposed action potentials. With each experiment the profile of the left ventricle wall and the right ventricle wall will be indicated in a little diagram which shows from endocardium to epicardium the area under the action potential at each location. The profile vectors are equal to the difference between these areas. For the models specified in the following paragraphs identical sequences of depolarization were used as in paragraph 4.1.1.

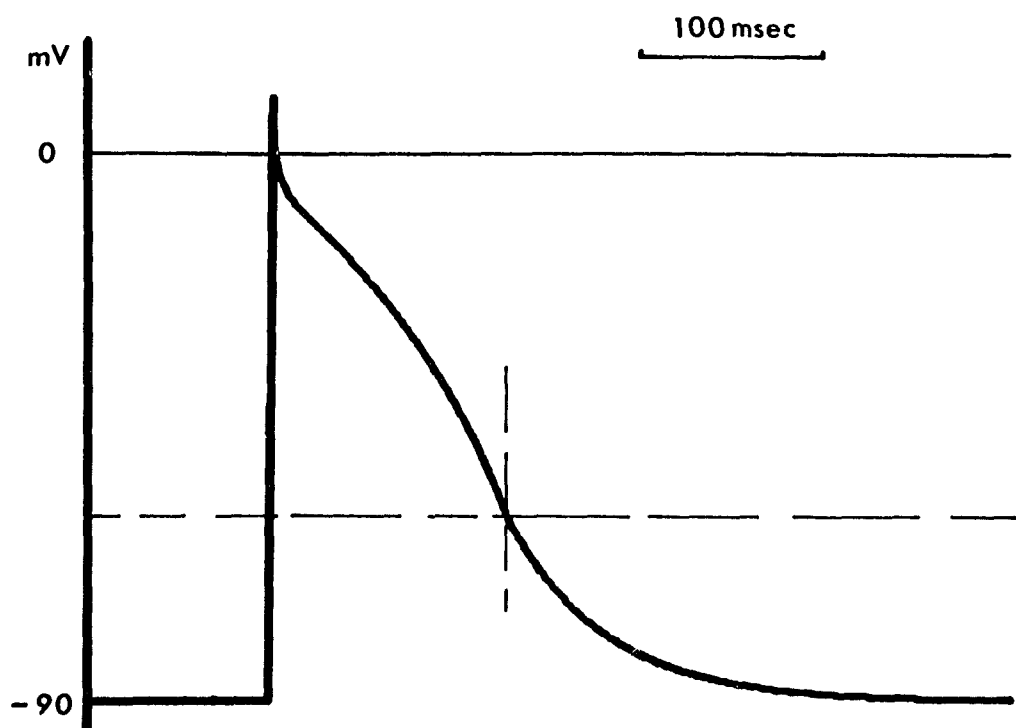


Fig. 4.7 The action potential of infarcted fibers. An example of the action potential used in the transitional zone of an infarction. Only parameter e (duration) and f (slope) (see legend fig. 4.6) are changed.

4.2.3.2 *Uniform profile*

No differences in type are assumed. The action potential for element type 5 is used for all elements. This model is used to test the 'reversed sequence' hypothesis of repolarization.

4.2.3.3 *Temperature profile*

Model 1A. Differences in type are arranged on the basis of the distance of the elements from the endocardial wall. The first layer around each cavity is typed No. 5, with the largest area under the action potential. The next layer is typed No. 6, etc. In Fig. 8A the typing of the cells is seen for Section No. 40. In this version both left and right cavities start with identical types of elements at the endocardium.

Model 1B. Assignment of element types from 5 to 15 for the left ventricle is the same as in model 1A. The right ventricle is assigned types 10 to 15, from endocardial to epicardial surface.

4.2.3.4 *Stress profile*

Model 2A. The distance to the left cavity was taken as measure for the typing. In the left ventricle wall and septum the type numbers 7,6,5,6,7,8 ...15 are assigned from endocardial to epicardial surface. The right ventricle is not typed, but is considered a part of the left ventricle. This results in type 15 mainly for the right ventricle wall (Fig. 4.9A).

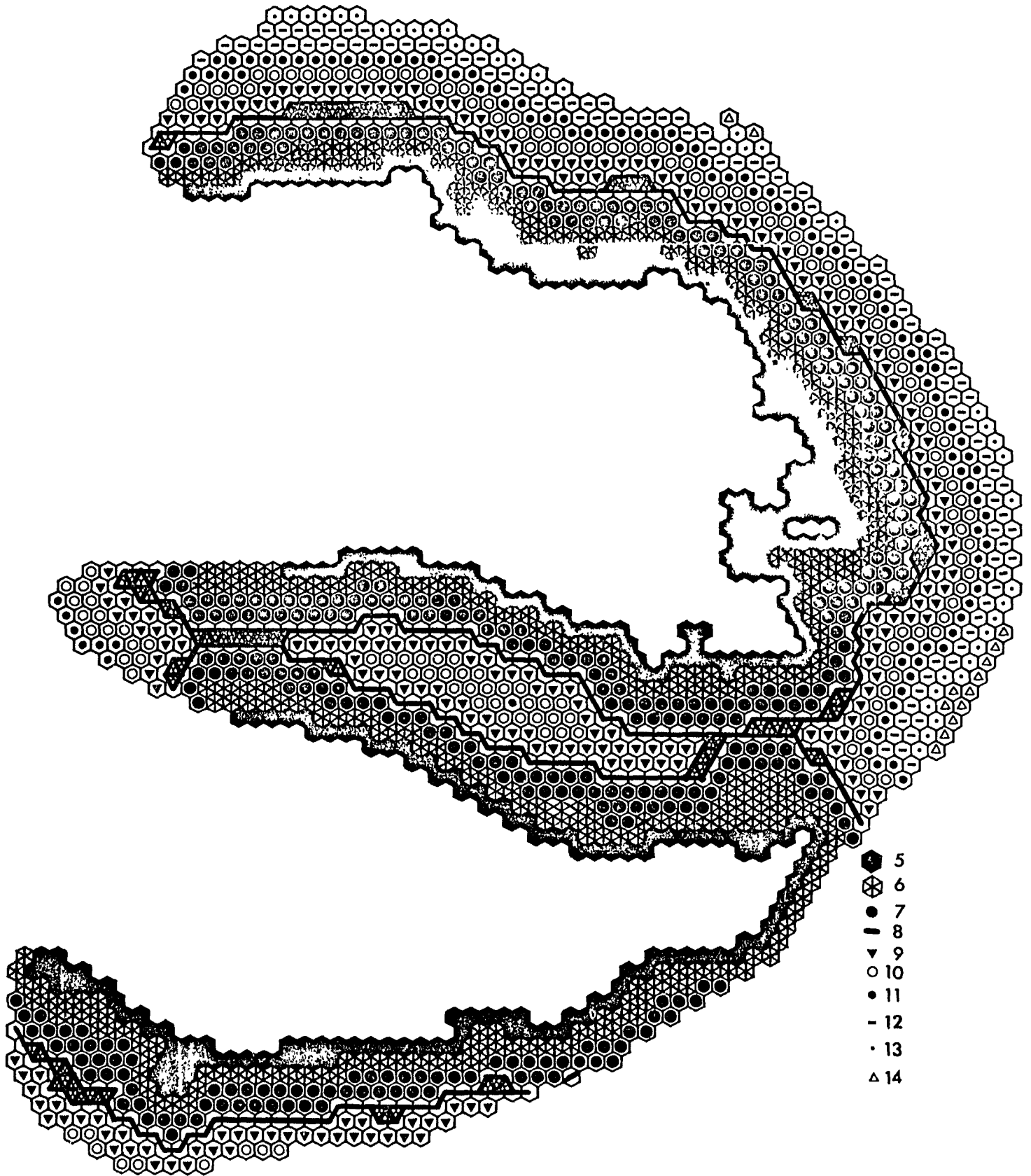


Fig. 4.8 A

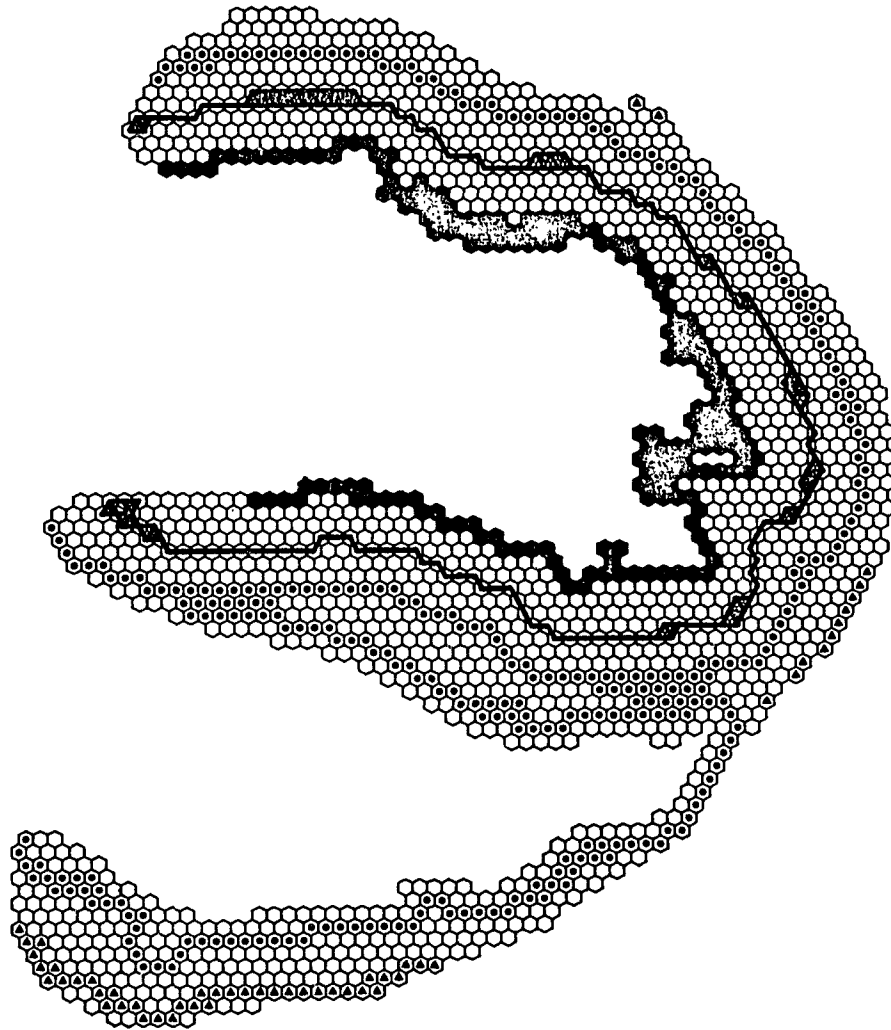


Fig. 4.8 A & B Typing of elements in repolarization model 1A,B

The element type numbers in section no. 40 are indicated. At both left and right endocardium the type numbers start with 5, increasing with each layer of elements with one. The symbol used for each type is indicated in the right hand bottom corner of Fig. 1A. In fig. 1B only type 5, 8, 11, and 14 are indicated. The symbol of type 14 (open triangle) is replaced by a solid triangle. In model 1B typing starts with 5 at the left endocardium and 10 at right endocardium.

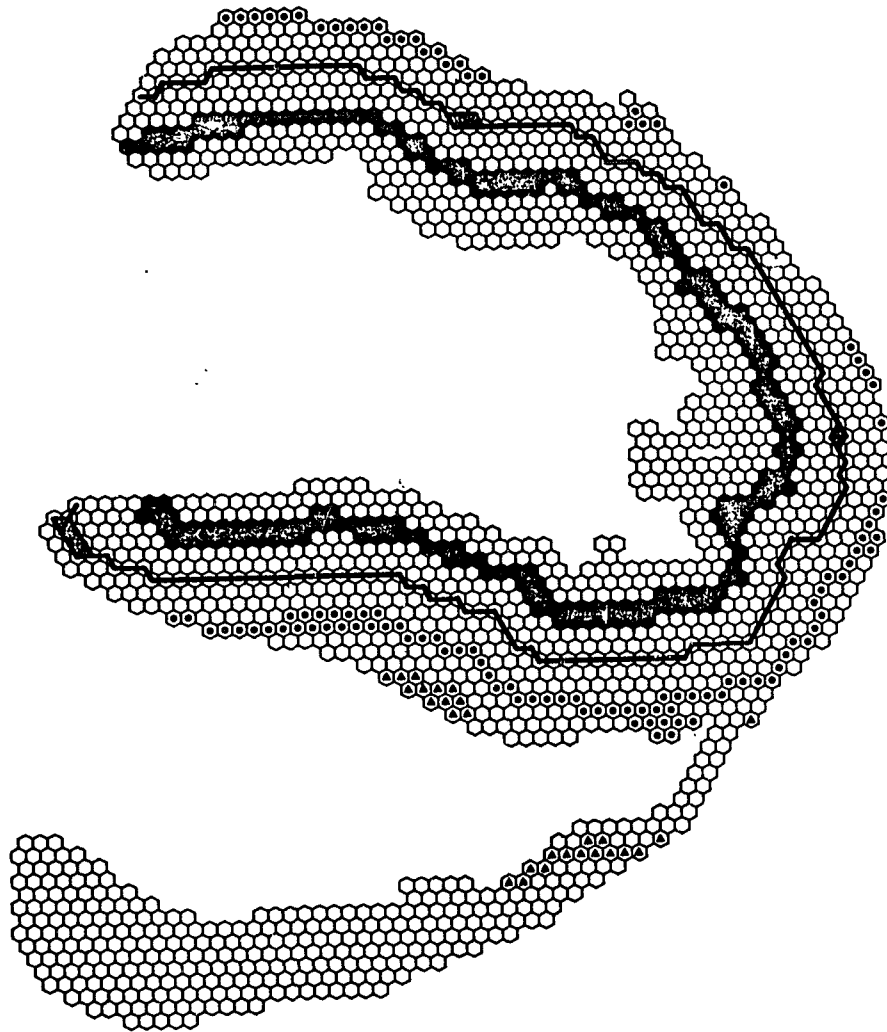


Fig. 4.9 A & B Typing of elements in repolarization model 2A,B

Only type 5, 8, 11, and 14 are indicated with the same symbols as used in fig. 4.8B. In model 2A the third layer of elements around the left cavity starts with type 5 the neighbouring elements increase with 1 etc. In model 2B, typing starts with 5 around the left cavity, and with 10 around the right cavity.

Model 2B. The distance to both left and right cavity was taken as measure for typing. The first two layers around the left cavity are typed 5, the next two 6, the next two 7, from here on each next layer with a type increase of 1. At the right endocardial site typing started with 10 and increased with each layer of elements. (Fig. 4.9B)

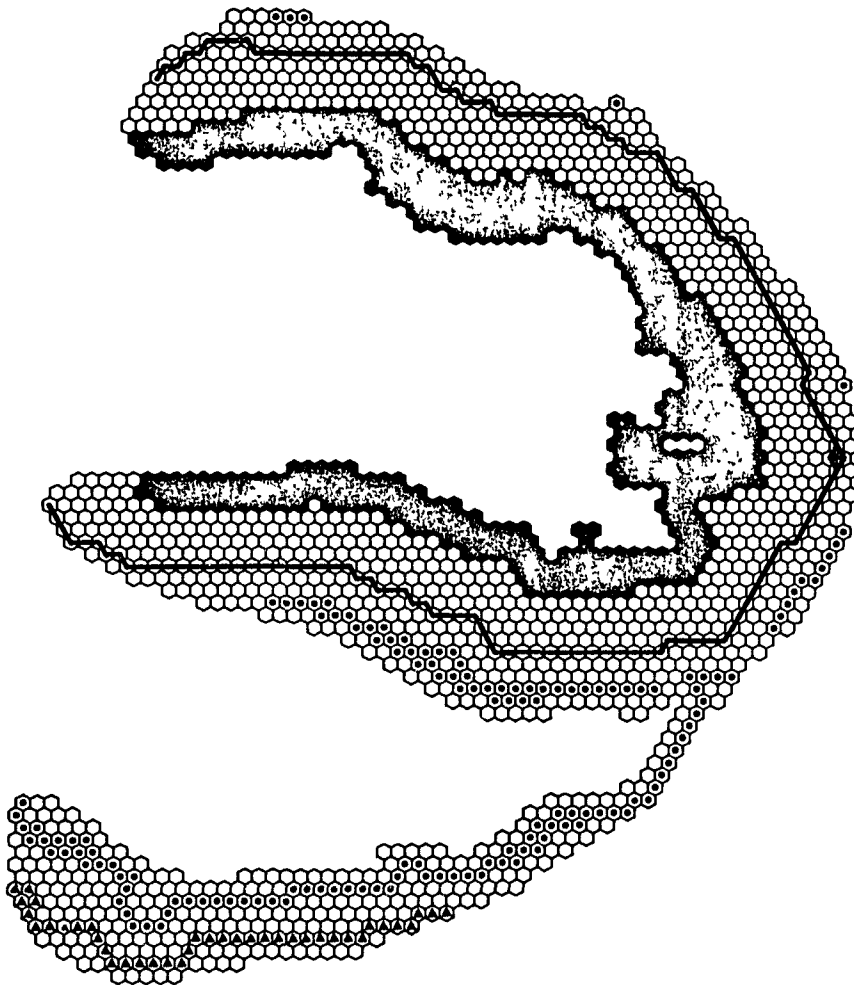


Fig. 4.9B

(See legend Fig. 4.9A)

4.2.3.5 *New hypothesis*

At the endocardial wall of the left ventricle typing starts with 5,6 etc.; whereas at the right endocardial wall typing increases from 5 with steps of 3, thus: 5, 8, 11. Furthermore the action potential duration of type 5 and 6 was increased by 20 and 10 msec respectively. This typing leads to the following profile of model 3. Immediately at the endocardial wall for both left and right ventricle long action potentials are found, however the transition in duration towards epicardium is much faster in the right ventricle wall than in the left ventricle wall.

Typing for above hypothesis is seen in Fig. 4.10.

4.2.4 *The lead systems*

For 9 instances of time during the depolarization and for 15 instances of time during repolarization the torso surface potential distribution was calculated from the 1239 distributed dipoles.

The potentials at the locations of the electrodes of the lead systems of interest were taken to form either the ECGs at these locations or to be synthesized to the VCGs of the appropriate lead systems. The lead systems studied were:

- a. the 12-lead system (154)
- b. the Burger-lead system (21)
- c. the Frank-lead system (52)
- d. the McFee-Parungao lead system (83)
- e. SVEC-111 lead system (124)

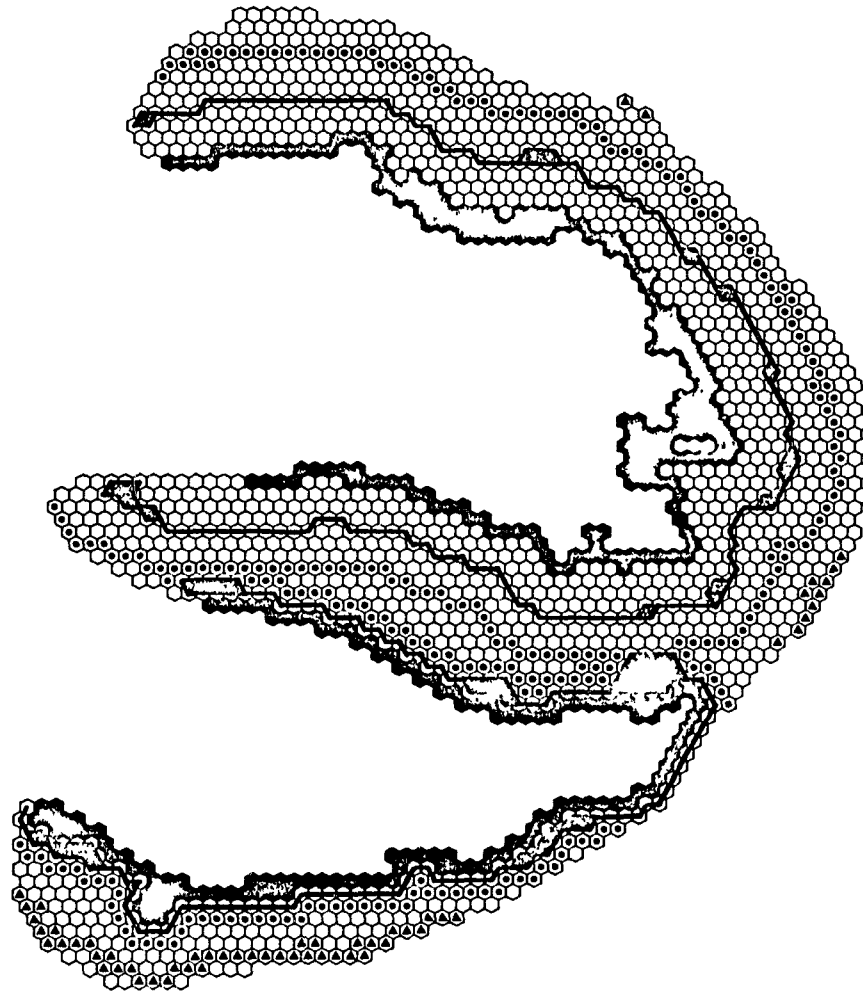


Fig. 4.10 Typing of elements in repolarization model 3. Only type 5, 8, 11, and 14 are indicated with the same symbols as used in Fig. 4.8B. At both endocardial sites typing starts with 5, in the right ventricle wall typing increases with 3, in the left ventricle wall with one.

4.3 Results

4.3.1 Normal excitation

The time for activation needed was 78 msec. The first wave-fronts are around the starting locations; at 20 msec after the onset of excitation the left ventricular endocardial surface is nearly completely excited. At 10 msec the earliest activation in the right ventricular wall starts. At 20 msec the first epicardial breakthrough is found at the area pretrabecularis on the right ventricular surface. The first breakthrough on the left ventricular surface occurs at 25 msec. The latest parts to be excited are the base of right ventricular free wall. Fig. 4.11 shows the isochrones for eight cross sections of the heart from base (Section A) to the apex (Section H).

4.3.2 Heart vectorcardiogram - depolarization

The QRS-complex of the H.V.C.G. as computed for the activation sequence described in paragraph 4.2.1 is seen in Fig. 4.12.

The inscription of the projection in the horizontal plane is counterclockwise. The centrifugal part of the loop in this projection starts out to the right and anterior, at 10 msec from the onset the rightward forces are at a maximum (Q wave in X), then the loop bends to the left anterior. The anterior forces are at their maximum at 15 msec (Q in Z), at 24 msec the maximum leftward forces are found (R in X), which rapidly diminish, to change into a rightward maximum at 40 msec (S in X). At that time the peak-posterior forces (R in Z) have been

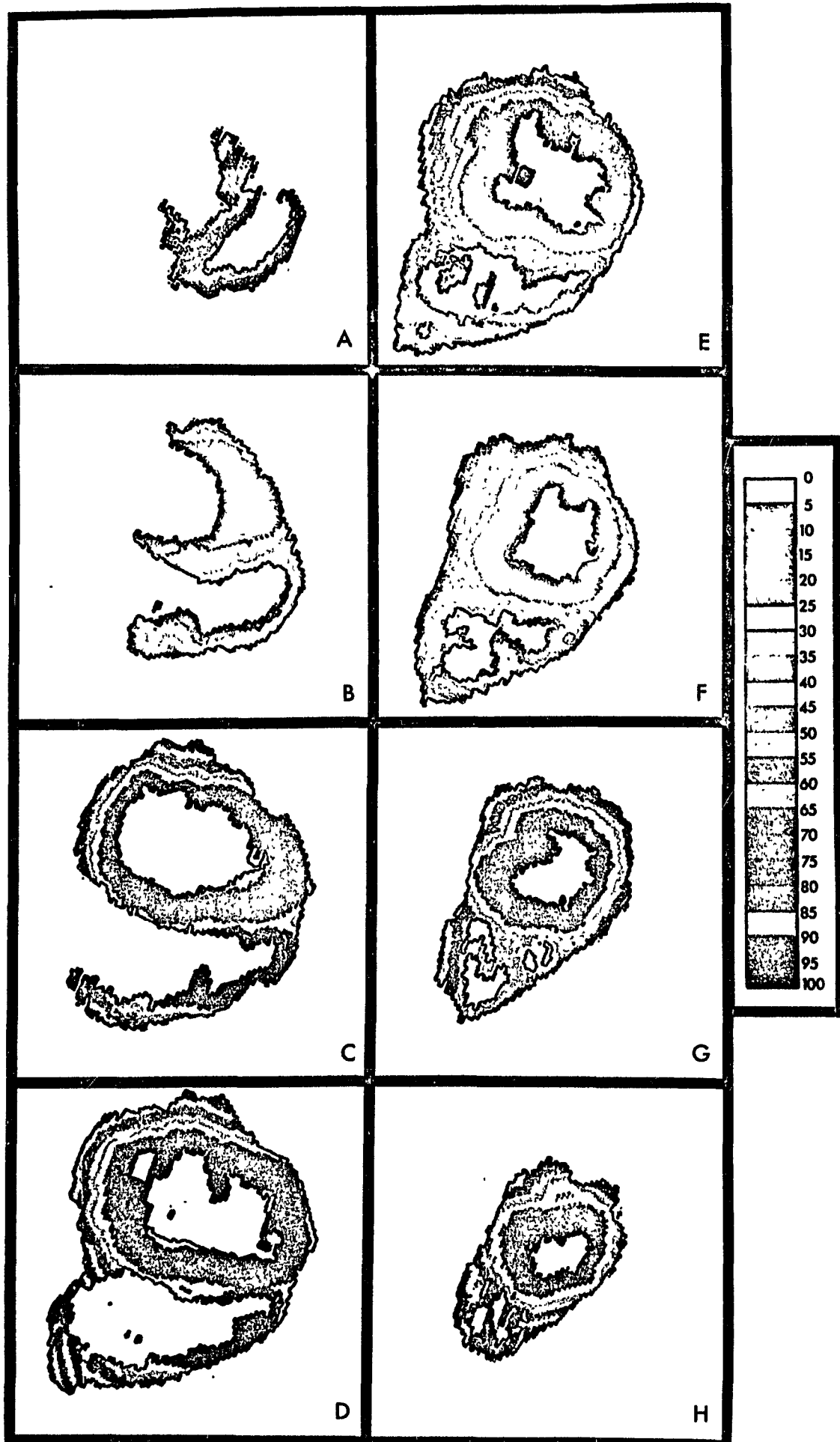
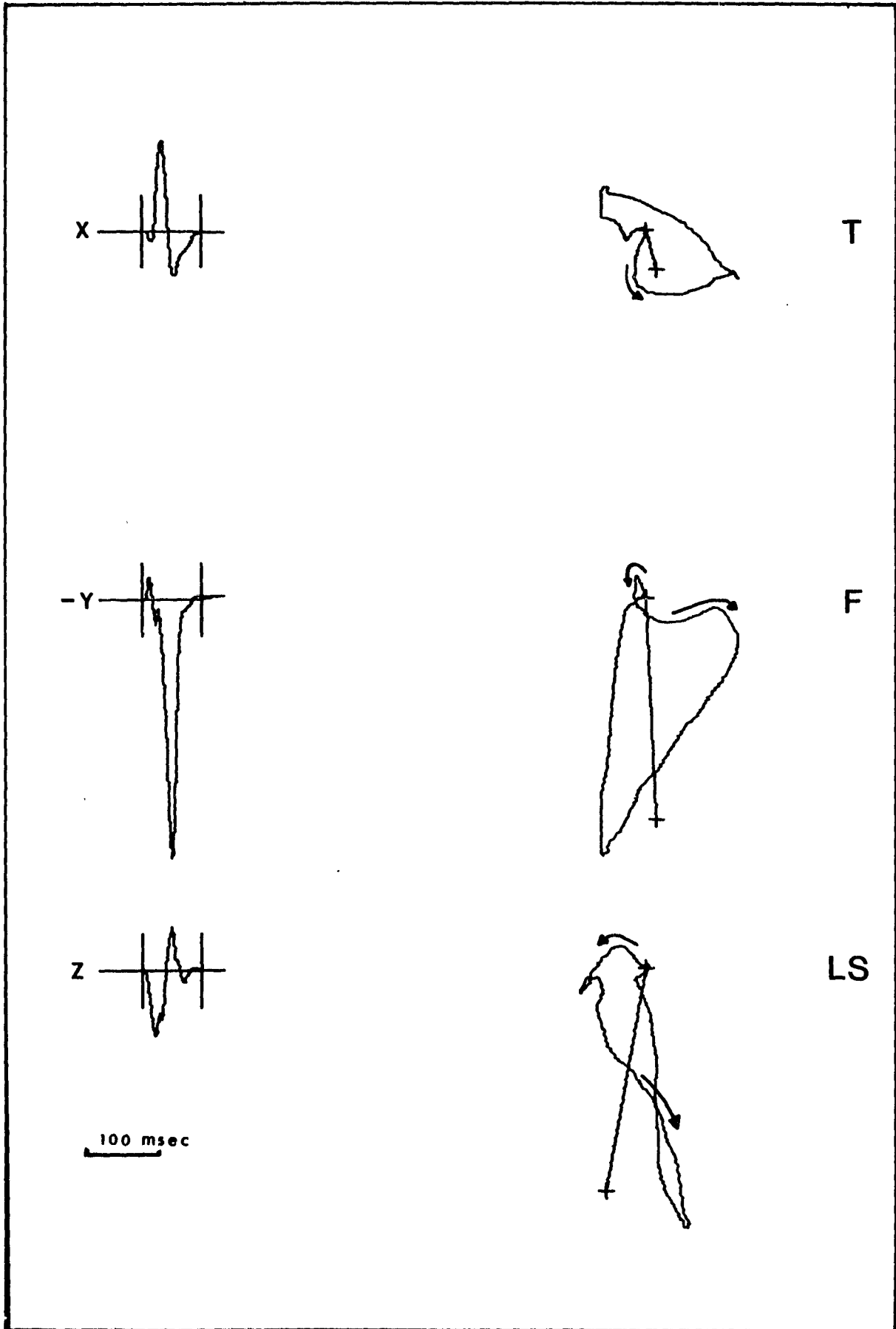


Fig. 4.11

Fig. 4.11 Isochronic representation of the simulated ventricular activation.

Sections A to H correspond to the intersections of the heart seen in Fig. 4.1. The sections are made at 1 cm interval perpendicular to an axis through the mitral valve opening and the left ventricle apex. The time scale is in msec after start of the first stimulation.

Fig. 4.12 The heart V.G.G. depolarization. Computed vectorcardiograms for the depolarization only. Left hand column contains the X, Y, and Z components of the vector cardiogram. Time scale is indicated at the bottom. Right hand column shows the projections of the spatial vector cardiogram on the principle planes, transverse, frontal and horizontal plane. The centrifugal limb is indicated with an arrow. The gradient vector is indicated with the + sign, and connected to the origin. Azimuth and elevation of the gradient vector are -75.6° and -79.5° respectively. The amplitude scale is arbitrary. Note that the Y component is displayed with reversed polarity.



TRADEMARK

Fig. 4.12

just passed (38 msec). The late and small forces are again directed anterior (S in Z at 56 msec), to return slowly to the origin. The general appearance of the loop is narrow. The inscription of the projection in the frontal plane is except for the first 16 msec, clockwise. The maximum superior forces are found immediately after the onset at 7 msec, to change in a small minimum at 16 msec. This rapid changes causes the loop to pass below the origin on the way from right to left. After the small minimum at 16 msec a transient upward deflection (seen as a notch in the y component) is encountered at 19 msec, after which the dominant inferior forces develop; with a maximum at 38 msec (S in Y), which quickly returns to the origin. The last centripetal part of this projection is smooth. The inscription in the left sagittal plane is predominantly counterclockwise, however the mid part of the loop shows a figure of 8 configuration.

The spatial vector loop is oriented parallel to the frontal plane, with a slight clockwise rotation around the y-axis. The main direction is inferior. The notches in Y and Z leads (at 16 and 22 msec respectively) are due to projections. The first deflection point a (6) is at 10 msec, the second deflection point b at 24 msec, the third deflection point c at 40 msec. The fourth is not discernable. The left/right ratio is $54/24$, the anterior/posterior ratio $35/24$, the superior/inferior ratio $13/142$. The H.V.C.G.s computed with the step function differed not essentially from the one computed with the artificial action potential as potential function of the elements.

The gradient for the QRS-complex has an elevation of -79.5 degrees and an azimuth of -75.6 degrees.

4.3.3 Heart vectorcardiogram - repolarization

4.3.3.1 Normal values of \vec{G}

Normal values computed for 650 Frank lead vectorcardiograms, recorded on male subjects in the age group between 40-70 are summarized in Table 1.

Table 1.				
<i>Ventricular gradient in 650 normal subjects (Frank-leads)</i>				
	\vec{G}_{QRS}	\vec{G}_T	$\vec{G}_{QRS,T}$	$\frac{\vec{G}_{QRS,T}}{\vec{G}_{QRS}}$
Magnitude (μVmsec)	66290.06 (SD 22699.80)	90960.69 (SD 27648.68)	122604.94 (SD 38633.39)	1.85
Elevation	-19.66° (18.04)	-26.59° (8.58)	-31.47° (12.43)	
Azimuth	39.93° (24.24)	-45.47° (15.64)	-10.50° (16.73)	
Angle $G_{QRS} G_T$	$= 74^\circ 46'$			
Minimum $G_{QRS,T}$	25550.78 μVmsec			
Maximum $G_{QRS,T}$	277573.87 μVmsec			

The ventricular gradient exceeds the gradient for QRS only, as seen from the values for the magnitude and the ratio of $\vec{G}_{QRS,T}/\vec{G}_{QRS}$. Note that the minimum $\vec{G}_{QRS,T}$ is still approximately half of the mean value for \vec{G}_{QRS} and note also that the directional SD value are much smaller for \vec{G}_T and $\vec{G}_{QRS,T}$ than for \vec{G}_{QRS} .

4.3.3.2 *Uniform profile*

The three components of the heart vector and its projections on transverse, frontal and left sagittal plane are seen in Fig. 4.13. The action potential used is also indicated. In the projection are entered the \vec{G}_{QRS} , \vec{G}_T . The vectors \vec{G}_{QRS} and \vec{G}_T are equal in magnitude and the spatial angle between them is 180° .

The profile diagram for right and left ventricle shows the area under the action potential in mVmsec, for the action potentials used from endocardium to epicardium. In the following illustrations the depolarization is omitted in the projections and replaced by \vec{G}_{QRS} . If $\vec{G}_{QRS,T}$ is not zero, it is entered in the projections as well.

4.3.3.3 *Temperature profile*

Fig. 4.14-16 contains the electrocardiograms for model 1A, for the different action potentials tried. In Fig. 4.14 the action potentials differ only in duration. In Fig. 4.15 the action potentials differ only in slope and have all identical durations. In Fig. 4.16 the action potentials are of different durations and different slopes.

Fig. 4.17, shows the results for model 1B for a few chosen combinations of duration and slope differences for the action potentials.

Not all combinations of the previous model are used, the less interesting ones are omitted. 4.17 B,C contains the results for different action potential durations. 4.17 A,D contains a combination of different durations and different slopes.

The ventricular gradients computed for this model, the angle subtended between \vec{G}_{QRS} and \vec{G}_T , and the ratio of $\vec{G}_{QRS,T}$ and \vec{G}_{QRS} are summarized in Table II.

Fig. 4.13 The heart V.C.G. - repolarization. Uniform profile.

Computed vectorcardiogram for depolarization and repolarization. Part A shows the X, Y and Z components, whereas part B shows the projections on the principal planes, from top to bottom, transverse, frontal and horizontal plane. \vec{G}_{QRS} and \vec{G}_T are marked with Q and T, respectively. Inscription sense of the loops is indicated. Part C shows the action potentials used for the computation, for fiber type 5, 10 and 15 (in this case identical). Part D shows the profile diagram for right and left ventricle. The vertical scale indicates the area under the action potential in mvmsec. The time scale for panel A and C is indicated below the Z-component, whereas the amplitude scale for panel A and B is arbitrary. Note that the Y component is displayed with inverse polarity, and that the vertical scale in panel D starts with 100 mvsec.

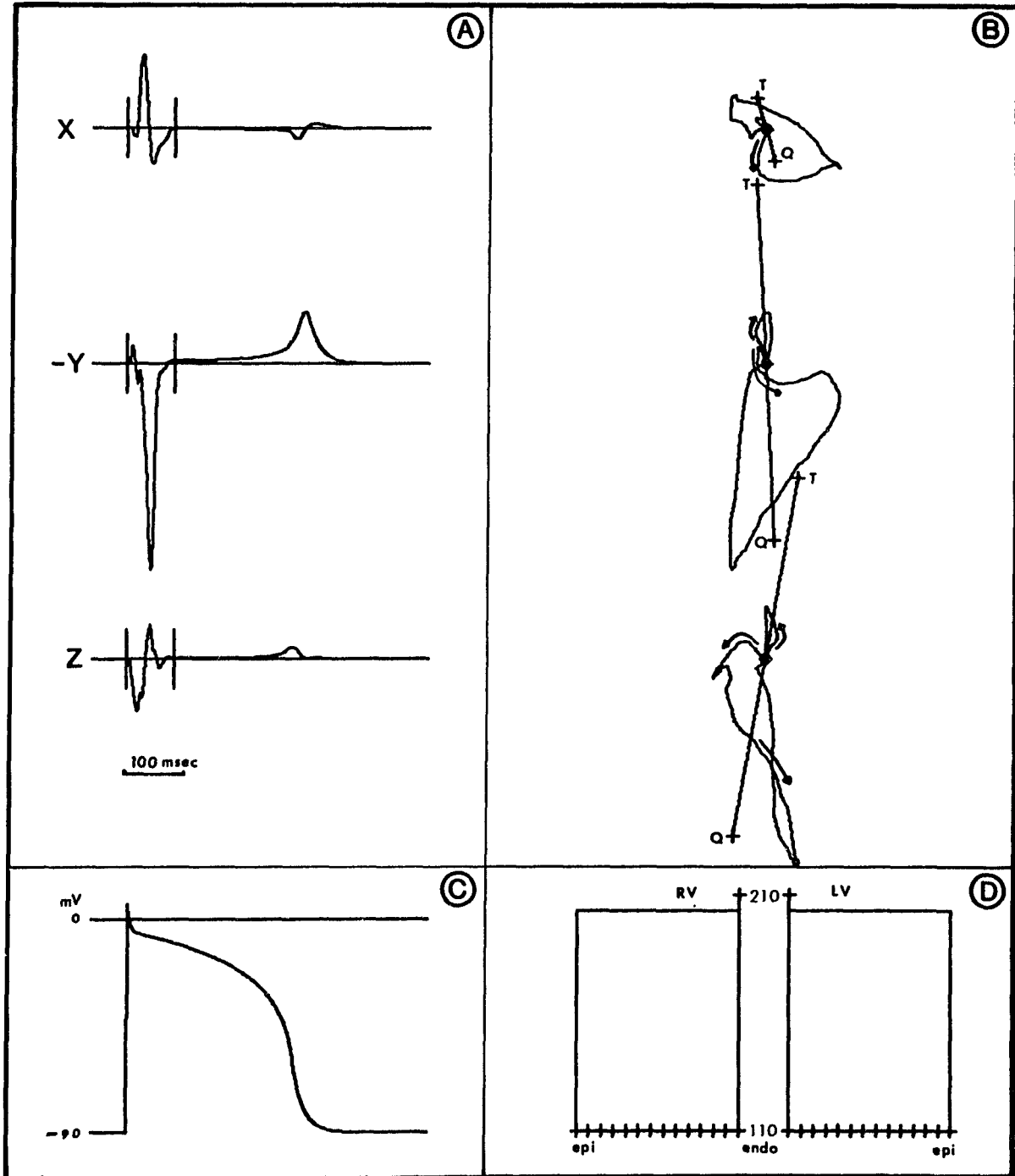


Fig. 4.13

Fig. 4.14 A,B,C,D Computed VCG for model 1A. Differences in duration only.

Each panel has the same outlay as the previous figure (4.13).

In the projections on the principle planes the depolarization vectors are omitted. G_{QRS} is indicated by the + sign, G_T with the open circle and $G_{QRS,T}$ with the solid circle.

Fig. 4.14 A,B,C,D shows the results for differences in duration of the action potential only. In A the maximal difference is 25 msec, in B 58 msec, in C 75 msec, and in D 100 msec. The area ranges with these differences from 190 mvmsec to 173, 154, 136, 129 mvmsec respectively.

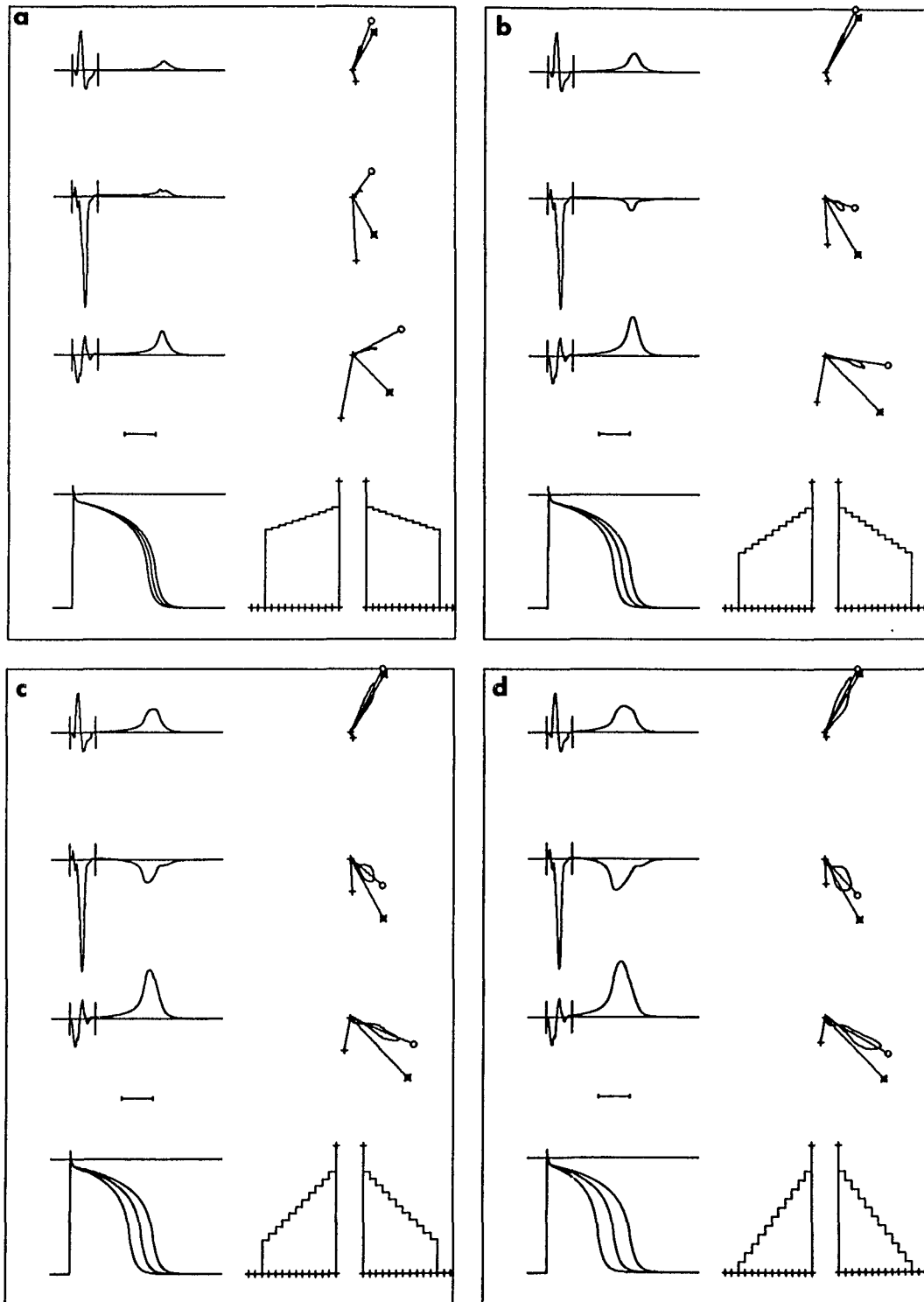


Fig. 4.14

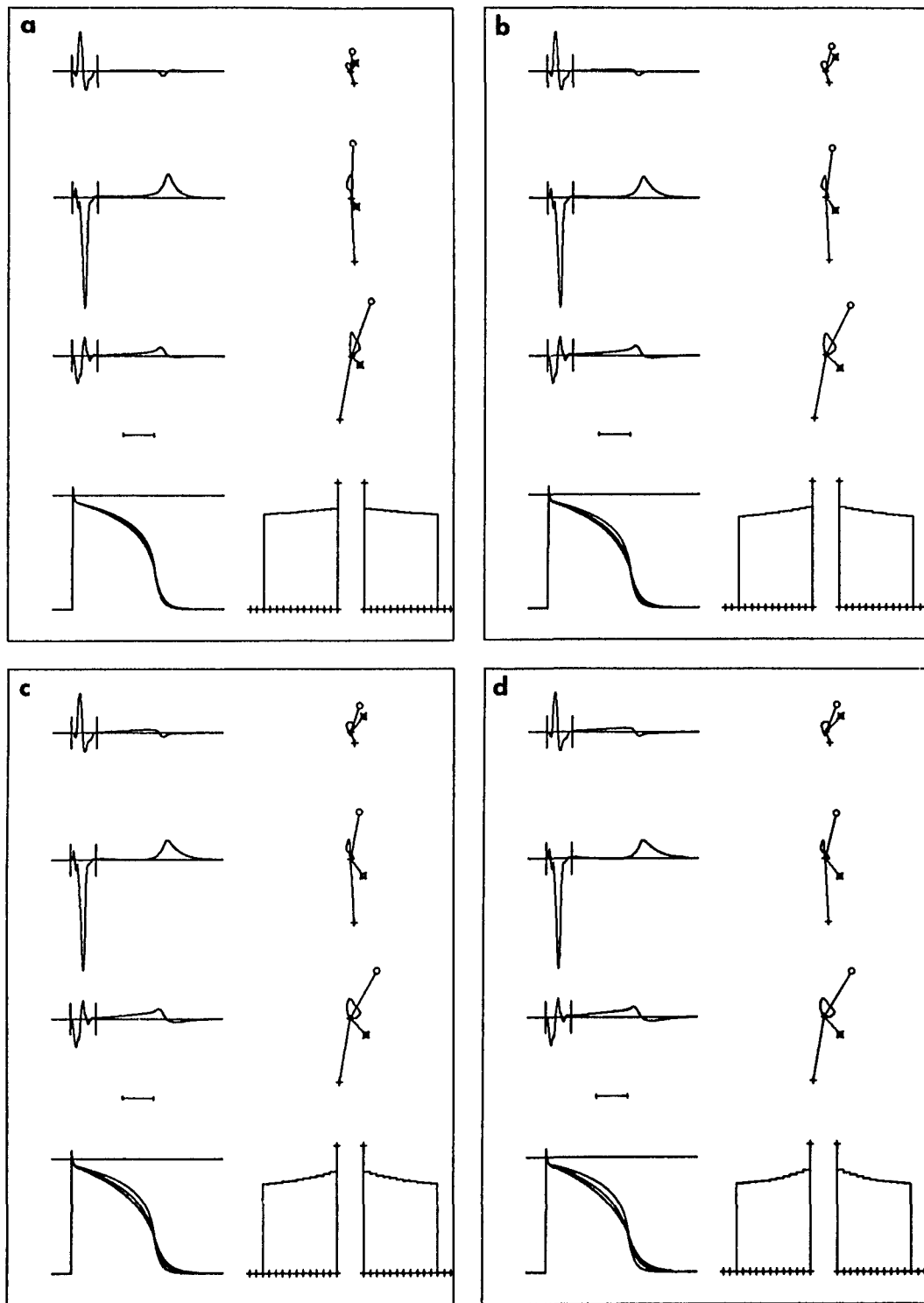


Fig. 4.15 A,B,C,D Computed V. C. G. for model 1A. Differences in slope only. For outlay and symbols used see figure legend of 4.14. Area ranges from 190 mvmsec. to 105, 82, 180 and 79 in A, B, C, and D respectively. The slope voltage (see paragraph 4.1.3.0 under f) is decreased with 25,50,75 and 100 mV for the maximum difference.

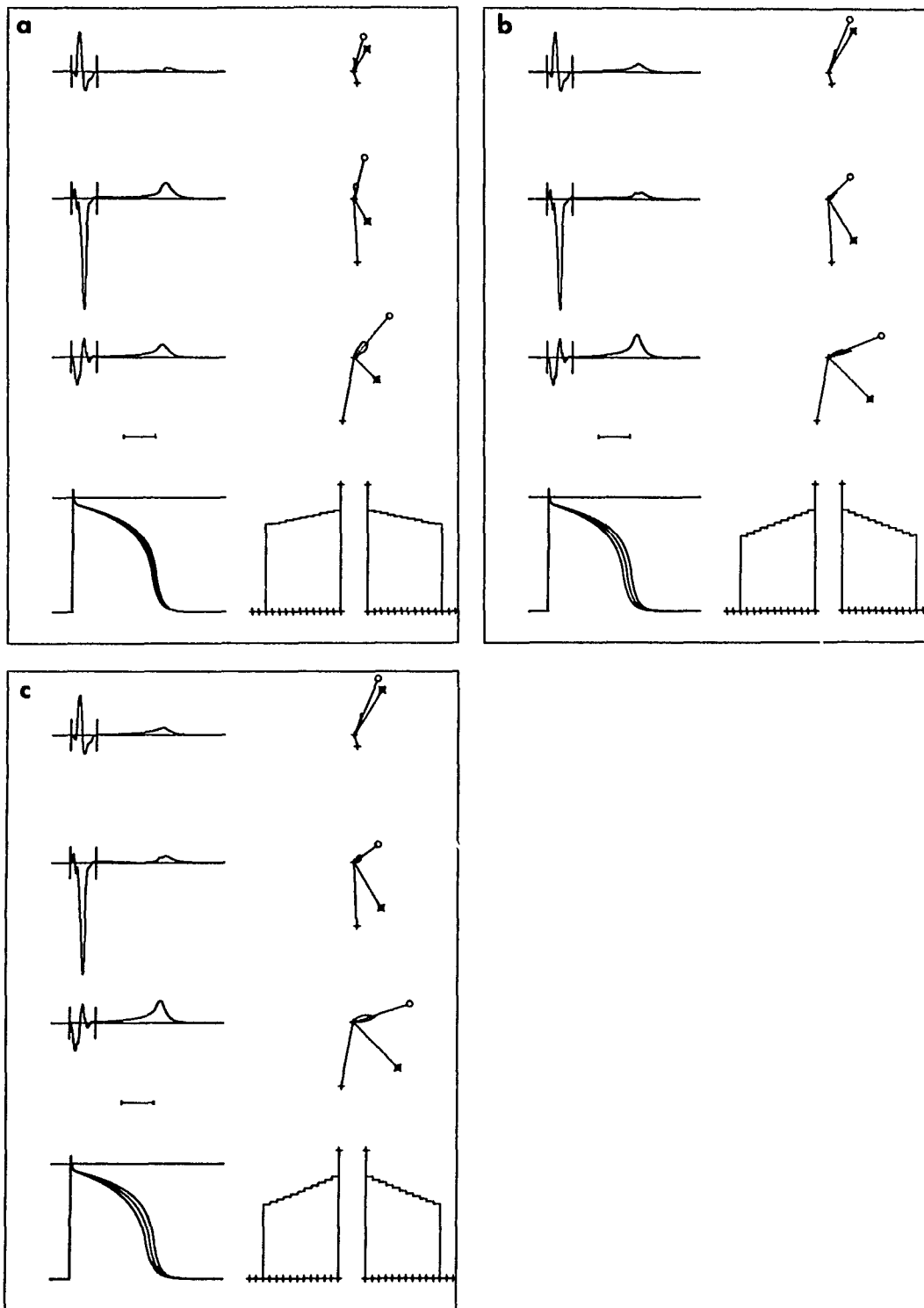


Fig. 4.16 A,B,C Computed VCG for model 1A. Differences in slope and duration.

For outlay and symbols used see figure legend of 4.14.

A. Duration differences of maximal 12 msec, with slope voltage differences of 12 mV maximally.

B. Maximal duration differences of 12 msec, slope voltage difference of 25 mV.

C. Duration differences with maximum of 25 msec, slope voltage difference of 25 mV.

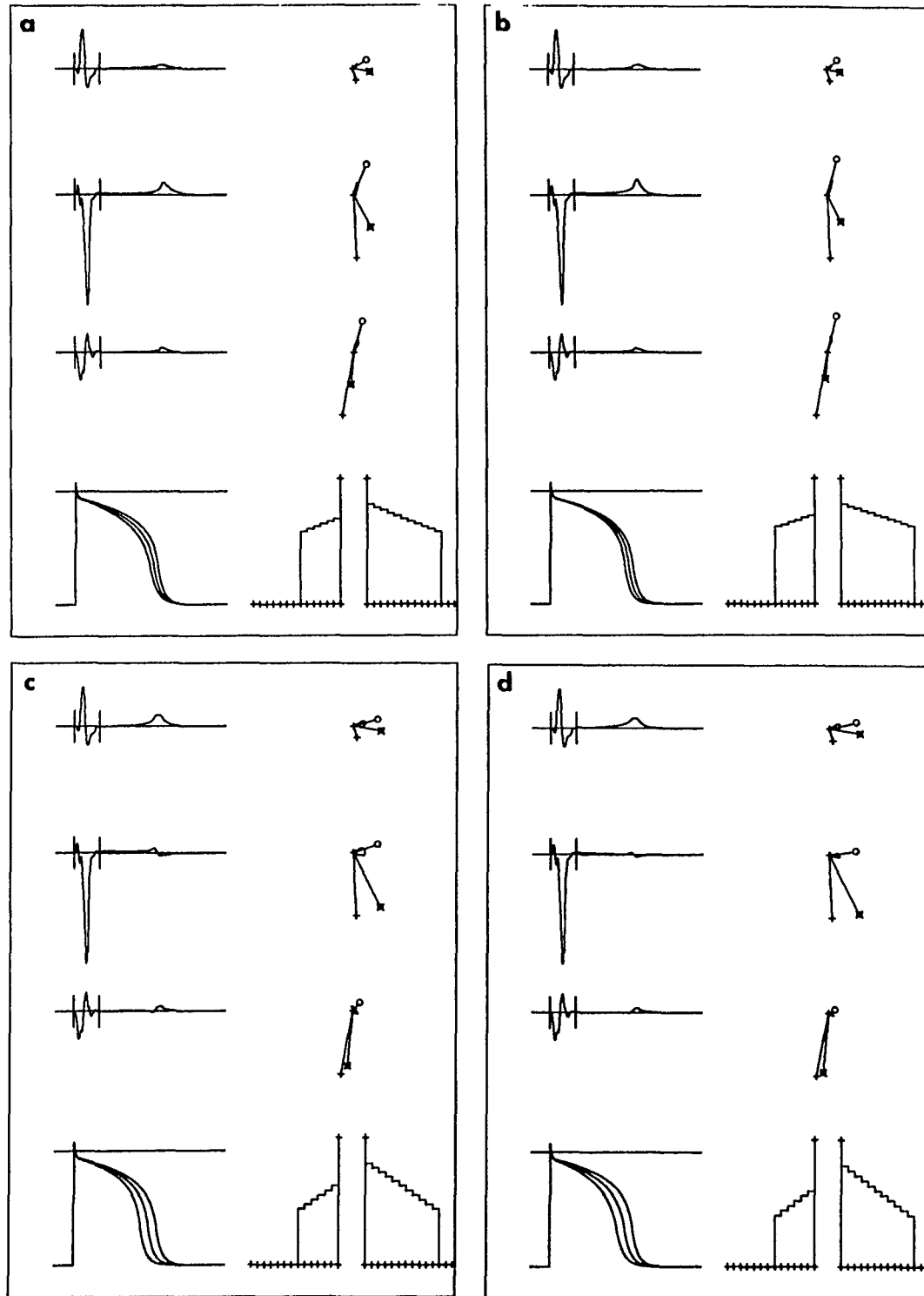


Fig. 4.17 A,B,C,D Computed VCG for model 1B. For outlay and symbols used see figure legend of 4.14.

A. Duration difference = 25 msec. Slope voltage differences 25 mV.

B. Duration difference = 25 msec. No slope changes.

C. Duration difference = 50 msec. No slope changes.

D. Duration difference = 50 msec. Slope voltage difference 25 mV.

Note that the elevation of $\vec{G}_{QRS,T}$ is within one standard deviation of the normal. The ratio of $\vec{G}_{QRS,T}/\vec{G}_{QRS}$ in Fig. 4.15 indicates extremely small gradient vectors. The increase of this ratio with larger differences between action potentials is as expected. The direction of $\vec{G}_{QRS,T}$ is changed in model 1B, as seen from azimuth and elevation angles. The azimuth now is within 2 standard deviations of the normal, however the elevation is outside 2 standard deviations of the normal.

4.3.3.4 *Stress profile*

Figure 4.18 A,B,C shows the results for model 2A with different action potential durations and Fig. 4.18 D,E,F and Fig. 4.19 A,B,C,D for differences in duration combined with differences in slope. The results for model 2B are seen in Fig. 4.20 D,E,F and Fig. 4.21 A,B,C,D for differences in duration combined with differences in slope. Table III summarizes the orientations of the ventricular gradients found in this model, as well as the angles subtended between \vec{G}_{QRS} , and \vec{G}_T and the ratio of $\vec{G}_{QRS,T}$ and \vec{G}_{QRS} .

In model 2A the direction of $\vec{G}_{QRS,T}$ in the transverse plane is practically anterior. Although the azimuth for both models are well outside 2 standard deviations of the mean for normals, the elevation is within 2 standard deviations for model 2B. None of the ratios of $\vec{G}_{QRS,T}/\vec{G}_{QRS}$ is close to normal.

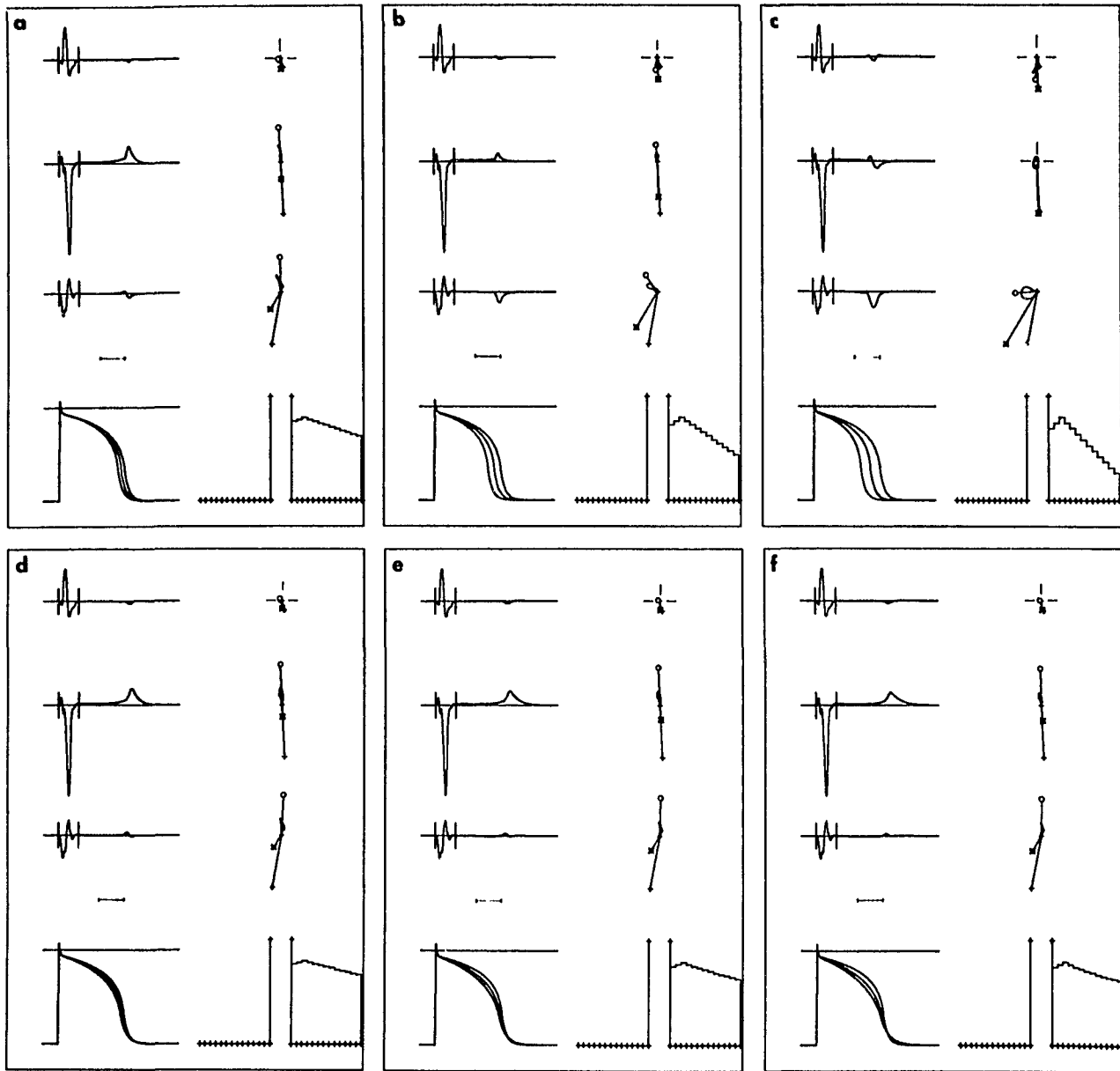


Fig. 4.18 A,B,C,D,E,F Computed VCG for model 2A. For outlay and symbols used, see figure legends of 4.14. A,B,C. Duration differences of 25, 50, 75 msec respectively. D,E,F. Duration differences of 12 msec and slope voltage differences of 25, 50, 75 mV respectively.

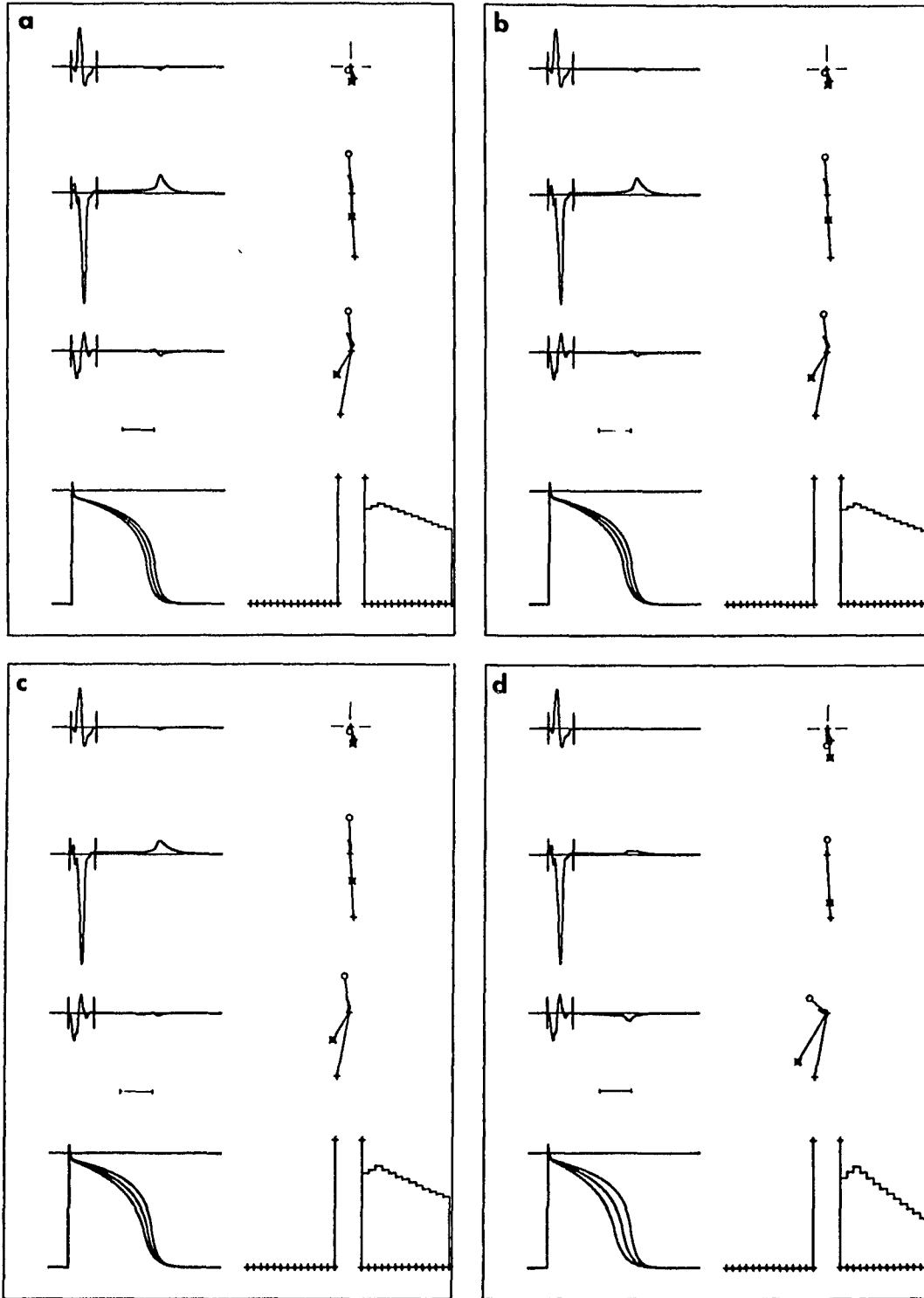


Fig. 4.19 A,B,C,D Computed VCG for model 2A. For outlay and symbols used see figure legend of 4.14. A,B,C. Duration differences of 25, with slope voltage differences of 12.5, 25, 50 mV respectively. D. Duration difference of 50 msec, slope voltage difference of 50 mV.

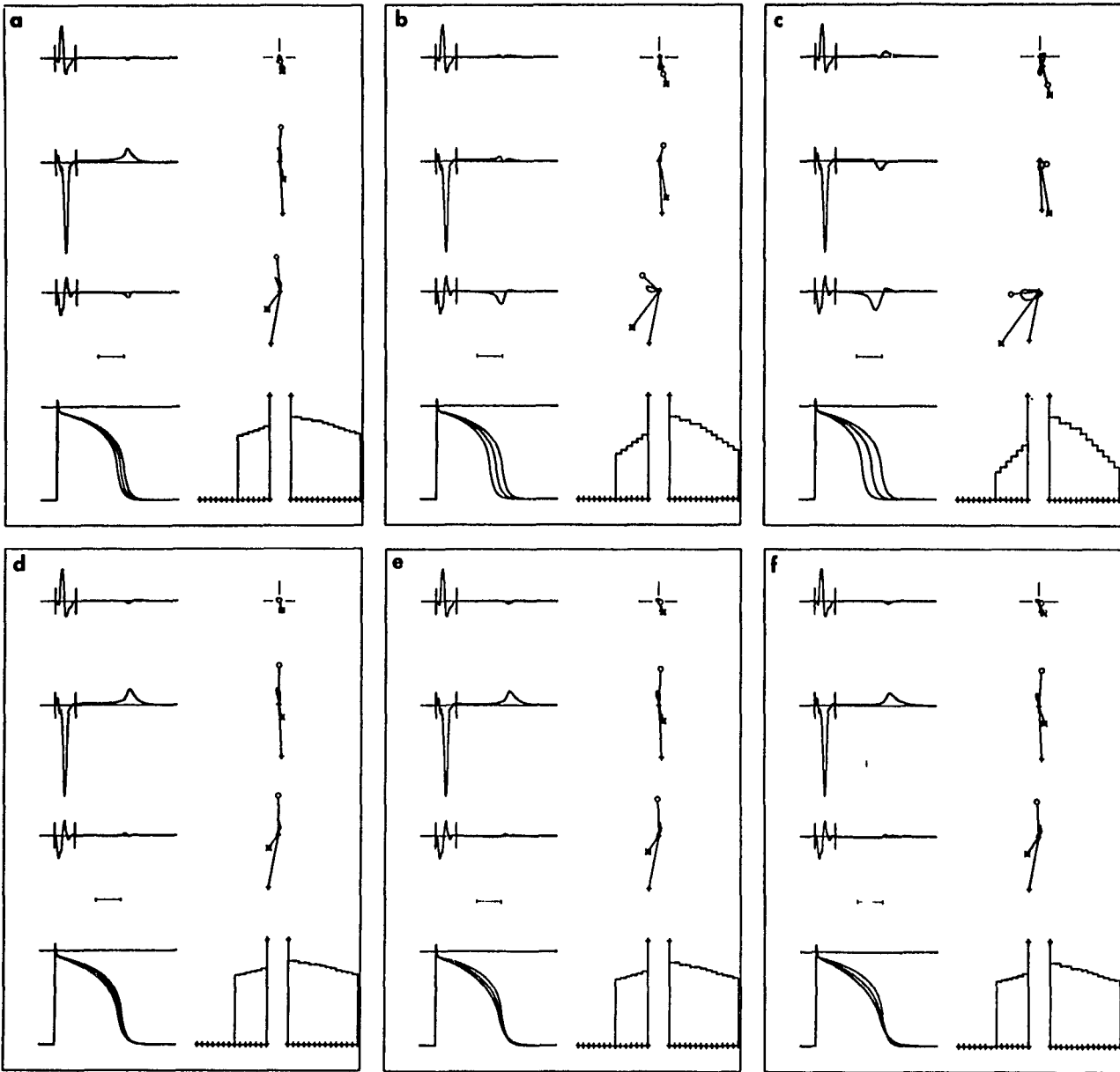


Fig. 4.20 A,B,C,D,E,F Computed VCG for model 2B. For outlay and symbols used see figure legends of 4.14. Duration and slope voltages are identical as in figure 4.18 A,B,C,D,E,F, respectively.

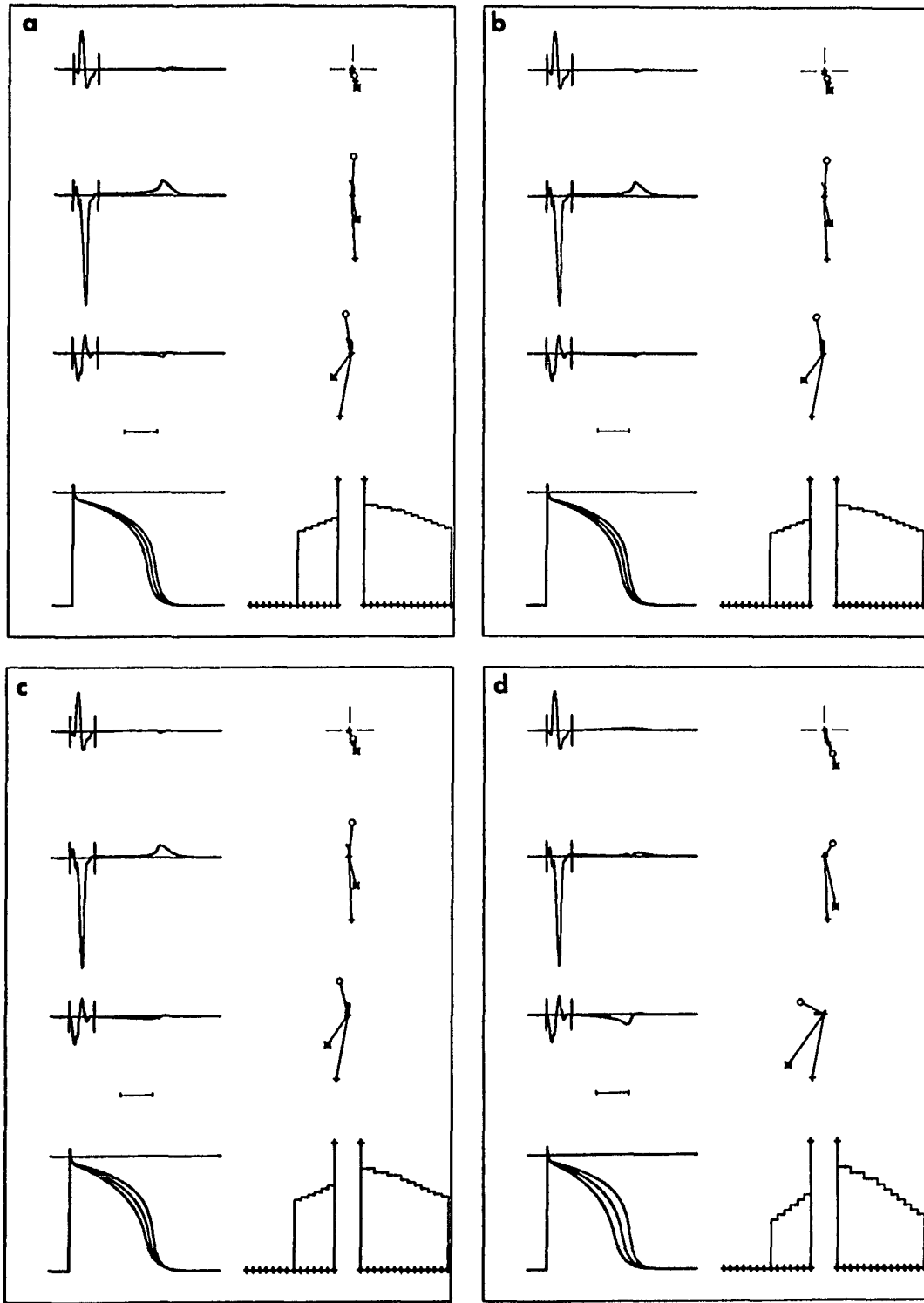


Fig. 4.21 A,B,C,D Computed VCG for model 2B. For outlay and symbols used see figure legends of 4.14. Durations and slope voltages are identical as in figure 4.19 A,B,C,D, respectively.

4.3.3.5 *Reversed sequence*

For each model the one or two electrocardiograms computed with the reversed sequence of repolarization are seen in Fig. 4.22 A,B,C,D and 4.23 A,B,C,D. The length and slopes of the action potentials were taken from these previous experiments, which yielded the best results. Orientations of the ventricular gradient vectors, the spatial angle between \vec{G}_{QRS} and the \vec{G}_T and the ratio $\vec{G}_{QRS,T}/\vec{G}_{QRS}$ are summarized in Table IV.

For model 0 both azimuth and elevation are well outside 2 SD of the mean for normals. The ratio $\vec{G}_{QRS,T}/\vec{G}_{QRS}$ is also small. Note that in the combined models all orientations are closer to the orientation of \vec{G}_{QRS} (azimuth -75.6° , elevation -79.5°).

4.3.3.6 *The new hypothesis*

Results for model 3 are seen in Fig. 4.24 A,B,C,D. Only combinations of action potential duration and slope differences are considered. Table V summarizes the orientations of the ventricular gradient vectors, the spatial angle subtended between $\vec{G}_{QRS,T}$ and \vec{G}_T and the ratio $\vec{G}_{QRS,T}/\vec{G}_{QRS}$. Note that all azimuth values are within 1 SD of the normal whereas 24 B and D are within 1 SD of the normal for the elevation, 24 A, and C are well within 2 SD. The ratio of $\vec{G}_{QRS,T}/\vec{G}_{QRS}$ for B and D are also closer to the normal ratio, than the ratio for A and C.

Fig. 4.22 A,B,C,D Computed VCG for the reversed sequence of repolarization.

For outlay and symbols used see figure legends of 4.14.

A,B. Uniform model, maximum differences in duration between first and last fibers 25 and 50 msec respectively.

C. Model 1A. Duration differences due to typing of elements to a maximum of 25 msec. No slope voltage differences. Maximum difference in duration due to depolarization sequence 25 msec.

D. Model 1A, as under C, except slope voltage differences due to typing of elements to a maximum of 25 mV.

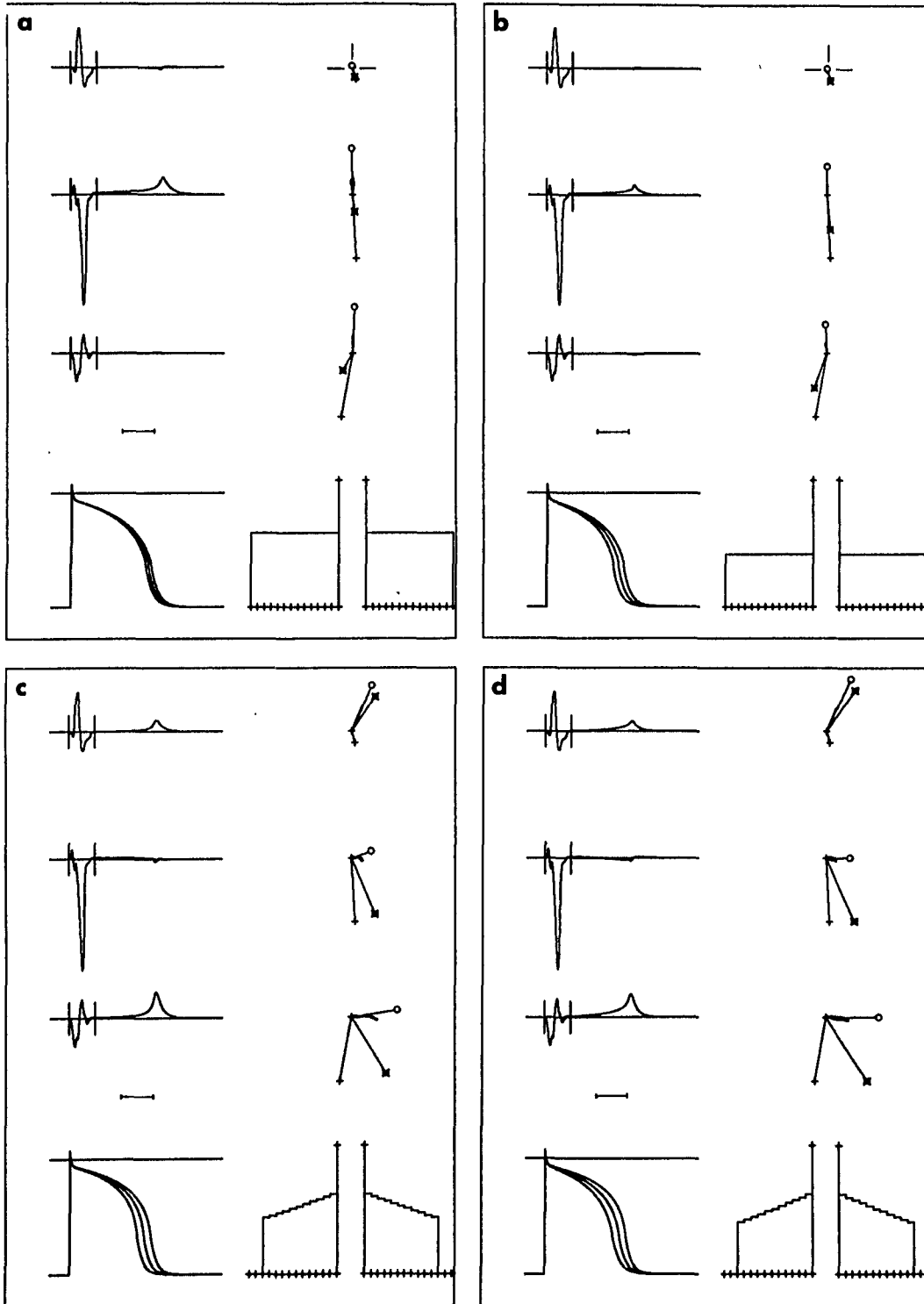


Fig. 4.22

Fig. 4.23 A,B,C,D Computed VCG for the reverse sequence of repolarization.

For outlay and symbols used see figure legends of figure 4.14.

A,B. Model 1B, durations and slope voltage differences as in Fig. 4.22
C,D respectively.

C. Model 2A. Duration difference due to typing of elements to a
maximum of 25 msec. No slope voltage difference. Maximum difference
in duration due to repolarization sequence 25 msec.

D. Model 2B, as under C.

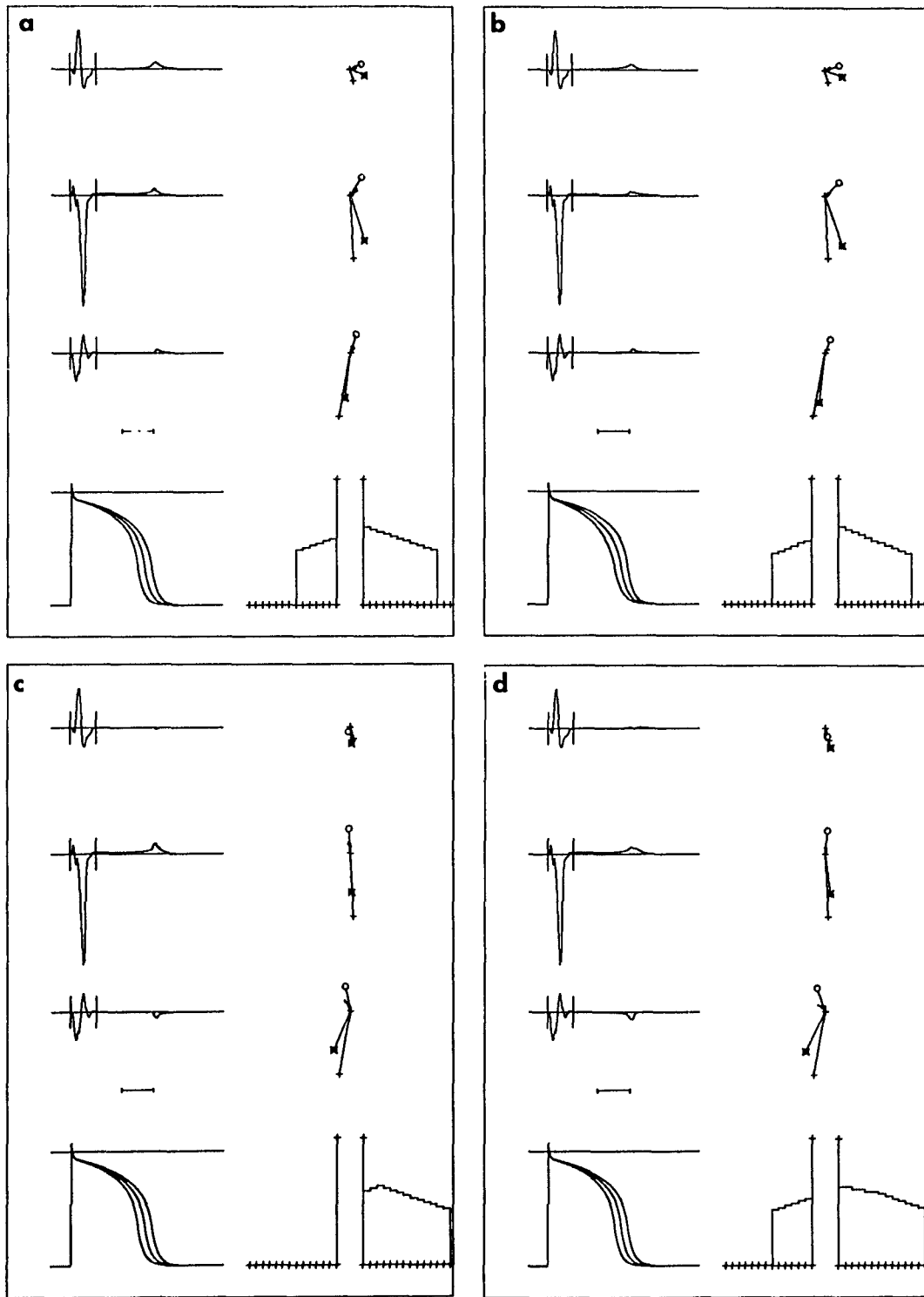


Fig. 4.23

Fig. 4.24 A,B,C,D Computed VCG for model 3. The new hypothesis.

Outlay and symbols used, see figure legends of figure 4.14.

- A. Duration differences 37.5 msec, no slope voltage differences.
- B. Duration differences of 55 msec, no slope voltage differences.
- C. Duration differences of 37.5 msec, slope voltage difference of maximal 17.5 mv.
- D. Duration differences of 55 msec, slope voltage difference of maximal 17.5 mv.

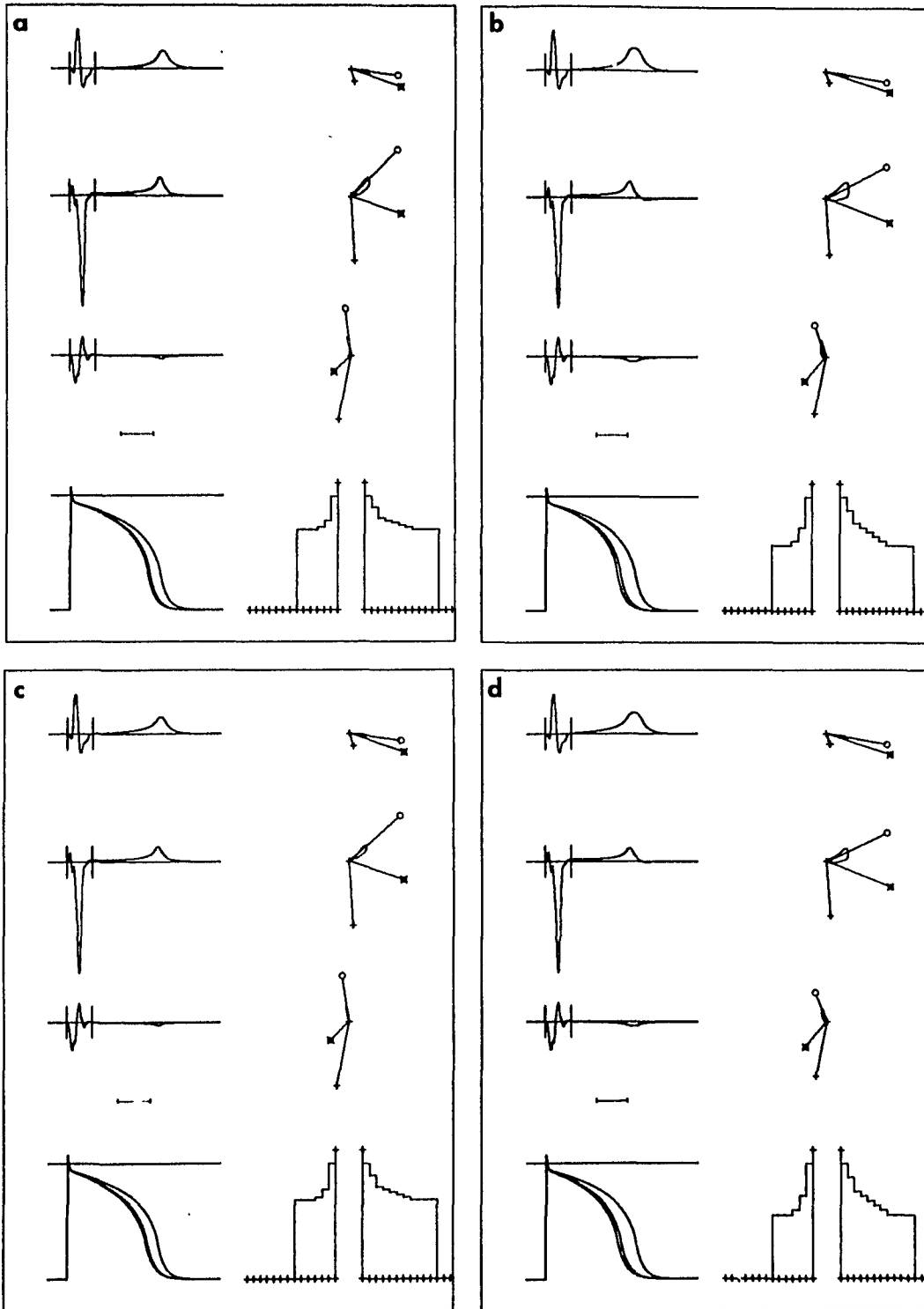


Fig. 4.24

4.3.4 The lead systems

4.3.4.1 The 12-lead system

The components of the 12 lead system are seen in Fig. 4.25. The commonly used symbolic abbreviations for each lead are used. Note that the precordial transition at V_4 and the persistent S-waves in the precordial leads. The negative T wave in III and positive T in aVL as well as the biphasic T-wave in aVF is unusual.

4.3.4.2 The VCG-lead systems

The VCGs of the orthogonal VCG-lead systems are seen in Fig. 4.26, 27, 28, 29. The small asterixes indicate the value in X, Y or Z at each time instant, as obtained by the lead-systems. The heart VCG is displayed as well. Both are scaled as to have an identical sum of squares for the 9 time instants of the QRS-complex compared, thus for example for the Frank system:

$$\sum_{i=1}^9 \left(V_{FX}^{(i)} \right)^2 + \left(V_{FY}^{(i)} \right)^2 + \left(V_{FZ}^{(i)} \right)^2 = \sum_{i=1}^9 \left(V_{HX}^{(i)} \right)^2 + \left(V_{HY}^{(i)} \right)^2 + \left(V_{HZ}^{(i)} \right)^2 \quad (50)$$

To compare the performance of each lead in the various lead systems, the difference number N is used. The difference number is defined as the sum of the absolute values of the differences at each time instant expressed as percentage of the sum of the absolute values at these time instances of the reference (heart vectorcardiogram), thus, for

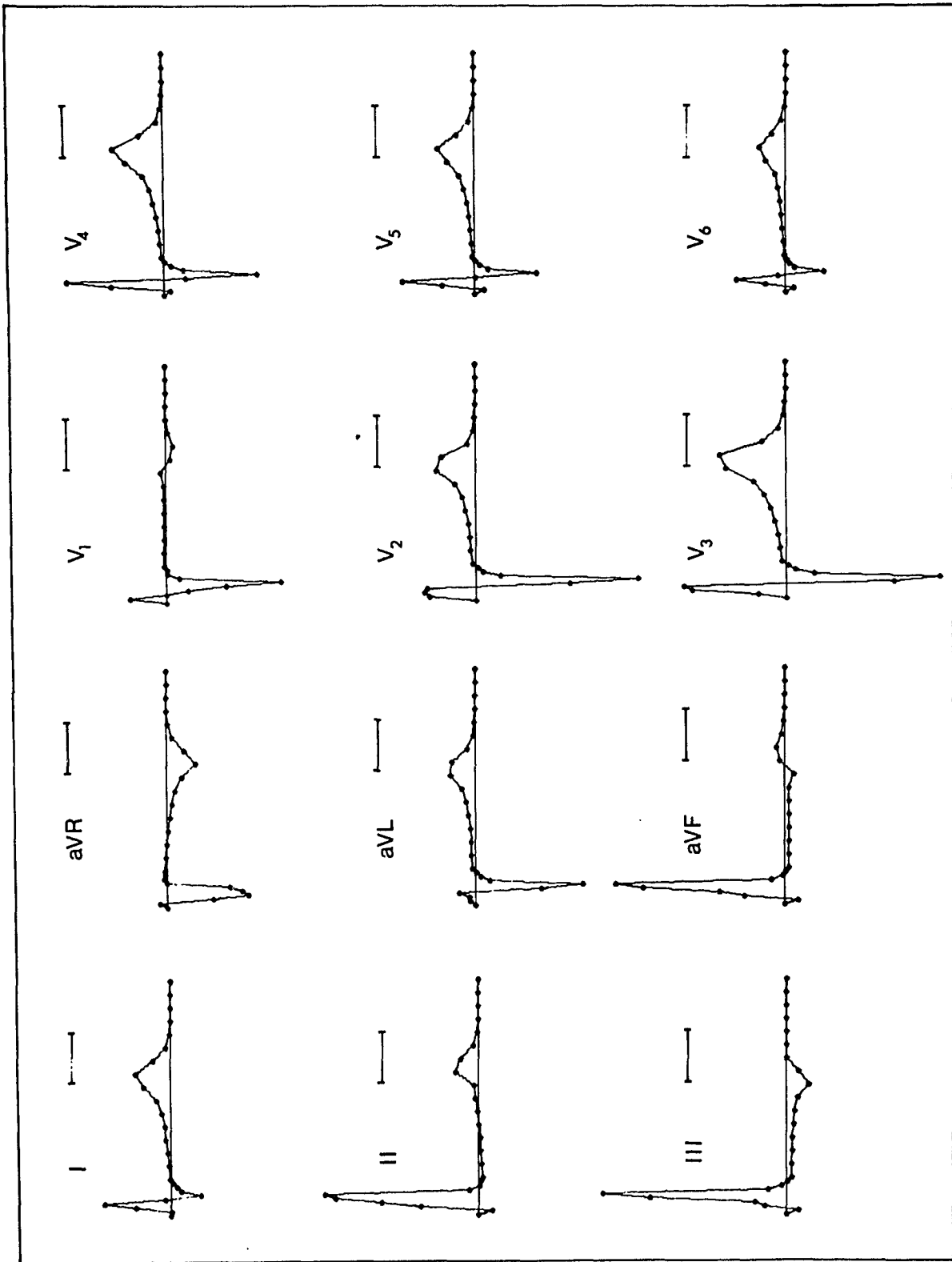


Fig. 4.25 Computed standard -12-lead electrocardiogram. The tiny asterixes indicate the points which were computed. Nine time instants during the depolarization and fifteen time instants during the repolarization were computed. The horizontal bars indicate 100 msec. The voltage scale is arbitrary, but identical in all leads.

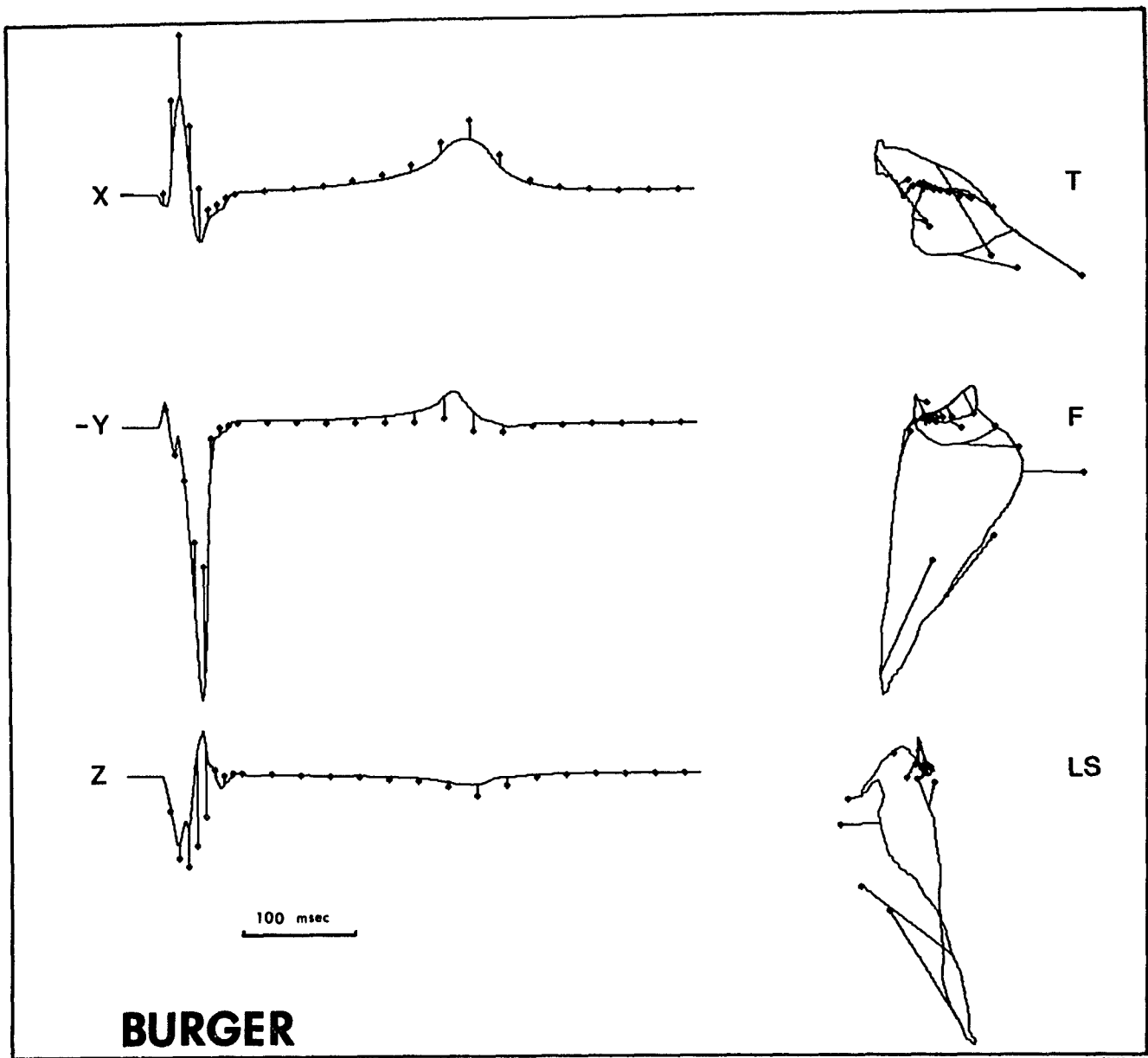


Fig. 4.26 Computed Burger - VCG.

At the left side are seen the X, -Y, and Z component of the Burger - VCG. The continuous line indicates the heart VCG, the tiny asterexes the value of X, Y, and Z for each time instant as computed with the Burger - VCG lead system. Scaling is done in such a way as to minimize the sum of the absolute values of the differences in X, Y, and Z simultaneously. Scaling is done for the QRS complex only, the same scale is maintained throughout ST,T segments. Note that the Y component is plotted with reversed polarity. On the right are seen the projections on the transverse, frontal, and left saggital planes. Scale of amplitude is arbitrary.

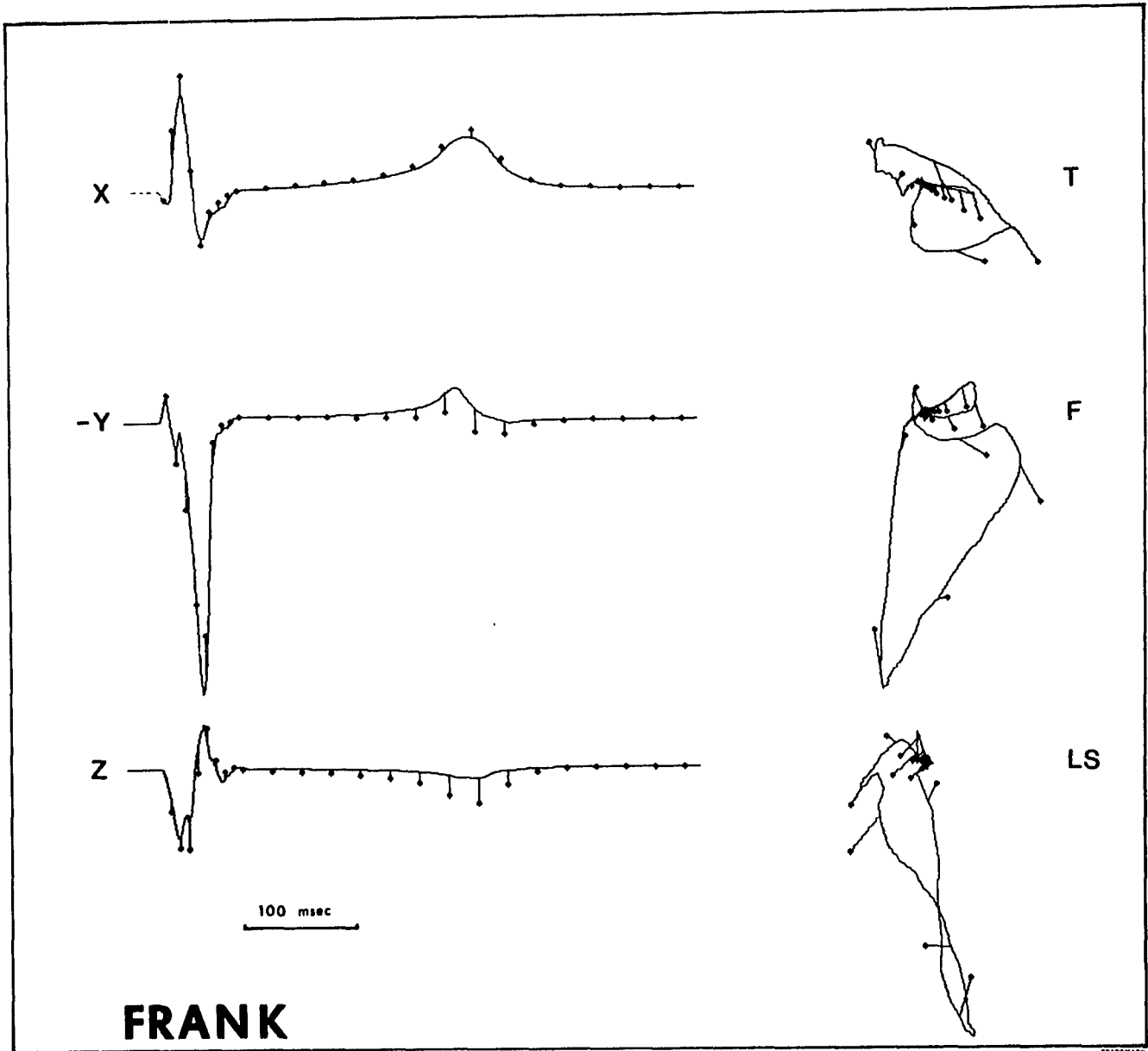


Fig. 4.27 Computed Frank - VCG.

The X, Y, and Z components of the Frank - VCG as computed from the body surface potentials, as compared with the heart VCG. For details see figure legend of Fig. 4.26.

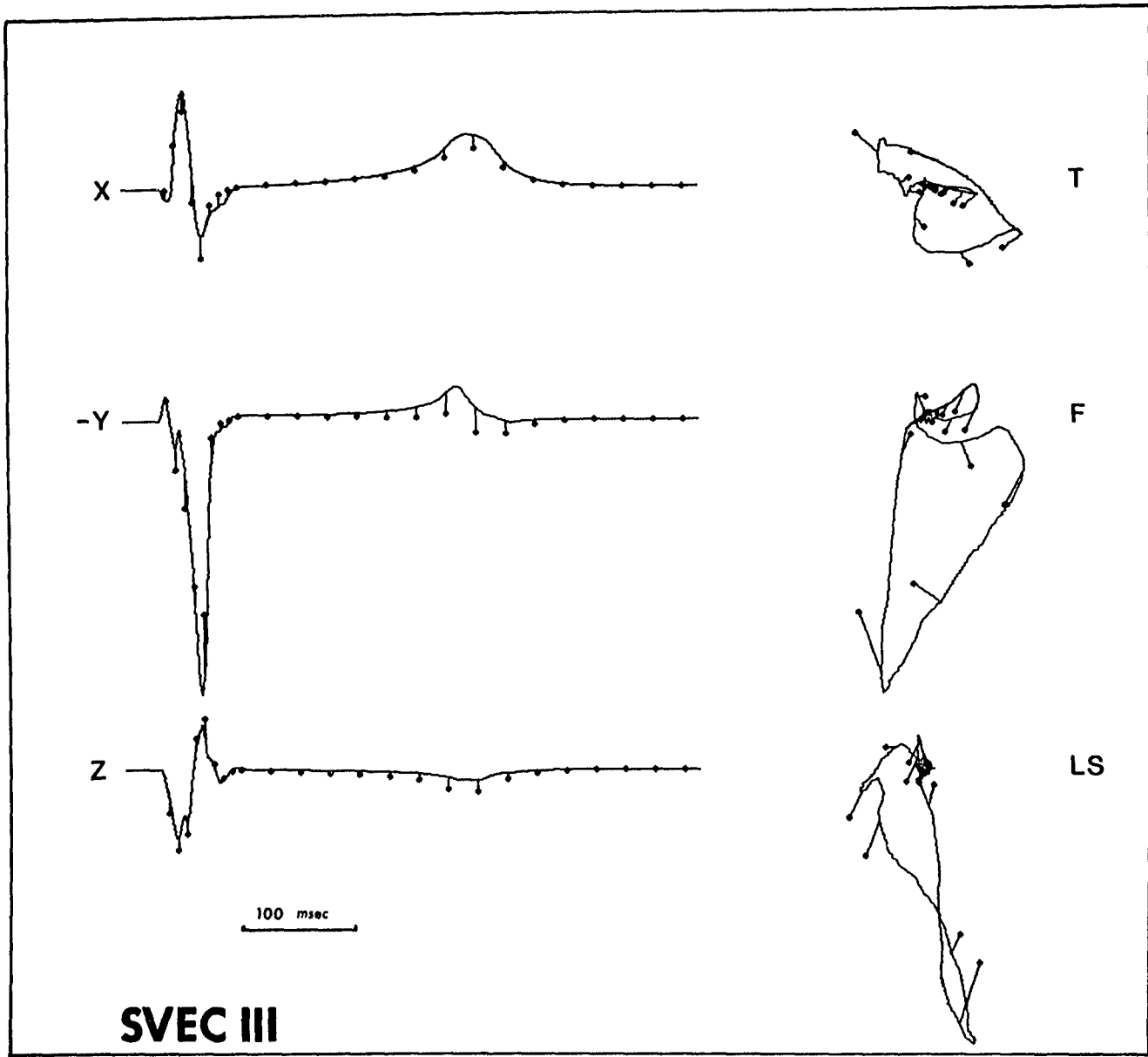


Fig. 4.29 Computed SVEC 111 - VCG.

The X, Y, and Z components of the computed SVEC - 111 - VCG, as compared with the heart VCG. See figure legend of Fig. 4.26 for details.

instance, for the QRS complex of the Frank X-leads:

$$N_{FX} = \sum_{i=1}^9 |V_{FX}^{(i)} - V_{PX}^{(i)}| \left(\sum_{i=1}^9 |V_{HX}^{(i)}| \right)^{-1} 100 \quad (51)$$

Leads to be compared are scaled as to have an identical sum of squares for the 9 time instants of the QRS-complex, to avoid bias of this number by any scale difference.

The same scale is maintained for the remaining part of the ECG. Also the correlation of QRS,ST and QRS,T is computed.

Table VI summarizes the difference numbers and correlations found for the four lead systems, separate for depolarization, repolarization (indicated with T) and combined. The highest correlation obtained in each category is underlined.

4.4 Discussion

4.4.1 Normal excitation

The total depolarization time, 78 msec, is short as compared with measured QRS durations. QRS durations in 110 normal men, aged 20-29 years, were reported to have a mean of 88 msec with a standard deviation of 12 msec (130). Durrer et al (42) pointed out that the conduction velocity as reported by them is probably 20% higher than the conduction velocity in the intact heart in situ. For dogs, they have shown a similar increase in conduction velocity after removal of the heart from the thorax. The reasons for this increase in conduction velocity are not known. Possible factors are neural and hormonal influences, composition of perfusion fluids used, work load on the heart, temperature

changes, etc. Durrer et al found, however, that all conduction velocities are proportionally affected. This suggests that the activation patterns are probably not affected by this change in conduction velocity. The total depolarization time of 78 msec compares very well with the total time of excitation in the surviving perfused human hearts.

The simulated early depolarization events are in very close agreement with those reported by Durrer et al. This is not surprising since the starting locations of excitation were chosen to match the reported observations, and the close agreement only proves that the starting locations, as chosen in the horizontal sections, were rightly identified. The most critical parts for comparison are the middle parts of the depolarization. Comparison of Fig. 4.11 with Fig. 1 from the article of Durrer et al (42) shows that the middle stages of depolarization are practically identical. This observation lends support to the validity of the assumptions made, especially assumptions A4 and B2.

The papillary muscles are excited almost at once, and very early in the systole. The physiological significance of this is obvious, since the papillary muscles support the AV-valves to withstand the increasing pressure in the ventricles during systole.

The right ventricular apex is among the first parts to be activated in the right ventricle. Inspections of the sections in Fig. 11.4 reveals that the heart wall in this region is very thin as compared with the other parts of the right ventricular wall. Early contraction in this

area will reduce the effective diameter of encompassed cavity and so greatly reduce the wall tension necessary to withstand the higher pressures which develop during later parts of the systole.

Although the isochronous lines nicely depict the excitation patterns, the distance of isochrones can be misleading in the assessment of conduction velocity, since the isochronous lines do not give any information about the direction in which the activation spreads.

The simulated excitation patterns during the last portion of excitation differ in detail from those reported by Durrer et al. This is understandable, since it is well known that the terminal events of activation are highly variable from subject to subject.

4.4.2 *The heart vectorcardiogram depolarization*

The general shape of the projections of the H.V.C.G. (and thus the QRS complexes of the orthogonal components) and the sense of inscription (phase relationship of the orthogonal components) are within the limits of normal variability.

The initial forces are to the right anterior and superior. At 10 msec the strong anterior forces, as seen in the Z-component, start to develop. The major feature of this H.V.C.G. is the vertical position of the loop, which makes the horizontal projection more narrow than is usually seen. A possible explanation for this vertical position and strong anterior forces might be found in the localization of the terminations of the right bundle. Other reported excitation patterns show that the initial excitation in the right ventricle may start near the apex at the side of the intraventricular septum. The deflection points described agree in general with those given by Arntzenius (6). The

first part (from origin to a) is supposedly due to septal activation, whereas the change from a towards b is caused by the right ventricular activation. Point b is expected to coincide with the first breakthrough on the right ventricular wall, point c with the first breakthrough on the left ventricular wall, and point d marks the disappearance of large forces and return to the origin. Point c at 40 msec appears to be 15 msec later than the left ventricular breakthrough. It is noted, however, that no substantial area of the left ventricular epicardial surface is excited until 35 msec from the start of excitation.

The most obvious deviation of a normal pattern is the S-wave in the Z-component. However, restraint should be exercised in comparing the patterns of the H.V.C.G. with V.C.G.'s derived from body surface potentials, and using normal standards derived from the latter to judge the normality of the former.

4.4.3 *The Heart VCG-repolarization*

The general appearance of the T-wave in scalar (X,Y,Z) display, as well as the usual VCG projections, as well as the magnitude and direction of the ventricular gradient can be used to evaluate the H.V.C.G. repolarization patterns. The following characteristics are known to appear in VCGs of clinically normal subjects. The T-waves are slightly assymmetric. Its initial part emerges slowly from the ST-segment and the terminal part returns more rapidly to the base line. The amplitude of the T-waves as compared with the QRS complex varies widely. It seldom exceeds the amplitude of the QRS complex, except in the Z-lead. In the VCG projections the orientation of the T-loop is generally in the same direction as the QRS loop (concordant T-loop),

though seldom in exactly the same direction. The average spatial angle subtended between mean QRS and mean T was 74° for the 650 normal male subjects of the present study. This explains why the T-waves in most leads are of the same polarity as the QRS complexes. The Z-lead, again, is an exception by showing in most cases negative T-waves. Normally the inscription sense (rotation) is identical to the one observed in the QRS complex. Normally the T-loop is open, except in infants in which narrow hooked T-loops are often seen. Caution should be exercised, as in the case of depolarization, in judging heart VCG patterns as 'normal' or 'abnormal'. The ventricular gradient vector in respect to G_{QRS} is more objective and suitable for comparison with our measured data. The orientation of the ventricular gradient vector is not influenced by the parameters regulating slope and duration of the action potentials as long as the profile has a constant slope. This could be anticipated from the theoretical introduction. However, the magnitude of the ventricular gradient is directly influenced by these parameters. Differences in upstroke and downstroke of the T-waves could be generated in every model by adjustment of the action potential slope parameter. This is caused by the relative shift of the action potential area difference towards earlier portions of the repolarization.

4.4.3.1 *Temperature profiles*

Model 1A is based on the assumption that the temperature inside the cavities is lower than inside the muscle and epicardial layers, and that the action potential duration is influenced by the absolute temperature. At lower temperatures the duration is longer. It is seen

from Fig. 4.14A that the magnitude and the orientation of the T-vectors changes substantially with relatively small changes in the action potential duration. A difference of maximally 25 msec in action potential duration between endocardial and epicardial layers can produce concordant relatively normal looking T-waves. All T-waves produced by model IA are, however, strikingly symmetrical and their spatial orientation is abnormally far in posterior and superior direction. It is also noted that with increasing differences in action potential durations the T-waves become disproportionately large, which is caused by the increased profile vectors. The orientation of $\vec{G}_{QRS,T}$ however does practically not change.

The increased magnitude of profile vectors force the T-vectors downwards, and reduce the QRS,T angle from 125° to 70° , which is practically the mean normal value. However, the posterior direction of $\vec{G}_{QRS,T}$ maintains also the posterior direction of the T-wave, which is abnormal.

If only differences in action potential slope voltages are used with constant action potential duration (Fig. 15A,B,C,D), the resulting T-waves are highly abnormal. This is mainly caused by the last part of the action potentials, where the fibers with the higher type numbers have a longer 'tail' in the action potential.

Although the typing is identical in the above experiments, the $\vec{G}_{QRS,T}$ has a slightly different direction, which also changes with increasing action potential slope changes. As mentioned in section 4.4.3, this will happen if the profile does not have a constant slope, which can be confirmed from the profile diagrams. The size of the profile

vectors which can be produced by merely changing the slope is not sufficient to bring the T-loops substantially down, and the QRS,T angle is accordingly large.

However, if slope and duration differences are considered simultaneously, the T-waves are very close to the ones generated with only duration differences, but now they are more assymetrical, the upstroke being slower than the downstroke, as is normally seen in adults. It should be noted here, that the T-loop configuration is very similar to the T-loop configuration seen in children, the so-called 'infantile' T-loop.

The gradient is also closer to the case with only duration differences. The additional increase in magnitude of the profile vectors due to slope changes forces the T-vectors further down with 25 msec difference in duration (Fig. 4.16,C) than if only duration differences are considered (Fig. 4.14,A).

The elevation of $\vec{G}_{QRS,T}$ is within one standard deviation of the normal, however, the azimuth is far outside the normal range. The ratio of $\vec{G}_{QRS,T}/\vec{G}_{QRS}$ is practically normal with maximal duration differences of 50 msec.

Model 1B differs from model 1A in assuming that in addition to the temperature differences in cavity and heart muscle, the temperature is lower in the left cavity than in the right cavity. This difference could be postulated by assuming that the blood is cooled down when passing through the lungs. The results are very similar with both of these models. With model 1B a change in $\vec{G}_{QRS,T}$ is seen. This change is

caused by the differences in the septal forces, since the profile vectors for all other parts are identical in both models. When using model 1B, $\vec{G}_{QRS,T}$ is directed much more anterior and inferior. The resulting T-orientation is closer to normal in the horizontal plane. The T-elevation, however, does not change sufficiently even with a steep profile, probably due to the fact that the ventricular gradient is rather small.

4.4.3.2 *Stress profiles*

These models were based on the assumption that the action potential duration or waveform is influenced by the stress under which the fibers operate. Model 2A is based on the fiber stress distribution at end systole (10), whereas Model 2B is based on the radial stress distribution (155). In the latter case, stress distribution in the right ventricle wall is also considered. The results for these two models are rather disappointing.

For Model 2A, the gradient is directed inferior and straight anterior and is in general small. The resulting T-waves point superior and slightly anterior. With a rather steep profile (4.18 B,C) negative T-waves in the Z-component can be brought about, whereas a biphasic T-wave in the Y-component results only with the steepest profile (Fig. 4.18C). The various combinations of duration and slope yield no essentially different result. The shape of the T-waves in all Y-components is rather abnormal, with a fast upstroke and slow downstroke. This is most likely caused by the right ventricular fibers, which practically all have identical (and short) action potentials. Support for this view is lent by the fact that the

upstroke in 4.18 E and F is less fast, whereas the profile is practically identical to the one in 4.18A. In 4.18A only differences of duration are considered, whereas 4.18 E and F have less duration difference, but obtain a similar profile by additional slope changes. The T-loops are in general discordant even with rather steep profile.

In Model 2B the ventricular gradient is directed less inferior and more to the left than in model 2A, but also rather small, consequently steep profiles are necessary to cause concordant T-waves, otherwise T loops result, which are pointing straight upwards.

4.4.3.3 *Reversed sequence of depolarization*

With a uniform model and 'reversed sequence' it is difficult to create concordant T-waves. The profile vectors are directed nearly in the same direction as the depolarization vectors, consequently much larger area differences are necessary to create concordant T-waves. A second obvious result is the orientation of $\vec{G}_{QRS,T}$ which is also nearly in the same direction as \vec{G}_{QRS} .

As a result, the T-vectors are practically opposite to the QRS-vectors, with a spatial angle of 172.6° between \vec{G}_{QRS} and \vec{G}_T . The ventricular gradient is also rather small, which makes a steep profile necessary to produce any substantial changes. Even with 50 msec difference between first and last fibers the results are hardly changed. The combination of the temperature profiles or the stress profiles with 'reversed' sequence produced no essentially different results. 'Reversed sequence' tends to make the spatial angle between \vec{G}_{QRS} and \vec{G}_T smaller and thus the

T-waves tend to become more concordant with the QRS vectors. This, however, happens at the expense of increased profile vectors.

4.4.3.4 *The new hypothesis*

Concordant T-waves are easily obtained in X and Z leads. The spatial position of \vec{G}_T is more anteriorly directed, which is caused by a more anteriorly directed $\vec{G}_{QRS,T}$. The spatial angle extended between \vec{G}_{QRS} and \vec{G}_T is approximately 120° .

The ventricular gradient is rather large, consequently a relatively shallow profile creates already concordant T-waves. The T-wave configuration is also reasonably correct, with faster downstroke than upstroke.

Both azimuth and elevation for $\vec{G}_{QRS,T}$ are within one standard deviation of the normal in 24.B and 24.D. The QRS-T angle is within normal limits (157). Except for the innermost layer (Purkyne - myocard junction) this profile shows a remarkable agreement with the one reported by Harumi et al (61), which was experimentally determined in dogs. This profile is also identical to the pressure distribution throughout the ventricle wall. Also the pressure distribution is sometimes held responsible for the sequence of repolarization (10).

The ratio of $\vec{G}_{QRS,T}/\vec{G}_{QRS}$ evaluates in all models described above less than normal, except for Model 1A, with action potential duration differences of maximally 50 msec. (With larger differences in the same model the ratio is substantially larger than normal.)

The elevation angle in most models (0, 1B, 2A and 2B) is outside or just inside two standard deviations of the normal mean. However, the azimuth angle in model 0, 1A, 2A, and 2B is well outside two standard deviations of the normal mean. Only Model 2 is for both parameters within two or one standard deviation of the mean.

The normal values used above are measured on a group of 650 healthy men, in the age group from 40-70. Changes in $\vec{G}_{QRS,T}$ and consequently in \vec{G}_T are known to occur with aging (129).

The values obtained served as a guideline. If more pertinent data on the factors which influence the $\vec{G}_{QRS,T}$ become available, it will be necessary to revise the models tested so far. However, as long as these detailed data are not available, the search for a perfect match of the simulated data with the measured data is unrealistic.

It should be noted that the above discussed T-wave models are all hypothetical. They are all based on the assumption that the non-zero values of $\vec{G}_{QRS,T}$ are due to differences in action potential duration or shape. So far no systematical differences in action potential duration throughout the ventricle wall are found. Moore, Preston and Moe (90) found that usually epicardial action potentials are shorter than endocardial action potentials, but these results were not confirmed by Durrer and van Dam (37) and Janse (73).

The effect of drinking ice water on the T-wave polarity (9,40) led many authors to speculate that local temperature differences may be the cause of the predominantly concordant T-waves. However, temperature differences across the ventricular wall in normal adults are only in the

order of 1^0 , and in which way they are distributed throughout the ventricle wall is unknown. The temperature profile model assumes a linear temperature distribution.

The influence of stress on a fiber's action potential is also postulated (118). A rather steep profile is necessary to create concordant T-waves in these models. No adequate explanation has been forwarded so far to adopt the 'reversed sequence' of activation. Abildskov and co-workers (4, 61, 1, 2) were able to reconstruct reasonable T-waves from the QRS complexes, by assuming the action potential duration to be dependent on the time of depolarization. One would expect, however, that under the assumption that the ventricular gradient will coincide in direction with the \vec{G}_{QRS} , which is clearly not the case in normal ECGs or VCGs. The effects of cancellation observed during depolarization (3,6), will also take place during repolarization (26,38). The more anterior directed and smaller gradient in model 1B can be explained on this basis. In model 1A profile vectors in the septum will nearly completely cancel, whereas the left ventricular wall will dominate over the forces in the right ventricular wall. In model 1B the left ventricular free wall and left septal profile vectors will cancel, however, the right ventricular free wall will dominate the very few profile vectors in the right septal wall.

Similarly, the small gradients in model 2A can be explained by the fact that the profile vectors are arranged in cup shapes around the left ventricle, causing most of them to cancel. Practically every distribution of profile vectors will result in a large amount of cancellation

around the left ventricle. The interventricular septum belongs functionally to the left cavity, so only the right ventricular free wall will be uncanceled and so dominate the resulting ventricular gradient.

Although the hypothesis of the new profile approached closest the T-wave configuration found in normal adults, the results are still not satisfactory. The upward directed T-loops, although within normal limits (157), result in too large a QRS-T angle. Further investigation is obviously required. The above observation of right ventricular wall dominance suggests that attention should be focused especially on the right ventricle. The resultant of all profile vectors in the left wall could account for the leftward direction of the ventricular gradient, whereas the more anterior located right ventricular wall will give the anterior displacement.

The lack of confirmation of any of the above profiles by experimental data forces one also to consider alternative explanations for the T-wave.

The influence of the mechanical systole and especially the movements of the ventricle wall in respect to the thorax on the repolarization pattern has to be assessed. Our present model is not suitable for such an assessment. Also, the effect of changed ventricular blood masses is not known. The effect of the blood masses in general will enhance the radially directed forces (the Brody effect) (15), and this effect can thus be expected to enhance radially directed profile vectors.

It is possible that some or all of the above mentioned effects can be accounted for by an equivalent profile. It could also be speculated that the profile which was most satisfactory is an equivalent profile for an unknown condition effecting the repolarization vectors.

4.4.4 *The lead systems*

4.4.4.1 *The 12-lead ECG*

The patterns as found in the 12-leads are in general in agreement with the heart VCG. Thus also a vertical electrical axis is seen as judged from leads II and III.

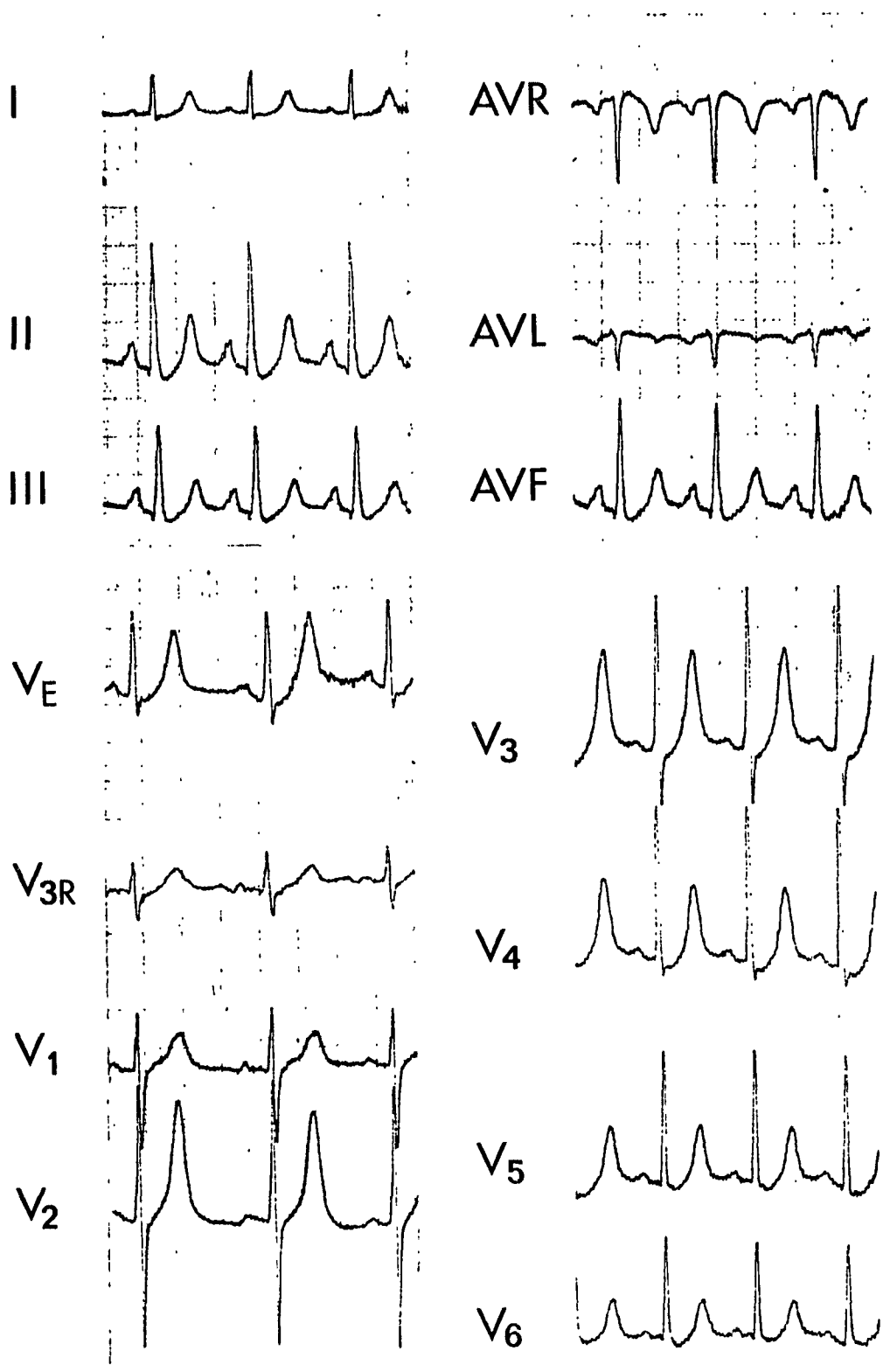
The most remarkable disagreement is found in the precordial leads, especially the leads V_1, V_2 and V_3 . The R/S ratio in these leads could be expected to be much larger than 1. However only lead V_4 displays a ratio which is just about 1. The small S-wave in the Z-component is not detectable in any of the precordial leads. The T-wave shows a similar disagreement in the precordial leads, where its amplitude was expected to be the largest in V_5 and V_6 (the mean T-wave has an azimuth of -10.9°). However, lead V_2 and V_3 show the largest T-waves. The T-axis is estimated to be horizontal, whereas in the heart VCG the elevation of the mean T is 25° .

Comparison of the computed 12-leads with the 12 lead ECG as recorded on the subject whose heart was studied by Durrer et al (see Fig. 4.30) shows a remarkable agreement in patterns as far as the QRS complex is concerned. The recorded 12-leads also show a vertical electrical heart axis, with small Q-waves and large R-waves in leads II and III. The precordial leads show less agreement, especially in the deep S-waves in V_4, V_5 , and V_6 in the simulated ECGs have no counterpart in the recorded ones. The 1:1 ratio in the recorded leads is found in V_2 instead of V_4 as in the computed ECGs. The latest parts of the depolarization are in general less similar; whereas, the simulated

Fig. 4.30 Recorded 12 - lead ECG.

The Standard 12 - lead - ECG as recorded by Durrer et al., from the subject who's heart was revived after death, perfused and studied . The excitation patterns of this heart served as a basis for comparison in this study.

HH 6



7-5-68

Fig. 4.30

T-waves, except for a horizontally directed axis are remarkably congruent to the measured ones. As mentioned in paragraph 4.3.1, the last parts of the depolarization are in general subject to variation.

4.4.4.2 *The VCG lead systems*

(a) *Burger lead system*

For the depolarization the Y lead shows the closest agreement both in area accounted for (difference number N) as well as the wave-shape (correlation coefficient), lead X is decidedly poorer, and lead Z is largely distorted. Especially from 24 msec on the discrepancy with the heart VCG is large. In contrast with this is the ST-T segment which shows a good agreement in wave shape for both X and Z and a much poorer one for Y. The overall performance shows again the dominance of the Y lead. The Z-lead is poor.

(b) *Frank lead system*

For the depolarization an excellent agreement in X is obtained, and Y and Z are both reasonable. Again the largest discrepancy exists at 24 msec and 32 msec. For the ST-T segment the X performs even better than for the depolarization, also the Z-lead is excellent, the Y-lead is in contrast rather poor. In overall performance, the X-lead is still the best, as could be anticipated, followed by the Y lead and the less perfect Z lead.

(c) *McFee and Parungao*

The Z lead is the best during depolarization, very closely followed by X and Y leads. Performance is similar during ST-T segment, except for the Y-lead which is poor. The overall rating is good for all leads.

(d) *SVEC 111*

For both depolarization and repolarization this system has the best Z-lead. The Y-lead is also very good during depolarization, this is however not the case during repolarization. The reverse situation is observed with respect to lead X, which is excellent during repolarization and worse during depolarization. The overall performance of leads X and Y is reasonably good, whereas lead Z is excellent.

If we compare the X lead performance of all systems Frank's X is the best, Burger's Y lead is best for depolarization but McFee's Y is best for repolarization. The Z lead of SVEC 111 is the best, closely followed by McFee. In overall performance McFee rates 1, Frank and SVEC 111 2 and Burger 3, which confirms the results of Horacek (68).

In the above rating the correlation coefficient was weighed heavily. The correlation, as performed here, measures the similarity of waveforms. The difference number N, on the other hand, is an index of absolute amplitude differences, after scaling for the QRS-complex, between HVCG and VCG recorded with various lead systems.

The X lead appears reasonably good for all systems except for the Burger system. The X lead during the last part of the depolarization,

which in the heart VCG could be interpreted as a conduction delay, is smooth in Frank and SVEC III, as is the terminal part of Y in all lead systems. In the Z lead Frank and Burger smooth this part, where SVEC III and McFee follow the heart vector exactly.

The disagreement in all systems starts at 24 msec, which is the time of right ventricular surface breakthrough.

All lead systems show an anterior displacement of the vectors, which is most pronounced in the Burger system. This displacement, especially during ST-T, enlarges the negative T-waves in Z, and is possibly the result of the Brody effect mentioned on page 4.41.

All systems have a low correlation in the Y lead for the ST-T segment. This is surprising since the QRS complex correlates quite well in all systems, and the Y leads as evaluated by Horacek (68) and Burger et al (21,22) are very stable and in general show good agreement.

The overall correlation is quite good, which raises the suspicion that the correlation coefficient is misleading on numerical basis, which could happen if a series of values (all very small) are scattered around the mean.

4.5 *Conclusions and summary*

The excitatory process was simulated in the model of the human ventricles, for which the data collection is described in chapter III. Reported data of a few clinically normal subjects served as a guideline. Such simulation was demonstrated to be feasible, under the assumptions adopted, for the major part of the ventricular excitation. The last part of the depolarization, however, was not compatible with the measured data. The heart VCG computed for this depolarization sequence showed remarkable 'normality', except for the late depolarizations. The deflection points of the heart VCG were in agreement with those reported by others. From the body surface potential distribution computed with the aid of a torso model of Dr. Horacek (68), the 12-lead electrocardiogram was extracted as well as the VCG's of four commonly used lead systems.

The general features of the 12-lead electrocardiogram are in agreement with the heart VCG, however the abnormality in the heart VCG at the end of the depolarization is not detectable in the 12-lead ECG.

A comparison of the computed 12-lead ECG with the ECG's recorded on the subject, who's heart was studied by Durrer et al (42), showed in general similar patterns, again with exemption of the late depolarizations. The VCG's of the four lead systems are compared with the heart VCG. The best representation of the X-component of the heart VCG is by the X-lead of the Frank system, followed by the McFee system, the SVEC III system and the Burger system. The Y-lead of the Burger system gives the best representation for the Y-component of the heart VCG, followed by Frank, McFee and SVEC III.

The Z-component is reproduced most closely by the Z-lead of SVEC III, followed by McFee, Frank and Burger.

The largest discrepancy with the heart VCG starts in each system at 24 msec. after onset of excitation. Two distinct wavefronts exist at this time instant, in contrast with the two preceding time instants. The SVEC III and the McFee lead system both give a very close approximation of the late depolarization patterns, in contrast to the Burger and Frank systems.

For all three components at the same time, the McFee system performs the best, followed by the Frank, SVEC III, and Burger system.

Simulation of repolarization is done on the basis of spatial and/or temporal distributed differences in voltage time function of the elements. These differences are expressed as profile vectors, which are defined in the context of the ventricular gradient concept. A simulated action potential is used as elemental voltage time function.

Four hypothetical explanations for the repolarization sequence are tested, on the basis of the direction and size of the ventricular gradient and T-wave configuration.

The hypothesis based on temperature differences yields satisfactory results in the frontal plane projection, however the results deviate strongly from normal in the horizontal projection. The hypothesis based on fiber stress distribution is generally less satisfactory, both in ventricular gradient direction and size, as well as in T-wave configuration. The hypothesis based on the "reversed sequence" of repolarization requires large profile vectors, and the direction of the ventricular gradient is abnormal. A new hypothesis offered yields the most satisfactory results,

both in size and direction of the ventricular gradient as well as in T-wave configuration. This hypothesis is based on physiological-histological data. Since all repolarization models are highly speculative, the need for more experimentally obtained data is stressed.

Body surface potentials are also computed for the repolarization, using the model which came closest to normal with its heart vectorcardiogram. The orientation of the T-loop in all four vectorcardiographic lead systems came closer to normal as compared with the T-loop of the heart VCG. The T-waves in the simulated 12-lead electrocardiogram, especially in the precordial leads, showed a similar change in orientation.

Chapter 5

IMPULSE CONDUCTION UNDER REPETITIVE STIMULATION

5.1 Introduction

5.2 Formulation of the interaction

- 5.2.1 Refractory periods
- 5.2.2 Conduction velocity
- 5.2.3 Impulse conduction with repetitive stimulation
- 5.2.4 Selfsustaining activity
- 5.2.5 Ventricular myocardium model

5.3 Methods

- 5.3.1 Action-potential duration
- 5.3.2 Conduction velocity
- 5.3.3 A simple structure of 2500 elements
- 5.3.4 Ventricular myocardium model

5.4 Results

- 5.4.1 Impulse conduction with repetitive stimulation
- 5.4.2 Selfsustaining activity
- 5.4.3 Ventricular myocardium

5.5 Discussion

- 5.5.1 The relationship functions
- 5.5.2 Selfsustaining activity
- 5.5.3 Ventricular myocardium model

5.6 Conclusions and summary

5.1 *Introduction*

In the previous chapter the properties of the heart were approached from a static point of view, i.e. only one excitation was considered without interaction of subsequent beats. Interaction of subsequent beats will appear either if the following beat occurs within the relative refractory period of the previous, or if by some mechanism the heart muscle cells are influenced by the overall heart rate. In the first case, only the immediate preceding interval is important, in the second case the immediate preceding interval has to be evaluated in the light of the total heart rate.

5.2 *Formulation of the interaction*

The interaction of cells is determined by the characteristics of the impulse of the donor cell and the response of the receiver cell. The response is mainly determined by the impulse conduction velocity, and the duration of the absolute and relative refractory periods. The interaction properties can be formulated without considering the action potential shape. However, a close relationship between excitability and membrane potential has been demonstrated (149,67). For this reason the duration of the absolute refractory period and the duration of the action potential (ADP) will be considered identical, and freely interchanged. Any impulse is either sufficient or insufficient to elicit a response (assumption B3).

5.2.1 *Refractory periods*

The refractory period of the heart is known to be dependent on the heart rate. The mechanism of this dependency, however, is not clear. Measurements in the dog's ventricle led Han and Moe (59) to the conclusion that the refractory period is only dependent on the previous interval. In a later paper (60), however, they report some influence of the total basic rhythm. Janse (73) clearly finds this influence in the canine heart, but he also points out the existence of a large difference between Purkyne fibers and ordinary heart muscle; Purkyne fibers being much more sensitive than ordinary heart muscle.

Prior to the availability of the microelectrode, several authors tried to infer from the QT-interval the relationship between the heart rate and the refractory period. Fredericia (53) proposed the following formula:

$$QT = k\sqrt[3]{R_0 R_1} \quad (52)$$

In 1920, Bazett (8) formulated this relationship as:

$$QT = k\sqrt{R_1 R_2} \quad (53)$$

Simonson et al (130) found that in 960 cases the following regression equation predicts the Q-T interval from the R-R interval and age with a standard error of .0164 sec.

$$QT = 0.2423 + (0.140 \pm 0.004)\overline{RR} + (0.00630 \pm 0.00004) \text{ age} \quad (54)$$

As pointed out by Hoffmann and Cranefield (66), a reasonably good prediction for the QT interval might be obtained by these formulae, but since the relationship between QT interval and the cellular action potential is not univocal little will be learned about the cellular refractory period. Carmeliet (27) studied the relationship of action potential duration and stimulus interval, in frog's Purkyne fibers. He found the following relation

$$A = R_{\infty} (1 - e^{-\alpha C}) \quad (55)$$

where A is the action potential duration, R_{∞} is the action potential duration at infinitely long interval and C the preceding stimulus interval. Vick (146) studied this relationship in dog Purkyne fibers, also specifically observing the action potential duration changes after a long series of stimuli, including changes taking place when the stimuli were stopped. He not only confirmed the exponential relationship found by Carmeliet, but also discovered a remarkable influence of the total driving rate on action potential duration. This influence was only fully developed after 400-800 beats. A similar influence with large time constants was established by Janse (73) in perfused surviving dog hearts, both for Purkyne and heart muscle fibers. Vick also focused attention on the relationship between preceding 'functional recovery period' and following action potential duration, rather than between preceding stimulus interval and action potential duration. This followed from his experimental setup, in which after 2-3 minutes of rest, a train of impulses

was started with fixed intervals. With the higher frequencies (i.e. shorter stimuli intervals) a remarkable electrical alternans (long and short refractory periods in alternating order) was observed, in which the correlation of action potential duration and 'functional recovery period' is obvious, whereas the stimuli intervals are constant.

'Functional recovery period' (FRP) is defined as the time interval between the end of the absolute refractory period and the next stimulus. Vick postulated an explanation for the electrical alternans and the earlier mentioned exponential relationship between functional recovery periods and action potential duration in the membrane model proposed by Noble (98). In this model the plateau phase is terminated by an increase in potassium conductance, g_K , due to activation of factor S. This factor S is deactivated after repolarization. If the interval after repolarization is only short, deactivation is not complete and the time for subsequent full activation is also shorter. In a later model, Nobel and Tsien (100,101) proposed the existence of a three component outward current, I_s , I_{x_1} and I_{x_2} . I_s is pure K^+ -current, whereas I_{x_1} and I_{x_2} are composed of the potassium current possibly mixed with other ions. In this model the termination of the plateau phase is attributed to activation of x_1 (the factor governing the conductance of I_{x_1}). Reported time constant for x_1 is voltage dependent, being smaller close to the plateau voltage and larger at resting membrane potentials.

5.2.2 *Conduction velocity*

A reduction in conduction velocity is found experimentally if a cell is depolarized shortly after the end of the absolute refractory period. A possible explanation for this was given by Weidmann (149), who determined the availability of the sodium carrying system. A cell will be able to react on the next stimulus only if sufficient sodium carrier is available, whereas activation of sodium carrier occurs only after repolarization beyond -60 mV. In direct relation with the available sodium carrier is the slope of the upstroke of the following action potential. The conduction velocity is related to the rate of rise of the action potential, and it will thus decrease with reduced sodium carrier availability, which will happen if there is a short interval between next excitation and end of previous refractory period. Though this is mentioned by many authors as an important factor in the behaviour of a large conglomerate of cells, very few systematic reports have appeared on the subject (39,147).

5.2.3 *Impulse conduction with repetitive stimulation*

The reaction of tissue 'en mass', especially to repetitive stimulation is of interest in connection with heart rhythm abnormalities. If stimulus intervals are of reasonably normal duration, it is easy to predict how the tissue will react. Similarly easy is the prediction of stimuli intervals of short duration if the tissue is homogeneous in properties. An example of such predictions is the study by Wiener and Rosenblueth (150) on flutter. However, if inhomogeneities in impulse

conduction properties are considered, the prediction becomes more complicated and has either to be on a statistical basis (150) or to be derived from simpler experiments under controlled conditions. Obviously, models provide a good opportunity to experiment under controlled conditions.

5.2.4 *Selfsustaining activity*

In 1965 a computer model of atrial fibrillation was proposed by Moe et al (89). Their procedures were along lines similar to the ones outlined below (5.3.3). They studied the interaction of elements (hexagons), for which a certain behaviour was specified. A brief outline follows:

The model consisted of 30 rows of 30 hexagons, each element was either absolute refractory, relative refractory or fully excitable. Time was considered in discrete steps of 5 msec. They proposed the length of the refractory period to be specified by

$$Q_1T_1 = \sqrt{KR_0R_1} \quad (56)$$

where Q_1T_1 is the refractory period, R_0R_1 is the preceding RR interval and K a constant, ranging from 10 to 20. K was randomly assigned to the 900 elements of the model. The above formula was based on observations by Mendez et al (84) and Alessi (5), in analogy to Bazett's (8) formula for the prediction of the QT-interval from the RR-interval. If an impulse reached an element within 15 msec after the end of the absolute refractory period also a conduction delay is imposed on the element.

Excitation was started in 4 adjacent elements at the same time, and repeated in the same elements immediately following the absolute refractory period. This was repeated till selfsustaining activity occurred, which continued indefinitely unless the computer was instructed to stop.

5.2.5 *Ventricular myocardium model*

For the conditions used by Moe et al in the above described model it does not seem worthwhile to extend this model to a three dimensional structure. Undoubtedly, if sufficient tissue mass is present, self-sustaining activity will occur. More attractive, however, is to test a hypothesis of a possible reentry mechanism in the ventricles.

Recently extensive work has been done on the properties of the Purkyne fiber network and transition from Purkyne fibers to ventricular myocardial fibers (94,93,85,36,35).

(a) It has been shown that the Purkyne fiber network is extremely sensitive to environmental changes, especially in respect to conduction velocity (85). Under experimental conditions in which a high extracellular potassium level (± 47 mM) was maintained extremely slow conduction velocities have been observed (35). Action potential changes are found under this condition similar to those obtained under conditions of hypoxemia or ischemia (66).

(b) Conduction block will occur first at the gates (85,94). Retrograde conduction from the heart muscle into the Purkyne fibers is possible longer than antegrade conduction (85).

(c) In an infarcted area conduction velocities are also lower (intrainfarction block) (158), as well as in the heart cells just around the infarcted area (perinfarction block) (158).

5.3 *Methods*

In the following paragraphs first the functional relationship of the elements will be defined, that is (1) the relationship of the functional recovery period (FRP) and the following action potential duration (APD), and (2) the relationship of the FRP and the conduction velocity (CV). Secondly, the impulse conduction under repetitive stimulation in a simple two dimensional sheet will be studied. Random inhomogeneity in respect of the first functional relationship is assumed. Thirdly, the nature of the induced selfsustaining activity will be evaluated and compared with the model of Moe et al. Fourthly, an attempt will be made to simulate one possible reentry mechanism in the heart model.

5.3.1 *Action potential duration*

Based on the above described model (100,101), the author used two exponential functions

$$f_1(t) = 1 - e^{-t/\alpha} \quad (57)$$

$$f_2(t) = e^{-t/\beta} \quad (58)$$

to predict the action potential duration from the previous functional recovery period. The approach is depicted schematically in Fig. 5.1.

If function f_2 depicts the x_1 -deactivation, then after time interval FRP, the remaining magnitude of x_1 is h , which initiates the following activation function f_1 h units closer to the threshold than normally. This results in a shortening of the time necessary to reach full activation of t_0-t_1 , after which deactivation starts again.

Using the time constants of $\alpha = .113$ sec and $\beta = .180$ sec for functions 1 and 2, respectively, the used algorithm results in an APD-FRP relationship as depicted in Fig. 5.2 A,B. Using the same relationship in a train of stimuli with fixed interval, the resulting APD's are seen in Fig. 5.2 C,D.

The ionic component I_{x_2} of Noble and Tsien's model could explain the long term change in action potential duration. When the heart rate is normal, the intervals are so short that x_2 will never be fully activated or deactivated. If the above described relationship is valid, the ratio of the 'functional recovery period' to the 'action potential duration' will increase with slow heart rates and decrease with high heart rates. In the latter case, the total time of deactivation will be smaller than the total time of activation, resulting in a larger contribution of I_{x_2} to outward current and thus shorter action potentials. Since the time constant of x_2 is much larger than that of x_1 , this effect will only be appreciable if longer series of stimuli are considered.

A similar scheme as in Fig. 5.1 is used to calculate the outward current component of I_{x_2} to outward current at the time of depolarization

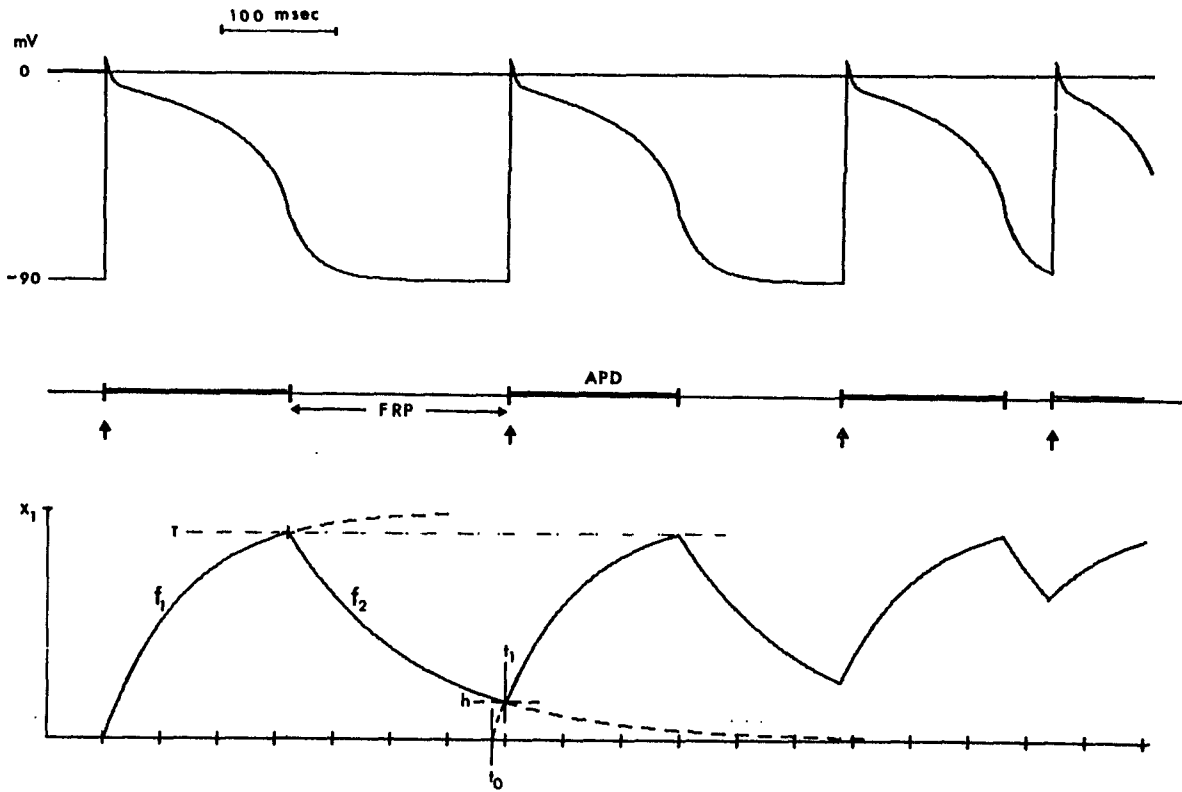


Fig. 5.1 Sequential relation of action potential duration (APD) and functional recovery period (FRP).

Bottom trace gives activation course of X_1 . Function 1 starts at time indicated by arrow. As soon as the threshold T is exceeded, deactivation function 2 starts. After interval FRP, at time t_1 , $F_2(t_1) = h$. For the following APD F_1 starts at this value. Resulting shortening of following APD is $t_1 - t_0$ in which t_0 is the theoretical time of activation of the element, if no preceding activation has occurred and the maximum APD - duration would have followed. Middle line indicates durations of action potentials, and functional recovery periods. Arrows indicate the time of excitations; which in this example happened after infinite duration of FRP for the first excitation, and after 190 msec and 40 msec FRP for the following excitations. Top tracing shows corresponding simulated action potentials.

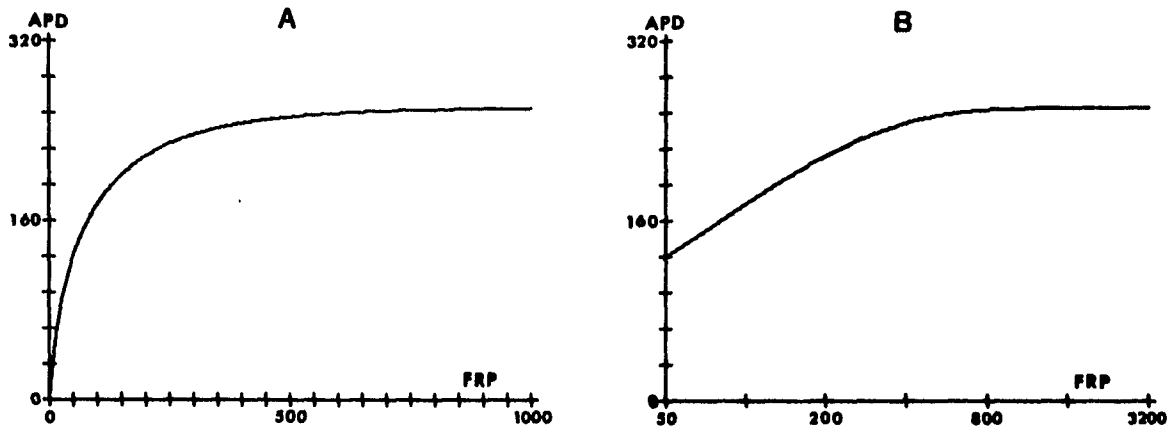


Fig. 5.2 A,B. Relationship of action potential duration and previous functional recovery period.

- A. Linear scale for APD and FRP, both in msec.
- B. Log scale for FRP, linear scale for APD, both in msec. Maximum APD obtained is 260 msec.

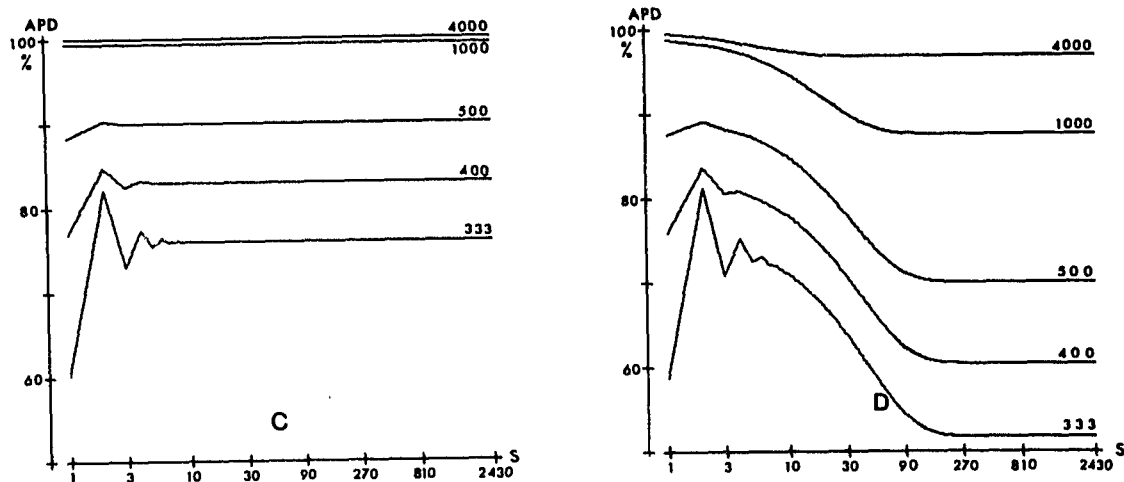


Fig. 5.2 C,D Simulated APD after a train of stimuli with fixed intervals.

- C. APD expressed as percentage of maximum action potential duration. The stimulus interval used is indicated on each trace. Horizontal scale indicates number of stimuli. Stimulus scale (S) is logarithmic.
- D. Scaling as under C. Long term influence of continuing stimulation considered.

is simply added to the one due to x_1 to determine the following action potential duration. Time constants used for activation and deactivation were .250 sec and 0.5 sec, respectively.

For stimulation with a train of stimuli with fixed intervals, the resulting shortening of action potential duration is seen in Fig. 5.2 D.

5.3.2 Conduction velocity

Based on the short time constant reported for activation and deactivation of the sodium carrier (149) the author used an exponential relationship between conduction velocity and functional recovery period (Fig. 5.3A). In one of the experiments the relationship given by Moe et al (89) was also used (Fig. 5.3B).

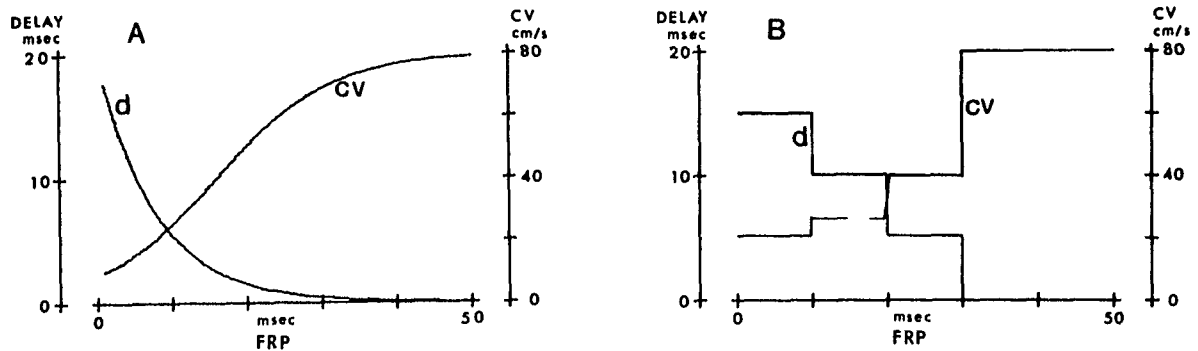


Fig. 5.3 A,B Relationship of conduction velocity and FRP.

A. Relationship of authors model.

B. Relationship as given by Moe. et al (*S2)

Curve labelled cv. refers to conduction velocity, with scale on the right. The same relationship given as delay function, labelled d, scale on the left. Assumed maximum conduction velocity 80 cm/sec.

5.3.3 *A simple structure of 2500 elements*

A sheet of 2500 elements comprising 50 rows and 50 columns was chosen. The interaction functions described in paragraph 5.2.1 and 5.2.2 were used. Since only a limited number of beats will be considered, the long term influence of action potential duration was excluded. Inhomogeneity was introduced by randomly assigning type numbers to each element. Ten different types were assigned. The type numbers are used in determination of the maximum action potential duration for each element. The relationship between action potential duration and functional recovery periods for the types with longest and shortest action potential is seen in Fig. 5.4A. The first activation is assumed to have occurred after infinite long interval, that is, the refractory periods of cells are long past, so no reduction in conduction velocity will occur and all elements are responsive. The above model is designated model R. To compare the author's results with those described by Moe, a second model (model M) was tested for which the functions as specified by Moe were used (Fig. 5.4B). The randomly assigned type numbers served as K-values in formula (56). For computational convenience the interval between the end of the previous refractory period and the following excitation (FRP-interval) was used to estimate the previous R-R interval. This estimated R-R interval was used for the calculation of the absolute refractory period. In both models activation was started in the same element, and this element was reexcited immediately after the end of the refractory period, and a third time after the end of the second refractory period,

etc. In the computation of electrocardiograms the simulated action potential described in 4.2.3.1 is used. Electrograms are computed as heart vectorcardiograms.

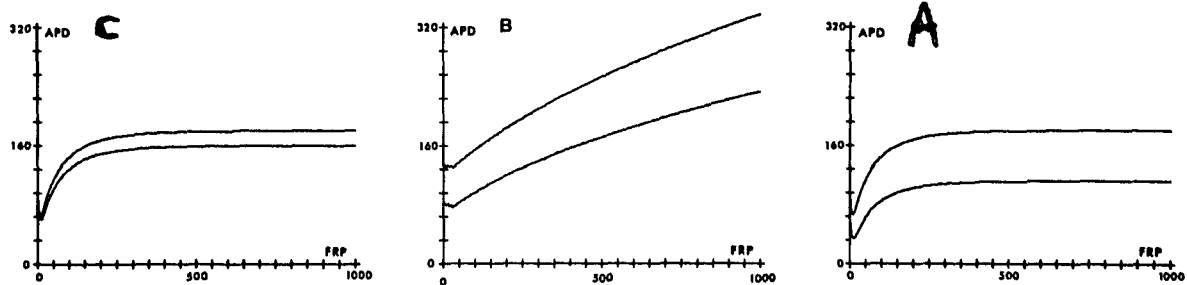


Fig. 5.4 A,B,C Relationship of APD and FRP

Linear scale, in msec.

- A. Author's model
- B. Model proposed by Moe et al.
- C. Author's model with decreased spacial dispersity.

5.3.4 *Ventricular myocardium model*

An infarcted area was created in the heart model along the anterior interventricular sulcus (see Fig. 5.5). The typing of the elements is seen in Fig. 5.6. The center of the infarcted area consists of type 3 elements, the transitional zone of type 4. Type 3 elements did not conduct at all, type 4 elements conducted with a conduction velocity of 8 cm/sec. Their refractory period was 130 msec. The Purkyne elements in contact with the transitional elements also conducted slowly and are not able to transmit an impulse towards the myocardial elements. Excitation was started at the normal locations.

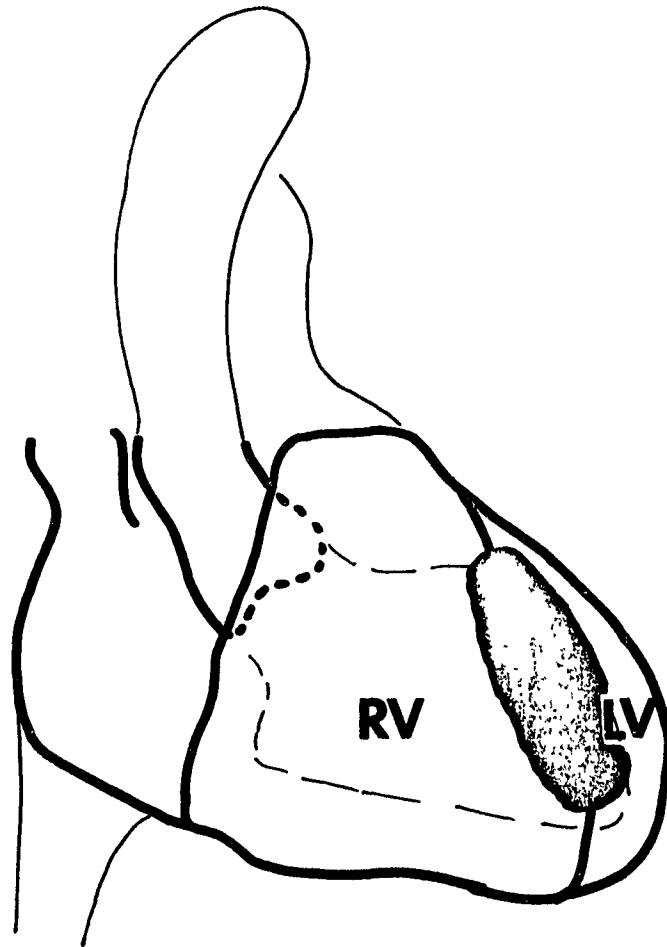
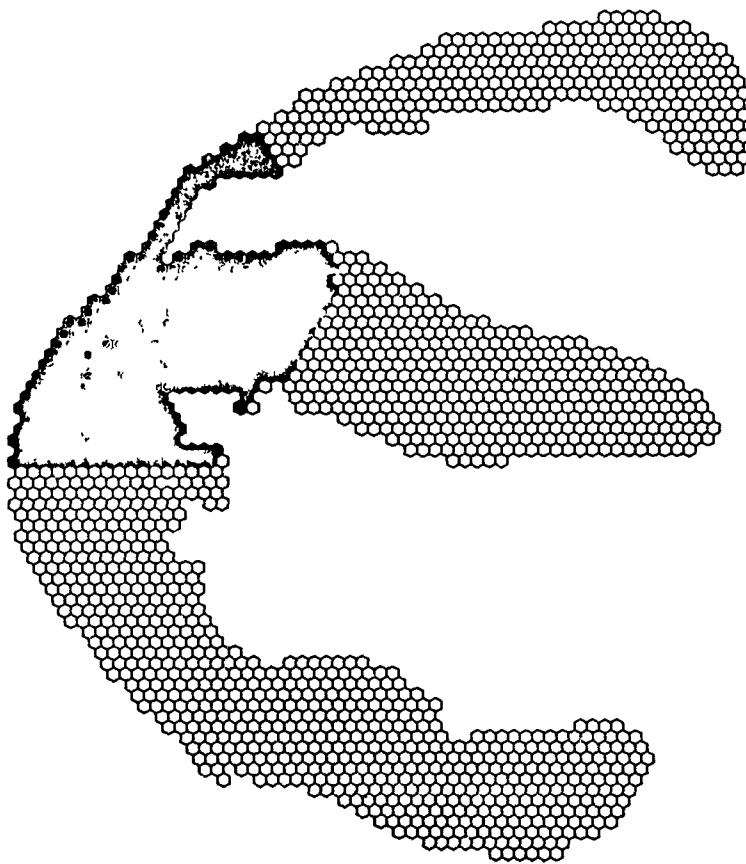


Fig. 5.5 Area of simulated infarction.

Area in which elements are typed as 'infarcted' is indicated in black.

Elements of nucleus of infarction are indicated with black solid circle, and black elements are elements in transitional zone. (Section 40).

Fig. 5.6 Typing of infarcted elements



5.4 Results

5.4.1 Impulse conduction with repetitive stimulation

For one single stimulation the results are seen in Fig. 5.7. The number of elements activated at each time step are indicated, as well as the computed electrocardiogram. The element in which excitation is started is excentrically located in column 26, row 16. The number of elements activated at each time step is rapidly increasing after the start of excitation. The abrupt changes in the curve are caused by the extinction of parts of the wave front at the edge of the sheet. The resultant electrogram shows in agreement with this, the first forces at the moment the closed wave front reached the edge of the sheet. Activity spontaneously ceased after 177 msec. In Fig. 5.8 A,B,C,D a first stimulation followed by a second stimulation at 132, 135, 153 and 156 msec intervals, respectively, is seen. The results of the first stimulation are identical to those of the single stimulation. A second stimulation of the same element after an interval of 132 msec does not result in a second excitation of the sheet. A second stimulation after three msec larger interval (Fig. 5.8B), however, resulted first in excitation of a few elements followed after a few msec by a reexcitation of the whole sheet, which however does not stop anymore. From the electrogram it can be appreciated that reexcitation occurs first in two or three more or less regular excitations, and afterwards becomes more chaotic. The computer run was terminated after 900 msec. A second

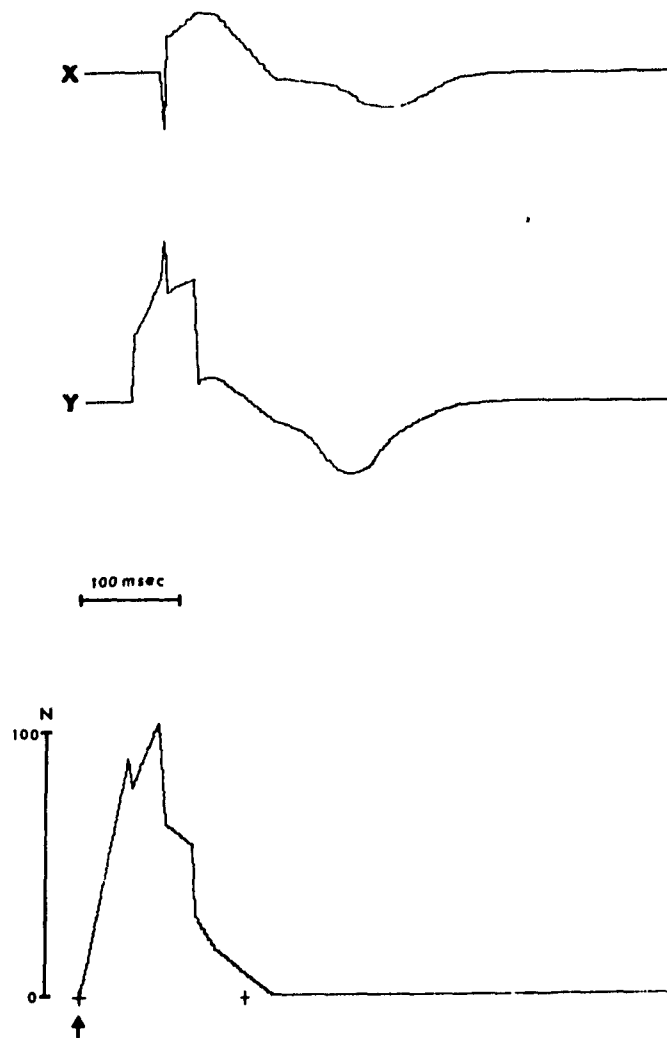


Fig. 5.7 Single excitation of simple sheet.

Excitation started in one element. Two top traces show X and Y components of computed electrogram. Amplitude is in arbitrary units.

Bottom trace indicates the number of elements excited at each time step.

The time of stimulus is indicated by arrow.

Fig. 5.8 A,B,C,D First and second excitation of simple sheet.

First and second excitation started in same element. In each panel top traces show X, and Y components of computed electrogram, bottom trace number of elements excited in each time step. Arrows indicate time of stimuli. APD - FRP relationship as seen in Fig. 5.4 A.

- A. Second stimulus after 132 msec.
- B. " " " 135 msec.
- C. " " " 153 msec.
- D. " " " 156 msec.

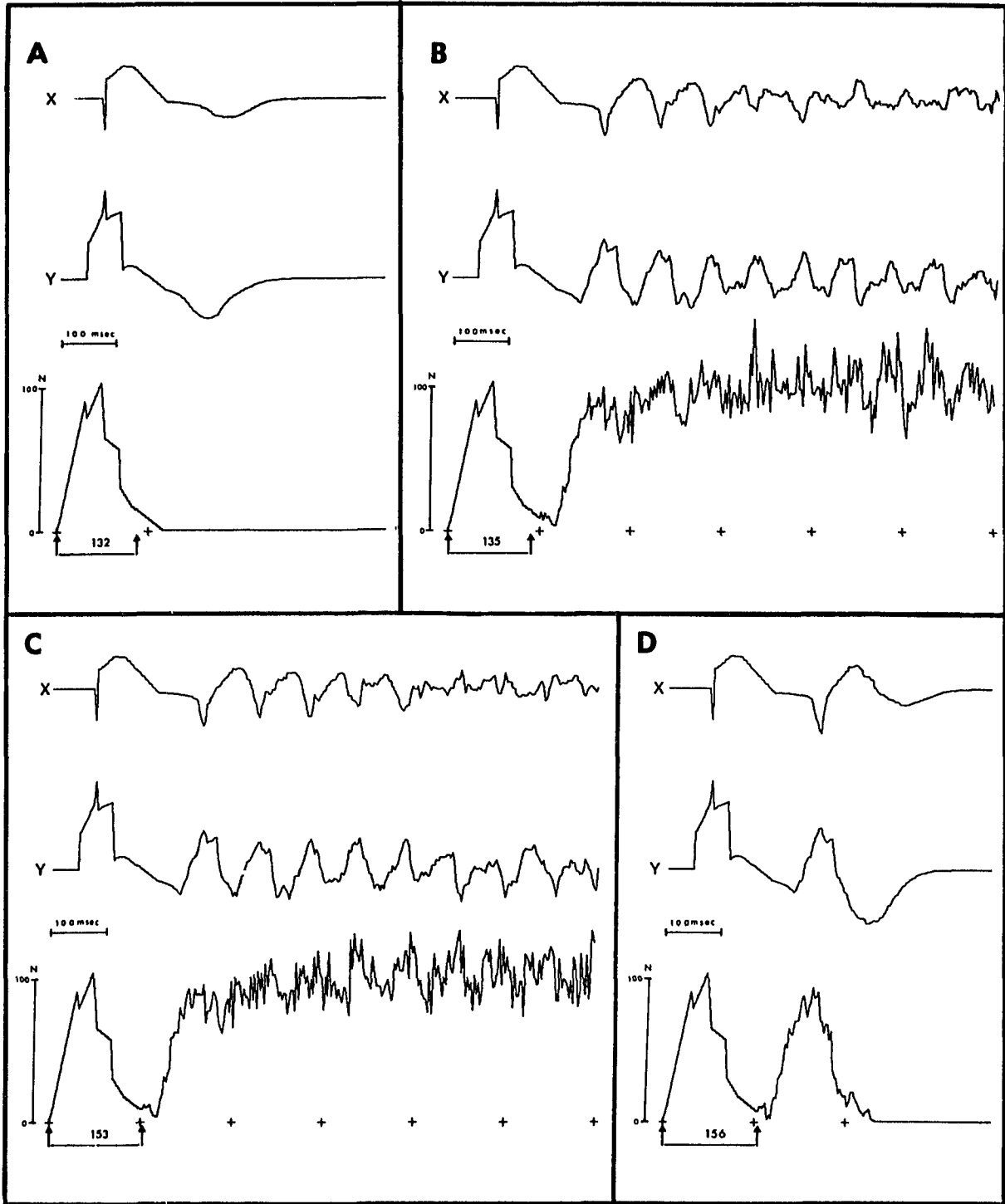


Fig. 5.8 A,B,C,D

stimulation after 153 msec interval (Fig. 5.8C) shows the same behaviour as just described, whereas a second stimulation after 156 msec (Fig. 5.8D) results in one single reexcitation which spontaneously stops after 198 msec. Note the irregular appearance of the reexcitation and the increased duration (198 msec) as compared with a 'normal' first excitation of 177 msec. For a long train of stimuli with decreasing intervals, the results are seen in Fig. 5.9.

The result of the first stimulation is identical to the above described single stimulation. Each following stimulation also results in complete excitation. With a stimulus interval of 120 msec the resulting excitation becomes irregular, whereas 75 msec interval sets off completely irregular chaotic activity. Note that the second, third and fourth stimulus are accompanied by an electrical alternans.

Introduction of selfsustained activity is also possible if the spacial dispersity is reduced. The relationship between APD and FRP is seen in Fig. 5.4C. A series of stimuli at the same element, properly timed, induced selfsustaining activity. A minimum of six additional stimuli was necessary to induce this activity, which continued indefinitely. Results are seen in Fig. 5.10 for the first 1.5 seconds.

Fig. 5.9 Excitation of simple sheet with train of stimuli with decreasing intervals.

Each stimulus applied in the same element. Intervals decreasing from 210 to 75 msec. X and Y components of computed electrogram, are on top, bottom trace shows number of elements excited in each time step. Arrows indicate time of stimuli. APD - FRP relationship as seen in Fig. 5.4 A.

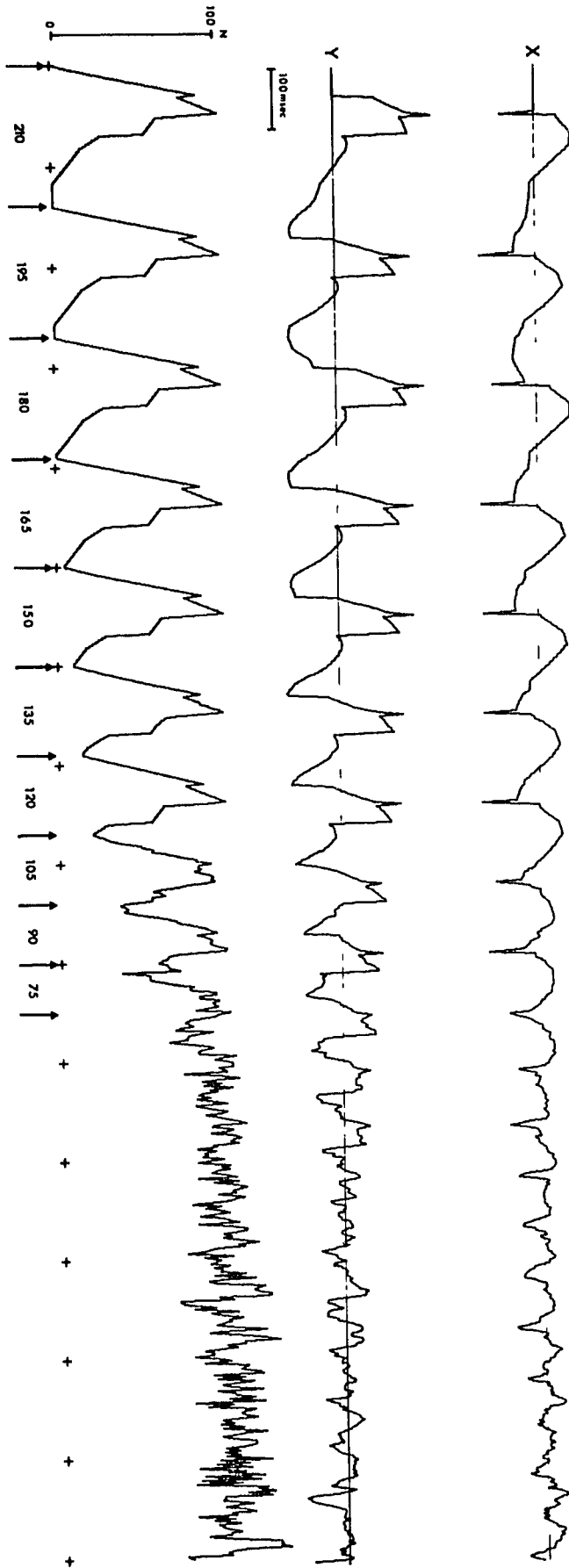


Fig. 5.9

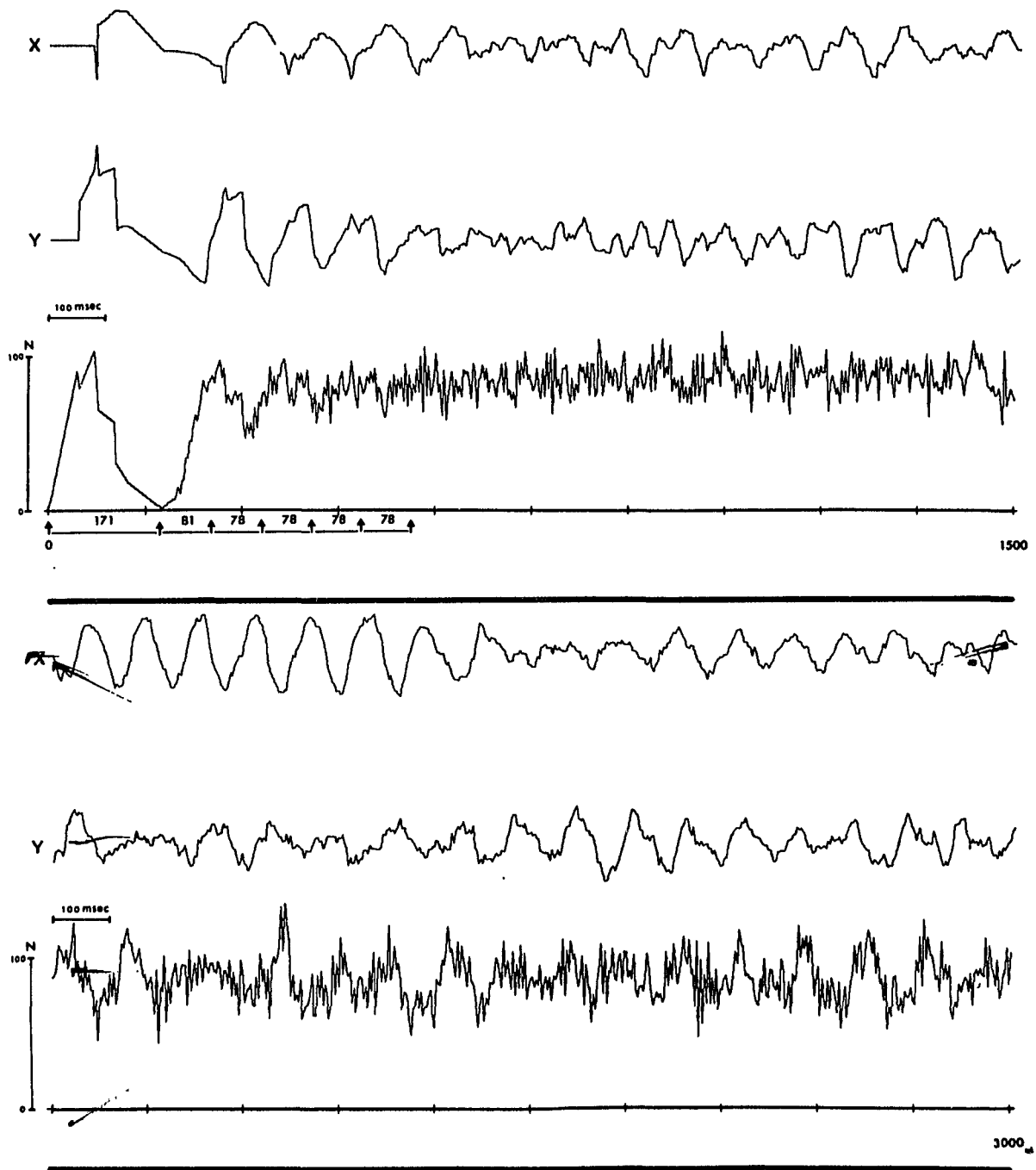


Fig. 5.10 Excitation of a simple sheet with reduced spatial dispersity.
Each stimulus is applied in the same element, with intervals of 171, 81, 78, 78, 78, and 78 msec respectively. Top tracings show X and Y components of computed electrograms, bottom trace the number of elements excited in each time step. Arrows indicate time of excitation. APD - FRP relationship as seen in Fig. 5.4 C.

5.4.2 *Selfsustaining activity*

In both models selfsustaining activity resulted. In the author's model (model R) the selfsustaining activity, which occurred after a second stimulation with 135 msec interval after the previous one, was maintained for 12 seconds, that is 4000 time steps. In the model proposed by Moe et al (89) (model M), selfsustaining activity occurred after 40 stimulations with an interval of 25 msec. No attempt was made to find the minimum number of stimuli which are still effective. The computer run was terminated after 4300 timesteps, that is, 21.5 seconds. For nine elements in the sheet the activity was sequentially analyzed. The location of these elements is seen in Fig. 5.11. A sequential histogram for the points are seen in the same figure, whereas Fig. 5.12 shows the corresponding serial correlograms.

The Chebyshev polynomial approximation for the interval sequence (the continuous line in the sequential histogram) shows slow trends in the intervals. The serial correlograms are computed without trend correction. A rather large oscillation of the trend is seen in element 3, 6, and 8. Table VII lists for each of the nine elements the number of times the element was excited, the mean interval, SD of the interval, and the type number of the element. The same elements were also analyzed in model M. The sequential histograms for the elements are seen in Fig. 5.13 and the serial correlograms in Fig. 5.14. Table VIII lists for each element the same data as was listed for model R in Table VII.

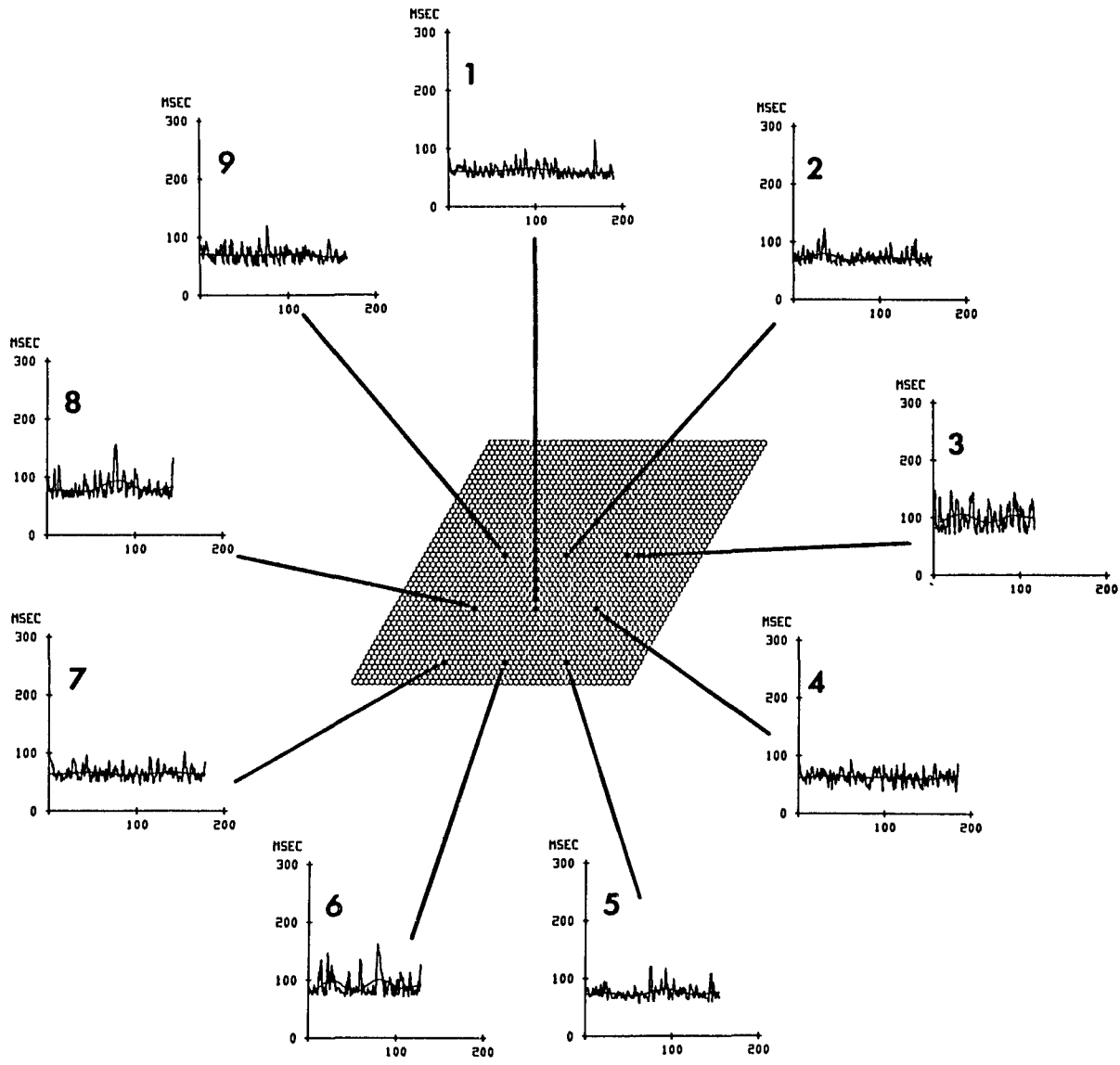


Fig. 5.11 Location of elements for sequential analysis. Author's model.
The sheet of elements (in center), with black dots identifying location of elements analyzed. Sequential interval histograms are shown for the elements chosen.

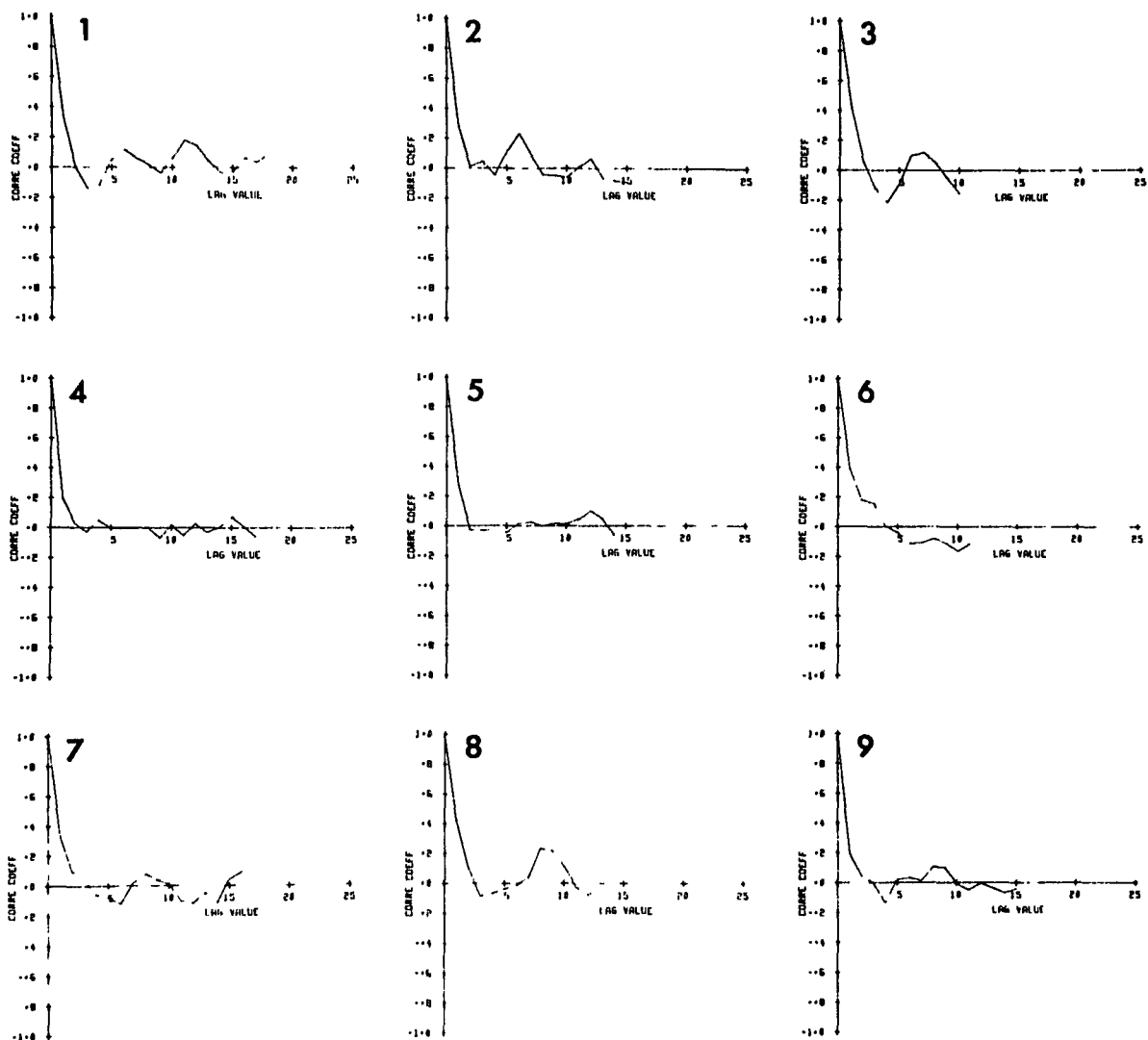


Fig. 5.12 Serial correlograms of sequential intervals. Author's model.
Correlograms computed from sequential intervals of the nine elements shown in Fig. 5.11 . Correlation coefficients plotted vs lag value.

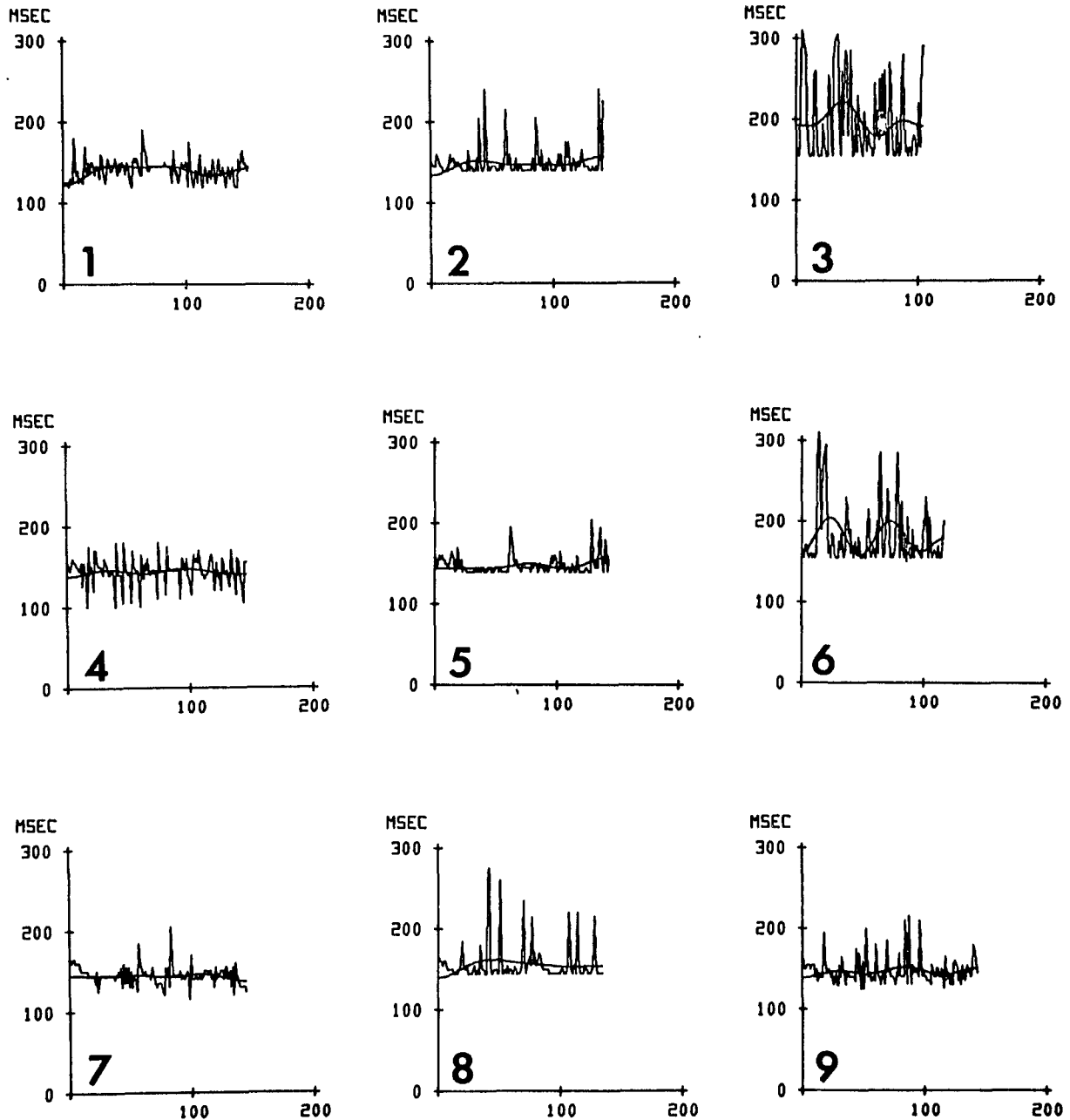


Fig. 5.13 Interval histograms of activity of elements. Model of Moe et al.
Sequential intervals plotted vs interval number as in Fig. 5.11.

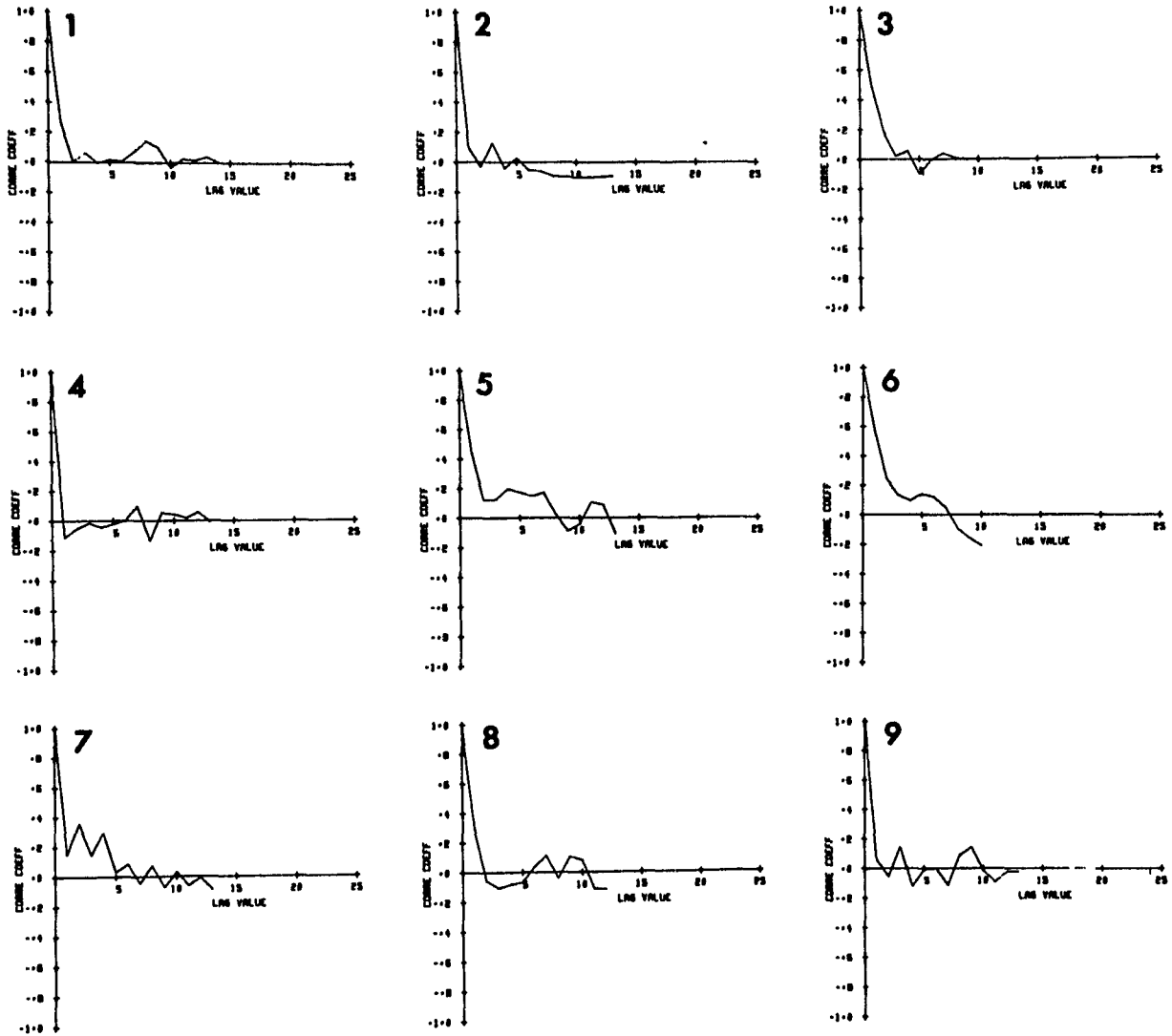


Fig. 5.14 Serial correlograms of sequential intervals. Model of Moe et al.
Correlograms computed from sequential intervals of the 9 elements shown
in Fig. 5.13.

5.4.3 *Ventricular myocardium model*

The components of the pure dipole VCG are seen in Fig. 5.15. After the first excitation a second excitation followed spontaneously; after this an increasingly chaotic activity takes place. After 1720 time steps the run was terminated. Note the ST-segment changes in the first excitation.

5.5 *Discussion*

5.5.1 *The relationship functions*

The purpose of paragraph 5.3.1 was to define the relationship of the refractory period and the functional recovery interval, rather than explaining it. The relationship used by Moe et al (89) and as given by Alessi (5) or Bazett (8) are clearly in disagreement with the physiological properties of interacting cells. First of all, it is known that a certain maximum action potential duration is associated with long stimulus intervals; the mentioned relationships do not incorporate this property. Secondly, it is unlikely that the influence of the preceding interval length or the heart rate should be mediated to the muscle cell, other than by some electrochemical or chemical process. These processes tend to follow first order kinetics, so any dependent variable will change exponentially with time. The relationship functions proposed in the present investigation, based on membrane model considerations, show a remarkably good agreement with measured data. The relationship of FRP and APD is in apparent agreement with the results of Carmeliet (27).

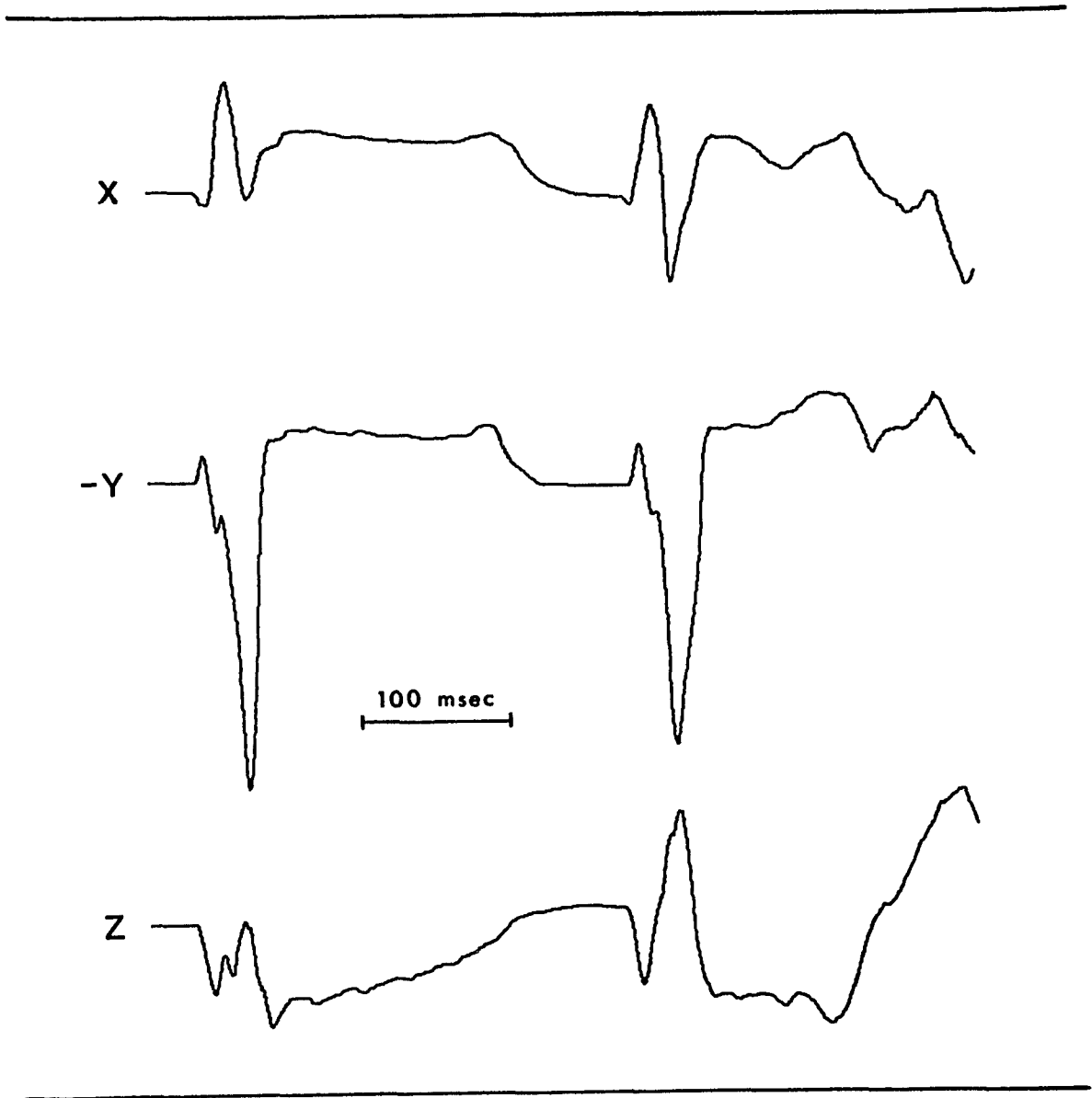


Fig. 5.15 Excitation of ventricular myocardium with anteroseptal infarction.
X, - Y, and Z components of heart vector cardiogram. First excitation is started at the normal locations (4.2.1). Second excitation occurs spontaneously and proceeds into increasingly irregular reexcitation sequence.

in a train of stimuli with fixed intervals, the electrical alternans is reproduced (Fig. 3C), however, not the decreasing action potential duration after a large series of stimuli. This decreasing action potential duration is sufficiently reproduced if the slow activating outward current I_{x_2} is also simulated (Fig. 3D). The shown relationship compares very well with the data from Vick (146).

The conduction velocity is expressed as a conduction delay between two elements. It can be argued whether this conduction delay effectively increases the functional recovery period and thus influences the following refractory period, or only increases the effective refractory period. In terms of the membrane model followed the question is: is there still a deactivation of x_1 and x_2 during the delay or not? Since activation and deactivation are membrane voltage dependent, it is difficult to make an exact prediction of what happens during a slow depolarization. For this reason, the delay is only considered to be an effective increase in refractory period. It should be noted that the fibrillation model of Moe et al (89) also takes the same stand. This effective increase in refractory period is seen in the relationship of APD and FRP in Fig. 5.4 A,B,C for FRP periods of less than 20 msec, causing a 'dip' in the curve.

The relationship described above between conduction velocity and functional recovery period is a functional one. Under normal conditions (i.e. functional recovery periods considerably longer than 20 msec), the maximum conduction velocity is obtained. It is also conceivable under pathological conditions that this maximum conduction velocity is reduced or enhanced (supernormal conduction) (39). Other interactions like summation or inhibition of impulses are not considered in the present

study.

5.5.1.1 *Repetitive stimulation*

The excitation following the first stimulation is conducted in a normal fashion throughout the sheet (Fig. 5.8). The refractory period of each element is set according to the relationship shown in Fig. 5.4A, each element obtaining its maximum refractory period, which are not identical. The dispersion of refractory periods is better appreciated if the relationship of Fig. 5.4A is transformed into the relationship of the refractory period following the second excitation and the interval length between the first and second stimulation ($R_0 - R_1$) (Fig. 5.16)

The second stimuli following the first with an interval shorter than a^1 will not excite any element. The second stimuli following the first with an interval ($R_0 - R_1$) where

$$a' < R_0 - R_1 \leq a'' \quad \text{will excite some elements, and if}$$
$$a'' < R_0 - R_1 \quad \text{all elements will respond.}$$

As a result of the first excitation, a spatially distributed inhomogeneity is created, which will influence the behaviour of the following excitations. The structure is 'conditioned' by the first excitation. Each following excitation will change the condition of the elements, consequently the behaviour of any excitation should be evaluated in the light of the previous conditioning excitation.

5.5.1.2 *The second stimulus*

Any stimulation with an interval after the first stimulation larger than b in Fig. 5.16 is normally conducted without any delay.

If the same element is excited, an identical excitation results, however, if the stimulus interval is less than approximately 500 msec, the following refractory periods are shorter. Any following stimulus with identical interval will thus always be conducted. A second stimulus with an interval between a^{11} and b^1 will be conducted throughout the sheet, though not normally. Those elements which have their 'dip' between a^{11} and b^1 will show slower conduction. After this beat the refractory periods are again shorter, permitting the next beat with an identical interval to be conducted normally. Second stimuli with intervals between a^1 and a^{11} will not only be conducted abnormally, but the possibility also exists that elements will be still in the absolute refractory period and do not participate at all in the conduction. The earlier the second stimulus follows the more elements will not conduct. Finally, if the interval is shorter than a^1 no response at all will be expected.

Stimuli with the intervals between a^1 and a^{11} possess the possibility to start a selfsustaining activity. For this selfsustaining activity it is necessary that the activation survives long enough to re-enter elements which are already passed the refractory periods of the second activation. This will happen if elements which could not be excited at their regular time are excited by elements which are slowly conducting. The maximum conduction delay of 20 msec is not sufficient by itself to make the elements desynchronized enough to allow the re-entry. With a minimum refractory period of 32 msec for the elements with the shortest refractory period a minimum of two maximally delaying elements must be passed to allow for the re-entry.

This possibility exists only if a number of elements are bypassed in the first excitation. As argued above, the earlier the second stimulus follows, the more elements are bypassed and the larger the likelihood of re-entry. Two factors emerge from the reasoning followed:

(a) The larger the differences in refractory periods between elements of the same structure, the larger the amount of non-conducting elements in an early second excitation. This will enhance the probability of re-entry.

(b) The slowdown in conduction velocity is a prerequisite for starting the reentry.

Fig. 5.8C shows the resulting selfsustaining activity after a second stimulus at 153 msec. A second stimulus started at 156 msec (Fig. 5.8 D) does not result in selfsustaining activity but yields a second excitation, which is not 'normal'. Second stimuli earlier than 135 msec do not yield any second excitation at all nor selfsustaining activity (Fig. 5.8A).

5.5.1.3 *Third and subsequent stimuli*

Third stimuli following with equal intervals the second one can be considered in the same way as a second stimulus, preceded by two conditioning stimuli. The question of interest is then how the conditioning differs from the one in the previous paragraph. For second stimuli more or less normally conducted no essential difference occurs, however, second stimuli which are not normally conducted and neither result in selfsustaining activity (i.e. no reentry occurs) cause a conditioning with even wider variety in possible responses than after a

first conditioning excitation. This is caused by the elements which did not conduct and where the third stimulus has a large previous interval. With such third stimuli the likelihood of selfsustaining activity is greatly increased.

Fig. 5.10 is an example of the stimulation of a sheet with reduced spatial dispersity. The differences between the elements with maximum and minimum refractory periods are very small (20 msec difference in maximum APD), decreasing to 4 msec at their 'dips' (see Fig. 5.4C).

5.5.1.4 *A long train of stimuli*

If second and third excitations are more or less normally conducted, i.e. all cells responded to excitation, continuation of stimuli with equal intervals will not result in selfsustaining activity. As outlined, this is caused by the shorter refractory periods due to the previous excitations. If the intervals are gradually shortened the decreasing refractory periods will allow higher and higher stimulus frequencies, of which the maximum is determined by the shortest refractory periods (at the 'dip' of the function curve). Such a series of decreasing intervals is seen in Fig. 5.9, in which finally a stimulus interval of 75 msec (stimulus frequency of 1250 bpm) resulted in self-sustaining activity. A second stimulus with this interval would not even be conducted. If the long term difference on refractory periods would also have been considered, even smaller intervals could have been obtained.

5.5.2 *Selfsustaining activity*

In both models selfsustaining activity is possible. The nature of this activity is irregular. This can be seen from Table VII, where elements reasonably close together are excited at different times (elements 7, 6, and 5 for instance are excited 179, 129, and 156 times, respectively), which could not have happened if regular wavefronts passed through all of them. The regularity could also occur on a smaller scale if certain pathways were reexcited every time. The serial correlograms, however, show little correlation between the intervals of successive excitations. This makes any regularity in excitation patterns unlikely. For lag value 1 sometimes a fair correlation exists (see Fig. 5.12). The serial correlograms of elements with the longer maximum action potential durations (elements 3, 6, and 8; type 20, 20 and 18 respectively) show rather large correlations for lag value 1 (.42, .39 and .43, respectively). It should be noted, however, that the total number of excitations (about 140) is relatively small for computation of a serial correlogram. No trend correction was done, which will especially influence these three elements which show a distinct trend. The difference between the two models is basically the relationship between the action potential duration and the functional recovery period. Although this relationship in the author's model represents more adequately physiological observations than the model of Moe et al, little difference is seen in the results regarding selfsustaining activity. The mean interval is practically twice as large in model M. This could be anticipated because the shortest possible refractory period in model M is practically twice as large as in model R. Much smaller differences

in spatial distribution of action potential duration still allow self-sustaining activity, as demonstrated in Fig. 5.10.

In the above discussion, the random nature of the selfsustaining activity was emphasized. According to Bootsma (14) this random activity is characteristic for fibrillation. However, in their evaluation one more unknown parameter is included, which is the impulse conduction in the AV-node.

The above simulation experiments show a striking similarity to the experiments in which a fibrillation-like activity was induced in dog atria by short bursts of repetitive stimulation of the auricle (88). This activity could be maintained if the vagus nerve was stimulated. Vagal nerve stimulation was found to create a spatial dispersity in refractory periods in dog atria as well as in dog ventricles (59). A number of other agents (hypoxia, hypercapnea, hyperhalaemia and several drugs) have also been found to be able to create this dispersity (59). The possibility to create and maintain the fibrillation-like activity was attributed to this dispersity in refractory periods. The model of atrial fibrillation as described by Moe et al (89) is based on the re-entry theory. The functional one-way block occurs if an element is excited in its absolute refractory period. This will only happen if the refractory period duration is different from one element to another. The differences introduced between the elements are thus an essential feature of this model. However, it does not follow automatically that the resulting activity is identical in nature to fibrillation. The activity might well be an artefact introduced by the formula used to

calculate the refractory periods.

In the dog experiments quoted, the activity seen was labelled atrial fibrillation on the basis of the recorded electrocardiograms, as well as on visual inspection of the contracting atria. Recently it was demonstrated, however, that atrial fibrillation induced artificially differs from autochtone occurring atrial fibrillation (137). The argument in this report is based on the interrelationship of ventricular excitation intervals, which is seen to be totally uncorrelated in spontaneous atrial fibrillation, but shows remarkable intercorrelation in artificially induced atrial fibrillations. The validity of the proof given is questionable, however, since the fibrillation was maintained by continuous direct electrical stimulation, whereas in Moe and Abildskov's experiment fibrillation was maintained under vagal nerve stimulation without direct stimulation of the atria.

The question is essentially, what type of activity is to be called fibrillation and what type is not. It is difficult, if not impossible, to provide a satisfactory answer to this question.

Clinically, fibrillation is diagnosed in physical examination if the atrial pulsations are irregular in time and unequal in strength (*pulsus irregularis et inequalis*). Electrocardiographically the following criteria are used (74): (1) the absence of P-waves, (2) the presence of fibrillation waves, at a rate between 350 and 600, which are irregular in spacing, timing, and amplitude, (3) grossly irregular beating of the ventricles. These criteria do not adopt an electrophysiological viewpoint on the cause of fibrillation or the mechanisms which maintain fibrillation.

Since the first reports by Engelman (47) and Mines (87) two different theories, both attempting to explain fibrillation, are advocated. The first is the ectopic focus theory, which states that fibrillation is started and maintained by one or more ectopic foci which fire with high frequency. The second is the reentry theory, advocating some mechanisms in which the impulse survives and subsequently reenters a tissue which is already past its refractory period. An extension of the last theory is the multiple wavelet hypothesis, which proposes that the activity is maintained by a large set of independent wavelets. To explain the onset of fibrillatory action the ectopic foci theory is more suitable. In the reentry theory, fibrillation will only start if an excitation survives at least for the duration of the refractory period. Under normal conditions for the atria this means a time of 180 msec. With an average conduction velocity of 80 cm/sec this amounts to a pathway of 14.4 cm in length, which seems unlikely even with a most tortuous path. For the ventricles an action potential duration of 260 msec and a conduction velocity of 45 cm/sec the pathway is 11.7 cm, which also seems unlikely. If, however, the conduction velocity is reduced under pathological conditions and/or the refractory period shortens, reentry might be possible. The ectopic focus theory is not so suitable to explain the apparent lack of periodicity indicated by the electrograms and electrocardiograms recorded under existing fibrillation. Either entry or exit block has to be assumed, to explain the occurrence of irregular rhythms. If the heart muscle is assumed to be functionally a syncytium, the reentry theory also needs to postulate a one-way block. The assumed blocks, either in the ectopic focus theory or in the

reentry theory, need not be continuous structural defects in the anatomical sense, but might as well be functional blocks occurring at a particular time instant.

The multiple wavelet hypothesis as proposed by Moe and Abildskov suggests an explanation for the continuation of fibrillatory action, independent of the mechanism which started it, be it either reentry or ectopic focus mechanism.

5.5.3 *Ventricular myocardium model.*

The experiment of which the results are seen in Fig. 5.15 is merely a demonstration of the possibility of reentry in the ventricular myocardium, if a sufficiently slow conduction and sufficiently short refractory period is postulated. The conduction velocity used (8 cm/sec) is on the conservative side as compared with the reported values in depressed Purkyne fibers (36). The action potential duration used is chosen rather arbitrarily. Once reentry occurred, the onset of fibrillation flutter-like action is no surprise. More experimental data are needed to create a more heuristic model for ventricular fibrillation. Experimental facts are particularly needed on electrophysiological behaviour of an infarcted area.

5.6 *Conclusions and summary.*

The relationship between functional recovery period and both action potential duration and conduction velocity is formulated on the basis of membrane model considerations.

The resulting relationship between action potential duration and functional recovery period agrees with experimental data reported in the literature. The behaviour of a simple conglomerate of elements is analyzed using the above mentioned relationship.

Second and subsequent stimulations are seen to result in self-sustaining activity, if applied in a certain time period after the first stimulations. This period can be lengthened by subsequent stimulations. The nature of the selfsustaining activity is analyzed and compared with the selfsustaining activity of a previously reported model of atrial fibrillation.

Though based on different relationship functions, both models exhibited similar behaviour.

Serial correlograms revealed a grossly chaotic and random activity in both models.

Under admittedly rather speculative constraints an infarcted area is simulated in the ventricular myocardium model. Infarction resulted in ST-segment changes in the heart VCG, and spontaneous occurrence of a second excitation followed by a chaotic activity.

Chapter 6

SUMMARY AND CONCLUSIONS

- 1) A digital computer model of ventricular excitation and repolarization in man was developed.
- 2) The geometry of the human heart obtained at autopsy served as anatomical basis for this model. The Purkyne fiber system was added on functional rather than anatomical basis.
- 3) Simulation of normal excitation was performed and seen in general to be a sufficiently accurate substitute for experimentally obtained data.
- 4) The electromotive forces generated by the excitation wave fronts were computed on the basis of the transmembrane potential distribution, and expressed either as a single dipole (the heart vector) or used, in the form of multiple distributed dipoles, to compute body surface potential distributions. A numerical substitute of the human torso was used for these last computations.
- 5) The heart vector cardiogram was essentially normal except for the late depolarization sequence.
- 6) The 12-lead ECG and VCG's of 4 commonly used vectorcardiographic lead-systems are extracted from computed surface potential distributions in order to compare them with the heart VCG.
- 7) The 12-lead electrocardiogram was seen to be within normal limits. Some abnormalities observed in the heart VCG disappeared in the 12-lead ECG. The largest discrepancies between HVCG and 12-lead ECG occurred in the precordial leads.
- 8) General agreement was found between the simulated 12-lead ECG and the 12-lead ECG recorded from the subject studied by Durrer et al. The late depolarizations again showed the largest discrepancies.

9) The performance of the four VCG lead systems were compared. All lead systems appeared to have satisfactory Y-leads. The X-lead of the Frank, McFee and SVEC III systems are relatively satisfactory and a reasonably accurate Z-lead is obtained by the McFee and SVEC III lead system. The McFee system ranked first in overall performance, followed by Frank and SVEC III, whereas the Burger system is less satisfactory.

10) Simulation of repolarization was done, assuming the repolarization process to be a non-conducted process. Lack of available data forced these models to be more speculative and general. Four hypotheses about ventricular repolarization were tested.

11) A generalized definition of the ventricular gradient vector is presented. Nonuniformities in different parts of the myocardium are represented by means of profile vectors which are operationally defined.

12) The repolarization hypothesis based on the temperature differences in the myocardium yields satisfactory results in the frontal plane projection; spatial discrepancies are observed, however, and the ventricular gradient is directed more posterior than expected.

13) The repolarization hypothesis based on stress distribution yields unsatisfactory results, both in direction and magnitude of the ventricular gradient created, as well as the shape of the resulting T-wave.

14) The hypothesis, which assumed the repolarization to develop in the reversed direction of the depolarization is also unsatisfactory.

15) The hypothesis based on physiological-histological data of Purkyne fiber distribution and action potential durations in Purkyne fibers and myocardium yields a heart VCG, which is closest to normal, both regarding the size and direction of the ventricular gradient as well as the configuration of the T-wave.

16) The T-waves computed from the body surface potential distribution appear much closer to normal T-waves than the T-waves of the heart VCG. The four VCG systems yield T-loops which are more anterior and inferior than the T-loop of the heart VCG and thus resemble much closer normal T-loops. The T-wave amplitudes in the 12-lead ECG are larger than anticipated from the heart VCG.

17) The relationship between action potential duration and functional recovery period is defined on the basis of membrane model considerations. Also a simple relationship between functional recovery period and conduction velocity is assumed.

18) Behaviour of a simple sheet of interconnected elements under repetitive stimulations is studied. The behaviours of this conglomerate of elements resembles in many regards functional behaviour of myocardial cells.

19) The elements exhibit a certain "vulnerable period" after each stimulation in which a second stimulation initiates a chaotic activity. If driven with a train of stimuli with increasing rate shorter intervals are possible than under resting conditions.

20) The nature of the chaotic selfsustaining activity is found compatible with the multiple wavelet hypothesis for atrial fibrillation.

BIBLIOGRAPHY

1. Abildskov, J.A., Burgess, M.J., Millar, K., et al :
The ventricular gradient and "primary" T wave.
Circulation 40: suppl. 3 : 1-34, 1969.
2. Abildskov, J.A., Burgess, M.J., Millar, K., et al :
The primary T wave - a new electrocardiographic waveform.
Amer. Heart J. 81 : 242-249, 1971.
3. Abildskov, J.A., and Klein, R.M. :
Cancellation electrocardiographic effects during ventricular
excitation.
Circulation Res. 11 : 247, 1962.
4. Abildskov, J.A., Millar, K., Burgess, M.J., and Green, L. :
Characteristics of ventricular recovery as defined by the
vectorcardiographic T-loop.
Amer. J. of Cardiology, 28 : 670-674, 1971.
5. Alessi, R., Nusynowitz, M., Abildskov, J.A., and Moe, G.K. :
Nonuniform distribution of vagal effects on the atrial refractory
period.
Am. J. Physiol., 194 : 406- , 1958.
6. Arntzenius, A.C. :
A model of excitation of the human heart.
Ph.D. Thesis, 1968. N.V. Drukkerij Levisson, Rijswijk, Z-H,
The Netherlands.
7. Barr, L., Dewey, M.M., and Berger, W. :
Propagation of action potentials and the structure of the nexus
in cardiac muscle.
J. of Gen. Physiol., 48 : 797-823, 1965.
8. Bazett, H.C. :
Analysis of time relations of electrocardiograms.
Heart 7 : 353- , 1920.
9. Becker, A., and Hellerstein, H.K. :
Effects of drinking iced water on the T loop of the spatial vector-
cardiogram and on the spatial ventricular gradient.
J. Electrocardiology, 2 : 145-158, 1969.
10. Beckwith, J.R. :
Grant's Clinical Electro-Cardiography.
McGraw-Hill Book Company, New York, 1970.
11. Den Boer, W. :
Vectorcardiografie.
Thesis, 1949. Rijksuniversiteit Utrecht.

12. Boineau, J.P., and Spach, M.S. :
The relationship between the electrocardiogram and the electrical activity of the heart.
J. Electrocardiology, 1 : 117, 1968.
13. Boineau, J.P., Spach, M.S., Pilkington, T.C., and Barr, R.C. :
Relationship between body surface potential and ventricular excitation in the dog.
Circulation Res. 19 : 489, 1966.
14. Bootsma, B.K., Hoelen, A.J., Strackee, J., Meijler, F.L. :
Analysis of R-R intervals in patients with atrial fibrillation at rest and during exercise.
Circulation, 41 : 783-794, 1970.
15. Brody, D.A. :
A theoretical analysis of intracavitary blood mass influence on the heart-lead relationship.
Circ. Res. 4 : 731, 1956.
16. Brody, D., and Romans, W.E. :
A model which demonstrates the quantitative relationship between the electromotive forces of the heart and the extremity leads.
Amer. Heart J., 45 : 263-276, 1953.
17. Bromberger-Barnea, B., Caldini, P., and Wittenstein, G.W. :
Transmembrane potentials of the normal and hypothermic human heart.
Circulation Res., 7 : 138-140, 1959.
18. Brückner :
Vielecke und Vielflache.
Leipzig, 1900.
19. Burger, H.C. :
A theoretical elucidation of the notion "Ventricular Gradient".
Amer. Heart J., 53 : 240- , 1957.
20. Burger, H.C.
Heart and Vector.
Philips Technical Library, 1967.
21. Burger, H.C., van Brummelen, A.G.W., and van Herpen, G. :
Heart-vector and leads.
Amer. Heart J., 61 : 317- , 1961.
22. Burger, H.C., van Brummelen, A.G.W., and van Herpen, G. :
Compromise in vectorcardiography. Displacement of electrodes as a means of adapting one lead system to another.
Am. Heart J., 62 : 398, 1961.

23. Burger, H.C., and van Milaan, J B. :
Heart-vector and leads I.
Brit. Heart J., 8 : 157-161, 1946.
24. Burger, H.C., and van Milaan, J.B. :
Heart-Vector and leads II.
Brit. Heart J., 9 : 154-160, 1947.
25. Burger, H.C., and van Milaan, J.B. :
Heart-vector and leads III.
Brit. Heart J., 10 : 229-233, 1948.
26. Burgess, M.J., Millar, K., and Abildskov, J.A. :
Cancellation of electrocardiographic effects during
ventricular recovery.
J. Electrocardiology, 2 : 101-108, 1969.
27. Carmeliet, E.:
Influence du rythme sur la durée du potentiel d'action
ventriculaire cardiaque.
Arch. Int. de Physiol. et de Biochimi, 63 : 222-232, 1955.
28. Casella, C., and Taccardi, B. :
The spread of excitation over short distances in heart muscle.
In Electrophysiology of the Heart. Ed. by B. Taccardi,
G. Marchetti. New York, Pergamon Press, pp. 153-162.
29. Churney, L., and Ohshima, H. :
Is the fundamental electrical response of the single heart
muscle cell a spike potential ?
J. of Gen. Physiology, 46 : 1029-1046, 1963.
30. Cooper, T., Gilmore, J.P., Manning, J.W., Peiss, C.N.,
Priola, D.V., Sarnoff, S.J., Smith, Jr., O.A., and Wallace, A.G. :
Nervous control of the heart.
Ed. by W.C. Randall.
The Williams and Wilkins Company, Baltimore, 1965.
31. Coraboeuf, E., and Weidmann, S. :
Temperature effects on the electrical activity of Purkinje fibers.
Helv. Physiol. et Pharmacol. Acta., 12 : 32-41, 1954.
32. Covino B.G., and D'Amato, H.E. :
Mechanism of ventricular fibrillation in hypothermia.
Circulation Res., 10 : 148- , 1962.
33. Coxeter, H.S.M. :
Regular polytopes.
Methuen & Co Ltd., London, 1948, p. 4.

34. Craib, H.W. :
A study of the electrical field surrounding active heart muscle.
Heart, 14 : 71 , 1927.
35. Cranefield, P.F., and Hoffman, B.F. :
Conduction of the cardiac impulse :
II. Summation and Inhibition.
Circulation Res., 28 : 220-233, 1971.
36. Cranefield, P.F., Klein, H.O., and Hoffman, B.F. :
Conduction of the cardiac impulse :
I. Delay, Block, and one-way block in depressed Purkinje fibers.
Circulation Res., 28 : 199-219, 1971.
37. van Dam, R.Th., and Durrer, D. :
Experimental study on the intramural distribution of the
excitability cycle and on the form of the epicardial T-wave
in the dog heart in situ.
Amer. Heart J., 61: 537- , 1961.
38. Van Dam, R.Th., and Durrer, D. :
T wave and ventricular repolarization.
Amer. J. Cardiol., 14 : 294- , 1964.
39. Van Dam, R.Th., Moore, E.N., and Hoffman, B.F. :
Initiation and conduction of impulses in partially depolarized
cardiac fibers.
Amer. J. of Physiol., 204 : 1133-1144, 1963.
40. Dowling, C.V., and Hellerstein, H.K. :
Factors influencing the T wave of the electrocardiogram :
II. Effects of drinking iced water.
Amer. Heart J., 41 : 58, 1951.
41. Durrer, D., Buller, J., Graaff, P., Lo, G.I., and Meijler, F.L. :
Epicardial excitation pattern as observed in the isolated revived
and perfused fetal human heart.
Circulation Res., 9: 29, 1961.
42. Durrer, D., van Dam, R.Th., Freud, G.E., Janse, M.J.,
Meijler, F.L., and Arzbaecher, R.C. :
Total excitation of the isolated human heart.
Circulation 41 : 899-912, 1970.
42. Durrer, D., Roos, J.P., and Buller, J. :
The spread of excitation in canine and human heart.
In Electrophysiology of the Heart. Ed. by B. Taccardi,
G. Marchetti. New York, Pergamon Press, pp. 203-214, 1965.

43. Durrer, D., and van der Tweel, L.H. :
Spread of activation in the left ventricular wall of the dog (I).
Amer. Heart J., 46 : 683, 1953.
44. Durrer, D., and van der Tweel, L.H. :
Spread of activation in the left ventricular wall of the dog (II).
Amer. Heart J., 47 : 192, 1954.
45. Einthoven, W. :
Die galvanometrische Registrirung der Menschlichen Elektrokardiogramms, zugleich eine Beurtheilung der Anwendung des Capillar-Elektrometers in der Physiologie.
Pflüger's Archiv für die gesammte Physiologie, 99 : 472-480, 1903.
46. Einthoven, W., Fahr, G., and de Waart, A. :
Ueber die Richtung und die manifeste Größe der Potential Schwankungen im menschlichen Herzen und über die Einfluss der Herzlage auf die Form des Elektrokardiogrammes.
Pflüger's Arch. für die gesammte Physiologie, 150 : 275, 1913.
47. Engelman, Th.W. :
Pflügers Archiv für die gesammte Physiologie, 62 : 543- , 1895.
48. Eycleshymer, H.C., and Schoemaker, P.M. :
"A cross-section anatomy".
Appleton-century-crofts, New York, 1911.
49. Fejes Toth, L. :
Lagerungen in der Ebene auf der Kugel und im Raum.
Springer Verlag. Berlin - Göttingen - Heidelberg. 1953.
50. Fisch, C., Edmands, R.E., and Greenspan, K. :
The effect of change in cycle length on the ventricular action potential in man.
Amer. J. Cardiol., 21 : 525- , 1968.
51. Frank, E. :
The image surface of a homogeneous torso.
Amer. Heart J., 47 : 757-768, 1954.
52. Frank, E. :
An accurate, clinically practical system for spatial vectorcardiography.
Circulation, 13 : 737, 1956.

53. Fredericia, L.S. :
Die Systolendauer im Elektrokardiogram bei normalen Menschen und bei Herzkranken.
Acta Med. Scand., 53 : 469-489, 1920.
54. Garrey, W.E. :
The nature of fibrillary contraction of the heart. Its relations to tissue mass and form.
Amer. J. Physiol., 33 : 397-414, 1914.
55. Gäyton, A.C. :
Chapt. Electrocardiography.
Textbook of Medical Physiology, 4th Ed. W.B. Saunders Co. Philadelphia.
56. Geselowitz, D.B. :
The concept of an equivalent cardiac generator.
In : "Biomedical Sciences Instrumentation".
Vol. 1, Planum Press, New York, 1963, p. 325.
57. Geselowitz, D.B. :
Dipole theory in electrocardiography.
The Amer. J. Cardiol., 14 : 301-306, 1964.
58. Goodman, D., van der Steen, A.B.M., and van Dam, R.Th. :
Endocardial and epicardial activation pathways of the canine right atrium.
Am. J. of Physiol., 220 : 1-11, 1971.
59. Han, J., and Moe, G.K. :
Non-uniform recovery of excitability in ventricular muscle.
Circulation Res., 14 : 44-60, 1964.
60. Han, J., and Moe, G.K. :
Cumulative effects of cycle length on refractory periods of cardiac tissues.
Amer. J. Physiol., 217 : 106, 1969.
61. Harumi, K., Burgess, M.J., and Abildskov, J.A. :
A theoretical model of the T wave.
Circulation, 34 : 657, 1966.
62. Hauswirth, O. :
Computer-rekonstruktionen der Effekte von Polarisationsströmen und Pharmaka auf Schrittmacher - und Aktionspotentiale von Herzmuskelfasern.
Thesis, 1971. Ruprecht-Karl-Universität, Heidelberg.
63. Hodgkin, A.L., and Huxley, A.F. :
A quantitative description of membrane current and its application to conduction and excitation in nerve.
J. Physiol., 117 : 500-544, 1952.

64. Hodgkin, A.L., Huxley, A.F., and Katz, B.:
Measurement of current-voltage relation in the membrane of the
giant axon of Loligo.
J. Physiol., 116 : 424-448, 1952.
65. Hoff, H.E., and Nahun, L.H. :
The factors determining the direction of the T-wave.
Amer. J. of Physiol., 131 : 700, 1941.
66. Hoffman, B.F., and Cranefield, P.F. :
Electrophysiology of the heart.
New York, McGraw-Hill Book Co., 1960.
67. Hoffman, B.F., Kao, C.Y., and Suckling, E.E. :
Refractoriness in cardiac muscle.
Amer. J. Physiol., 190 : 473- , 1957.
68. Horacek, B. :
The effect on electrocardiographic lead vectors of conductivity
inhomogeneities in the human torso.
Ph.D. Thesis, 1971. Dalhousie University, Halifax
69. Horacek, B., and Ritsema van Eck, H.J. :
The forward problem of electrocardiography.
Satellite Symposium of the XXVth International Congress
of Physiol. Sciences : "The electrical field of the heart".
Brussels, 2-3 aug., 1971, In Press.
70. Horan, L.G., Flowers, N.C., and Brody, D.A. :
Body surface potential distribution; comparison of naturally and
artificially produced signals as analyzed by the digital computer.
Circulation Res., 13 : 373-387, 1963.
71. Kepler, :
Harmonice Mundi.
Opera Omnia : Vol. 5. Frankfurt, 1864, p. 123.
72. Janse, M.J. :
Influence of the direction of the atrial wavefront on AV nodal
transmission in isolated rabbit hearts.
Circulation Res., 25 : 439, 1969..
73. Janse, M.J. :
The effect of changes in heart rate on the refractory period of
the heart.
Ph.D. Thesis, 1971. University of Amsterdam
74. Katz, L N., and Pick, A. :
Clinical Electrocardiography - Part I. The Arrhythmias.

75. Lepeschkin, E. :
Role of the temperature gradients within ventricular muscle in genesis of normal T wave of electrocardiogram and ventricular gradient responsible for it.
Fed. Proc. Amer. Physiol. Soc., 10 : 81, 1951.
76. Lewis, T. :
On the spread of the excitatory process in the vertebrate heart. Part III. The Dog's Ventricle. Part IV. The Human Ventricle.
Phil. Trans. (London), B., Vol. 207, p.247-297, 1916.
77. Lewis, T. :
The mechanism and graphic registration of the heart beat.
London, Shaw & Sons, 1920.
78. Lewis, T., Feil, H.S., and Stroud, W.D. :
Observations upon flutter and fibrillation.
Part II : The nature of auricular flutter.
Heart, 7 : 191, 1920.
79. Ling, T., Gerard, R.W. :
The normal membrane potential of frog sartorius fibers.
J. Cellular Comp. Physiol., 34 : 383-396, 1949.
80. Matsuda, K., Kamiyama, A., and Hoski, T. :
Configuration of the transmembrane action potential at the Purkinje-ventricular fiber junction and its analysis.
In Electrophysiology and ultrastructure of the heart, pp. 177-188.
Grune and Stratton, Inc. New York and London.
Ed. by T. Sano, V. Mizuhira, and K. Matsuda.
81. McAllister, R.E. :
Computed action potentials for Purkinje fibers membranes with resistance and capacitance in series.
Biophysical Journal, 8 : 951-964, 1968.
82. McFee, R., and Johnston, F.D. :
Electrocardiographic leads. I. Introduction.
Circulation, 8 : 554, 1953.
83. McFee, R., and Parungao, A. :
An orthogonal lead system for clinical electrocardiography.
Amer. Heart J., 62 : 93, 1961.
84. Mendez, C., Gruhzt, C., and Moe, G.K. :
Influence of cycle length upon refractory period of auricles, ventricles, and A-V node in the dog.
Amer. J. Physiol., 184 : 287, 1956.

85. Mendez, C., Mueller, W.J., and Urguiaga, X. :
Propagation of impulses across the Purkinje Fiber-muscle
junctions in the dog heart.
Circulation Res., 26 : 135-150, 1970.
86. Meredith, J., and Titus, J.L. :
The anatomic atrial connections between sinus and A-V node.
Circulation, 37 : 566-579, 1968.
87. Mines, G.R. :
On dynamic equilibrium in the heart.
J. Physiol. (London)46 : 349-383, 1913.
88. Moe, G.K., and Abildskov, J.A. :
Atrial fibrillation as a self-sustaining arrhythmia independent
of focal discharge.
Amer. Heart J., 58 : 59-70, 1959.
89. Moe, G.K., Rheinboldt, W.C., and Abildskov, J.A. :
A computer model of atrial fibrillation.
Amer. Heart J., 67 : 200-220, 1964.
90. Moore, E.N., Preston, J.B., and Moe, G.K. :
Durations of transmembrane action potentials and functional
refractory periods of canine false tendon and ventricular myocardium.
Circulation Res., 17 : 259, 1965.
91. Moore, D., and Ruska, H., Electron microscope study of
Electron microscope study of mammalian cardiac muscle cells.
J. Biophys. Biochem. Cytol., 3 : 261-268, 1957.
92. Myerburg, R.J. :
The gating mechanism in the distal atrioventricular conducting system.
Circulation, 43 : 955, 960, 1971.
93. Myerburg, R.J., Gelband, H., and Hoffman, B.F. :
Functional characteristics of the gating mechanism in the canine
A-V conducting system.
Circulation Res., 28 : 136-147, 1971.
94. Myerburg, R.J., Stewart, J.W., and Hoffman, B.F. :
Electrophysiological properties of the canine peripheral A-V
conducting system.
Circulation Res., 26 : 361-378, 1970.
95. Naylor, T.H., Balintfy, J.L., Burdich, D.S., and Chu, K. :
Computer simulation techniques.
John Wiley and Sons, Inc., New York, London, Sidney, 1966.

96. Nelson, C.V. :
Human thorax potentials.
Ann. N.Y. Acad. Sci., 65 : 1014-1050, 1957.
97. Nims, L.F., Kartin, B., Chernoff, N.M., and Nahum, L.H. :
Heart temperature and its relation to the T-wave.
Fed. Proc., 7 : 86, 1948.
98. Noble, D. :
A modification of the Hodgkin-Huxley equations applicable to
Purkinje fibre action and pacemaker potentials.
J. Physiol., 160 : 317-352, 1962.
99. Noble, D., and Tsien, R.W. :
Outward membrane currents activated in the plateau range of
potentials in cardiac Purkinje fibers.
J. Physiol., 200 : 205-231, 1969.a.
100. Noble, D., and Tsien, R.W. :
The kinetics and rectifier properties of the slow potassium
current in cardiac Purkinje fibers.
J. Physiol., 195 : 185-214, 1968.
101. Noble, D., and Tsien, R.W. :
Reconstruction of the repolarization process in cardiac
Purkinje fibers based on voltage clamp measurements of
membrane currents.
J. Physiol., 200 : 233-254, 1969, b.
102. Okajima, M., Fujino, T., Kobayashi, T., and Yamada, K. :
Computer simulation of the propagation process in excitation
of the ventricles.
Circulation Res., 23 : 203-211, 1968.
103. Van Oostrum, A. :
Personnal Communication.
104. Pal, I. :
Descriptive geometry with three dimensional figures.
Budapest - Műszaki Könyvkiado - 1966, 3ed, pp. 85.
105. Peper, K., and Trautwein, W. :
A note on the pacemaker current in Purkinje fibers.
Pflügers Arch., 309 : 356-361, 1969.
106. Plonsey, R. :
Bio-electric phenomena.
McGraw-Hill Book Company, New York, 1969. pp. 211.

107. Plonsey, R. :
The biophysical basis for electrocardiography.
C.R.C. Critical reviews in Bio-engineering, 1 : 1-48, 1971.
108. Porter, W.T. :
Pflügers Arch. ges. Physiol., 55 : 366- , 1894.
109. Rautaharju, P.M., and Simonson, E. :
Die Grenzen der Klinischer Anwendbarkeit des in der
Frontal ebene konstruierter Ventrikel Gradienten.
Ztschr. Kreislaufforsch., 50: 282, 1961.
110. Rheinboldt, W., Ledley, R.S., Abildskov, J.A., and Oestreich, A.E. :
Simulation of the ventricles of the heart.
Proc. 16th Ann. Conference on Eng. in Med. and Biol.,
5 : 32, 1963.
111. Robertson, W. van B., and Dunihue, F.W. :
Water and electrolyte distribution in cardiac muscle.
Am. J. Physiol., 177 : 292-297, 1954.
112. Rosenblueth, A., and Wiener, N. ;
The role of models in science.
Philosophy of Science, 12 : 316-321, 1945.
113. Rosenblueth, A., and Garcia Ramos, J. :
Studies on flutter and fibrillation.
II. The influence of artificial obstacles on experimental
auricular flutter.
Amer. Heart J., 33 : 677- , 1947.
114. Rossi, L. :
Histopathologic features of cardiac arrhythmias.
Milano, Casa Editrice Ambrosiana, 1969.
115. Rothberger, C.J., and Winterberg, H. :
Über Vorhofflimmern und Vorhofflattern.
Pflügers Arch. ges. Physiol., 160 : 42- , 1914.
116. Sano, T., Tahayama, N., and Shimamoto, T. :
Directional difference of conduction velocity in the cardiac
ventricular syncytium studied by micro-electrodes.
Circulation Res., 7: 262- , 1959.
117. Sano, T., and Yamagishi, S. :
Spread of excitation from the sinus node.
Circulation Res., 16 : 423-430, 1965.

118. Scheafer, H., Pena, A., Schölmerich, P. :
Der Monophasische Aktionsstrom von Spitze und Basis des
Warmblüterherzens und die Theorie der T-Welle des EKG.
Pflügers Arch. ges. Physiol., 246 : 728-745, 1943.
119. Schaefer, H., and Trautwein, W. :
Über die elementaren elektrischen Prozesse im Herzmuskel
und ihre Rolle für eine neue Theorie des EKG.
Arch. ges. Physiol., 251 : 417, 1949.
120. Scher, A.M. :
Excitation of the heart.
Handbook of Physiology, Section 2 : The circulation, Vol. 1.
American Physiological Society, Washington, D.C., pp. 287-322,
Ed. by Field, J. 1962.
121. Scher, A.M. :
Newer data on myocardial excitation.
In "Electrophysiology of the Heart".
Ed. by B. Taccardi, G. Marchetti.
New York, Pergamon Press, pp. 217-228, 1965.
122. Scher, A.M., and Paton, R.R. :
Spread of electrical activity through the wall of the ventricle.
Circulation Res., 1 : 539, 1953.
123. Scher, A.M., and Young, A.C. :
Ventricular depolarization and the genesis of QRS.
Ann. New York Acad. Sci., 65 : 768, 1957.
124. Schmitt, O.H., and Simonson, E. :
The present status of vectorcardiography.
Arch. Intern. Med., 96 : 574, 1955.
125. Selvester, R.H., Collier, C.R., and Pearson, R.B. :
Analog computer model of the vectorcardiogram.
Circulation, 31 : 45, 1965.
126. Selvester, R.H., Kalaba, R., Collier, R., Bellman, R., and
Kagiwada, H. :
A digital computer model of the V.C.G. with distance
and boundary effects : Simulated myocardial infarction.
Amer. Heart J., 74 : 792-808, 1967.
127. Selvester, R.H., Kalaba, R., Bellman, R., Kagiwada, H., and
Collier, R. :
Simulated myocardial infarction with a mathematical model of
the heart containing distance and boundary effects.
Proc. of the Long Island Jewish Hospital Symp. on V.C.G.
May 11-13, 1965, North Holland Publ. Co., 1966, Amsterdam.

128. Selvester, R.H., Solomon, J.C., and Gillespie, T.L. :
Digital computer model of a total body electrocardiographic surface map. An adult male-torso simulation with lungs.
Circulation, 38 : 684-690, 1968.
129. Simonson, E. :
Differentiation between normal and abnormal in electrocardiography.
The C.V. Mosby Company, St. Louis, 1961.
130. Simonson, E., Cady, L.D., and Woodbury, M. :
The normal Q-T interval.
Amer. Heart J., 63 : 747, 1962.
131. Sjöstrand, F.S., Anderson, G.E., and Dewey, M.M. :
The ultrastructure of the intercalated discs of frog mouse and guinea pig cardiac muscle.
J. Ultrastruct. Res., 1 : 271-287, 1958.
132. Solomon, J.C., and Selvester, R.H. :
Myocardial activation sequence simulation.
Proc. XIth Intern. Vectorcardiographic Symposium. New York, May 15-17, 1970. North Holland Publ. Co. Amsterdam, 1971. pp. 175-182.
133. Solomon, J.C., and Selvester, R.H. :
Current dipole moment density of the heart.
Amer. Heart J., 81 : 351- , 1971.
134. Sperelakis, N. :
Additional evidence for high-resistance intercalated discs in the myocardium.
Circulation Res., 12 : 676-683, 1963.
135. Sperelakis, N., Hoshiko, T., and Berne, R.H. :
Nonsyncytial nature of cardiac muscle : membrane resistance of single cells.
Amer. J. Physiol., 198 : 531-536, 1960.
136. Stephen Weens, H., and Gay, Jr., B.B. :
In : "The Heart, arteries and veins", pp. 318-320.
Ed. by Hurst, J.W., Logue, R.B., McGraw-Hill Book Company. New York, 1970.
137. Strackee, J., Hoelen, A.J., Zimmerman, A.N.E., and Meijler, F.L. :
Artificial atrial fibrillation in the dog : an artifact ?
Circulation Res., 28 : 441-445, 1971.
138. Szekeres, L., and Papp, G.J. :
Experimental cardiac arrhythmias and antiarrhythmic drugs.
Akadémiai Kiadó. Budapest, 1971.

139. Taccardi, B. :
Distribution of heart potentials on the thoracic surface of normal human subjects.
Circulation Res., 12 : 341-352, 1963.
140. Taccardi, B. :
Body surface distribution of equipotential lines during atrial depolarization and ventricular repolarization.
Circulation Res., 19 : 865-878, 1966.
141. Trautwein, W., Kassebaum, D.G., Nelson, R.M., and Hecht, H.H. :
Electrophysiological study of human heart muscle.
Circulation Res., 10 : 306-312, 1962.
142. Truex, R.C., and Smythe, M.Q. :
Recent observations on the human cardiac conduction system, with special considerations of the atrioventricular node and bundle.
In : "Electrophysiology of the heart. Ed. by B. Taccardi, G. Marchetti.
New York, Pergamon Press, pp. 177-198.
143. Unknown Author.
Genesis
In the "Old Testament".
144. Van der Ark, C.R., and Reynolds, Jr., E.W. :
An experimental study of propagated electrical activity of the canine heart.
Circulation Res., 26 : 451-460, 1970.
145. Verduyn Lunel A.A. :
The localization of the atrio-ventricular conduction system in normal hearts and in cases of congenital openings in the septum cordis.
Ph.D.Thesis, Rijksuniversiteit Leiden, Drukkerij Albani, Den Haag.-1964.
146. Vick, R.L.
Action potential duration in canine purkinje tissue :
Effects of preceding excitation.
J. Electrocardiology, 4 : 105-115, 1971.
147. Viersma, J.W., Bouman, L.N., and Mater, M. :
Frequency, conduction velocity and rate of depolarization in rabbit auricle.
Nature, 217 : 1176-1177, 1968.
148. Waller, A.D. :
A demonstration on man of electromotive changes accompanying the heart's beat.
J. Physiology (London), 8 : 229, 1887.
149. Weidmann, S. :
The effect of the cardiac membrane potential on the rapid availability of sodium carrying system.
J. Physiology (London), 127 : 213- , 1955.

150. Wiener, N., and Rosenblueth, A.:
The mathematical formulation of the problem of conduction of impulses in a network of connected excitable elements, specifically in cardiac muscle.
Arch. Inst. Cardiol. Mexico, 16 : 205, 1946.
151. Wilson, F.N., Johnston, F.D., and Kossman, C.E. :
The substitution of a tetrahedron for the Einthoven triangle.
Amer. Heart J., 33 : 594, 1947.
152. Wilson, F.N., Macleod, A.G., and Barker, P.S. :
The distribution of the currents of action and injury displayed by the hearts muscle and other excitable tissue.
Vol. 18. Ann. Arbor, Mich. : Univ. of Michigan Press, 1933, p. 58.
153. Wilson, F.N., Macleod, A.G., Barker, P.S., and Johnston, F.D. :
Determination and the significance of the areas of the ventricular deflections of the electrocardiogram.
Amer. Heart J., 10 : 46, 1934.
154. Wilson, F.N., et al :
Recommendations for standardization of electrocardiographic and vectorcardiographic leads.
Circulation, 10 : 564, 1954.
155. Wong, A.Y. :
Personnal communication.
156. Woodbury, J.W. : Cellular electrophysiology of the heart.
In *Handbook of Physiology, Circulation, Sect. 2, Vol. 1.*
Washington D.C., Amer. Physiol. Soc., 1962.
157. Ziegler, R., and Bloomenfield, D.K. :
A study of the normal QRS-T angle in the frontal plane.
J. Electrocardiology, 3 : 161-168, 1970.
158. Durrer, D., van Lier, A.A.W. and Buller, J. :
Epicardial and intramural excitation in chronic myocardial infarction.
Am. Heart J., 68 : 765-776, 1964.

APPENDICES

Appendix I

COLLECTION OF ANATOMICAL DATA

Preparation of the heart specimen for digital processing

The heart was obtained during autopsy, performed as soon as possible after death of the donor. After opening the chest, two orientation needles were inserted into the heart in an anterior-posterior direction. Both needles were lying in the same sagittal plane.

The large vessels were cut as far as possible from the heart, the pericard was cut with sufficient space in order to permit removal of the heart without disturbing the position of the inserted orientation needles. After cleaning with fresh water and removal of blood clots, the heart was submerged in a 20% gelatine solution and incubated for 4 days at 37°C.* Next, the free openings of all the large vessels were closed with suitable cork stoppers. The vessels were ligated around the corks with surgical thread, and the corks secured. The 20% gelatine solution, heated to 40°C was injected by means of large size syringe needles into the right and left side of the heart through the corks which closed off the vena cava and venae pulmonales, respectively. Two medium size syringe needles of the Luer-Lock type (B.O. -20) were inserted obliquely through the right and left ventricular wall into the right and left ventricular cavity, respectively. A 3-way valve (B-D, MS -10) permitted injection of gelatin under pressure

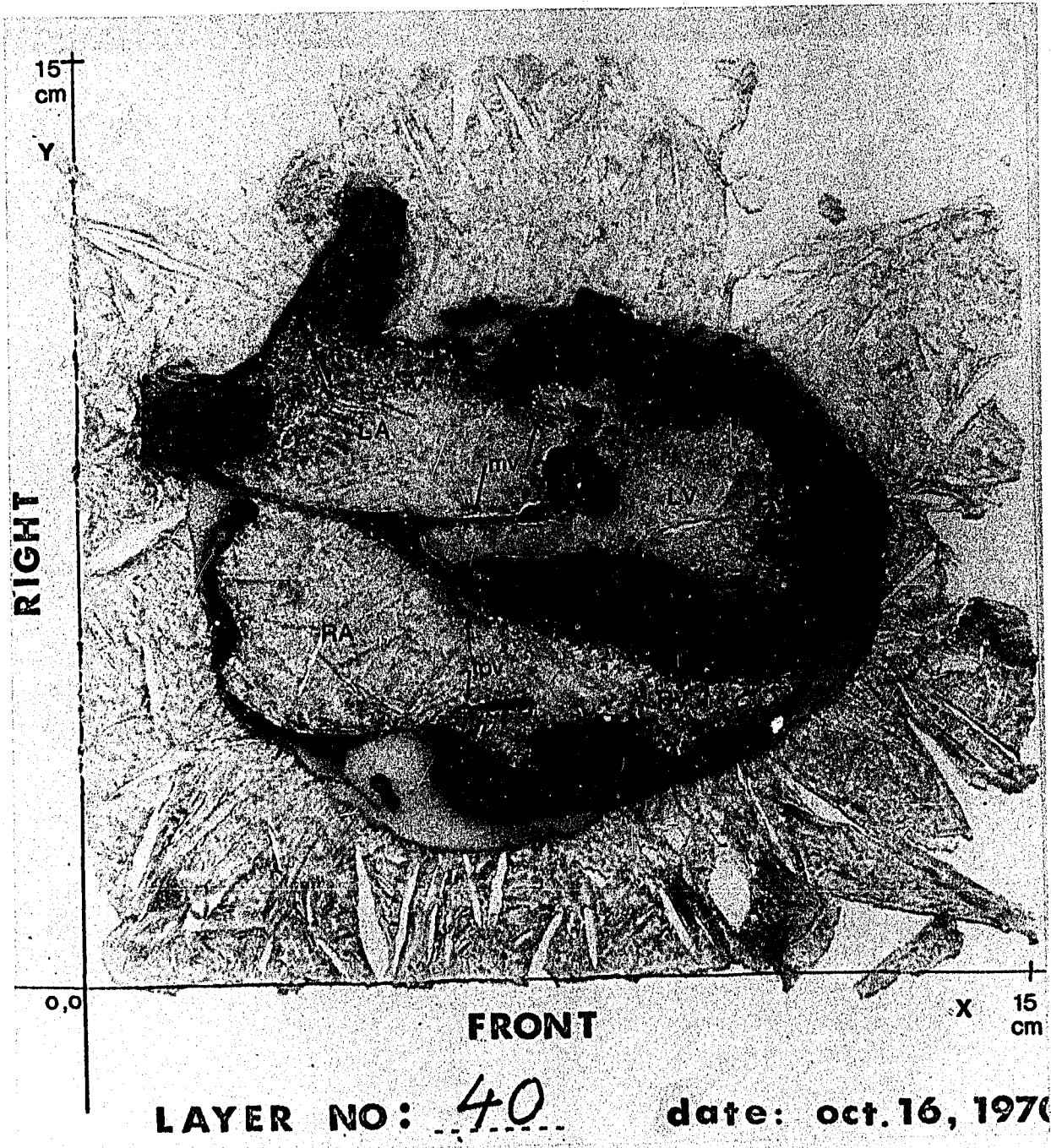
* At this stage, 5 cc of phenol (carbolic acid) was added per liter of gelatine, to avoid bacteria from growing during the incubation.

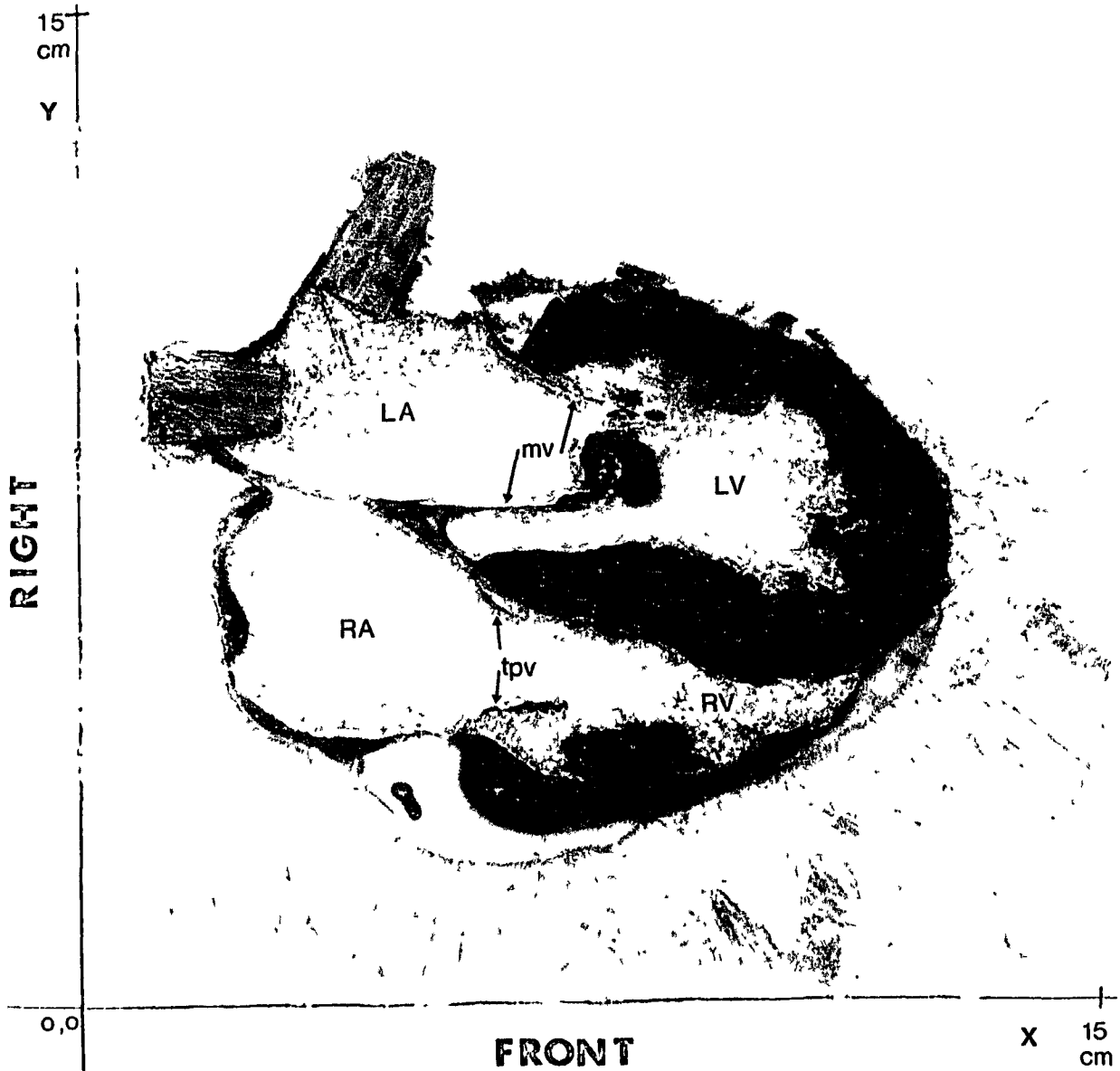
By this means, further filling of both ventricles was done until a pressure of 20 mm Hg and 80 mm Hg was obtained in the right and left ventricular cavity, respectively. Gradually the whole preparation was cooled to a temperature of 4°C under alternating control of pressure in left and right ventricle. At 4°C the gelatine has sufficient viscosity to prevent possible leakage of gelatine through the needle holes or alongside the orientation needles, or possible leaks at the sides of the corks.

The heart was kept at 4°C for a period of about 48 hours. Next, it was positioned in a wooden box of which the inside measurements were 15 x 15 x 15 cm. If the bottom of the box is designated the horizontal plane, and the anterior wall the frontal plane, the heart was positioned in respect to these planes as it was in the body, by means of the orientation needles. A fresh amount of gelatine was prepared and warmed to a fair viscosity. The empty spaces surrounding the heart were then filled and the whole box frozen to -20°C. Forty-eight hours later, the wooden box was removed and the frozen gelatine block, containing the specimen, positioned on a large microtome (Carl Zeiss, Jung-Tetrandler 1) and fixed by freezing it to the microtome with liquid CO₂.

The whole block was cut into 1 mm slices. Each slice was accurately placed on a paper sheet which showed a reference scale and photographed (Fig. 1.1). The reference scale served to maintain orientation and proper scaling factors after magnification of the photographs. On the enlarged prints (twice real size) the boundaries of the muscular parts

of the ventricles could easily be identified and as such be designated for further processing with the digitizer-pencil-follower.





LAYER NO: 40

date: oct. 16, 1970

Fig. 1.1 Photograph of Section 40. The photograph taken of Section 40 against a background with two coordinate axes (X and Y). The edges of the gelatin block are aligned with the coordinate axis. The medium dark part in the section is muscle. The black areas are blood clots. The sleeves of the mitral valve (MV) and tricuspid valve (TpV) are indicated with an arrow. Also two corks are seen, which were used to close off the pulmonary veins. Left (L) and right (R) atrium (A) and ventricle (V) are also indicated. Both right and left coronary artery can be easily identified.

Appendix II

PREPARATION OF THE DIGITAL MODEL

(a) *Conversion of the boundaries into series of coordinates*

The enlarged photographs were placed on the drawing board of the pencil follower coordinate digitizer (D-mac, Computer Equipment Corp., Peripheral System Division, Rockville, Md., U.S.A.). The intersection of the coordinate axis was established as origin, and it was positioned so that all X and Y coordinates coded had positive values. The coordinates of a vertical scale on the photographs were coded first to provide a scaling factor and to retain information necessary for correction of possible translation and rotation of the photographs with respect to the new coordinate axes. The coordinate digitizer automatically punched once per second the coordinates of its position into computer cards. Thus by moving the pencil forward along the borderlines of the myocardium series of coordinates were obtained. Care was taken to move the pencil follower slowly enough to code the position coordinates with adequately close spacing. The pencil was moved slowly when there were rapid changes in the contours. The boundaries were followed in such a way that their paths formed closed loops, so the last and first coordinate pair of a series were identical. Preceding such series of coordinates was an identification card signifying the anatomical part to which the boundary belonged. At the front card of a deck of cards for one section the section number was stored. A total of 50.492 coordinate pairs were obtained for 78 sections.

The coordinates were read from card onto digital magnetic tape. Corrections were made for possible scale differences and for rotation of the photographs on the drawing board in respect of X and Y axis.

(b) *Second order interpolation and smoothing*

The curves as obtained in digital form are a non-continuous representation of the original continuous surface in three dimensions. Since the sampling was done manually, the samples were not equally spaced and inaccuracies in positioning the pencil produced minor irregularities or 'noise' in the contour lines. A moving average filter was used to smooth the curves. The moving average was applied to the X and Y coordinates separately.

To allow the use of a simple moving average, the series of coordinates were converted into series of coordinates with equidistant sample points. The following procedure was used:

Let a series of N coordinate pairs be designated

$$(X_n, Y_n), \text{ where } n=1, 2, \dots, N.$$

Let us extend this series by 5 more pairs to a total of L, where

$$X_{N+m} = X_m \text{ and } Y_{N+m} = Y_m, \text{ for } m \text{ from } 1 \text{ to } 5 \text{ and } L=N+5$$

Now X and Y can be redefined as a function of distance S_l , which is

$$S_l = \sum_{i=1}^l \sqrt{(X_{i+1} - X_i)^2 + (Y_{i+1} - Y_i)^2}, \text{ for } l=L \Rightarrow S_l = S$$

For each function a new function can be defined $X'(S')$ and $Y'(S')$ for which

$$S_l = S_3 + C_l, \text{ for } l=1, 2, \dots, N \text{ and } C_N = S_N.$$

The relation between $X'(S')$, $Y'(S')$ and $X(S)$, $Y(S)$ is given by

$$X'(S'_l) = A(S_l)^2 + B(S_l) + C$$

in which A, B and C are the coefficients of the parabola

$$X(S) = A(S)^2 + B(S) + C$$

which is fitted by least square fit through the points

$$X(S_i) \text{ for } i = j-2, j-1, \dots, j+2,$$

where j is the value for which $(S_j - S'_1)^2$ is the smallest.

The new derived functions have equidistant sample points, with distance c . For c the value of .5 mm was used. A total of 115.824 coordinate-pairs were obtained. To this function a moving average filter (the lowpass type) was applied, with 9 terms and weighting function as shown in Fig. (II, 1). The overlap of the beginning and the end of each series assures a smooth continuation between end and beginning of the closed loops. An example of the total procedure is given in Fig. (II, 2).

(c) *Hexagonal Approximation of the boundaries and filling of the sections with rhombododecahedron.*

For each coordinate pair of a series an approximated hexagonal coordinated pair was substituted. These approximated hexagonal coordinates are the coordinates as measured along the X_H and Y_H axis, rounded off to the nearest integer value. The origin of this coordinate system was chosen in the same location as the origin for the orthogonal coordinate system, however, unit distance along X_H or Y_H axis equaled $(\sqrt{6}/6)$ * unity along X_O or Y_O axis. A total of 93.609 hexagonal coordinate pairs were obtained. A check was done to verify whether the coordinate series were continuous, i.e. consecutive coordinates were unit distance apart, and whether the series formed still loops, i.e. the last and first coordinates pair were unit distance apart. Next, the sections were filled with rhombododecahedra, by approximating each points inside the section boundaries by a point in integer hexagonal coordinates.

$$X'_n = \left(5X_n + 4(X_{n-1} + X_{n+1}) + 3(X_{n-2} + X_{n+2}) + 2(X_{n-3} + X_{n+3}) + (X_{n-4} + X_{n+4}) \right) / 25$$

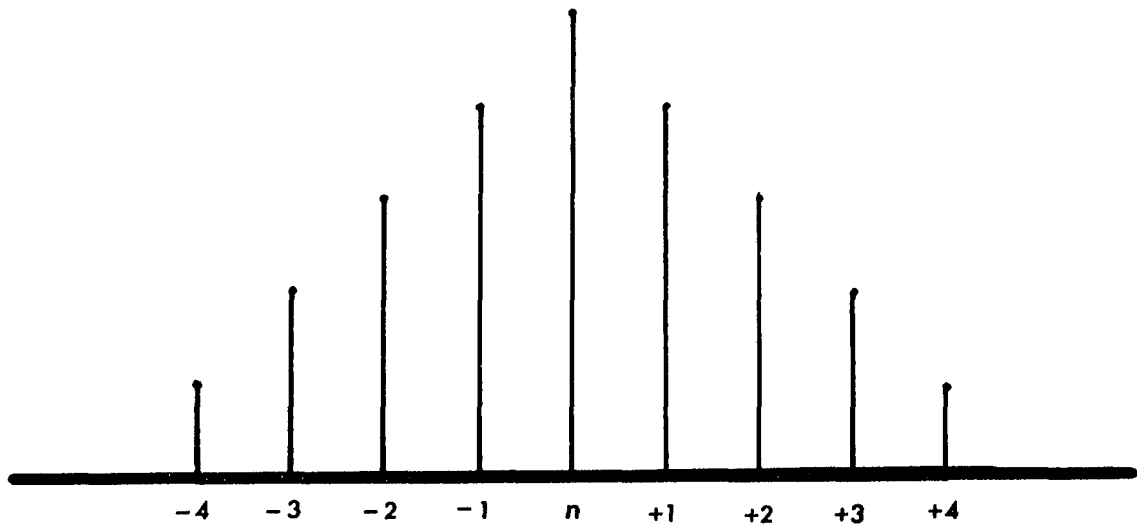


Fig. 11.1 Weighting function of moving average filter. Value X'_n is obtained by taking a weighted average of X_{n-4} till X_{n+4} . This filter is of the low pass type, without phase shift.

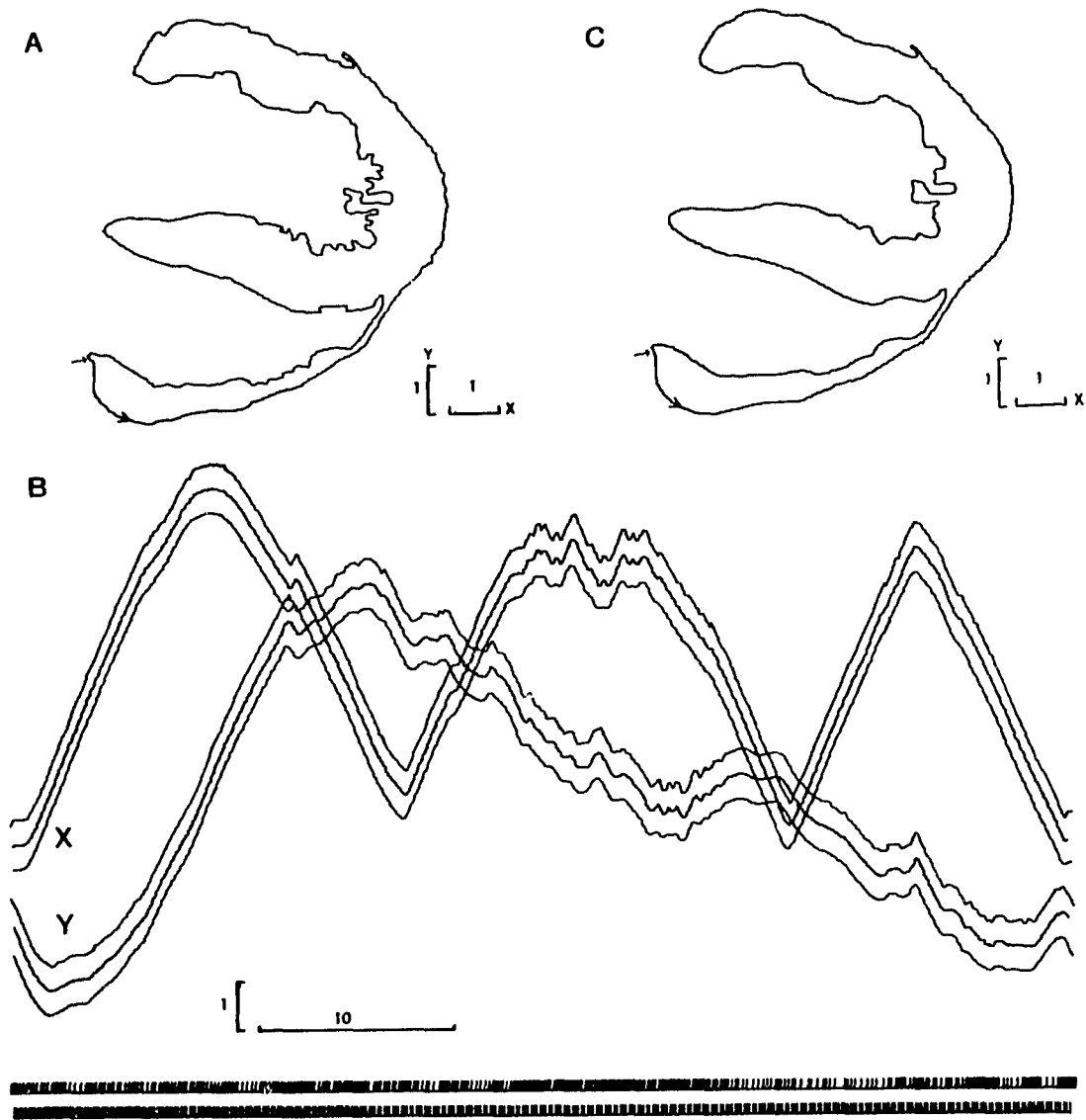


Fig. 11.2 Smoothing of the curves representing the sections. At (A) the original measured data are seen. The little arrow indicates the starting point of the series of coordinates, the bigger arrow head indicates the direction in which the series develops. In (B) the same loop is displayed in its two components X and Y, against distance measured along the loop from the origin (top tracing for X and for Y). At the bottom is indicated at which distance the samples are taken (top row). The second tracing in (B) for X and Y shows the same curve after second order interpolation, with equal sample spacing (bottom row). The third tracing (still with equal sample spacing) shows X and Y after smoothing with the moving average filter. In (C) the X and Y are again synthesized to form the smooth section.

(d) *Alignment of the Sections.*

In order to ensure proper alignment of all sections correction was made for translation and rotation of the coordinates. In the first instance, a rough correction was made for translation. Each rhombododecahedron was assigned a unit weight, and the center of the gravity for each section was determined. Under the assumption that a smooth transition in location of the center of gravity between consecutive sections should exist, a translation of coordinates was done. The coordinates of the center of gravity for each section were plotted against the section number separately for X and Y coordinates. A least square fit using a moving nine point parabolic approximation was performed.

Figure (II,3) shows the original X and Y coordinates of the center of gravity for each section and the new coordinates after translation. Following this procedure the alignment of sections was inspected by observing the projections of the sections on top of each other in the horizontal plane. Where necessary a finer adjustment of the translation of any particular section was done. For such a section the projection of sections above and below onto this section was taken and the difference area with each of them calculated. The section was then shifted until this difference area was a minimum.

In the X-Y plane, rotational correction was judged not to be necessary, since the alignment as obtained was satisfactory within the limits of the anatomical resolution. The final alignment was applied to the data as obtained after the procedure described in part B of this appendix. Then a procedure similar to the one in part C was applied.

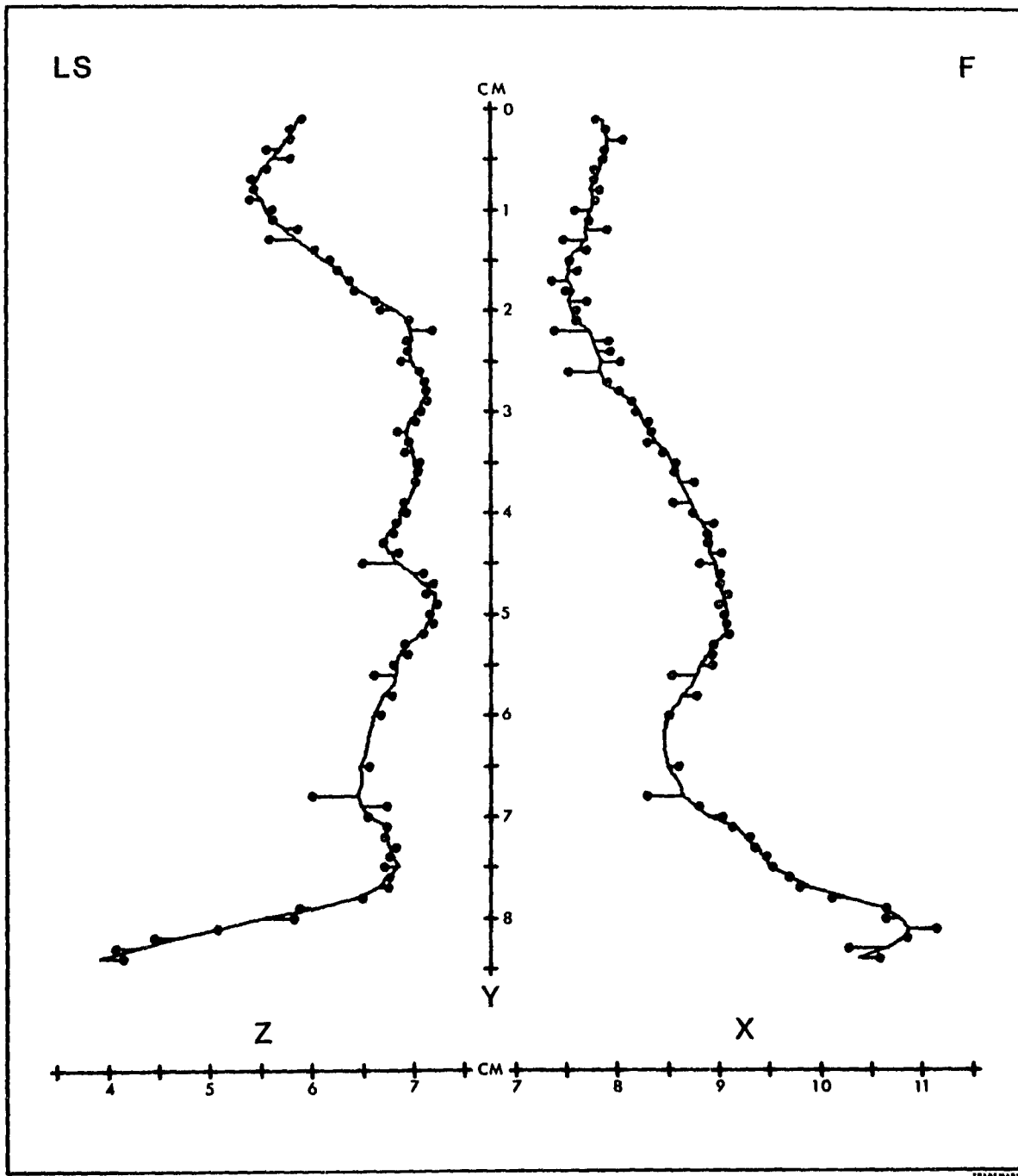


Fig. 11.3 Translation of coordinates according to center of gravity. Black dots indicate in left saggital and frontal projection the original position of the center of gravity of each section. The continuous lines connect the center of gravities after correction. The horizontal bars indicate for each section the amount of translation used (N.B. The vectorcardiographic convention for X,Y and Z directions is used.) The scale is in centimeters from the origin used.

The approximation as described in part C was an approximation of X and Y coordinates. To each coordinate pair was added a Z coordinate which was equal to the section number x0,1 cm. This placed the origin of the cartesian coordinate system 0.1 cm above the first section with the Z axis directed footwards. The approximation now was done with unity along X_H , Y_H , and Z_H axis equalling $(\sqrt{6}/3)$ unity along X_O , Y_O , and Z_O axis, which makes the size of units twice as large as before.

(e) *Addition and correction of data.*

The sections which were incomplete or missing in the original photographs were dealt with as follows: First, sections parallel to the X - Z plane were constructed from the horizontal sections. A total of 200 sections 1 mm apart were obtained. These were displayed on the cathod ray tube of the computer terminal. A program was devised which allowed changing coordinates or adding coordinates. For the missing or incomplete horizontal sections, the coordinates were identified and coded using the control thumbwheels of the display terminal. The adjustments were checked by reconstructing the horizontal sections again. The incomplete sections allowed comparison of the parts still available with the manually created sections. Luckily enough very few sections were incomplete for parts with complicated fine structures like the atria and the right ventricle. Section 38, 57, 59, 61, 62, and 64 were missing completely, and in sections 63, 66, and 67 small parts of the left ventricle were missing. As judged from frontal sections and superimposition of horizontal sections a satisfactory result was obtained. Figure (11.4) shows the ventricle parts as finally used. A total of 156.349 rhombododecahedrae dispersed over 84 horizontal sections were necessary to represent the ventricles.

Fig. 11.4 Section 1-84. All horizontal sections as used in the ventricular model are seen from top (Section 1) to bottom (Section 84) of the heart as positioned in the torso. The tracings shown are the data in hexagonal coordinates after smoothing, positioning, correction and addition of elements. The Purkinje elements are not shown.

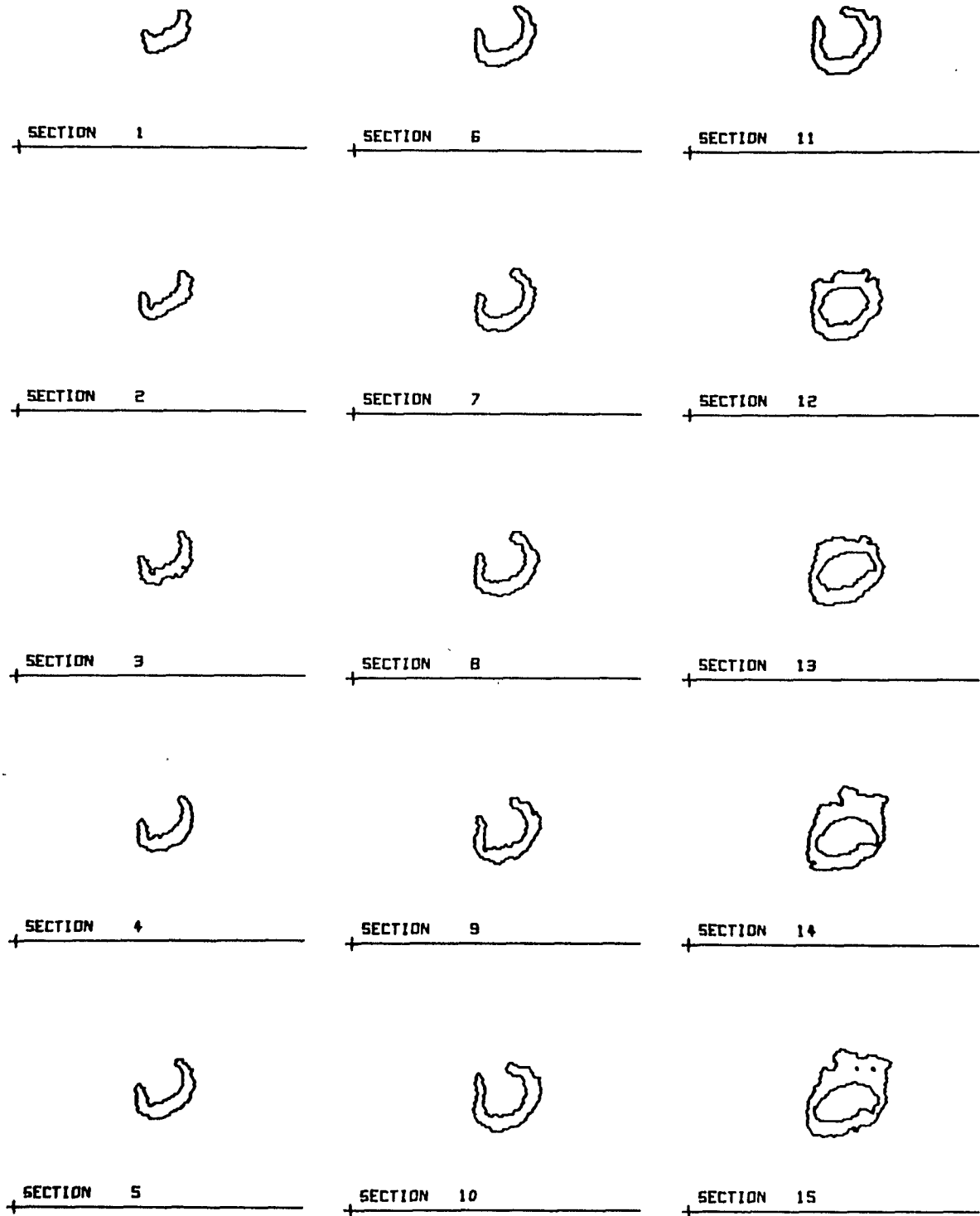


Fig. 11.4(1)

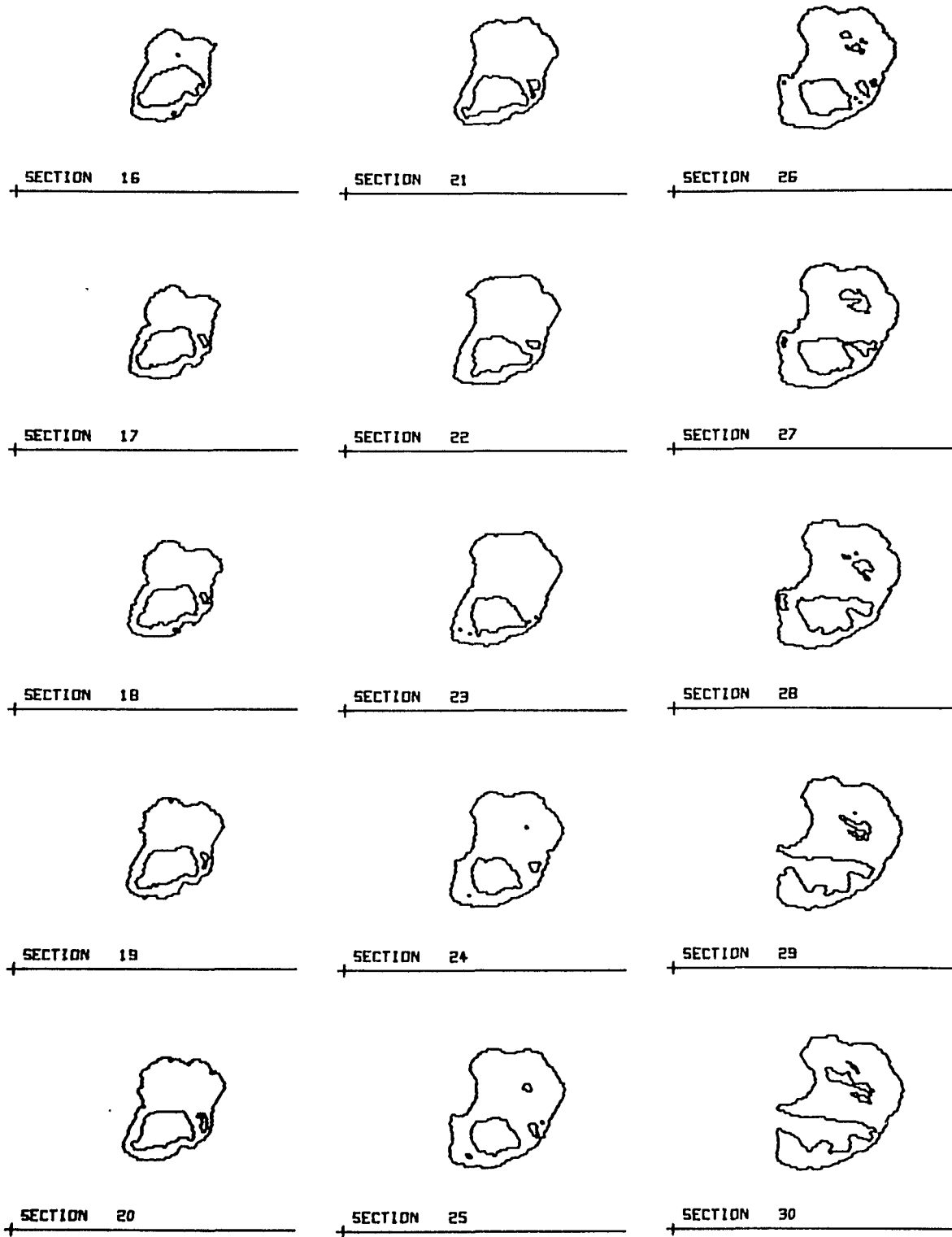


Fig. 11.4(2)

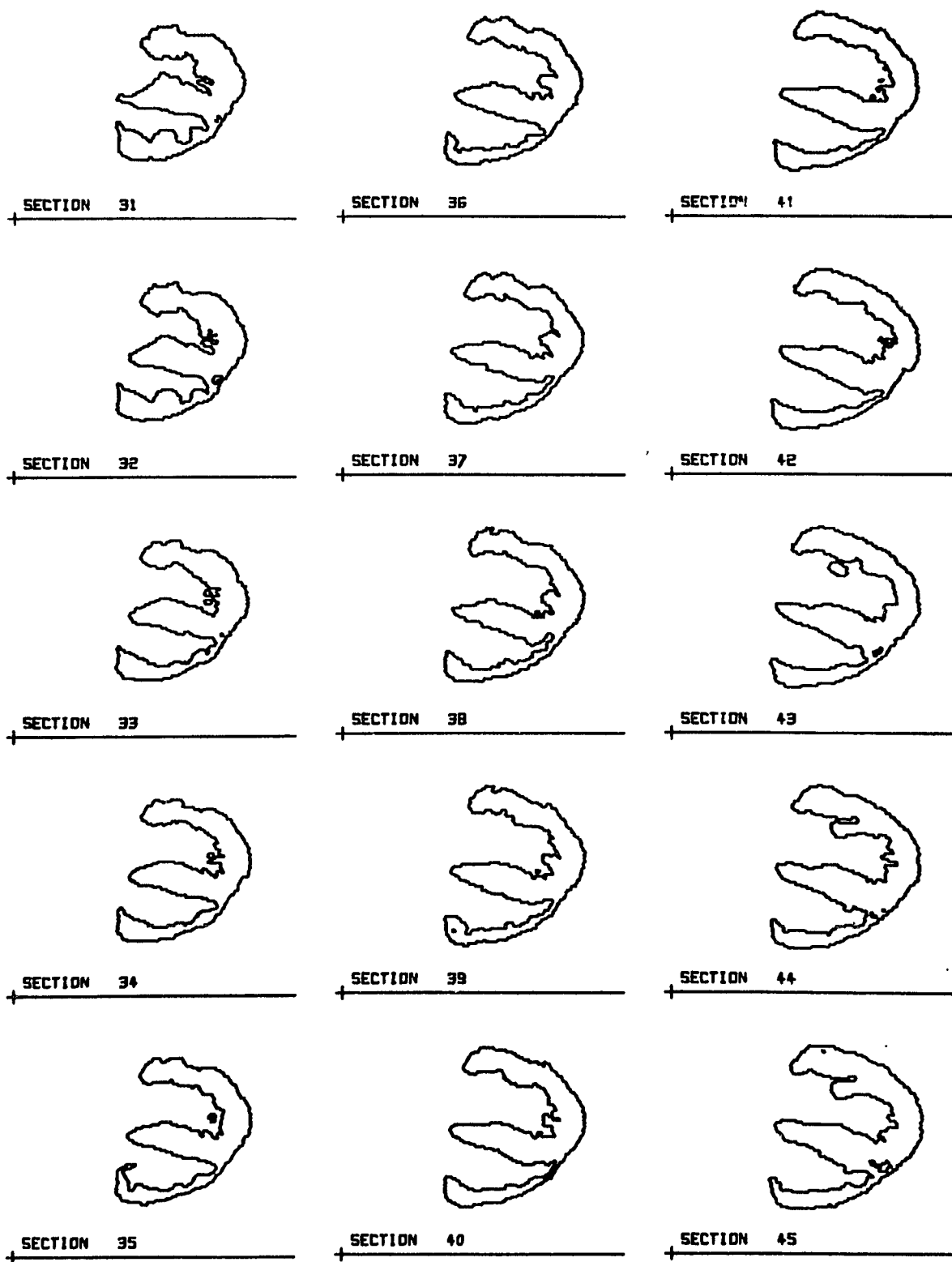


Fig. 11. 4 (3)

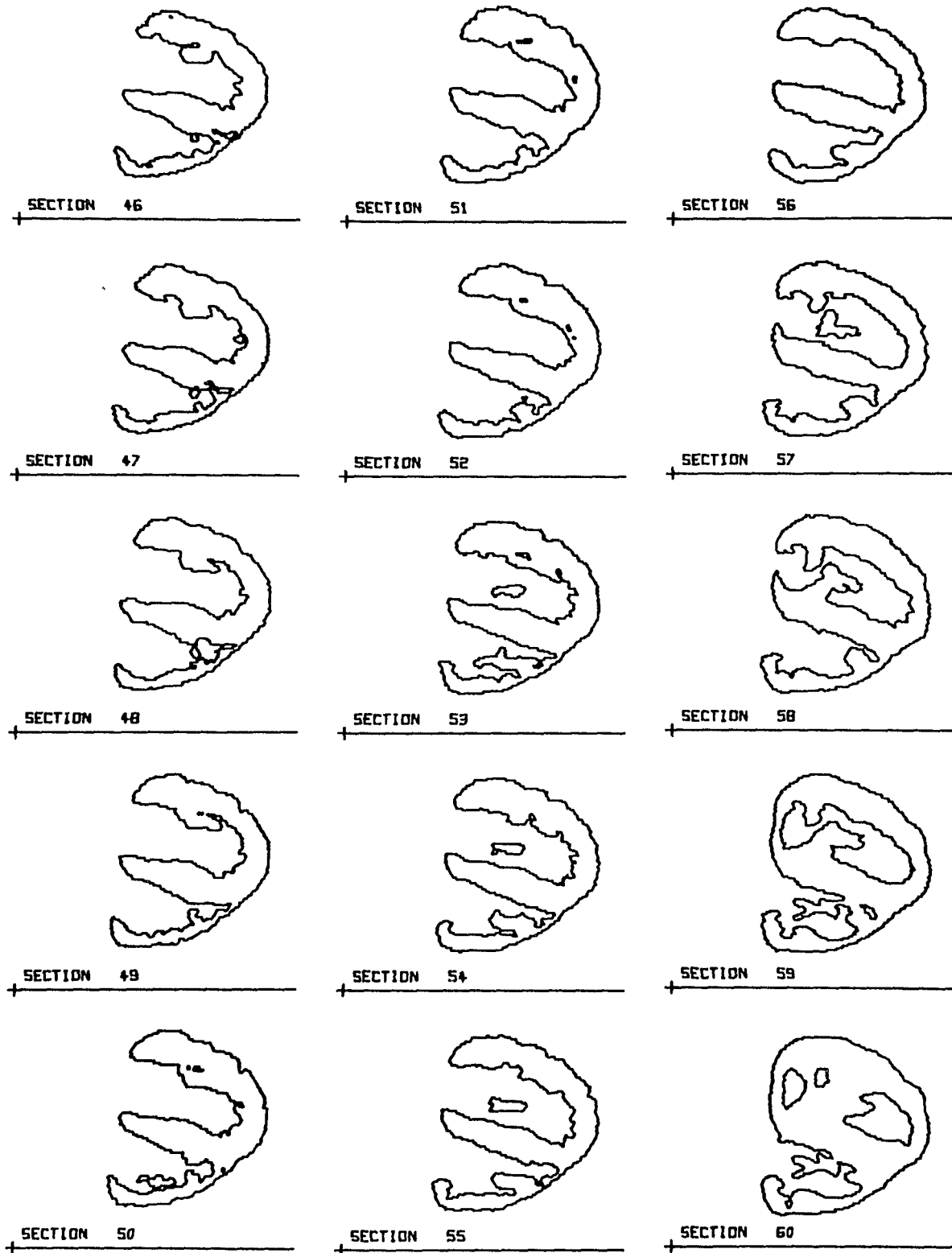


Fig. 11.4 (4)

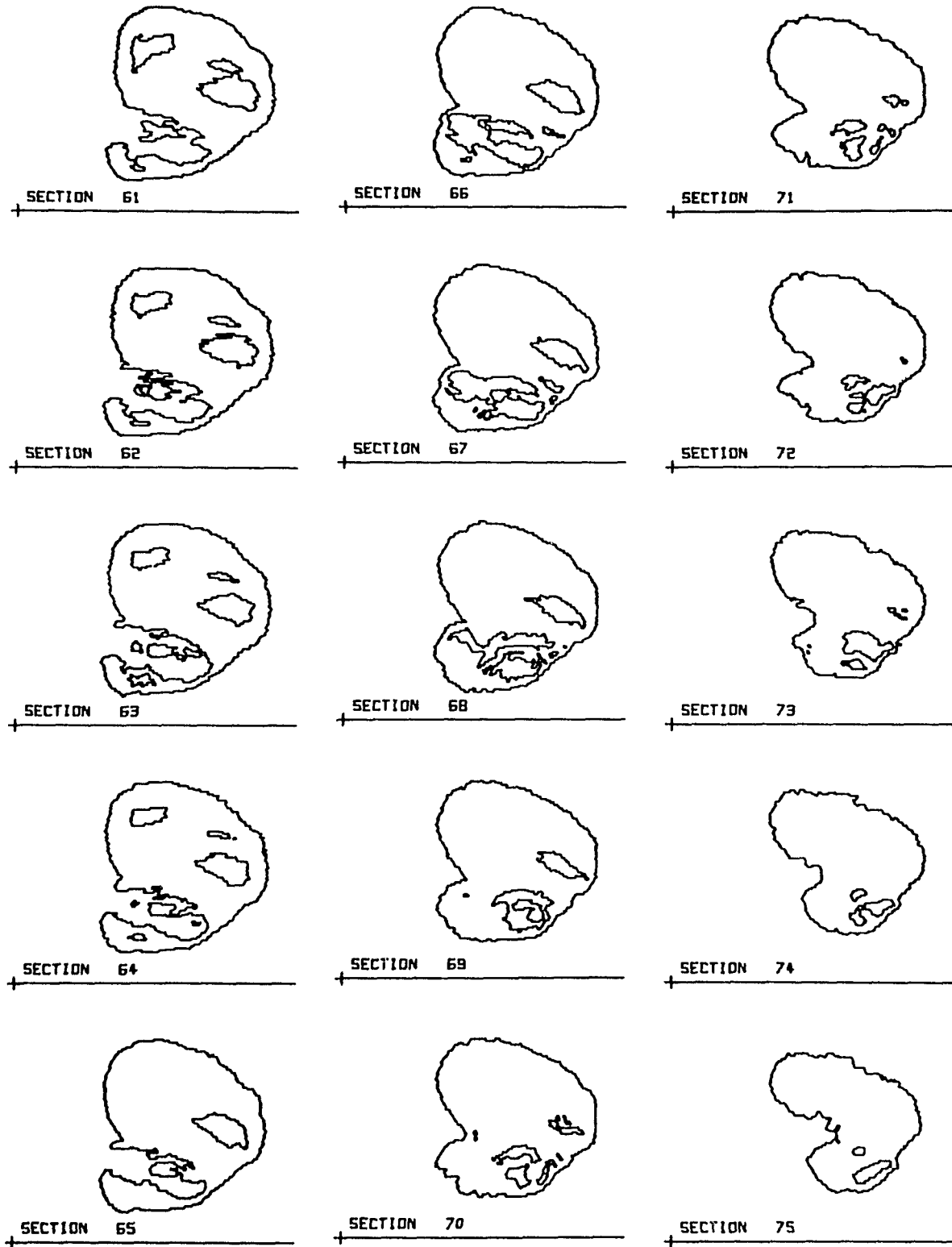


Fig. 11.4 (5)

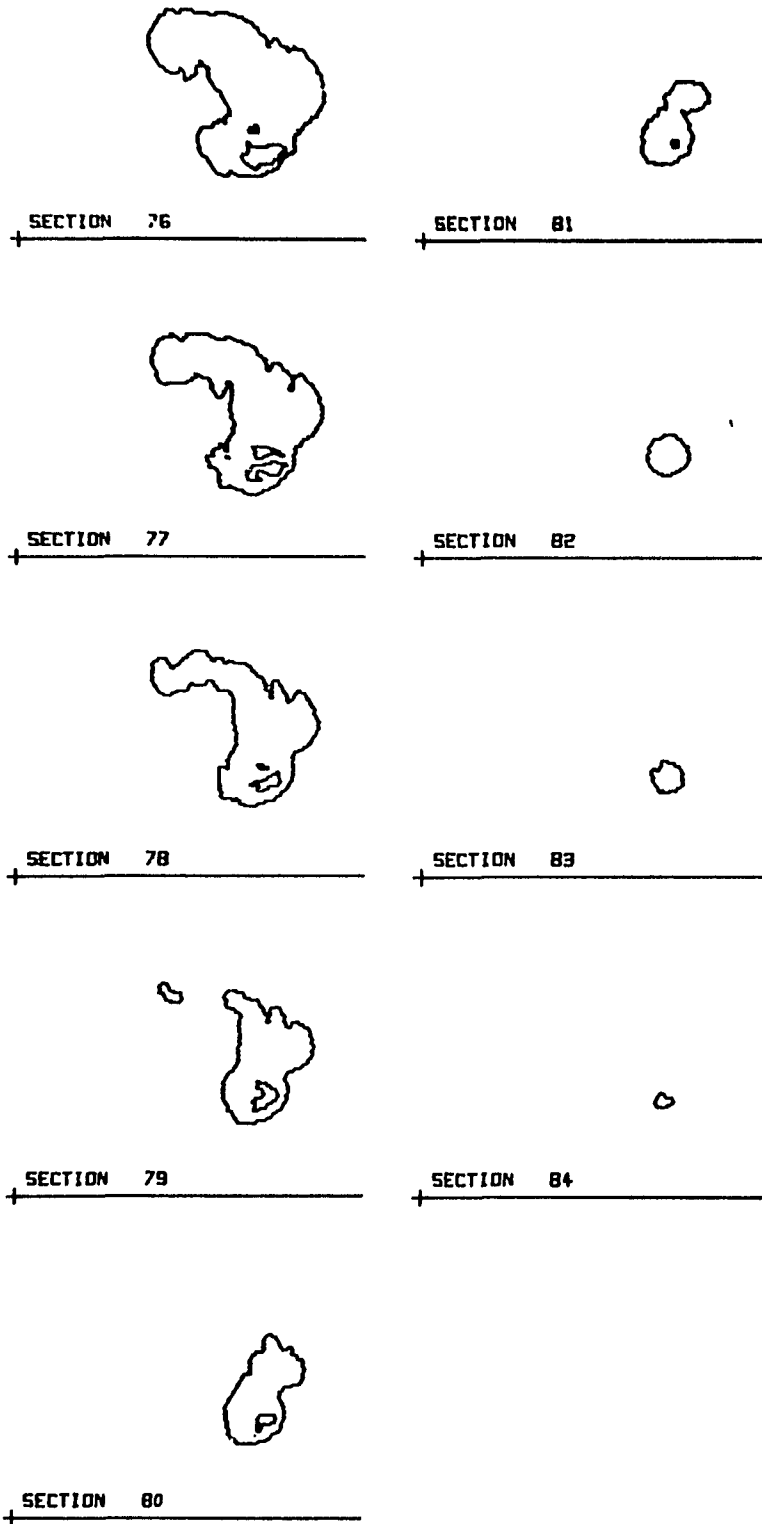


Fig. 11.4 (6)

(f) *Addition of Purkyne fibers*

A layer of elements labelled Purkyne elements were added inside the ventricles in order to allow for faster spreading of excitation. On displays on the terminal CRT was determined where and to which extent possibly Purkyne elements inside the cavities occur. These Purkyne elements were then manually added to the total structure. In this way, a total of 19.283 Purkyne elements were added. Special attention was paid to reconstruct also the false tendons. False tendons are Purkyne fibers which are running free from the intraventricular septum through the cavities to the papillary muscles.

N.B.

After selection of the termination location of the left and right bundle a second version of the model was created in which only the Purkyne elements were retained which are reached within the first 25 msec after onset of excitation at this termination locations. This model is finally used in the simulation experiments and referred to as "restricted" model.

Appendix 111

THE RHOMBODODECAHEDRON (RDH)

The Rhombododecahedron (RDH)

A rhombododecahedron is a polyhedron. A polyhedron may be defined as a finite, connected set of plane polygons, such that every side of each polygon belongs also to just one other polygon, with the proviso that the polygons surrounding each vertex form a single circuit (33).

In the large family of polyhedrons, we can distinguish:

(a) *Regular solids*

These are the five platonic solids. A regular solid is defined as a solid whose faces are congruent, regular polygons, so arranged that the same number of edges meet at each vertex (104). The five platonic solids are the tetrahedron, octahedron, icosahedron, hexahedron, and dodecahedron (pentagonal).

(b) *Semiregular solids*

These are the Archimedean solids as well as those solids having dual features with them.

b1. Archimedean solids are convex solids with regular faces, not all of which are the same kind, and with non-regular polyhedral angles, all of which are identical (104).

b2. Duals of Archimedean solids are convex solids with non-regular faces, all of which are identical and with regular polyhedral angles, not all of the same kind.

A polyhedral angle is the solid angle of the vertex. If the midpoints of the sides of one vertex form the vertices of a regular polygon, the polyhedral angle is said to be regular.

A rhombododecahedron falls into category b(2). Its 12 faces are equal rhombi. Each face has diagonals in the ratio $1:\sqrt{2}$. To build a rhombododecahedron: Take two identical solid cubes. Cut one of them in six square pyramids based on six faces, with their common apex at the center of the cube. Place these pyramids on the respective faces of the second cube. Result: A solid rhombododecahedron (18). If we pack rhombododecahedra with their centers on the above described grid lines (Fig. 3.2) they fill all space just once. If the distance between the integer coordinates is a , then the volume occupied by one rhombododecahedron is $a^3\sqrt{2}/2$ and the surface area of each rhombic face is $a^2\sqrt{2}/4$. The normals of two adjacent rhombic faces make an angle of 60° , consequently all the dihedral angles are 120° .

From the way we can build up a rhombododecahedra (see above) it follows that if we connect the short diagonals of each rhombic face we obtain a hexahedron. In 6 from the 14 vertices 4 faces meet, in the other 8 three faces come together. The regular polyhedral angles are $\frac{2}{3}\pi$ and π respectively. The distance from the center of the RDH to each face is equal, and $\frac{1}{2}$ the packing distance a . The distance from the center to the vertex with four sides is $a\sqrt{2}/2$, to the vertex with 3 sides $a\sqrt{6}/4$.

In the packing used, the orthogonal Z axis intersects with two opposing vertices of 3 sides; and one vertex of 4 sides has polar coordinates of 30° azimuth and an elevation of $35^\circ.16'$. The orientation of the RDH in space is thus unambiguously defined. The first known description

of a RDH is attributed to Kepler (1619) (71). More well known is the pentagonal dodecahedron, which is one of the five platonic solids. Although this solid is more regular and has less difference with its inscribed sphere (24.54% difference volume for the pentagonal dodecahedron and 25.95% for the RDH) it is not suitable for packing, since its dihedral angle is 108° . One more polyhedron deserves attention. It is a dodecahedron whose faces are made of six rhombi and six trapezoids, which can be obtained from the RDH by cutting this in two equal pieces by a plane perpendicular to the orthogonal Z axis, and rotating the halves 60° in respect to each other. This polyhedron allows a similar dense packing as the RDH. However, it is not suitable for our purposes since no regular grid fits the center points.

Appendix IV

HEXAGONAL COORDINATES AND VECTOR OPERATIONS IN HEXAGONAL SPACE

Hexagonal cartesian coordinates

A hexagonal cartesian coordinate system is a system in which the location of a point in space is specified by three coordinates, which are the intersections of hexagonal coordinate axis with the plane through this point parallel to the plane formed by the other axes. A hexagonal coordinate axis is an axis which makes an angle of 60° with the other two axes.

The following formulae transform coordinates in hexagonal cartesian coordinate system into coordinates in an orthogonal cartesian coordinate system:

$$X_o = X_H + Y_H \cos(\pi/3) + Z_H \cos(\pi/3)$$

$$Y_o = Y_H \sin(\pi/3) + \frac{1}{3} Z_H \sin(\pi/3)$$

$$Z_o = \frac{1}{3} \sqrt{6} Z_H$$

The opposite transformation is given by:

$$X_H = X_o - Y_o \tan(\pi/6) - \frac{1}{6} \sqrt{6} Z_o$$

$$Y_H = Y_o / \sin(\pi/3) - \frac{1}{6} \sqrt{6} Z_o$$

$$Z_H = \frac{1}{2} \sqrt{6} Z_o$$

Unit distance in both systems is equal. The sections were made at an orthogonal distance of 1 mm. We preferred to have the Z_h grid-points exactly in these layers. This is accomplished by using the constant $C(\sqrt{6}/3)$ as unity in the hexagonal coordinate system. The two sets of transformation formulae then look like:

$$X_o = 1/c (X_H + 0.5 Y_H + 0.5 Z_H)$$

$$Y_o = 1/c (0.866025 Y_H + 0.288675 Z_H)$$

$$Z_o = Z_H$$

and

$$X_H = c (X_o - 0.57735 Y_o - 0.40825 Z_o)$$

$$Y_H = c (1.154701 Y_o - 0.40825 Z_o)$$

$$Z_H = Z_o$$

In this set, X_o, Y_o, Z_o are measured in millimeters as unity and X_H, Y_H, Z_H , with $1/3\sqrt{6}$ millimeters as unity.

Vector Operations

All vector operations are done in the same way as in an orthogonal coordinate system. However, it should be kept in mind that the unit vectors $\vec{i}, \vec{j}, \vec{k}$, make 60° angles with each other. The dot products of two vectors can be derived as follows:

$$\text{Let vector } \vec{A} = A_1\vec{i} + A_2\vec{j} + A_3\vec{k} \quad \text{and} \quad \vec{B} = B_1\vec{i} + B_2\vec{j} + B_3\vec{k}$$

$$\begin{aligned} \vec{A} \cdot \vec{B} &= A_1B_1\vec{i} \cdot \vec{i} + A_2B_2\vec{j} \cdot \vec{j} + A_3B_3\vec{k} \cdot \vec{k} + \\ &\quad + (A_2B_3 + A_3B_2)\vec{j} \cdot \vec{k} + (A_1B_3 + A_3B_1)\vec{i} \cdot \vec{k} + (A_1B_2 + A_2B_1)\vec{i} \cdot \vec{j} \end{aligned}$$

In case of an orthogonal coordinate system $\vec{i} \cdot \vec{i} = \vec{j} \cdot \vec{j} = \vec{k} \cdot \vec{k} = 1$ and the products of the other unit vectors are zero (cosine $90^\circ = 0$) in an

hexagonal coordinate system, however, these products all equal to 0.5 (cosine 60°), and the dot product of the two vectors A and B is

$$\vec{A} \cdot \vec{B} = A_1B_1 + A_2B_2 + A_3B_3 + 0.5[(A_1B_2 + A_2B_1) + (A_2B_3 + A_3B_2) + (A_1B_3 + A_3B_1)]$$

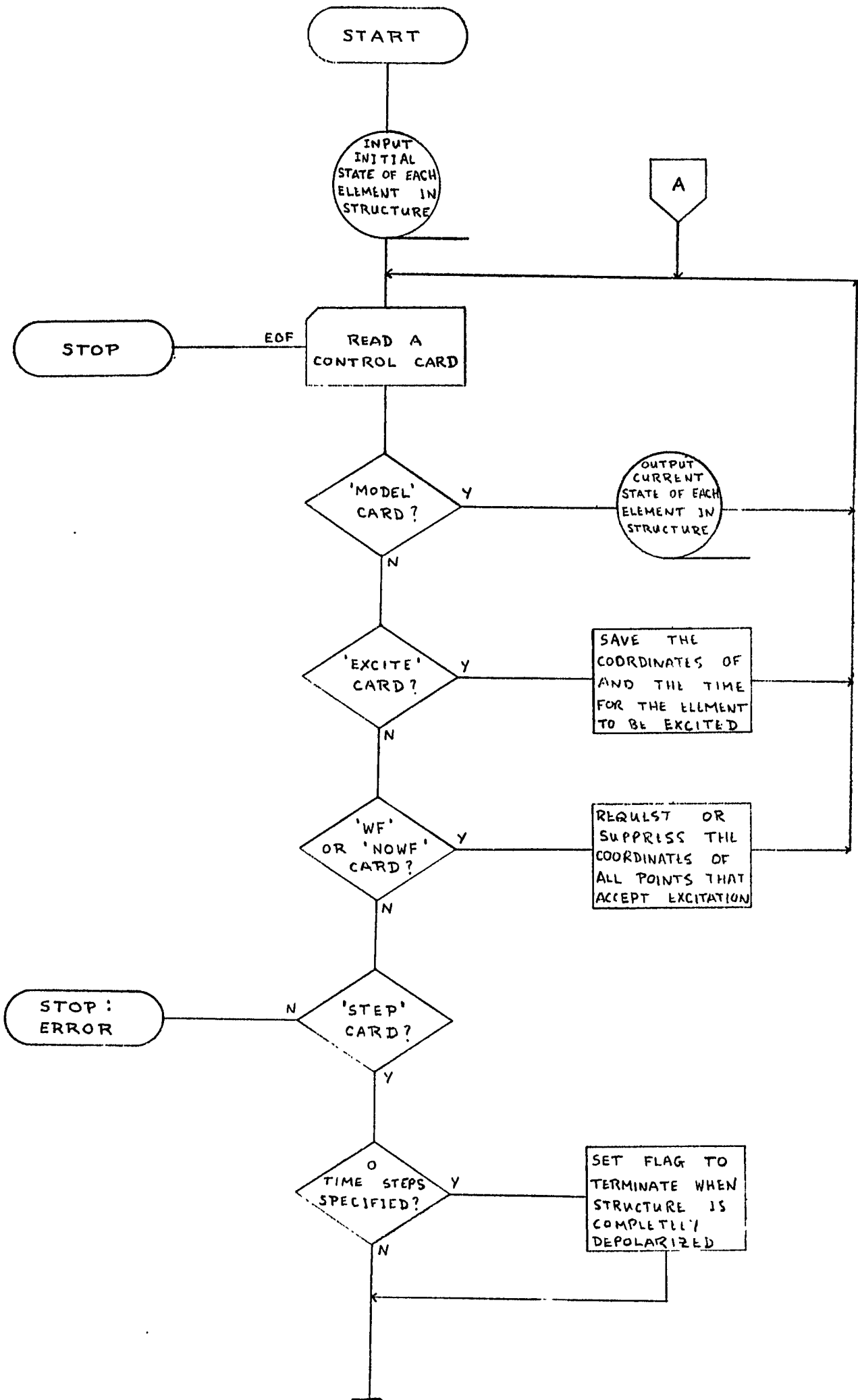
If two points, P_1 and P_2 , have hexagonal coordinates (X_1, Y_1, Z_1) , and (X_2, Y_2, Z_2) , respectively, then the distance is given by the formula :

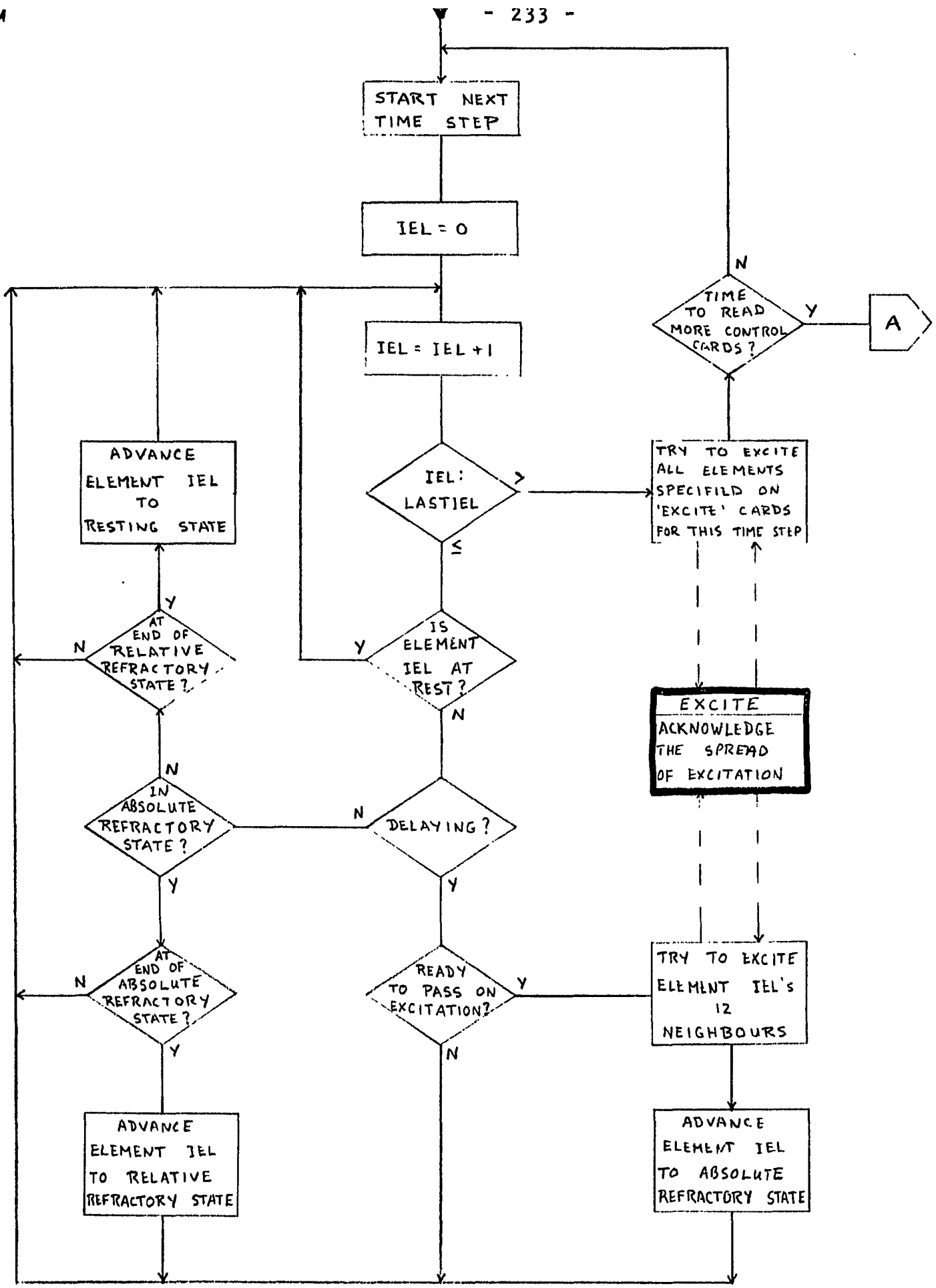
$$\overline{P_1P_2} = \left((X_2 - X_1)^2 + (Y_2 - Y_1)^2 + (Z_2 - Z_1)^2 + (X_2 - X_1)(Y_2 - Y_1) + (X_2 - X_1)(Z_2 - Z_1) + (Y_2 - Y_1)(Z_2 - Z_1) \right)^{-1/2}$$

For each center point (0,0,0) and any of the twelve coordinate triplets given above (page 1V.1) this distance evaluates as 1.

Appendix V

FLOW CHART OF PROGRAM HEXCITE





TABLES

TABLE II

Elevation and azimuth angles of ventricular gradients of model I^A and I^B; angle subtended between \vec{G}_{QRS} and \vec{G}_T and the ratio of $\vec{G}_{QRS,T}/\vec{G}_{QRS}$

Data relating to figure	azimuth (degrees)	elevation (degrees)	QRS-T-angle (degrees)	$\vec{G}_{QRS,T}/\vec{G}_{QRS}$	
IA	4.14.a	59.9	-41.1	125.0	.89
	.b	59.9	-41.6	90.3	1.80
	.c	59.8	-41.7	77.2	2.70
	.d	59.8	-41.8	70.8	3.61
	4.15.a	58.9	-38.1	169.4	.20
	.b	55.4	-39.4	161.6	.33
	.c	51.9	-39.7	157.0	.40
	.d	48.2	-39.9	154.8	.44
	4.16.a	60.1	-40.7	148.4	.53
	.b	59.6	-41.2	119.2	.99
	.c	59.1	-41.2	114.7	1.07
IB	4.17.a	- 9.0	-62.0	154.4	.56
	.b	-10.0	-63.0	162.1	.46
	.c	-10.1	-63.5	108.6	.95
	.d	-10.0	-62.7	97.9	1.04

TABLE III

Elevation and azimuth angles of ventricular gradients of model II^A and II^B, the angle subtended between \vec{G}_{QRS} and \vec{G}_T and the ratio $\vec{G}_{QRS,T}/\vec{G}_{QRS}$.

Data relating to figure	azimuth (degrees)	elevation (degrees)	QRS-T-angle (degrees)	$\vec{G}_{QRS,T}/\vec{G}_{QRS}$
II A				
4.18 a	-88.1	-57.9	168.0	.38
b	-87.8	-58.6	133.5	.79
c	-87.3	-58.8	75.4	1.18
d	-87.8	-57.29	172.7	.27
e	-84.0	-58.1	171.3	.31
f	-80.1	-58.6	171.0	.33
4.19 a	-87.3	-58.2	165.8	.43
b	-86.3	-58.4	164.2	.46
c	-83.8	-58.8	162.2	.50
d	-84.9	-59.1	121.1	.87
II B				
4.20 a	-76.1	-52.2	163.2	.43
b	-75.7	-52.9	120.2	.87
c	-75.4	-53.2	72.7	1.31
d	-74.1	-51.9	169.5	.31
e	-70.2	-52.6	166.9	.37
f	-65.9	-53.1	165.4	.40
4.21 a	-75.3	-52.5	160.0	.48
b	-74.2	-52.8	157.3	.52
c	-71.4	-53.2	153.6	.57
d	-72.5	-53.4	105.1	.98

TABLE IV

Elevation and azimuth angles of ventricular gradients in models with reversed sequence of repolarization, the angle subtended between \vec{G}_{QRS} and \vec{G}_T and the ratio $\vec{G}_{QRS,T}/\vec{G}_{QRS}$

Data relating to figure	azimuth (degrees)	elevation (degrees)	QRS-T-angle (degrees)	$\vec{G}_{QRS,T}/\vec{G}_{QRS}$	
Fig. 22.a	a	-77.33	-60.3	172.6	.303
	b	-76.1	-69.4	167.3	.58
	c	56.5	-54.0	106.9	1.08
	d	56.1	-52.1	98.4	1.24
23.a	a	-22.1	-71.2	146.5	.74
	b	-19.9	-69.5	132.0	.82
	c	-85.5	-67.1	158.4	.66
	d	-76.0	-63.1	150.0	.70

TABLE V

Elevation and azimuth angles of ventricular gradients in model 3, the angle subtended between \vec{G}_{QRS} and \vec{G}_T and ratio $\vec{G}_{QRS,T}/\vec{G}_{QRS}$

Data relating to figure	azimuth (degrees)	elevation (degrees)	QRS-T-angle (degrees)	$\vec{G}_{QRS,T}/\vec{G}_{QRS}$
Fig. 24.a	-19.5	-17.8	130.8	.85
b	-18.5	-20.5	112.4	1.24
c	-19.3	-18.3	126.9	.92
d	-18.4	-20.6	109.7	1.30

TABLE VI

Difference numbers and correlation of the various leadsystems as compared with the pure dipoleVCG

	BURGER	FRANK	McFEE	SVEC III
X QRS	N = 69.1 R = .92	<u>N = 21.9 R = .99</u>	N = 28.7 R = .97	N = 48.2 R = .92
Y QRS	N = 19.9 R = .98	N = 20.8 R = .97	N = 21.1 R = .97	N = 24.8 R = .96
Z QRS	N = 79.4 R = .49	N = 31.5 R = .94	N = 16.7 R = .98	<u>N = 13.4 R = .99</u>
X _T	N = 7.33 R = .99	<u>N = 2.3 R = .99</u>	N = 10.5 R = .99	N = 14.8 R = .99
Y _T	N = 85.14 R = .51	N = 91.3 R = .46	<u>N = 79.9 R = .56</u>	N = 99.1 R = .36
Z _T	N = 38.43 R = .95	N = 223.5 R = .98	N = 165.7 R = .98	<u>N = 89.3 R = .99</u>
X _{QRS,T}	N = 43.5 R = .87	<u>N = 13.8 R = .98</u>	N = 21.1 R = .97	N = 34.4 R = .93
Y _{QRS,T}	<u>N = 28.4 R = .98</u>	N = 30.0 R = .97	N = 28.8 R = .97	N = 34.4 R = .97
Z _{QRS,T}	N = 73.9 R = .53	N = 57.3 R = .93	N = 36.7 R = .97	<u>N = 23.6 R = .98</u>

Table VII

Number of times of excitation (N), mean and S.D. of the intervals and type number of the elements. Model R.

Duration of activity analyzed: 4000 time steps (12 seconds).

Element	N	Mean	SD	Type
1	191	62.1	10.2	10
2	161	73.7	10.7	17
3	118	100.4	21.3	20
4	186	63.7	10.9	10
5	156	75.7	11.2	17
6	129	91.5	19.1	20
7	179	65.6	11.2	13
8	144	82.3	17.3	18
9	169	70.0	11.7	15

Table VIII

Number of times of excitation (N), mean and SD of the intervals and type number of the elements. Model M.

Duration of activity analyzed: 4300 time steps (21.5 seconds)

Element	N	Mean	+	SD	Type
1	152	141.3		12.4	10
2	143	149.3		17.2	17
3	106	199.9		49.1	20
4	147	144.5		15.5	10
5	144	148.5		11.3	17
6	118	181.2		37.5	20
7	146	145.1		11.5	13
8	136	156.4		22.5	18
9	145	147.3		15.7	15